# Development and characterisation of novel mouse models of human prostate cancer

Helen Pearson

Ph.D.

Cardiff University

2005-2008






ProQuest LLC
789 East Eisenhower Parkway
P.O. Box 1346
Ann Arbor, MI 48106-1346

**DECLARATION**

This work has not previously been accepted in substance for any degree and is not concurrently submitted in candidature for any degree.

Signed.....H. Pearson..... (candidate) Date ...26.03.08.....

**STATEMENT 1**

This thesis is being submitted in partial fulfilment of the requirements for the degree of PhD.

Signed.....H. Pearson..... (candidate) Date ...26.03.08.....

**STATEMENT 2**

This thesis is the result of my own independent work/investigation, except where otherwise stated. Other sources are acknowledged by explicit references.

Signed.....H. Pearson..... (candidate) Date ...26.03.08.....

**STATEMENT 3**

I hereby give consent for my thesis, if accepted, to be available for photocopying and for inter-library loan, and for the title and summary to be made available to outside organisations.

Signed.....H. Pearson..... (candidate) Date ...26.03.08.....

**STATEMENT 4: PREVIOUSLY APPROVED BAR ON ACCESS**

I hereby give consent for my thesis, if accepted, to be available for photocopying and for inter-library loans **after expiry of a bar on access previously approved by the Graduate Development Committee.**

Signed....H. Pearson..... (candidate) Date ....26.03.08.....

# Acknowledgements

Special thanks must go to my supervisor Prof. Alan Clarke and Toby, whose advice, support and constant optimism has been invaluable. I would also like to thank and all members of the lab for their excellent advice throughout my Ph.D. and for many unforgettable work parties!

Many thanks to my family and friends for their continual support and for distracting me from my constant worrying!

I am also greatly indebted to Mark Bishop, Lucie Pietzka and Luke Piggott for carrying out the genotyping, Derek Scarborough for histology services and Anthony Hann for assisting with electron microscopy (all based at Cardiff University). I would also like to thank Andrew Suttie (ILS Inc, New Zealand) for providing me with a detailed prostate microdissection protocol and Dylan Edwards and Caroline Pennington (University of East Anglia, Norwich) for carrying out qRT-PCR analysis of human prostate samples. Many thanks also to Prof. Chris Collins (Bristol Royal Infirmary, Bristol) for providing me with detailed pathology reports and my undergraduate student Jennifer Howard.

This Ph.D. was supported by Tenovus.

# Table of Contents

# List of Figures

# List of Tables

# Abstract

To date, prostate cancer is the most common male cancer diagnosed in the United Kingdom. Our rudimentary knowledge of the aetiology and molecular pathways implicated in prostate tumourigenesis is probably responsible for its poor prognosis. To address this, a conditional transgenic approach was employed to investigate the role of the tumour suppressor Lkb1 and the proto-oncogenes β-catenin and K-ras within the murine prostate.

LKB1 is a tumour suppressor commonly mutated in Peutz-Jegher's syndrome (PJS), which predominantly predisposes to gastrointestinal hamartomas and various extra-intestinal tumours. Using a conditional transgenic approach, recombination of a LoxP-flanked *Lkb1* transgene was mediated by the inducible *Ah (p450 CYP1A1)* promoter. Loss of Lkb1 in un-induced $AhCre^{+}Lkb1^{fl/fl}$ mice predisposed to prostate intra-epithelial neoplasia (PIN) within 2-4 months. Molecular analysis revealed that neoplastic foci had lost cellular polarity and showed enhanced PI3K/AKT and Wnt signalling pathway activity, ultimately leading to tumour growth. Loss of Lkb1 did not result in activation of the AMPK/mTOR pathway, suggesting that a feedback mechanism suppresses mTOR in Lkb1 deficient conditions. Study of disease progression in this model is limited owing to decreased longevity, which is thought to be caused by the development of bulbourethral gland cysts. Additional GU tract phenotypes were also observed in un-induced $AhCre^{+}Lkb1^{fl/fl}$ urethral glands and seminal vesicles and all $Lkb1^{fl/fl}$ male mice were infertile.

To address the problem of reduced longevity in the $AhCre^{+}Lkb1^{fl/fl}$ cohort, $PBCre^{+}Lkb1^{fl/fl}$ transgenic mice were derived. Here, *Cre*-recombinase expression is mediated by the composite rat *Probasin* promoter. All cohorts showed life-spans comparable to *wild-type* mice at 500 days. $PBCre^{+}Lkb1^{+/fl}$ prostates were normal, while $Cre^{-}Lkb1^{fl/fl}$ mice developed low grade-PIN, demonstrating the hypomorphic nature of the *Lkb1* floxed allele. $PBCre^{+}Lkb1^{fl/fl}$ mice demonstrated atypical hyperplasia of the prostate, arguing a critical role for *Lkb1* levels in cancer initiation. Long-term Lkb1 deficiency also predisposed to kidney abnormalities, preputial gland squamous metaplasia and PJS-linked phenotypes, including stomach hamartomas and Sertoli-cell-only syndrome at 500 days.

To investigate the deregulation of Wnt signalling in the murine prostate, conditional transgenic mice carrying a dominant stable form of β-catenin in the prostate were generated ($PBCre^{+}Catnb^{+/lox(ex3)}$). At 3 months, males manifested PIN-like keratinised squamous metaplasia that advanced to adenocarcinoma by 6 months. No evidence for synergy was

determined between Lkb1 loss and activated β-catenin, although investigations were limited to *PBCre*$^{+}$*Lkb1*$^{+/fl}$:*Catnb*$^{+/lox(ex3)}$ mice owing to a time constraint and partial embryonic lethality of *Lkb1*$^{fl/fl}$ mice.

Synergism between Wnt and Ras signalling has been well documented in many human cancers, including intestine, liver and kidney. To address the cooperativity of these pathways in the prostate, the *PBCre* transgenic line was employed to express an activated K-*ras*$^{V12}$ mutation and a dominant stabilised form of β-catenin (*PBCre*$^{+}$*K-ras*$^{+/V12}$;*Catnb*$^{+/lox(ex3)}$). *PBCre*$^{+}$*K-ras*$^{+/V12}$ mice were predisposed to low grade-PIN at 16 months and demonstrated elevated MAPK signalling. Double mutants demonstrated rapid tumourigenesis to invasive carcinoma at 6 months, which displayed elevated Wnt and MAPK signalling. Further molecular analysis determined that activated K-ras and β-catenin synergise to facilitate prostate tumourigenesis by elevating the number of androgen receptor positive cells and upregulating Wnt targets, such as COX-2 and c-Myc. This evidence suggests androgen-independent tumour growth and presents a direct mechanism whereby tumour progression is accelerated via the canonical Wnt pathway.

In summary, this thesis reports the first correlation between Lkb1 loss and prostate neoplasia, and demonstrates synergy between Wnt and Ras signalling in murine prostate tumourigenesis. Together, these data provide a valuable resource for genetic based studies and establish the multi-step nature of tumourigenesis.

# Abbreviations

ADP - Adenosine diphosphate.
AH - Atypical hyperplasia.
AKT - v-akt murine thymoma viral oncogene homolog 1 (PKB).
AMACR - α-methylacyl-CoA racemase.
AMP - Adenosine monophosphate.
AMPK - AMP activating protein kinase.
AP - Anterior prostate.
APC - Adenomatous polyposis coli.
AR - Androgen receptor.
ARE - Androgen response element.
ARR - Androgen receptor regulated promoter region.
ATP - Adenosine triphosphate.
bp - base pairs.
BrdU - Bromodeoxyuridine.
BRG1 - Brahma related gene-1.
BUG - Bulbourethral gland.
BZS - Bannayan zonana syndrome.
Catnb -β-catenin (CTNNB1).
CD - Cowden's disease.
CD44 - CD44 antigen (homing function and Indian b blood group system).
CK2 - Casein kinase-2.
Cre - Cyclisation recombination.
CZ - Central zone.
DEPC - Diethyl pyrocarbonate.
DHT - 5-alpha-dihydrotestosterone.
DLP - Dorsolateral prostate.
DP - Dorsal prostate.
DPX - Distrene plasticizer and xylene.
Dsh - Dishevelled.
E - Embryonic day.
EM - Electron microscopy.
ERK - Extracellular signal-regulated kinase.
FAP - Familial adenomatous polyposis.
FGF - Fibroblast growth factor.
Fl - Floxed.
Foxa1 - Forkhead box A1.
FSH - Follicle stimulating hormone.
GSK3β - Glycogen synthase kinase-3β.
GU - Genitourinary.
H&E - Haematoxylin and eosin.
HG-PIN - High-grade prostate intra-epithelial neoplasia.
Hh - Hedgehog.
HK2 - Human kallikrein-2.
HNPCC - Hereditary non-polyposis colorectal cancer.
HPC-1 - Hereditary prostate cancer-1.
IGF-1 - Insulin growth factor-1.

i.p. - intra-peritoneal.
JNK - Janus kinase.
JPS - Juvenile polyposis syndrome.
kDa - kilodalton.
Ki-67 - antigen identified by monoclonal antibody Ki-67 (MKI-67).
LCMD - Laser capture microdissection.
LG-PIN - Low-grade prostate intra-epithelial neoplasia.
LH - Luteinising hormone.
LIP1 - LKB1 interacting protein-1.
LKB1 - Serine threonine kinase-11 (STK11).
LOH - Loss of heterozygosity.
LoxP - Locus x of crossover P1 site.
LP - Lamina propria.
MAPK - Mitogen-activated protein kinase.
MARK - Microtubule affinity regulated kinases.
MeCP2 - Methyl CpG binding protein 2.
MEK1/2 - Mitogen-activated protein kinase kinase 1/2.
mRNA - Messenger RNA.
mTOR - FK506 binding protein 12-rapamycin associated protein 1 (FRAP1).
Nkx3.1 - NK-3 transcription factor, locus 1.
NLS - Nuclear localisation sequence.
O/N - Overnight.
p53 - Transformation related protein 53, Trp53.
p63 - Transformation related protein 63, Trp63.
PAP - Prostate acid phosphatase.
PAR1A - MAP/microtubule affinity-regulating kinase 3 (MARK3), Cdc25C-associated kinase 1 (cTAK1).
PB - Probasin promoter.
PBS - Phosphate buffered saline.
PCR - Polymerase chain reaction.
PDK1 - Pyruvate dehydrogenase kinase, isozyme 1.
PI3K - Phosphoinositol-3 kinase.
PIN - Prostate intra-epithelial neoplasia.
PJS - Peutz-Jeghers syndrome.
pS6 - p70 S6 ribosomal protein (RpS6).
PSA - Prostate specific antigen.
PSCA - Prostate stem cell antigen.
PTEN - Phosphatase and tensin homolog deleted on chromosome 10, MMAC1.
PZ - Peripheral zone.
Rb - Retinoblastoma.
RHEB - Ras homolog enriched in brain.
RT-PCR - Reverse transcription polymerase chain reaction.
S6K - Ribosomal protein S6 kinase, 70kDa, polypeptide 1 (RPS6K).
SCID - Severe combined immunodeficiency.
SCOS - Sertoli-cell-only syndrome.
SD - Standard deviation.
SDS - Sodium dodecyl sulphate.
Sox17 - Sry-related HMG box gene 17.
STRAD - Ste20-related adaptor.
SqM - Seminal vesicle squamous metaplasia.

SV - Seminal vesicle.
T - Testosterone.
TBS - Tris buffered saline.
TCF/LEF - T-cell factor/ lymphocyte enhancer factor.
TCF4 - Transcription factor-4.
TGFβ - Transforming growth factor-β.
TZ - Transitional zone.
TSC1 - Tuberous sclerosis 1 (hamartin).
TSC2 - Tuberous sclerosis 2 (tuberin).
UG - Urethral glands.
UGH - Urethral gland hyperplasia.
UGS - Urogenital sinus.
VEGF - Vascular endothelial growth factor.
VP - Ventral prostate.
Wnt - Wingless type MMTV integration site family member.
Xeek1 - *Xenopus* egg and embryonic kinase-1.
ZO-1 - Zona occludens-1.

# Chapter 1: Introduction

## 1.1 The prostate

The prostate is a small gland of the male reproductive system consisting of a network of ducts that are growth stimulated by androgens, such as testosterone. This section shall focus on the function, morphology, growth and development of the prostate. Moreover, a description of the similarities and differences between human and mouse prostate highlights the benefits of this model organism in the study of prostate cancer.

### 1.1.1 Prostate function

The male accessory glands consist of the prostate, seminal vesicles, bulbourethral glands, urethral glands, preputial glands and ampullary glands. The prostate is fundamental to the male reproductive tract and primarily functions to secrete a protease-rich milky fluid (pH 6.5) that contributes to approximately 30% of the ejaculate (Fair and Cordonnier, 1978). To increase sperm motility and viability, prostatic fluid contains hormones, lipids, growth factors, nutrients, citric acid for ATP production and enzymes for seminal liquefaction (Fair and Cordonnier, 1978; Zaichick *et al.*, 1997). In humans, prostate acid phosphatases (PAPs), prostate specific antigen (PSA, also termed kallikrein-related peptidase 3, KLK3) are also present. PAPs convert phosphatidic acid to diacylglycerol and functions in glycerolipid synthesis and phospholipase D signal transduction. PSA is believed to participate in the liquefaction of seminal coagulum by cleaving seminogelins, which allow sperm to swim more freely (Fair and Cordonnier, 1978; Zaichick *et al.*, 1997). The serum level of these enzymes is frequently used to determine tumour stage at diagnosis and to monitor prostate cancer progression (Deras *et al.*, 2008). More recently, the *PCA3* (prostate cancer antigen 3, *DD3*) gene has emerged as a clinical prostate cancer marker, where a high level of *PCA3* mRNA in urine correlates to prostate cancer (Deras *et al.*, 2008). One study has shown that 95% of primary prostate cancer specimens over-express the *PCA3* gene (deKok *et al.*, 2002).

All mammals have a prostate and the principle functions remain analogous between species, despite the varying number of accessory glands. For example, aquatic cetaceans lack seminal vesicles, ampullary glands and bulbourethral glands (Price, 1963). Furthermore, the female prostate termed the gland of Skene is histologically similar to the male prostate (Price, 1963).

### 1.1.2 Development of the prostate

Development of the human prostate has been previously well documented (Holyrood, 1997). In brief, at week 7 the male human embryo undergoes degeneration of the paramesonephric ducts to form the prostatic utricle. The urethers separate from the mesonephric ducts to become the proximal urethra and the mesonephric ducts differentiate to generate the ejaculatory ducts. During week 10, the urogenital sinus (UGS) mesenchyme induces epithelial buds in the early prostatic urethra and lumens of primitive acini develop. During weeks 13-15, testosterone levels elevate and remain high until week 25 to induce epithelial differentiation. The secretory cells become functional and the basal and neuroendocrine cell populations arise. At week 25, testosterone production is reduced and the gland remains in a quiescent state until puberty, in a similar manner to mice (Wang *et al.*, 2001). During puberty, testosterone levels increase to induce epithelial proliferation of membrane infoldings, to generate a mature prostate. At 45-50 years of age, androgen levels deplete and the prostate involutes. With increasing age, atrophication of the gland may occur, increasing the risk of prostate disorders (Holyrood, 1997).

Mouse prostate development has been described in detail previously (Kasper and Matusik, 2000; Staack *et al.*, 2003). Briefly, during E10-11 the UGS begins to emerge and the testes commence androgen production at E12.5-13, which peaks during E17-18 and then drops until puberty. At E14.5, the Wolffian ducts differentiate into the epididymis, seminal vesicles and ductus deferens and the Mullarian duct degenerates. By E18.5, the rudimentary prostate can be distinguished as a pair of ventral buds and anterior lobe outgrowths. At birth, the prostatic lobes have differentiated and over the next 1.5 months mucosal membranous infoldings form and further growth occurs, until sexual maturation is complete (Kasper and Matusik, 2000; Staack *et al.*, 2003).

In mammals, the development of organs composed of epithelial parenchyma relies upon mesenchymal-epithelial cross-talk, where paracrine signals from the mesenchyme direct epithelial differentiation and morphology (Cunha *et al.*, 2004; Hayward and Cunha, 2000). Early prostate ductal budding and morphogenesis is accompanied by the transient elevation of multiple signalling molecules; Shh, Bmp4, Fgf7/10, Foxa1, Notch1 (Mirosevich *et al.*, 2005) and Homeobox (HOX) genes (Shappell *et al.*, 2004).

### 1.1.3 Prostate morphology

The prostate is essentially a collection of tubular-alveolar glands that secrete components of the seminal fluid into the prostatic urethra (Shappell *et al.*, 2004). Figure 1.1

depicts a cross-section of normal human prostate epithelium composed of three established different cell types; basal, luminal (also termed secretory cells) and neuroendocrine (Lam, 2006). A fourth controversial population of prostate stem cells also exists and is speculated to give rise to a fifth population, termed the transit-amplifying cells (discussed in section 1.1.4). Currently, the relationship between the prostate cell lineages is not well understood.

In humans, basal cells form a continuous layer adjacent to the basement membrane and express a number of specific biomarkers; p63 (a p53 homologue), cytokeratins 5 and 14, Bcl-2, CD44, telomerase and GST-π (Huss *et al.*, 2001; Lam, 2006; Tang *et al.*, 2007). The basal cell lineage comprises ~10% of the prostate epithelial cells, is generally undifferentiated and display a low proliferative index (0-1%) and apoptotic index (0-1.3%) (Faith *et al.*, 2005; Thorson *et al.*, 2003). Although basal cells are considered to be androgen-independent, they have been shown to express a low level of androgen receptor (AR) mRNA, suggesting they have the potential to respond to androgens (Lam, 2006). Luminal (secretory) cells face the lumen and function to secrete seminal protein from the apical surface. The luminal cells are androgen-dependent and express AR, CD57, PSA, PAP, 15-lopoxygenase-2 (15-LOX-2) and cytokeratins 8/18 (Lam, 2006; Tang *et al.*, 2007).

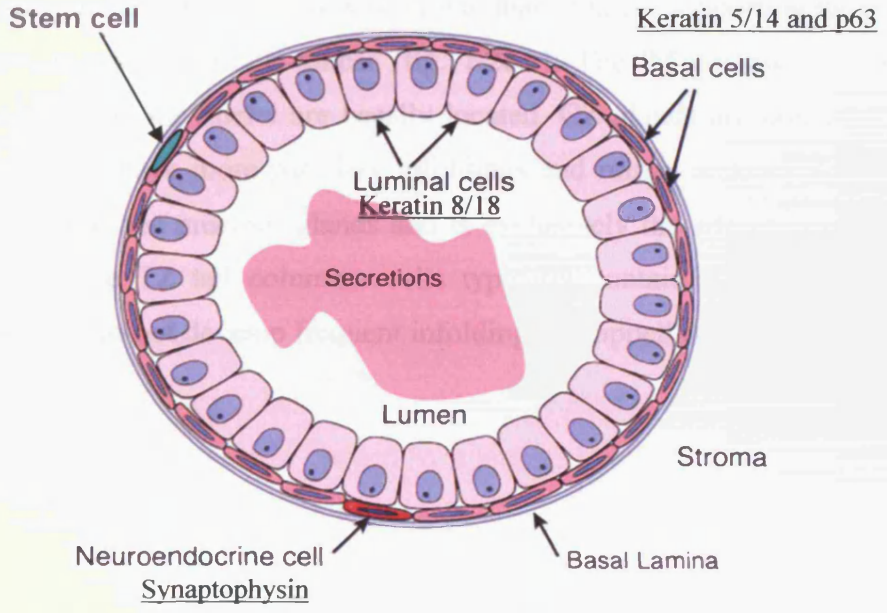


**Figure 1.1: Schematic cross-section of a human prostatic duct.** Basal cells are positioned adjacent to the basement membrane and are sandwiched in by the luminal (secretory) cells. The rare neuroendocrine cells representing 1% of the cellular population are morphologically distinguishable from the basal cells (red). Stem cells are speculated to form ~1% of the basal cell layer (green) and may give rise to the transit-amplifying cells. Specific biomarkers for each cell type have been underlined and this figure is adapted from Abate-Shen and Shen 2002.

The androgen-independent neuroendocrine cells comprise only 1% of the prostate epithelial cells (<0.3% in mice) and express synaptophysin and chromogranin A (Shappell *et al.*, 2004). Neuroendocrine cells secrete a variety of growth factors and paracrine signals that are considered to support the growth and maintenance of the luminal cells (Garabedian *et al.*, 1998; Roy-Burman *et al.*, 2004). Finally, the stroma consists of connective tissue containing smooth muscle fibres that surround the ducts and is rich in blood vessels and nerve endings (Price, 1963).

#### 1.1.3.1 Human prostate

Human prostate is located at the base of the bladder and rectum and surrounds the urethra, forming an anatomically compact structure enclosed by a fibromuscular sheath (figure 1.2a) (Shappell *et al.*, 2004). The gland is divided into three compartments, the peripheral (PZ), central (CZ) and transitional (TZ) zones (figure 1.2b). The PZ accounts for 70% of the glandular tissue and comprises the posterolateral aspects of the prostate, as it surrounds both the CZ and TZ (Roy-Burman *et al.*, 2004; Shappell *et al.*, 2004). The CZ surrounds the ejaculatory ducts and the TZ is located interiorly between the urethra and the surrounding PZ and CZ.

Human prostate acini histologically resemble that of mice, supporting the generation of murine models to study prostate cancer (fig. 1.2c-e). The PZ consists of a moderate amount of infoldings and the nuclei are basally located. CZ glands are larger in diameter than the PZ glands and have more papillary infoldings and roman arches (Shappell *et al.*, 2004). The TZ contains the mucosal glands and is exclusively the site of benign prostatic hyperplasia (BPH). The TZ tall columnar cells typically contain basally located nuclei within small acini that do not develop frequent infoldings (Shappell *et al.*, 2004).

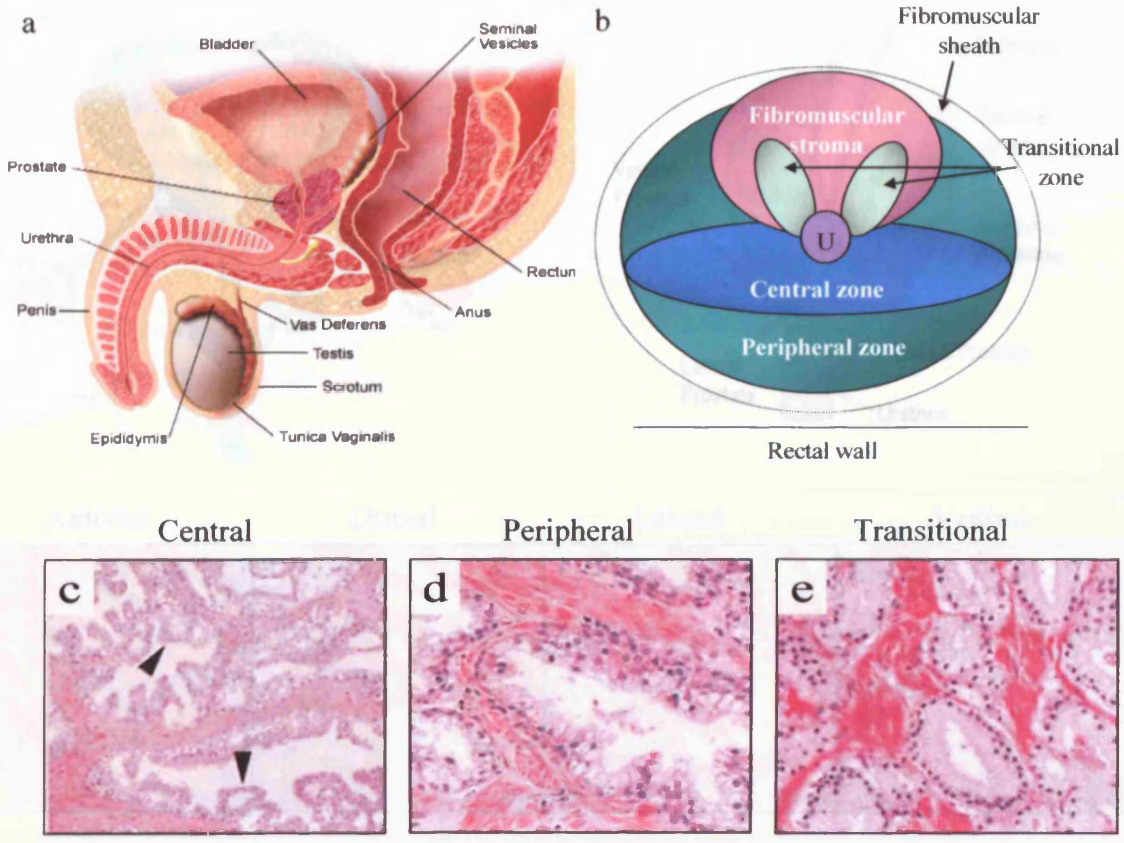


**Figure 1.2: Anatomy and histology of normal human prostate.** (a) Human prostate (box) is located beneath the bladder and is contained within a fibromuscular sheath that surrounds the prostatic urethra (U). (b) The three human prostate lobes; central, peripheral and transitional form an anatomically compact structure. H&E staining of normal human central zone (arrows indicate roman arches) (c), peripheral zone hyperplasia (d) and a typical transitional zone BPH showing large nuclei with prominent nucleoli (e). Figures were adapted from (a) medicalcenter.osu.edu, (b) Abate-Shen and Shen (2002) and (c-e) Shappell *et al* (2004).

### 1.1.3.2 Mouse prostate

Although mouse and human prostate differs in several respects, there are similarities between the two species. Figure 1.3a illustrates the male murine genitourinary (GU) tract, indicating that the murine prostate is located in a similar position to the human prostate, surrounding the neck of the bladder. Mouse prostate consists of four distinct lobes termed the anterior (AP), dorsal (DP), lateral (LP) and ventral (VP) prostate (figure 1.3a-b) (Pinheiro *et al.*, 2003; Shappell *et al.*, 2004; Xue *et al.*, 1997c). The luminal epithelium of each lobe is specialised to produce specific protein products (Kasper and Matusik, 2000) and have distinct histology (figure 1.3c-f).

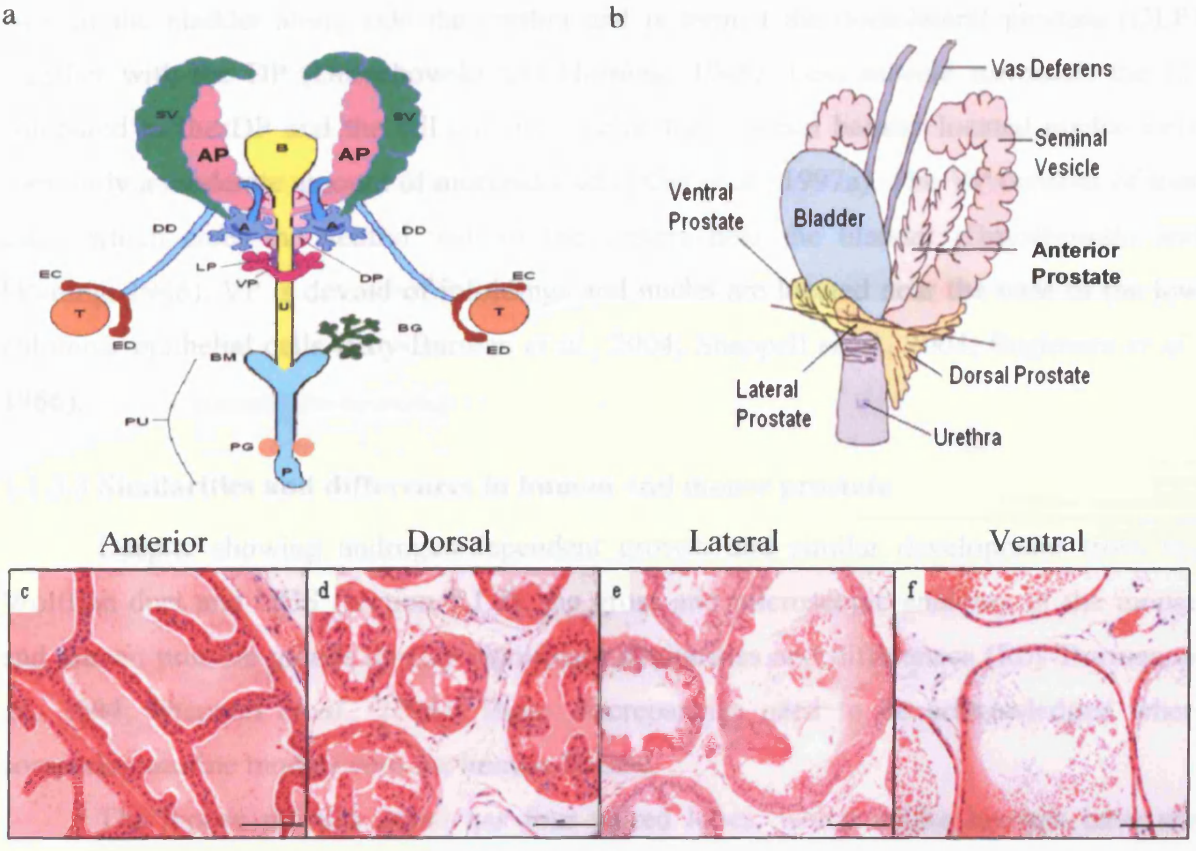


**Figure 1.3: Anatomy and histology of normal mouse prostate.** (a) Ventral view of the male murine genitourinary (GU) tract where A=Ampullary, AP=Anterior prostate, B=Bladder, BG=Bulbourethral Gland, BM= Bulbourethral Muscle, DD=Ductus Deferens, DP=Dorsal Prostate, EC=Epididymis Caput, ED=Epididymis Cauda, LP=Lateral Prostate, P=Penis, PG=Preputial Gland, PU=Penile Urethra, SV=Seminal Vesicle, T=Testis, U=Urethra, VP=Ventral Prostate. (b) Lateral view of the murine prostate. The anterior prostate branches to lie underneath the seminal vesicles, while the dorsal, lateral and ventral lobes surround the neck of the bladder. Histological analysis of formalin-fixed, paraffin-embedded H&E sections from the anterior (c), dorsal (d), lateral (e) and ventral (f) prostate lobes of an adult mouse shows similarities with human prostate. Pictures were taken at 20x magnification and scale bars represent 100 μm. Figures were adapted from (a) Pinheiro *et al* (2003) and (b) Shappell *et al* (2004).

The AP is a paired gland embedded in the peritoneal sheath along the concave surface of the seminal vesicles. The AP functions to secrete a seminal fluid coagulation enzyme, hence its alternate name, the coagulating gland (Dmochowski and Horning, 1946). Within each AP acinous, the mucous membrane is thrown into many mucosal folds, creating finger-like projections into the lumen. Here, the epithelial columnar cells contain small, round, central nuclei (Xue *et al.*, 1997a). The AP and DP are both androgen sensitive and secrete similar products, although DP ducts all enter the dorsal wall of the urethra, whereas the two AP ducts enter the anterior urethra (Dmochowski and Horning, 1946). Compared to the AP, the DP lobes are narrower, surrounded by a thick muscle layer and the nuclei are larger in a more granular cytoplasm (Xue *et al.*, 1997b). The LP is positioned adjacent to the

base of the bladder along side the urethra and is termed the dorsolateral prostate (DLP) together with the DP (Dmochowski and Horning, 1946). Less muscle surrounds the LP compared to the DP and the tall columnar cells, that contain basally located nuclei, only form only a moderate amount of mucosal folds (Xue *et al.*, 1997a). The VP consists of four ducts which enter the ventral wall of the urethra near the bladder (Dmochowski and Horning, 1946). VP is devoid of infoldings and nuclei are located near the base of the low columnar epithelial cells (Roy-Burman *et al.*, 2004; Shappell *et al.*, 2004; Sugimura *et al.*, 1986).

#### 1.1.3.3 Similarities and differences in human and mouse prostate

Despite showing androgen-dependent growth and similar development from the Wolffian duct and UGS (section 1.1.2), the gross and microscopic anatomy of the mouse and human prostate glands display significant similarities and differences (Roy-Burman *et al.*, 2004; Shappell *et al.*, 2004). These discrepancies need to be acknowledged when comparing murine models with the human disease.

The mouse prostate gland has four paired lobes, which unlike humans have not merged into a compact single lobular structure, which consists of three zones (Shappell *et al.*, 2004). Besides this anatomic difference, acini from both species contain basal, neuroendocrine and luminal epithelial cells, albeit with some discrepancy in the ratio and location (Shappell *et al.*, 2004). In humans, basal cells lie adjacent to the basement membrane, forming a layer underneath the luminal cells (Roy-Burman *et al.*, 2004). In mice, the basal cell population is discontinuous and contains a significantly lower ratio of basal to luminal cells (Roy-Burman *et al.*, 2004; Wang *et al.*, 2001). In addition, human basal cells are positive for p27 and BCL-2, whereas murine basal cells only occasionally express p27 and BCL-2 (Wang *et al.*, 2006b). Rare neuroendocrine cells are scattered across both human and murine acini, however, the population of this lineage is significantly smaller in the mouse prostate (i.e. 1% in humans and <0.3% in mice) (Roy-Burman *et al.*, 2004). Tall columnar luminal cells that secrete prostatic proteins and fluids from their apical surfaces into the lumen are common to both species (Roy-Burman *et al.*, 2004).

The stromal content of the human and mouse prostate is significantly different and must be taken into account when comparing the local invasiveness of prostate cancer (Roy-Burman *et al.*, 2004). Human prostate ducts are encapsulated by a thick fibromuscular sheath, while the individual lobes of the murine prostate are surrounded by a thin stromal component (Roy-Burman *et al.*, 2004). Both human and mouse stroma expresses AR,

indicating it is hormone regulated (Cunha *et al.*, 2003). It should also be noted that in the developing rodent prostate smooth muscle differentiates adjacent to the epithelium, while in the developing human prostate the smooth muscle initially differentiates some distance away from the epithelium and gradually fills in the space between the differentiated muscle and the epithelial basement membrane (Hayward *et al.*, 1998). The different location of the neurovasculature within the stroma also prevents a direct comparison of disease progression between species (Roy-Burman *et al.*, 2004). Despite these differences, many studies have supported a functional relationship between the murine DLP and the human PZ, where 70% of carcinomas arise (Roy-Burman *et al.*, 2004). The mouse AP is considered analogous to the human CZ, which rarely transforms in humans (Huss *et al.*, 2001). The VP has no known human equivalent and the TZ, predominantly associated with benign prostatic hyperplasia (BPH), is not considered to have a murine homologue (Roy-Burman *et al.*, 2004). It is important to note that these connections are based on descriptive information and are yet to be defined by molecular characterisation (Lamb and Zhang, 2005).

### 1.1.4 Prostate stem cells

Somatic stem cells function to maintain the normal turnover of cells within an organ. These cells are generally characterised by their ability to self-renew, proliferate indefinitely and ultimately provide all the different cell types required by the tissue they reside in (Lam, 2006; Tysnes and Bjerkvig, 2007). To ensure self-renewal, stem cells are considered to undergo both symmetric and asymmetric divisions, producing either two identical daughter cells with stem cell properties or one stem cell and a progenitor cell respectively (Lam, 2006). The progenitor cell is thought to have a limited self-renewal potential and following several divisions (transit-amplification) may become terminally differentiated. The transit-amplifying cells are considered the major contributors to normal tissue renewal, while the stem cells are regarded as quiescent and do not proliferate (Lam, 2006). Stem cells are thought to reside in a "niche", where interactions of the stem cell with its microenvironment regulate stem cell function (Lam, 2006). The presence and identification of prostate stem cells may be vital for generating novel therapeutic interventions and is currently a highly controversial topic.

The rodent prostate can undergo multiple rounds of castration-induced regression and testosterone-induced regeneration, suggesting the presence of stem cells (Isaacs and Isaacs, 2004; Lawson and Witte, 2007). Androgen-deprived adult prostate regresses, with nearly all epithelial cells reported to undergo apoptosis (predominantly luminal cells), while

the androgen-independent basal cells are thought to remain (Sawicki and Rothman, 2002). Further evidence for prostate stem cells arises from grafting experiments. Prostate epithelial cells (e.g. LAPC-4/9 derived from lymph node and bone metastases respectively) have been shown to form prostate glands when transplanted under the renal capsule with UGS mesenchymal cells (Tang *et al.*, 2007). Current literature presents two potential scenarios for the observed regenerative capacity of the adult prostate; (a) independent self-renewal of basal and luminal cells or (b) multipotent stem cells that comprise 1-15% of the basal cell population (Collins *et al.*, 2005; English *et al.*, 1989; Tokar *et al.*, 2005). Current consensus favours a stem cell-driven hierarchical renewal mechanism, similar to that demonstrated for other epithelial tissues, such as the skin and colon (Sawicki and Rothman, 2002). Consistent with multi-potent stem cell coordination, a transit-amplifying compartment has also been postulated in the prostate, harbouring a subset of cells morphologically classified as intermediates between basal and luminal cells (Signoretti *et al.*, 2000; Wang *et al.*, 2001). Nonetheless, the exact location of prostate stem cells remains under debate.

#### 1.1.4.1 Prostate stem cell location

In humans and mice, each prostate gland comprises a proximal region that connects to the urethra, an intermediate region and a distal tip. The majority of the literature indicates that stem cells are proximally located (Tsujimura *et al.*, 2002; Watabe *et al.*, 2002; Zhou *et al.*, 2007). Compared to the intermediate and distal regions, the proximal cells have been shown to display elevated telomerase activity and a higher proliferative index *in vitro* (Tsujimura *et al.*, 2002; Watabe *et al.*, 2002). Experiments taking advantage of the fact that stem cells probably retain the long-term S-Phase marker BrdU (bromodeoxyuridine), have shown that while the rapidly dividing cells of the transit-amplifying layer quickly dilute the BrdU label, label-retaining cells are concentrated in the proximal region (Tsujimura *et al.*, 2002). This region is characterized by a thick band of morphologically distinct smooth muscle cells that secrete high levels of TGF-β, making it a compelling location for the prostate stem cell niche, since this factor is known to promote stem cell quiescence (Lawson and Witte, 2007). In addition, studies in mice deficient in p53 and Rb have also reported that the proximal region of mouse prostatic ducts enrich for stem cells (Zhou *et al.*, 2007). However, it is possible that stem cells are not restricted to the proximal zone, as some studies have shown that not all the regenerative capacity is located in the proximal region (Kinbara *et al.*, 1996; Lawson and Witte, 2007; Watabe *et al.*, 2002). Indeed, the distal tip also shows a relatively high rate of proliferation when transplanted under the kidney capsule

with UGS mesenchymal cells (Kinbara *et al.*, 1996). The fact that the distal tip is positive for PSCA has led to the hypothesis that the distal tip comprises the bulk of the transit-amplifying cells (Watabe *et al.*, 2002).

The notion that the basal lineage contains the prostate stem cells is widely accepted, although not definitively demonstrated. Consistent with this, basal cells have been shown to express survival factors, such as BCL-2 (Verhagen *et al.*, 1992). Furthermore, *p63* null mice (basal cell deficient) that die shortly after birth, develop defects in prostatic bud development in addition to rudimentary limb development and loss of skin (Signoretti *et al.*, 2000). Signoretti *et al* (2000) also showed that chimeric animals created from $p63^{-/-}$ blastocysts complemented with $p63^{+/+}$ β-galactosidase–positive ES cells, produced β-galactosidase–positive luminal cells in prostate epithelium. This suggests that the basal cells are probably required to restrict multipotent UGS endodermal cells to a prostate lineage and implicates $p63^{+}$ cells in prostate maintenance and luminal cell survival (Signoretti *et al.*, 2000). Morphometric analysis of basal and luminal cells, before and after androgen ablation, has shown that basal cells are highly proliferative during regeneration (Bonkhoff and Remberger, 1996). Together, this evidence suggests that the basal cells can differentiate into luminal cells however, this trans-differentiation process is yet to be confirmed (Collins *et al.*, 2001; Foster *et al.*, 2002; Uzgare *et al.*, 2004). In support of this hypothesis, both rat and human basal cell lines have been shown to differentiate into luminal cells in response to different growth medium (Danielpour, 1999; Robinson *et al.*, 1998). Furthermore, Tran *et al* (2002) also reported that PSCA (prostate stem cell antigen) identifies late intermediate (transit-amplifying) prostate epithelial cells *in vitro*. PSCA-negative cells were shown to give rise to more differentiated PSCA-positive cells that express both basal and luminal cytokeratins but do not express p63, resembling the characteristics of a putative transit-amplifying cell (Tran *et al.*, 2002).

In contrast, a luminal self-renewing population of putative stem cells has also been speculated (Kurita *et al.*, 2004; Lawson and Witte, 2007). Kurita *et al* (2004) argue that luminal cells can develop independently of basal cells. Experiments grafting normal or *p63* null UGS into male adult nude mice revealed that *p63* deficient grafts developed androgen-dependent prostate ducts, where basal cells are absent (Kurita *et al.*, 2004). This data was speculated to imply that $p63^{+}$ cells are required for the differentiation of the basal cells and maintenance of proper luminal cell differentiation, but are not required to regenerate prostate acini following androgen ablation. However, there are other explanations for these observations, one example being that loss of p63 expression causes differentiation defects

that make basal cells unidentifiable in regenerated tissue (Lawson and Witte, 2007). Alternatively, distinct luminal and basal progenitor cells may exist (Lawson and Witte, 2007).

### 1.1.4.2 Prostate stem cell markers

Although the exact number and location of prostate stem cells is yet to be determined, the general consensus is that prostate stem cells reside within the basal cell population. Currently, several potential human prostate stem cell markers have been identified, such as p63, CD44, Keratin 5, Keratin 6, BCL-2, CD133 (AC133), integrin $\alpha_2\beta_1$ and integrin $\alpha_6$ (Collins *et al.*, 2005; Collins *et al.*, 2001; Hurt *et al.*, 2008; Liu *et al.*, 1997; Schmelz *et al.*, 2005). Mouse prostate markers include, prominin (CD133), stem cell antigen-1 (Sca-1) and CD49f (Lawson *et al.*, 2007; Tsujimura *et al.*, 2007; Xin *et al.*, 2005). The discovery of prostate stem cell markers is summarised in Table 1.1.

Richardson *et al* (2004) combined the use of $\alpha_2\beta_1^{hi}$ and $CD133^+$ markers to enrich the prostate stem cell population from normal human prostate. Recently, Lawson *et al* (2007) demonstrated that the $CD45^-/CD31^-/Ter119^-/Sca\text{-}1^+/CD49f^+$ mouse prostate cell subpopulation is enriched for cells capable of both colony and sphere formation *in vitro*. These cells can self-renew to form spheres for multiple generations and can differentiate to produce prostatic tubule structures containing both basal and luminal cells *in vivo*, similarly to the $\alpha_2\beta_1^{hi}/CD133^+$ subpopulation in humans (Richardson *et al.*, 2004). In mice, prominin (CD133) expressing cells from the basal layer within the proximal region of the dorsal prostate also enrich for prostate stem cells and can generate large branched structures in 3D culture, while prominin negative cells did not form these structures (Tsujimura *et al.*, 2007).

Notably, CD133 is also a stem cell marker of kidney, lung, brain, mammary gland and primitive haematopoietic stem cells (Singh *et al.*, 2003; Tsujimura *et al.*, 2007; Yin *et al.*, 1997). Furthermore, CD49f is a known marker of mammary gland, neural and haematopoietic stem cells (Lawson *et al.*, 2007; Stingl *et al.*, 2006). Together, these data suggest that common stem cell markers may exist in an array of different tissues and also in humans and mice.

Sca-1 enriches for murine prostate cells capable of regenerating tubular structures containing basal and luminal cell lineages, demonstrated by transplanting $Sca1^+$ cells under the kidney capsule of immunodeficient mice with UGS mesenchyme (Xin *et al.*, 2005). Androgen ablation studies have also shown enrichment of androgen-independent and $Sca\text{-}1^+$ cells, which can initiate tumourigenesis in conjunction with activated AKT *in vivo* (Xin *et*

*al.*, 2005). Consistent with this, mice harbouring a *Pten* deficiency in the prostate (*PBCre*$^{+}$ *Pten*$^{fl/fl}$) also enhances the proportion of pre-malignant cells expressing p63, Sca-1 and Bcl-2 *in vivo* (Wang *et al.*, 2006b). Furthermore, elevated Sca-1 expression has been associated with mammary tumour stem cell activity (Li *et al.*, 2003).

**Table 1.1: Prostate stem cell markers**

| Human | Description | Reference |
|---|---|---|
| CD44 | CD44+ basal cells purified and co-cultured with stromal cells and DHT, PSA secretions are elevated suggesting differentiation of CD44+ cells into luminal cells. | (Liu *et al.*, 1997) |
| $\alpha_2\beta_1$-integrin | $\alpha_2\beta_1$-integrin cells represent ~1% of the basal cell population | (Collins *et al.*, 2001) |
| CK6 | 4.9% of basal cells express CK6, which possess a high proliferative potential. | (Schmelz *et al.*, 2005) |
| $\alpha_2\beta_1^{hi}$ CD133, CD44$^{+}$ | CD133+/$\alpha_2\beta_1^{hi}$ cells represent 0.75% of basal cell population, possess a high proliferative index and can reconstitute prostate acini *in vivo*.<br>$\alpha_2\beta_1^{hi}$/CD133$^{+}$/CD44$^{+}$ cells isolated from human prostate tumours enrich for prostate cancer stem cells. | (Richardson *et al.*, 2004)<br>(Collins *et al.*, 2005) |
| CD44$^{+}$ CD24$^{-}$ | CD44+/CD24- LNCaP cells form tumours when injected into NOD/SCID mice. These cells express genes required for stem cell maintenance e.g. BMI-1, Oct3/4 and β-catenin. | (Hurt *et al.*, 2008) |
| **Mouse** | **Description** | **Reference** |
| p63 | p63$^{-/-}$ mice develop small prostatic buds demonstrating p63 is essential for basal cell differentiation and normal luminal cell differentiation. | (Signoretti *et al.*, 2000) |
| K5 and Bcl2 | K5+/BCL2+ mouse prostate epithelial cells demonstrated self-maintenance *in vitro*. | (Sawicki and Rothman, 2002) |
| Sca-1 | An *in vivo* prostate reconstitution assay determined that Sca-1+ cells isolated from the murine proximal region show high regenerative abilities. Sca1+ cells can also initiate tumourigenesis upon Akt activation. | (Burger *et al.*, 2005)<br>(Xin *et al.*, 2005) |
| Prominin (CD133) | Prominin positive cells from the mouse proximal region basal layer enriched for prostate stem cells that generate prostatic ducts in culture. | (Tsujimura *et al.*, 2007) |
| CD49f+ (integrin α6) | CD45-/CD31-/Ter119-/Sca-1+/CD49f+ proximal duct prostate cells self renew *in vitro* and *in vivo* and can differentiate into luminal and basal cells within prostate tubule structures. | (Lawson *et al.*, 2007) |

The expression status of androgen receptor (AR) in stem cells is also controversial. Although basal cells do not express detectable levels of AR, it is thought that stem cells may gain the ability to express AR in androgen deficient tissue (Lawson *et al.*, 2007). This has been observed *in vivo* where elevated AR expression correlates to the development of

hormone refractory tumours (Chen *et al.*, 2004; Maitland and Collins, 2005). Hormone ablation therapy essentially destroys all AR-expressing cells, while the prostate stem cells and cancer stem cells that do not express AR remain. It is speculated that the surviving cells may begin to over-express AR, allowing prostate growth to occur in response to low androgen levels (Chen *et al.*, 2004; Maitland and Collins, 2005).

### 1.1.4.3 The origin of prostate cancer

To account for prostate cancer heterogeneity, recent evidence suggests that prostate tumourigenesis may arise as a result of malignant transformation of normal prostatic epithelial stem cells or transit amplifying cells (Li *et al.*, 2007a). Consistent with this, cancer stem cells are thought to retain some phenotypic properties of the original normal stem cell. Prostate cancer stem cells have been isolated from primary and metastatic human prostate tumours, with a $\alpha_2\beta_1^{hi}/CD133^+/CD44^+$ phenotype (Collins *et al.*, 2005). In culture, these cells were capable of self-renewal and generated phenotypically mixed populations that expressed differentiated cell products, such as AR, suggesting that these cells are tumour initiating (Collins *et al.*, 2005). This is suggestive of a prostate cancer stem cell population that has the capacity to proliferate, self-renew, differentiate and invade. Furthermore, $CD133^+$ cells enrich for brain tumour stem cells and have been shown to differentiate into tumours that resemble the original human tumour, *in vitro* and *in vivo* (Singh *et al.*, 2003; Singh *et al.*, 2004). Singh *et al* (2004) demonstrated that $CD133^+$ cells can form tumours when grafted into NOD-SCID (non-obese diabetic, severe combined immunodeficient) mouse brains, while $CD133^-$ cells cannot, further implicating that $CD133^+$ cells are tumour initiating.

Currently, it remains unclear whether prostate cancer is derived from the normal prostate stem cell or the transit-amplifying population (Lam, 2006; Signoretti and Loda, 2006 ; Tang *et al.*, 2007). In the first scenario, a slight change in stem cell number leads to a dramatic expansion of the transit-amplifying population, which is considered to serve as a precursor for luminal epithelial cells. In this case, the tumour-initiating cells are the mutated stem cells (Wang *et al.*, 2006b). The second scenario suggests that oncogenic transformation of the stem cells does not occur and the transit-amplifying cells, with limited proliferative capacity, can be transformed by acquiring self-renewal potential (Wang *et al.*, 2006b).

Understanding normal stem cells and cancer stem cells is of paramount importance and could provide insights into the origin of prostate cancer and novel therapeutic strategies that specifically target the elimination of the cancer stem cells (Maitland and Collins, 2005).

Potential therapeutic targets include pathways implicated in the regulation of stem cell self-renewal. These include hedgehog, Notch, Wnt, PTEN/AKT, p53 and TGFβ cascades (Korkaya and Wicha, 2007; Tysnes and Bjerkvig, 2007). Telomerase is also emerging as a therapeutic drug target, given the synergistic relationship between telomerase, senescence and the cancer stem cell (Keith *et al.*, 2007). Telomerase activity is a hallmark of cancer and its inhibition in cancer has highlighted how important the induction of cellular senescence can be as a tumour suppressor mechanism (Keith *et al.*, 2007). To conclude, further characterisation of surface markers and signalling pathways specific to cancer stem cells remains crucial to targeting them for elimination.

### 1.1.5 Introduction to prostate cancer

Prostate cancer is a heterogeneous and multifocal disease arising from multiple genetic and epigenetic changes (Hill, 2005). It is currently the most common malignancy in men and accounts for 24% of the newly diagnosed male cancers (CRUK, 2004). The life-time risk of developing prostate cancer is 1 in 14 in the UK (CRUK, 2004). The most significant single risk factor for prostate cancer is age, yet ethnicity (particularly African Americans), family history and a high fat diet all increase the risk of prostate tumourigenesis. The majority of cases are diagnosed between 70 and 74 years of age (figure 1.4a), although these figures are expected to increase in concert with increasing life-time expectancy (CRUK, 2004).

Survival rates over the last 4 decades have improved drastically owing to early detection and novel treatment strategies (figure 1.4b), (CRUK, 2004). Interestingly, one study has shown that men taking Aspirin regularly have a 15-18% reduced risk of developing prostate cancer (CRUK, 2004; Jacobs *et al.*, 2005).

Prostate problems or symptoms tend to fall into three common categories; (a) non-life threatening prostatitis, or chronic inflammation of the gland, (b) benign prostatic hyperplasia (BPH), a non-neoplastic growth common to the transitional zone that constricts the urethra and (c) prostate cancer, often located in the peripheral zone (Bostwick *et al.*, 1996). Human prostate cancer that has breached the basement membrane commonly results in metastasis to the lymph nodes in the pelvis, bone and pancreas (Shappell *et al.*, 2004).

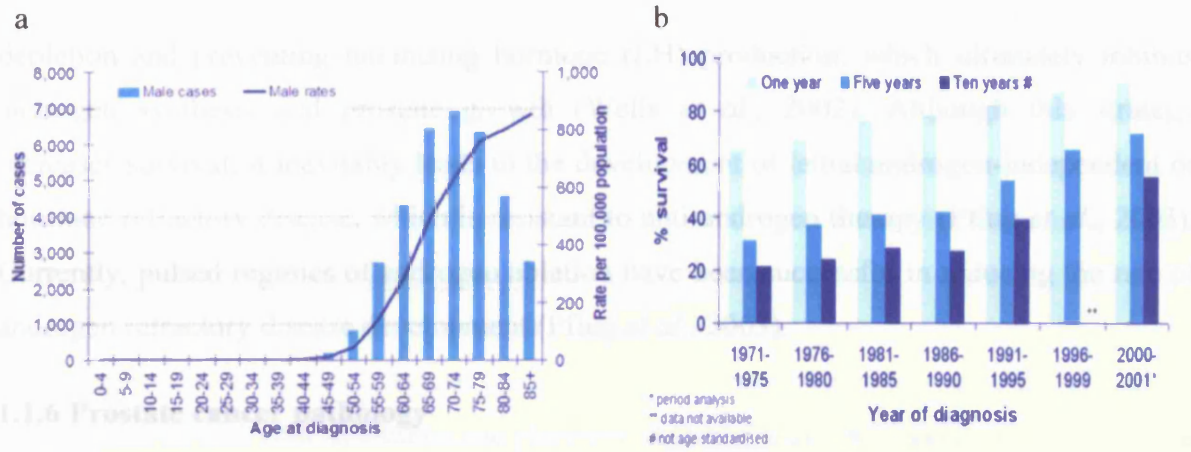


**Figure 1.4: Prostate cancer incidence and risk associated with age.** Statistical data indicates the average age at diagnosis of prostate cancer is 72 (a). The 5 year relative survival rate of prostate cancer patients was 70% during 2000-2001 in the UK (b). Figures are adapted from CRUK (2004).

There are three major treatment options currently available; surgical treatment, radiation therapy and androgen ablation (hormone therapy), (Duchesne, 2001; Quade, 2005). Benign prostatic hyperplasia (BPH) is commonly treated by a surgical procedure known as TURP (Transurethral resection of the prostate). This technique removes portions of the hyperplastic prostate to relieve pressure on the urethra (Quade, 2005). A radical prostectomy is common in patients under 70 years old who have been diagnosed with low-grade prostate cancer (grades I-II). Radiation treatment includes brachytherapy and external beam radiation, although these processes have a low success rate (Duchesne, 2001; Quade, 2005). Brachytherapy is also known as sealed source radiotherapy and is used to treat localised form of prostate cancer, where the radioactive source is placed inside or next to the area requiring treatment (Quade, 2005). More recent strategies include cryosurgery, where prostate cancer cells are destroyed by intermittent freezing of the prostate tissue with cryoprobes (Quade, 2005). In addition, a flavanoid anti-oxidant called Silibinin has also been shown to prevent hormone refractory prostate cancer by inhibiting AR-mediated proliferation and inducing $G_1$ arrest (Amanatullah *et al.*, 2000).

Following surgical failure, the first line of effective treatment for malignant prostate cancer is androgen ablation, which has been shown to dramatically increase survival. Anti-androgens administered include steroidal anti-androgens (e.g. Cyproterone) that inhibit AR and testosterone production and non-steroidal anti-androgens (e.g. Flutamide and Casodex) that are competitive inhibitors of AR (Amanatullah *et al.*, 2000). Zoladex, a synthetic analogue of luteinising hormone releasing hormone (LHRH) is also commonly used to treat prostate cancer. Zoladex antagonises LHRH receptors on pituitary cells, causing their

depletion and preventing luteinising hormone (LH) production, which ultimately inhibits androgen synthesis and prostate growth (Wells *et al.*, 2002). Although this strategy increases survival, it inevitably leads to the development of lethal androgen-independent or hormone refractory disease, which is resistant to anti-androgen therapy (Pflug *et al.*, 2003). Currently, pulsed regimes of androgen ablation have been successful in reducing the rate of androgen refractory disease development (Pflug *et al.*, 2003).

### 1.1.6 Prostate cancer pathology

Prostate cancer is a linear multi-step process whereby normal prostatic epithelium progresses to invasive prostate cancer via several intermediate steps (Mitsumori and Elwell, 1994; Shappell *et al.*, 2004; Trotman *et al.*, 2003); atypical hyperplasia (AH) → dysplasia/low grade prostate intra-epithelial neoplasia (LG-PIN) → high grade intra-epithelial neoplasia (HG-PIN) → locally invasive prostate cancer (adenocarcinoma) → diffuse prostate cancer (invasive carcinoma) and metastasis (figure 1.5). This process is considered to require the acquisition of multiple genetic mutations and the later stages of progression frequently develop hormone refractory disease.

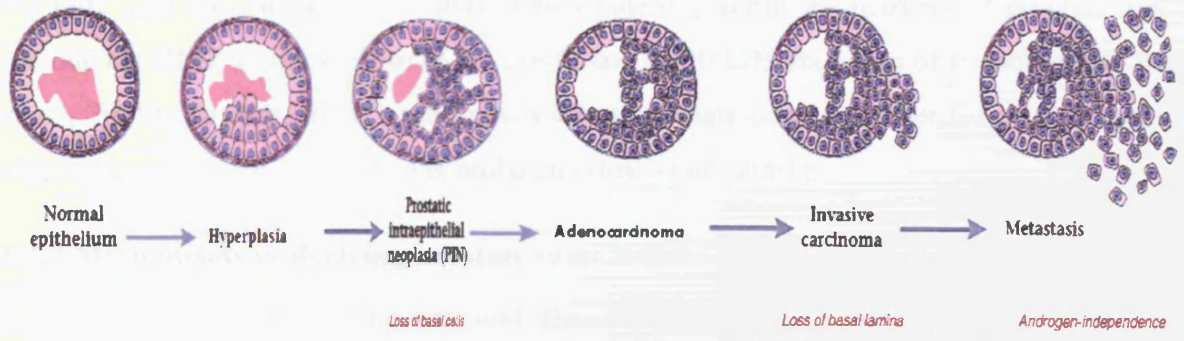


**Figure 1.5: Linear pathway of human prostate cancer progression.** Stages of progression reveal hyperplasia as a precursor to PIN, which progresses to adenocarcinoma and invasive carcinoma that may become androgen-independent. This process is thought to require the acquisition of multiple genetic mutations. Ultimately invasive lesions result in incurable metastatic disease where secondary tumour formation occurs at distant locations. This figure is adapted from Shappell *et al* (2004).

Human prostate biopsies are scored using the Gleason grading system, where a high score correlates with increasing severity (DeMarzo *et al.*, 2003). The proliferation of non-neoplastic cells, termed hyperplasia, is the least severe phenotype and is considered to be a precursor to PIN (Shappell *et al.*, 2004). PIN is classified as the neoplastic proliferation of atypical epithelial cells which may predispose to invasive carcinoma. PIN is characterised

by four architectural patterns; tufting, micropapillary, cribriform and flat (Bostwick *et al.*, 1996). Invasive carcinoma consists of malignant cells penetrating the basement membrane into the stroma, resulting in invasive carcinoma, a malignant epithelial neoplasm (Shappell *et al.*, 2004). If glandular differentiation is maintained, the invasive carcinoma is classified as an adenocarcinoma (Shappell *et al.*, 2004). Squamous cell carcinoma is an invasive malignant epithelial neoplasm that exhibits squamous differentiation, such as keratinisation and/or intercellular bridges (Shappell *et al.*, 2004). An adenosquamous carcinoma consists of a mixture of foci with squamous and glandular differentiation. Mucinous adenocarcinoma is a variant of the classic acinotubular adenocarcinoma of the prostate that displays differentiated cells that secrete mucin (Curtis *et al.*, 2005; Odom *et al.*, 1986).

Specific biomarkers of epithelial-mesenchymal interactions, deemed necessary for prostate differentiation and stromal responses to tumourigenesis, have provided a valuable resource for the detection and diagnosis of prostate cancer (Cunha *et al.*, 1987). In humans, elevated PSA (prostate specific antigen) levels in serum and high tissue expression of AMACR (α-methylacyl-CoA racemase) label HG-PIN and in some cases, BPH (DeMarzo *et al.*, 2003). PSA is a serine protease and AMACR is responsible for converting the 2R-isomer of pristanic acid (as the coenzyme A ester) to its 2S form, facilitating β-oxidation of the fatty acid (Bostwick *et al.*, 1996). Other potential serum biomarkers of prostate cancer include the RM2 antigen (Saito *et al.*, 2005) and an 80 kDa fragment of E-cadherin (Kuefer *et al.*, 2005). To date, there is no known serum prostate cancer marker for murine models, although one possible candidate is probasin (Huss *et al.*, 2001).

### 1.1.7 Mechanisms underlying prostate tumourigenesis

Several genetic mutations and the deregulation of endogenous hormones and environmental influences that induce differentiation and proliferation of the prostate epithelium have been shown to play a role in prostate tumourigenesis (Cunha *et al.*, 2004). These processes shall be discussed in this section.

Familial/hereditary prostate cancer (HPC) has been shown to be associated with germline mutations in a number of genes, particularly *HPC1* that encodes the tumour suppressor ribonuclease L (RNASEL) and *PCAP (HPC2)* that map to the 1q24-25 locus, where many mutations linked to prostate cancer have been found (DeMarzo *et al.*, 2003; Xu *et al.*, 1998). The X-linked *HPCX* gene is also highly mutated in hereditary prostate cancers (16%) (Xu *et al.*, 1998). Additional modes of genomic instability in prostate cancer include microsatellite instability (defective DNA mismatch repair) and structural changes to

chromosomes (DeMarzo *et al.*, 2003). For instance, the length of the polymorphic CAG repeat in exon 1 of the *AR* gene correlates inversely with *AR* transcriptional activity (Zitzmann *et al.*, 2003). Mutations in the *AR* gene may also alter ligand specificity to non-androgens or anti-androgens (Zitzmann *et al.*, 2003). Functional mutations in AR co-activators or co-repressors that regulate AR activity can also facilitate tumour progression and provide rationale for androgen-independent prostate cancer (DeMarzo *et al.*, 2003).

Common signalling cascades that are deregulated in prostate cancer include the PI3K/AKT, Wnt, Ras, Hedgehog (Hh) and the Notch signal transduction pathways (Belandia *et al.*, 2005; Le-Page *et al.*, 2006; Sheng *et al.*, 2004; Weber and Gioeli, 2004; Yardy and Brewster, 2005). Notably, all of these pathways can regulate AR signalling and play vital roles within the cell, including cell proliferation, polarity and differentiation (Belandia *et al.*, 2005; Le-Page *et al.*, 2006; Sheng *et al.*, 2004; Weber and Gioeli, 2004; Yardy and Brewster, 2005). As such, deregulation of these pathways can further promote prostate tumourigenesis and progression.

PTEN (MMAC1) is a tyrosine phosphatase homologous to tensin that acts as a tumour suppressor by antagonising PI3K and inhibiting AKT activation (Di Cristofano *et al.*, 2001; Di Cristofano *et al.*, 1998). PTEN interactions with AR inhibit AR nuclear translocation (Lin *et al.*, 2004a). This evidence suggests that PTEN loss of function in prostate cancer may activate the PI3K/AKT pathway to drive proliferation and survival, as well as permitting androgen signalling (Lin *et al.*, 2004a). Consistent with this, inactivating mutations in PTEN are a common event in human prostate cancer (Yoshimoto *et al.*, 2007) and elevated expression levels of AKT are associated with a poor prognosis (Le-Page *et al.*, 2006; Malik *et al.*, 2002). In mice, *Pten* loss predisposes to invasive carcinoma and metastasis, concomitant with elevated Akt expression, resembling the kinetics of human disease progression (Wang *et al.*, 2003).

PTEN contains multiple phosphorylation sites that play a crucial role in regulating its stability and activity (Okahara *et al.*, 2004). Post-translational regulation of PTEN by phosphorylation of a cluster of serine and threonine residues in its C-terminus has been shown to regulate the stability and half-life of PTEN (Al-Khouri *et al.*, 2005) however, this process is not fully understood. In general, unphosphorylated PTEN is considered more active than the phosphorylated form, however its conformation is more open to allow substrate interactions and is thought to reduce PTEN stability (Shukla *et al.*, 2005). Casein kinase II (CK2) has been shown to phosphorylate PTEN, reducing its biological activity *in vitro* (Al-Khouri *et al.*, 2005). Given the fact that PTEN loss is associated with prostate

tumourigenesis and that CK2 is over-expressed in human prostate cancer, it is speculated that PTEN post-translational regulation by CK2 plays a fundamental role in promoting prostate cancer formation by decreasing PTEN activity (Wang *et al.*, 2006a).

Wnt signalling plays a crucial role in prostate epithelium proliferation, survival, androgen signalling and differentiation (discussed in section 1.4). Activation of the Wnt pathway results in β-catenin nuclear translocation where it binds additional transcription factors to mediate transcription of Wnt target genes (Yardy and Brewster, 2005). β-catenin has also been shown to act as an AR co-activator (Yardy and Brewster, 2005). Aberrant Wnt signalling is a common occurrence in human prostate cancer and can occur following mutations in the oncogenes *β-catenin* and *APC* (Voeller *et al.*, 1998; Yardy and Brewster, 2005). In mice, *Apc* loss and *β-catenin* hyperactivation predispose to keratinised squamous metaplasia of the prostate and adenocarcinoma (Bierie *et al.*, 2003; Bruxvoort *et al.*, 2007; Gounari *et al.*, 2002). Targets of the Wnt pathway are also upregulated in prostate cancer, driving disease progression. For example, c-Myc expression has been shown to correlate to tumour progression in humans and mice (Thompson *et al.*, 1989; Yang *et al.*, 2005).

Ras signalling results in the activation of numerous Ras effector signalling pathways, such as the mitogen-activated protein kinase (MAPK) cascade, to coordinate essential cellular events that include proliferation, differentiation and cell polarity (Schubbert *et al.*, 2007), (detailed in section 1.5). The MAPK pathway has also been shown to activate AR-mediated transcription via Src, indicating that Ras signalling can regulate prostate growth (Weber and Gioeli, 2004). Hyperactivating mutations of the proto-oncogene Ras are uncommon in human prostate cancer, yet enhanced Ras signalling during human prostate tumourigenesis is a frequent event (Papatsoris *et al.*, 2007; Weber and Gioeli, 2004). Elevated Ras signalling in prostate tumours is postulated to equate to increased levels of growth factors that can stimulate Ras activation by binding to tyrosine kinase receptors (RTKs) (Weber and Gioeli, 2004). Consistent with this, oncogenic Ras transformations in transgenic mice have shown that elevated Ras signalling causes hyperplasia and LG-PIN (Barrios *et al.*, 1996; Scherl *et al.*, 2004).

Hedgehog (Hh) signalling pathways are required for prostate development and have been shown to play a role in stem/progenitor cell proliferation (Shaw and Bushman, 2007). There are three mammalian Hh genes; Sonic, Desert and Indian. The Hh genes are ligands for the trans-membrane receptor Patched (PTCH), which upon activation alleviates suppression of smoothened (SMO) and leads to the stimulation of Gli transcription factors

that in turn initiate transcription of Hh target genes (Shaw and Bushman, 2007). Transgenic loss of Gli2 function demonstrated a developmental role for the Hh pathway in the mouse prostate. Ductal budding abnormalities were associated with decreased Hh target gene expression, decreased expression of the stem cell marker Nestin and hyperplasia of $p63^+$ basal cells (Shaw and Bushman, 2007). Interestingly, Hh signalling components have been observed to co-localise to the $p63^+$ basal cells in hyperplastic foci, speculated to reflect transformation of prostate stem cells into cancer stem cells (Chen *et al.*, 2007).

Several recent reports have highlighted a role for the Hh pathway in prostate cancer (Karhadkar *et al.*, 2004; Shaw and Bushman, 2007; Sheng *et al.*, 2004). Advanced tumours have demonstrated high levels of Hh target genes, namely PTCH1 and hedgehog-interacting protein (HIP), consistent with a low expression of Su(Fu) (Sheng *et al.*, 2004). Su(Fu) is a negative regulator of the Hh pathway and Su(Fu) mutations have been reported in human prostate cancer (Sheng *et al.*, 2004). Whether this data represents mutational activation or an increased responsiveness of the tumour cell or ectopic stroma to Hh ligand is not known (Shaw and Bushman, 2007). Molecular analysis of the LADY transgenic mouse model (see section 1.2.3) did not report any generalised increase in Hh signalling during tumour development, although elevated Indian Hh expression correlated to decreased expression of terminal differentiation markers and increased progenitor cell markers (Gipp *et al.*, 2007). Furthermore, *in vitro* studies have shown conflicting reports as to whether inhibition of Hh signalling in human prostate cancer cell lines prevents cell growth (Sanchez *et al.*, 2004; Zhang *et al.*, 2007). Zhang *et al* (2007) recently reported that three different human prostate cancer cell lines does not respond to the Hh signalling pathway inhibitor Cyclopamine and that expression of Ptch and Gli1 is lower than normal human prostate tissue. Meanwhile, Sanchez *et al* (2004) previously reported that Cyclopamine can inhibit cell proliferation of PC3 and LNCaP cell lines in culture. In support, human prostate cancer xenografts showed tumour regression following Cyclopamine treatment (Karhadkar *et al.*, 2004). To conclude, further investigation is necessary to fully comprehend the role Hh signalling in prostate cancer, together with the generation of models that accurately represent the disease.

Notch signalling also plays a vital role in the prostate, particularly during development and growth, as well as coordinating stem/progenitor cell maintenance (Wang *et al.*, 2006c; Wang *et al.*, 2004b). This suggests that deregulation of the Notch pathway in prostate epithelium may play a role in tumourigenesis. Consistent with this notion, an *ex vivo* organ culture system revealed that treating rat ventral prostate lobes with a γ-secretase inhibitor (that prevents Notch protein maturation), results in reduced branching of the

prostate ducts, elevated proliferation and increased numbers of cells co-expressing basal (K14) and luminal (K8) cell markers (Wang *et al.*, 2006c). This data suggests that Notch signalling plays a role in prostate development and differentiation. A Notch1 conditional transgenic mouse model also revealed that loss of Notch signalling results in hyperplastic foci (Wang *et al.*, 2006c). This evidence correlates to human studies that have reported Notch signalling is elevated in human prostate cancer and Hey1, a mediator of notch signalling and an AR co-repressor, is frequently mislocalised in prostate tumours (Belandia *et al.*, 2005). Jagged1 (a notch receptor ligand) is also found to be elevated in a large number of human prostate patients and Notch signalling is thought to augment AKT signalling, further promoting growth and survival of prostate epithelial cells (Santagata *et al.*, 2004).

Interestingly, Nguyen *et al* (2006) showed that p63 expression is suppressed by Notch1 activation in human and mouse keratinocytes. In turn, elevated p63 expression was shown to prevent Notch signalling from restricting cell growth and inducing differentiation (Nguyen *et al.*, 2006). Together, this evidence suggests that p63 regulation of Notch signalling could in fact play a role in basal cell differentiation and self-renewal within prostate epithelium.

### 1.1.8 Male hormone regulation and AR signalling

The steroidal androgens, principally testosterone (T) and its metabolite 5-Alpha-Dihydrotestosterone (DHT), mediate a wide range of physiological processes. Androgens play a key role in the development and maintenance of the male GU tract, sexual maturation, spermatogenesis and regulation of male gonadotrophin (Heinlein and Chang, 2002). Gonadotrophin-releasing hormone (GnRH) is secreted by neurons in the hypothalamus to stimulate androgen production (Chang and Heinlein, 2004). GnRH is transported by capillaries to the anterior pituitary gland where it triggers the production of pituitary gonadotrophins termed luteinising hormone (LH) and follicle stimulating hormone (FSH) (Scher *et al.*, 2004). LH and FSH are transported through the blood to the testes or ovaries where they stimulate the production of steroid hormones from cholesterol. Female (oestrogen and progesterone) or male (testosterone) steroid hormones to maintain ova or sperm production respectively, as well as maintaining the sex organs (Lattouf *et al.*, 2006). In response to LH, Leydig (or interstitial) cells in the testis synthesise testosterone which diffuses into the seminiferous tubules to maintain spermatogenesis (together with FSH) and into the blood to maintain hormone homeostasis. This hormone cascade is controlled by a

series of feedback mechanisms (figure 1.6a). For example, elevated levels of testosterone in the blood results in decreased GnRH, which in turn reduces LH secretion (Scher *et al.*, 2004). The adrenal glands that are positioned above the kidneys also produce androgens, in a process regulated by ACTH (adrenocorticotrophic hormone) produced in the anterior pituitary (Lattouf *et al.*, 2006).

Androgen receptor (AR) is a member of the nuclear receptor family that functions as a ligand-inducible transcription factor (Chang and Heinlein, 2004). Androgens predominantly bind to AR in the cytoplasm, which upon activation dimerize and translocate to the nucleus (figure 1.6b). In the nucleus, the AR homodimer binds to the ARE (Androgen Response Element) and recruits co-regulators, such as steroid coactivator-1 (SRC-1) and Creb-binding protein (CBP) to trigger transcription of target genes (Lee and Chang, 2003). In its unbound ligand conformation, AR is bound to heat-shock proteins and co-repressors, such as prohibitin and Hey1 to repress transcription (Belandia *et al.*, 2005).

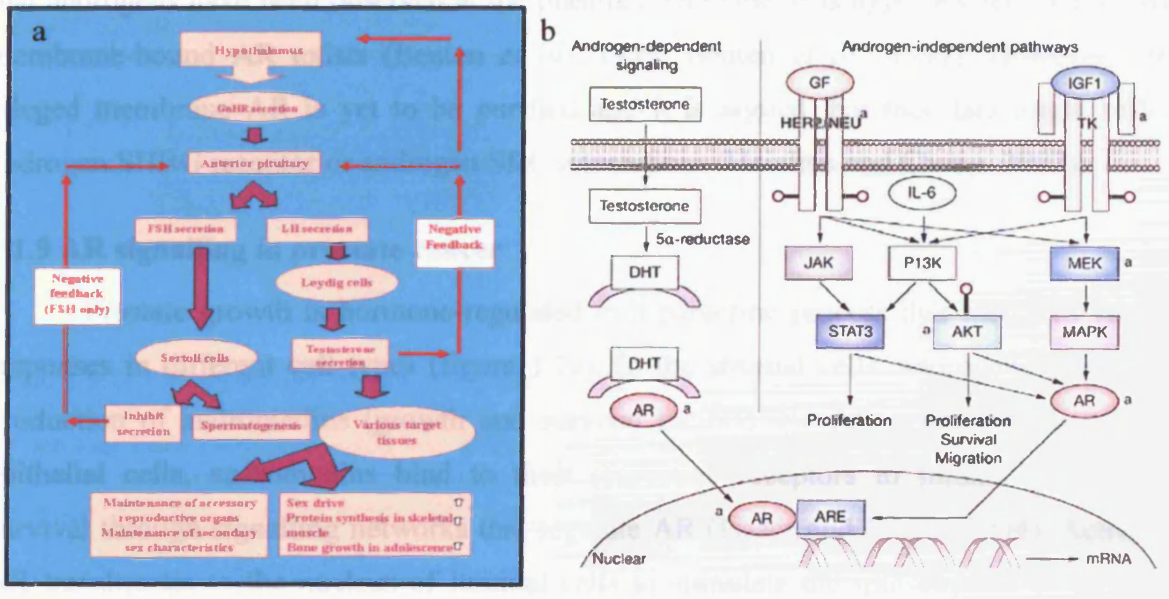


**Figure 1.6: Male hormone regulation and AR signalling.** (a) Hormone regulation in males is controlled by gonadotrophin-releasing hormone (GnRH) from the hypothalamus, which stimulates the production of both follicle stimulating hormone (FSH) and luteinising hormone (LH) in the anterior pituitary. LH stimulates testosterone production in the Leydig cells to maintain the Sertoli cells and spermatogenesis, together with FSH. FSH and LH also act to maintain the male accessory organs. (b) AR is stimulated by its ligand 5α-dihydrotestosterone (DHT), metabolised from testosterone by 5α-reducatse in the cytoplasm. Here, DHT binds to the AR and causes its dimerisation and nuclear translocalisation. In the nucleus, AR binds to the Androgen Response Element (ARE) and initiates transcription of target genes. Alternatively, androgen-independent pathways exist, including the JAK/STAT3 pathway, the PI3K/AKT pathway and the MAPK cascade. Figure (a) is adapted from http://en.wikibooks.org/wiki/Human _Physiology/Print_Version and (b) is adapted from Lattouf *et al* (2006).

AR is also reported to form heterodimers with other nuclear receptors, including the estrogen receptor (ER), glucocorticoid receptor (GR) and testicular orphan receptor-4 (TR4), reducing AR transcriptional activity (Isaacs and Isaacs, 2004). Androgen-independent AR activation can also occur in response to growth factors (figure 1.6b). For example, hormone-refractory prostate cancer cells have been shown to mediate AR signalling by alternative mechanisms, such as the MAPK, AKT and Jak/Stat3 pathways and more recently, through Wnt signaling (Lattouf *et al.*, 2006; Terry *et al.*, 2006; Yardy and Brewster, 2005).

Androgens are also thought to modulate intracellular events independently of AR by interacting with the SHBG (sex hormone binding globulin) receptor to regulate intracellular calcium levels. In addition, AR interactions with the SH3 domain of SRC stimulates kinase signalling pathways, including the MAPK cascade, which induces transcription of AR (Heinlein and Chang, 2002). Given that androgens can regulate ion channel activation and that androgens have been observed at the plasma membrane, it is hypothesized that a novel membrane-bound AR exists (Benten *et al.*, 1999; Benten *et al.*, 1997). However, the alleged membrane AR is yet to be purified and it is argued that this data might reflect androgen:SHBG receptor or androgen:SRC interactions (Heinlein and Chang, 2002).

### 1.1.9 AR signalling in prostate cancer

Prostate growth is hormone-regulated in a paracrine process that mediates various responses in different cell types (figure 1.7a). In the stromal cells, androgens induce the production of andromedins (growth and survival factors) and AR activation. In prostate epithelial cells, andromedins bind to their respective receptors to initiate growth and survival through signalling networks that regulate AR (Isaacs and Isaacs, 2004). Activated AR translocates to the nucleus of luminal cells to stimulate the transcription of prostate-specific differentiation markers, such as PSA, NKX3.1 and human kallikrein-2, HK2 (Isaacs and Isaacs, 2004). Although AR stimulates transcription of these markers, it does not stimulate growth and survival, instead, it is considered to prevent andromedin-induced proliferation of the luminal cells (Isaacs and Isaacs, 2004).

Anti-androgen therapy inevitably results in hormone refractory disease where AR is over-expressed in prostate epithelial cells, resulting in them becoming supersensitive to androgens, rather than being independent of them (Litvinov *et al.*, 2003). It has been speculated that supersensitivity is a consequence of accumulating molecular changes that trigger a gain of function in the AR signalling pathways (Litvinov *et al.*, 2003). During this

process, the paracrine mechanism of AR action is thought to be replaced by an autocrine mechanism, whereby cancer cells are less dependent on stromal cell factors and have gained the ability to activate novel AR signalling pathways for their proliferation and survival, without requiring the physiological androgen ligand binding (Isaacs and Isaacs, 2004; Litvinov *et al.*, 2003), (figure 1.7b). Paradoxically, prostate epithelial cells may also become sensitive to anti-androgens, rather than becoming androgen-independent (Isaacs and Isaacs, 2004).

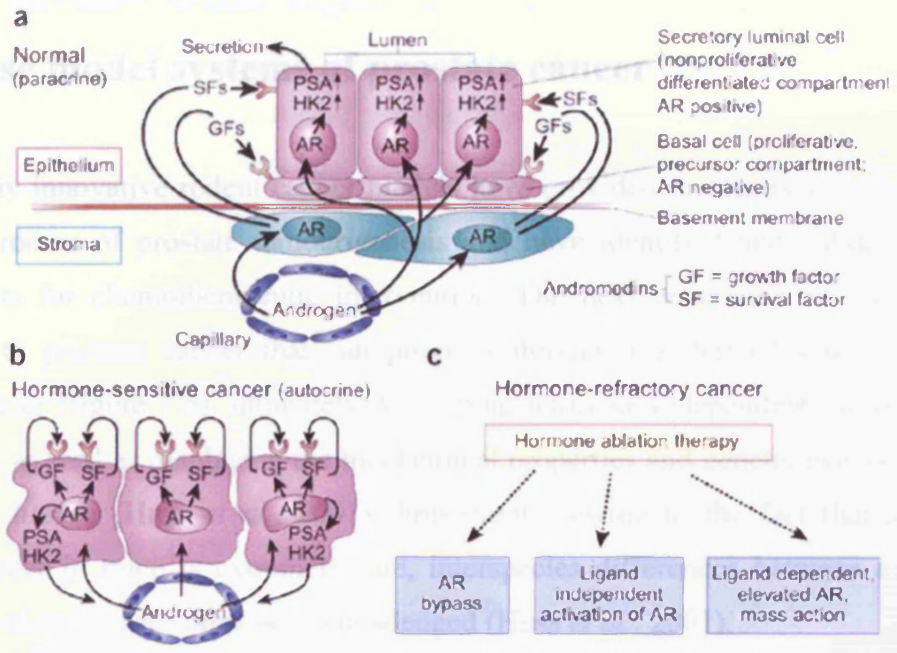


**Figure 1.7: AR signalling in the normal and malignant prostate epithelium.** (a) Growth and maintenance of normal prostate epithelium depends on growth factors and survival factors produced by stromal cells (smooth muscle and fibroblasts) in response to androgens. (b) Model depicting hormones sensitive prostate cancer as an autocrine process. (c) Mechanisms for AR deregulation in hormone-refractory prostate cancer. This figure is adapted from Isaacs and Isaacs (2004).

Currently, there are three mechanisms believed to explain the development of hormone refractory disease (Isaacs and Isaacs, 2004), (figure 1.7c). First, AR signalling may be bypassed by alternative signalling pathways that drive proliferation and growth. Second, ligand-independent activation of the AR could be a direct consequence of deregulated signalling cascades (such as activated MAPK or Wnt pathways) or indeed indirect activation owing to altered AR co-activator and co-repressor ratios. Third, AR mutations might allow AR activation in response to alternative ligands, such as estrogen or AR antagonists (Isaacs and Isaacs, 2004). About 30% of human prostate cancer patients harbour an AR mutation, suggesting that the majority of hormone refractory prostate cancers are likely to be caused by AR independent mechanisms or through aberrant AR signalling

(Isaacs and Isaacs, 2004). Evidence for deregulated AR signalling stems from the fact that microarray-based profiling of isogenic prostate cancer xenograft models showed hormone refractory prostate cancer correlates with increased AR mRNA expression 2-5 fold, (Chen *et al.*, 2004). This data suggests that AR upregulation is both necessary and sufficient for hormone-refractory progression (Chen *et al.*, 2004). Current studies are now focusing on the generation of therapies that inhibit AR function or expression using heat-shock protein inhibitors and RNA interference mechanisms respectively (Chen *et al.*, 2004).

## 1.2 Mouse model systems of prostate cancer

Many innovative rodent cancer models have provided mechanistic insights into the multistep process of prostate tumourigenesis and have identified and validated potential novel targets for chemotherapeutic intervention. The next generation of models aim to predispose to prostate cancer that can progress through the defined kinetics of human prostate cancer (figure 1.5), ultimately developing hormone-independent tumours that can metastasise, as well as displaying the biochemical properties and genetic events common to the human disease (Huss *et al.*, 2001). Importantly, owing to the fact that spontaneous prostate cancer in mice is extremely rare, interspecies differences between experimental models and clinical cases must be acknowledged (Huss *et al.*, 2001).

### 1.2.1 Xenograft prostate cancer models

Human prostate cancer cell lines have played a fundamental role in studying prostate cancer. Some common lines include LNCaP hormone sensitive cells that were derived from a lymph node metastasis and harbour an AR mutation in the steroid binding domain, T877A (Veldscholte *et al.*, 1992). Androgen-independent cell lines include PC-3 and DU145 that originated from the bone and brain metastases respectively. Although these *in vitro* cell lines have identified key genetic events and validated the use of novel therapeutics in treating prostate cancer, they are difficult to establish, lack certain features of the disease, including PSA, and are frequently derived from rare sites of metastases from patients who have received hormone ablation therapy. *In vivo* xenograft studies have proved beneficial in resolving the latter problem, allowing the onset and progression of prostate cancer to be investigated as a 3-dimensional structure, complete with angiogenesis, stromal interactions, metastasis and paracrine and hormonal factors (Lamb and Zhang, 2005). Xenografts involve

cell lines being transplanted into immunodeficient mice, typically male SCID mice in prostate studies. The host is compromised immunologically to prevent rejection of the transfected tissue at the cost of increasing the risk of opportunistic infections.

Recent advances have investigated the role of interleukin-6 (IL-6), an important growth regulator in prostate cancer (Steiner *et al.*, 2003). Male nude mice inoculated with either LNCaP cells or LNCaP-IL6$^{+}$ transfected cells have shown that IL-6 expression reduces Rb expression and elevates the MAPK pathway to accelerate tumour growth (Steiner *et al.*, 2003). Rodent prostate cancer cell lines have also been utilised and genetically manipulated to examine the role of tumour suppressors and oncogenes in the prostate. For example, the dunning rat prostate adenocarcinoma cell line AT2.1 transfected with *v-H-ras* showed increased metastatic frequency, suggesting that aberrant Ras signalling may play a role in prostate cancer progression (Treiger and Isaacs, 1988). Furthermore, xenografts have been employed to demonstrate subpopulations of cells enrich for prostate stem cells. Lawson *et al* (2007) have shown that a subpopulation of cells expressing CD45$^{-}$ /CD31$^{-}$/Ter119$^{-}$/Sca-1$^{+}$/CD49f$^{+}$ enriches for prostate stem cells that can self renew *in vivo* when injected subcutaneously into SCID mice.

Xenograft models have also proved beneficial in validating potential chemotherapeutic targets. For example, Ke *et al* (2006) employed an inducible lentiviral RNAi vector to silence the known cancer therapeutic target mTOR in PC3 cells. Once transplanted into male hosts, induction with Doxycycline resulted in tumour regression *in vivo* (Ke *et al.*, 2006). This novel approach permits staged tumour progression and target validation without the limitations associated with conventional siRNA techniques, which often fail to establish tumours in hosts (Ke *et al.*, 2006). To conclude, xenograft models stimulate genetic and clinical manifestations of the human disease *in vivo*, facilitating research into the physiological mechanisms involved.

### 1.2.2 Mouse prostate reconstitution (MPR) models

MPR models involve grafting the murine foetal urogenital sinus (UGS) under the renal capsule of adult isogenic male hosts, resulting in differentiation into a mature prostate. Genetic manipulation is achievable in the UGS using the retroviral transduction method (Navone *et al.*, 1998). For example, MPR models have successfully manifested dysplasia and hyperplasia when the UGS is transfected with activated *vHa-Ras* or *Myc* oncogenes respectively prior to transplantation into the renal capsule of a male host (Thompson *et al.*, 1989). Experiments analysing the synergy between *vHa-Ras* and *c-Myc* mutation in the

MPR model revealed accelerated progression to a more advanced phenotype, highlighting the multi-step nature of prostate cancer (Thompson *et al.*, 1989).

### 1.2.3 Transgenic mouse prostate cancer models

Knockout and knockin transgenic mice have provided powerful insights into the molecular mechanisms of prostate carcinogenesis. Two genes in particular, *Nkx3.1* and *Pten* have been well characterised using knockout mouse models, revealing their importance in suppressing prostate tumourigenesis.

The *Nkx3.1* homeobox gene is a prostate cancer tumour suppressor that undergoes epigenetic inactivation, which is essential for prostate function (Kim *et al.*, 2002a). *Nkx3.1* undergoes allelic deletion in about 80% of human prostate cancers and has been implicated at the onset and during progression of the disease (Abate-Shen *et al.*, 2003). *Nkx3.1* null mice exhibit hyperplasia and dysplasia (within 2 months), mimicking early stages of human prostate cancer (Kim *et al.*, 2002a). PIN-like lesions from *Nkx3.1* mutants have also been shown to undergo progressively severe histopathological alterations after serial transplantation in nude mice, suggesting that loss of *Nkx3.1* plays a role in prostate cancer progression (Kim *et al.*, 2002a).

In humans, the tumour suppressor PTEN has been reported to be frequently deleted in prostate adenocarcinomas (Schmitz *et al.*, 2007; Trotman *et al.*, 2003; Wang *et al.*, 2003). PTEN is required to regulate the normal proliferation and differentiation of the intestinal mucosa, prostate and skin (Wang *et al.*, 2003). *Pten* null mice are embryonic lethal and $Pten^{+/-}$ mice are viable (Podsypanina *et al.*, 1999). *Pten* haploinsufficiency results in pathologies with features similar to those of Cowden's disease (CD), such as intestinal hamartomas, thyroid and breast tumours, and Bannayan-Zonana Syndrome (BZS), which predisposes to intestinal polyps, enlarged heads and a developmental delay (Di Cristofano *et al.*, 1998). $Pten^{+/-}$ mice develop PIN and neoplasms of the endometrium, liver, thyroid, thymus and the gastrointestinal tract (Di Cristofano *et al.*, 1998; Podsypanina *et al.*, 1999). This phenotype can be accelerated by additional homozygous deletion of *Cdkn1b* or *Nkx3.1*, with carcinomas occurring within 3 months on this background, thus highlighting the multi-step nature of tumourigenesis (Di Cristofano *et al.*, 2001; Kim *et al.*, 2002b). For example, $Nkx3.1^{+/-}$:$Pten^{+/-}$ compound mutant transgenic mice have demonstrated that loss of function of *Nkx3.1* cooperates with loss of function of the *Pten* tumour suppressor gene in cancer progression *in vivo* (Kim et al., 2002b). This cooperativity results in increased HG-PIN/early carcinoma incidence within 3 months and the synergistic activation of Akt, a key

modulator of cell growth and survival (Kim *et al.*, 2002b). This compound transgenic model has also proved beneficial in the validation of novel chemotherapeutic agents. Interestingly, vitamin D treatment reduced PIN incidence and severity in the *Nkx3.1:Pten* mutants (Banach-Petrosky *et al.*, 2006). This suggests that the chemopreventative actions of vitamin D (1,25 $D_3$), presumed to be mediated by its interaction with vitamin D receptor, are likely be useful in the treatment of human prostate cancer (Banach-Petrosky *et al.*, 2006).

Although knock-out/in models have been extremely beneficial in recapitulating disease progression and validating chemotherapeutic strategies, these models have two major limitations; (a) development of multiple phenotypes in non-prostate tissues and (b) disease progression can be limited by embryonic lethality in knock-out/in studies of essential genes, such as *Pten*. To address this, the next generation of transgenic mouse models aim to specifically target transgenes to prostate epithelium.

To elicit a phenotype in the prostate, a strong, prostate-specific promoter is necessary, such as the rat *probasin* (Prostatic basic protein, *PB*), *prostate specific antigen* (*PSA*), prostate steroid binding protein *C3(1)* and *Keratin-5* (*K5*) promoters and the mouse *Cryptdin-2* (*CR2*) promoter (Kasper, 2005). Many target genes have been investigated using this approach, including growth factors, cell cycle regulators, pro- and anti-apoptotic proteins, steroid hormone and growth factor receptors, oncogenes, tumour suppressors, and homeobox genes (Kasper, 2005). To this end, many experimental approaches have been utilised to derive genetically modified mice that permit up/down-regulated, knock-out/in and conditional (Cre-LoxP technology) expression of the transgene in prostate epithelium.

The most widely exploited prostate-specific promoter to generate transgenic prostate cancer models is the rat probasin (PB) promoter. PB is a member of the lipocalcin superfamily and is found in the secretions and nuclei of prostate epithelial cells. PB expression is regulated by hormones (e.g. androgens) and zinc (Johnson *et al.*, 2000; Kasper and Matusik, 2000). The function of PB is unknown, although it is speculated to play a role in shuttling an unidentified hydrophobic ligand in seminal fluid (Johnson *et al.*, 2000).

The PB promoter contains two androgen receptor binding sites (*ARBS-1/2*) within the *PB* promoter's androgen responsive region (*ARR*, +244/-96 bp). The presence of the *ARR* in the PB promoter is required for elevated expression of transgene reporter constructs (Kasper, 2005). Novel PB promoters were generated bearing the *ARR*, including the minimal *PB* promoter (-426/+28 bp), the long *PB* promoter (*LPB*) (12 kb of the *PB* promoter region) and the composite *PB* promoter ($ARR_2PB$), where two *ARR*s are linked to the endogenous *PB* promoter (Kasper, 2005).

The first *PB* promoter prostate cancer models were the TRAMP (Transgenic Adenocarcinoma of Mouse Prostate) and LADY (*LPB-Tag*) transgenic mice. In TRAMP mice, the minimal *PB* promoter is used to drive the expression of the SV40 viral large T antigen within prostate epithelium, while the *LPB* promoter drives the expression of both the large T and small t tumour antigens in the LADY prostate (Abate-Shen and Shen, 2002). The SV40 viral large T antigens act as oncogenes through interactions with Rb and p53 tumour suppressors and the small t antigen interacts with protein phosphatase 2A to facilitate tumourigenesis (Greenberg *et al.*, 1995). The TRAMP model develops androgen-dependent PIN by 12 weeks and metastasis by 30 weeks, primarily to the lung, lymph nodes, bone, kidneys and adrenal gland (Greenberg *et al.*, 1995; Pflug *et al.*, 2003). The LADY model is less aggressive than the TRAMP model and develops multi-focal LG-PIN between 12-20 weeks that progresses to early invasive carcinoma but generally fails to metastasise (Abate-Shen and Shen, 2002).

In combination with knockout/knockin mice, the LADY and the TRAMP models have provided mechanistic insights into prostate tumourigenesis. For example, TRAMP:*Pten*$^{+/-}$ mice have shown invasive adenocarcinoma and frequent metastasis to the lung, liver, lymph nodes and kidney, demonstrating the role of *Pten* loss in promoting late stage progression (Kwabi-Addo *et al.*, 2001). TRAMP:*Fgf2*$^{-/-}$ mutant mice show decreased tumour progression/metastasis and improved survival, implicating *Fgf2*-mediated angiogenesis and intranuclear activities in prostate cancer progression (Polnaszek *et al.*, 2003). Recently, Gipp *et al* (2007) reported no generalised increase in Hh signalling during tumour development in the LADY transgenic mouse model, although Indian Hh expression was shown to increase with enhanced expression of progenitor cell markers.

The LADY and the TRAMP models have also validated several potential chemotherapeutic agents. For example, reduced primary tumour incidence and metastasis has been demonstrated in response to the COX-2 selective inhibitor Celecoxib (Pandha *et al.*, 2005), green tea polyphenols that inhibit IGF1-induced signalling (Adhami *et al.*, 2004), dietary restriction (Suttie *et al.*, 2005), the γ-secretase inhibitor E-7869 (R-Flurbiprofen) (Wechter *et al.*, 2000) and anti-estrogen (Raghow *et al.*, 2002).

Although these models are highly successful at recapitulating the full spectrum of human prostate disease progression, it is important to note that the viral antigens and the phenotype observed are not naturally associated with human prostate cancer. Furthermore, the SV40 models exhibit neoplastic neuroendocrine cells which are uncommon in clinical

cases (Roy-Burman *et al.*, 2004). To this end, the *PB* promoter has also been utilised to over-express a number of genes. These include *AR*, *FGF8b*, *FGF7*, *FGFR1/2* and *SKP2* (to target $P27^{Kip1}$ for proteolysis), all of which predisposed HG-PIN (Kasper, 2005) and *PB-H-ras* transgenic mice that manifest LG-PIN and metaplastic changes towards an intestinal goblet cell phenotype (Scherl *et al.*, 2004).

The *PB* promoter has also been exploited to over-express Akt, highlighting its crucial role during prostate tumourigenesis and progression (Majumder *et al.*, 2003). AKT promotes cell survival and growth by targeting GSK-3β, BCL-2, eNOS, S6K1, angiogenein-3, the mTOR pathway and forkhead box (FOX) transcription factors (Majumder *et al.*, 2003). The MPAKT (Murine Prostate restricted Akt Kinase activity in Transgenic mice) model showed that over-expressing *Akt1* in the prostate causes PIN (Majumder *et al.*, 2003). Consistent with this, loss of *PTEN*, which suppresses Akt activity, predisposes to an approximate phenocopy of the MPAKT model (Kwabi-Addo *et al.*, 2001).

In addition to the PB promoter, the *C3(1)*, *K5* and *CR2* promoters have proven to be successful in targeting gene expression to the prostates of transgenic mice. The *C3(1)* promoter has been employed to drive expression of *Bcl2*, *c-Myc* and the SV40 tumour antigens in the VP, giving rise to hyperplasia, LG-PIN and adenocarcinoma respectively (Kasper, 2005; Zhang *et al.*, 2000). The *K5* promoter specifically targets basal cells and has been employed to over-express the insulin growth factor-1 (*Igf1*). *K5-Igf1* mice developed epithelial hyperplasia at 8 weeks, which progressed to adenocarcinomas (DiGiovanni *et al.*, 2000). The *CR2* promoter is expressed endogenously post-puberty (week 7-8 onwards) and was originally employed in intestinal studies. CR2 targets the neuroendocrine lineage and has been employed to drive expression of the SV40 large T antigen (*CR2-T-Ag*). Mice demonstrated PIN within 1 week of *CR2*-mediated T antigen expression and progressed to androgen-independent carcinoma and metastasis by 6 months of age (Garabedian *et al.*, 1998). The X-linked transcription factor, early growth response gene-1 (Erg-1) regulates cell growth, differentiation, apoptosis and wound healing and is frequently upregulated in human prostate cancer (Eid *et al.*, 1998). *CR2-T-Ag:Erg*$^{-/-}$ mice showed that loss of *Erg1* delays tumour progression to invasive carcinomas from PIN, suggesting that Erg1 plays a role in driving progression to late stage disease (Abdulkadir *et al.*, 2001; Eid *et al.*, 1998).

More recently, the EZC-prostate model has emerged, permitting both *ex vivo* and *in vivo* imaging of the prostate by utilising the human *kallikrein2* based promoter, *hK2-E3/P*, to incorporate firefly *Luciferase* and enhanced green fluorescent protein expression in

prostate epithelium (Xie *et al.*, 2004). This allows therapeutics to be monitored throughout an entire treatment regime by visualising these fluorescent molecules (Xie *et al.*, 2004). In a similar project, the human *PSA* promoter has also been employed (Lyons, 2005). Additional non-invasive techniques include magnetic resonance imaging (MRI) and positron emission tomography (PET), which ultimately permit the tracking of transgene expression and visualisation of tumour progression (Lyons, 2005).

### 1.2.4 Cre-LoxP technology

The *Cre*-LoxP recombination system is a powerful molecular approach for the conditional and tissue specific inactivation or expression of target genes (Hoess and Abremski, 1984). *Cre*-LoxP technology provides a means to circumvent some of the limitations of conventional gene knockouts, such as embryonic lethality, permitting direct evaluation of gene function *in vivo* (Maddison and Clarke, 2005). The bactriophage P1 *Cre* gene (Cyclisation recombination, a type-1 topoisomerase) encodes a site-specific DNA recombinase that excises intervening DNA flanked between two 34 bp unidirectional bacterial LoxP sites ('floxed', fl) (Lakso *et al.*, 1992). The reciprocal recombination event produces a circular excised fragment of DNA containing one LoxP sequence which is quickly degraded, while the second LoxP site remains within the linear DNA (Clarke, 2002; Wu *et al.*, 2001). This approach can be employed to target gene ablation and gene expression. A floxed gene, where LoxP sites flank the gene of interest will result in excision of the gene (figure 1.8a). Gene ablation may also be accomplished by flanking the activating domain of the gene of interest with LoxP sites. Gene expression can occur by floxing the deactivating domain of the target gene or by inserting a floxed STOP cassette upstream of the target gene (figure 1.8b). Upon *Cre recombinase* expression, the STOP cassette is excised and transcription of the target gene is permitted.

The Rosa26 reporter system has been used extensively to confirm the profile of endogenous recombination events (Soriano, 1999). This construct contains a LoxP-flanked NEO-STOP cassette situated upstream of the *LacZ* reporter gene, similar to that depicted in figure 1.8b. *Cre recombinase* expression results in excision of the STOP cassette and transcription of β-galactosidase, which forms a blue product upon LacZ staining (Soriano, 1999). As the Rosa26 reporter transgene is present in all cells of the organism (e.g. mouse), this facilitates the visualisation of recombination driven by different promoters.

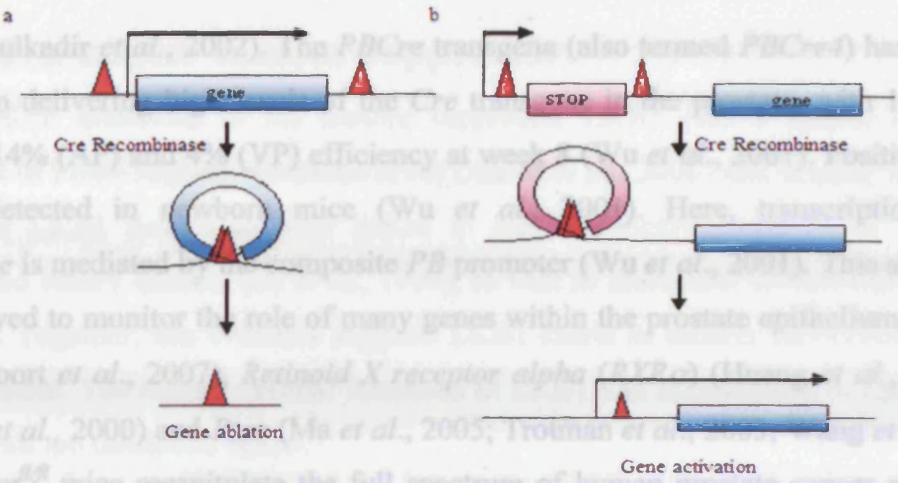


**Figure 1.8: The Cre-LoxP system.** (a) Conditional knockout: Transgenic mice harbouring a floxed gene of interest (i.e. flanked by LoxP sites, red arrow heads) are inter-crossed with mice bearing *Cre recombinase* under the control of a tissue specific promoter. Upon *Cre recombinase* expression, recombination at the LoxP sites takes place and the target gene is excised from the genome. (b) Conditional knockin: Transgenic mice carrying a floxed STOP cassette upstream of the silenced gene of interest are crossed to mice bearing the tissue-specific *Cre recombinase*. Expression of *Cre recombinase* results in cleavage at LoxP sequences, excision of the STOP cassette and transcription of the target gene. This figure is adapted from Maddison and Clarke (2005).

To regulate the *Cre*-LoxP system it is necessary to create a transgenic organism (initially via pronuclear injection) with a tissue specific promoter to drive *Cre recombinase* expression, either constitutively or by induction. This method allows researchers to isolate the effects of genes in tissues of interest and is only limited by the availability of a transcriptionally strong promoter and its specificity. It is important to avoid spontaneous background recombination, which may cause multiple phenotypes. Inducible promoters are a useful tool for transgenic models, allowing temporal and spatial regulation of the transgene (Maddison and Clarke, 2005). For example, xenobiotics, such as β-naphthoflavone, target the dioxin response element within the *Cyp1a1 p450* (*Ah*) promoter to drive *Cre-recombinase* expression, resulting in the over-expression, activation, deficiency or inactivation of floxed transgenes in the liver, kidneys and gastrointestinal tract (Ireland *et al.*, 2004).

### 1.2.5 Conditional transgenic mouse prostate cancer models

*Cre*-LoxP technology has become a powerful strategy for generating conditional transgenic mouse prostate cancer models (Abate-Shen and Shen, 2002; Kasper, 2005). The PSA promoter has been employed to drive *Cre recombinase* expression, allowing genetic manipulation to take place within the prostate. For example, *PSACre-Nkx3.1*$^{fl/fl}$ mice deficient for *Nkx3.1* develop hyperplasia and dysplasia, similar to the *Nkx3.1* knockout

model (Abdulkadir *et al.*, 2002). The *PBCre* transgene (also termed *PBCre4*) has also been successful in delivering high levels of the *Cre* transgene in the prostate, with 100% (LP), 33% (DP), 14% (AP) and 4% (VP) efficiency at week 8 (Wu *et al.*, 2001). Positive staining was also detected in newborn mice (Wu *et al.*, 2001). Here, transcription of *Cre Recombinase* is mediated by the composite *PB* promoter (Wu *et al.*, 2001). This strategy has been employed to monitor the role of many genes within the prostate epithelium, including *Apc* (Bruxvoort *et al.*, 2007), *Retinoid X receptor alpha* (*RXRα*) (Huang *et al.*, 2002), *Rb* (Maddison *et al.*, 2000) and *Pten* (Ma *et al.*, 2005; Trotman *et al.*, 2003; Wang *et al.*, 2003). *PBCre4*$^{+}$*Pten*$^{fl/fl}$ mice recapitulate the full spectrum of human prostate cancer progression from hyperplasia, LG-PIN, HG-PIN, androgen independent carcinoma and metastasis (Wang *et al.*, 2003). This phenotype has also been shown using the *PSA-Cre* transgenic line to mediate *Pten* biallelic excision (Ma *et al.*, 2005).

To conclude, rodent transgenic prostate cancer models have proved to be beneficial in determining the genetic events that predispose to prostate tumourigenesis (summarised in figure 1.9). The primary objective of the next generation of prostate cancer models is to derive animal models that display all the pathophysiological characteristics of the human disease, including androgen-independence and metastasis.

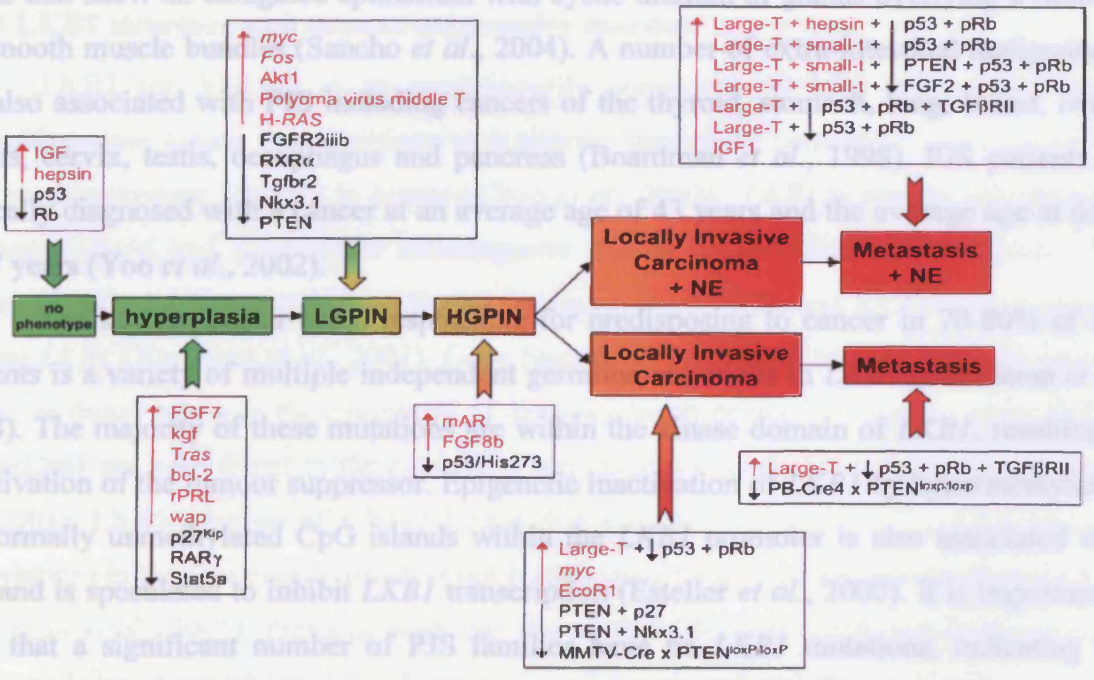


**Figure 1.9 Summary of the multi-step nature of prostate cancer and current transgenic mouse models.** This diagram depicts the large number of prostate cancer mouse models available and how synergy between tumour suppressors and/or oncogenes is a common event for the development of advanced stages of tumour progression. This figure was adapted from Kasper (2005).

## 1.3 LKB1: a master tumour suppressor

Germline mutations of the tumour suppressor LKB1 play a central role in the development of Peutz-Jeghers syndrome (PJS) (Alessi *et al.*, 2006) and somatic inactivating mutations of LKB1 have also been linked to lung adenocarcinomas (Ji *et al.*, 2007), pancreatic and biliary cancers (Su *et al.*, 1999), as well as malignant melanomas (Guldberg *et al.*, 1999). Together, this evidence suggests LKB1 exerts its tumour suppressive role in a variety of tissues. The normal cellular functions of LKB1 and implications of LKB1 loss in tumourigenesis are discussed below.

### 1.3.1 Peutz-Jeghers syndrome

PJS was first described in 1922 by Dr. Johannes Peutz and further characterised by Dr. Harold Jeghers and colleagues in 1940 (Alessi *et al.*, 2006). PJS is a rare, autosomal dominant human disorder (estimated 1 per 250,000 - 300,000 people) characterised by melanin deposits on the buccal mucosa, lips and digits and an increased lifetime risk (10-fold) of developing malignant neoplasia (Yoo *et al.*, 2002). Patients are particularly predisposed to hamartomatous polyps and carcinomas throughout the gastrointestinal tract (with a 93% risk) (Giardiello *et al.*, 1987). PJS hamartomas are benign overgrowths of tissue that show an elongated epithelium with cystic dilation of glands overlying a network of smooth muscle bundles (Sancho *et al.*, 2004). A number of extra-intestinal malignancies are also associated with PJS including cancers of the thyroid, stomach, lung, breast, ovary, uterus, cervix, testis, oesophagus and pancreas (Boardman *et al.*, 1998). PJS patients are typically diagnosed with a cancer at an average age of 43 years and the average age at death is 57 years (Yoo *et al.*, 2002).

The key molecular event responsible for predisposing to cancer in 70-80% of PJS patients is a variety of multiple independent germline mutations in *LKB1* (Boardman *et al.*, 1998). The majority of these mutations are within the kinase domain of *LKB1*, resulting in inactivation of the tumour suppressor. Epigenetic inactivation of *LKB1* by hypermethylation of normally unmethylated CpG islands within the *LKB1* promoter is also associated with PJS and is speculated to inhibit *LKB1* transcription (Esteller *et al.*, 2000). It is important to note that a significant number of PJS families have no *LKB1* mutations, indicating the existence of a second causative locus for PJS. However, no mutations in proteins known to interact with LKB1, such as LKB1 interacting protein-1 (LIP1), MO25, STRAD or BRG1 have been identified (Alhopuro *et al.*, 2005; Yoo *et al.*, 2002).

Whether haploinsufficiency of *Lkb1* is sufficient for tumour formation is currently under debate. It is possible that transgenic mice lack human tumour suppression mechanisms and allow haploinsufficiency to cause gastrointestinal polyps (Karuman *et al.*, 2001). Consistent with this, heterozygous, *Lkb1*$^{+/-}$ knockout mice develop PJS symptoms, predominantly gastrointestinal hamartomatous polyposis, directly resembling the human disorder (Miyoshi *et al.*, 2002; Nakau, 2002). Currently, haploinsufficiency of *LKB1* is linked to the onset of cancer yet loss of heterozygosity (LOH) is deemed necessary in human disease progression (Gruber *et al.*, 1998; Yoo *et al.*, 2002). *LKB1* mutations commonly arise in the epithelium and not the stroma in PJS polyps. This directly connects germline mutations with cell proliferation after the loss of a second allele and supports a hamartomas-adenoma-carcinoma sequence in neoplastic transformation (Bosman, 1999). However, a recent study on human PJS polyps demonstrated that the wild-type *LKB1* allele is present in both epithelial and stromal cells of the hamartomatous polyp (Hernan *et al.*, 2004). The evidence indicates that biallelic inactivation of *LKB1* is not required for hamartomatous polyp formation and may provide some further growth advantage (Katajisto *et al.*, 2007). It is hoped that conditional knockouts of *Lkb1* will help resolve this debate (Sakamoto *et al.*, 2005).

### 1.3.2 LKB1 structure and tumour suppressive function

LKB1 (or STK11) is an evolutionarily conserved 60 kDa (433 amino acids) serine/threonine kinase that functions as a tumour suppressor consisting of 10 exons that map to chromosome 19p13.3 in humans (Yoo *et al.*, 2002). *LKB1* is also an orthologue of *C.elegans Par4* and *Drosophila melanogaster dLKB1* mammalian polarity genes. The mouse (*Lkb1*) and *Xenopus laevis* (*Xeek1*) homologues are 88% and 83.7% homologous to human *LKB1* (Karuman *et al.*, 2001). Gene function is speculated to vary between species; Xeek1 is found solely in the cytoplasm of *Xenopus laevis* primarily oocytes, while hLKB1 and mLkb1 are both found in the cytoplasm and nucleus (Conde *et al.*, 2007; Marignani *et al.*, 2001). LKB1 consists of a large kinase domain, two NLSs and a $C_{433}$AAX box (for prenylation) in the C-terminus which is not homologous to any known protein (figure 1.10a) (Karuman *et al.*, 2001). Previous work has shown that LKB1 is highly regulated by many post-translational modifications and is capable of autophosphorylation at residues Thr185, Thr189, Thr366 and Ser404, to regulate its own catalytic activity (Alessi *et al.*, 2006), (figure 1.10a). p90 ribosomal protein kinase (RSK) and PKA are also thought to regulate cell growth by phosphorylating LKB1 at Ser431 (Alessi *et al.*, 2006). Consistent with this,

mutation at Ser431 determined that this residue regulates LKB1's ability to suppress growth in G361 cells (Alessi *et al.*, 2006). Phosphorylation at Thr366 in response to ionising radiation is thought to be carried out by the DNA-damage activated ataxia-telangiectasia-mutated (ATM) kinase (Alessi *et al.*, 2006). In addition, the fact that Ser31 lies in a consensus sequence for AMP-activated protein kinase (AMPK) mediated phosphorylation suggests that AMPK or an AMPK-related kinase may regulate LKB1 activity at this residue (Alessi *et al.*, 2006).

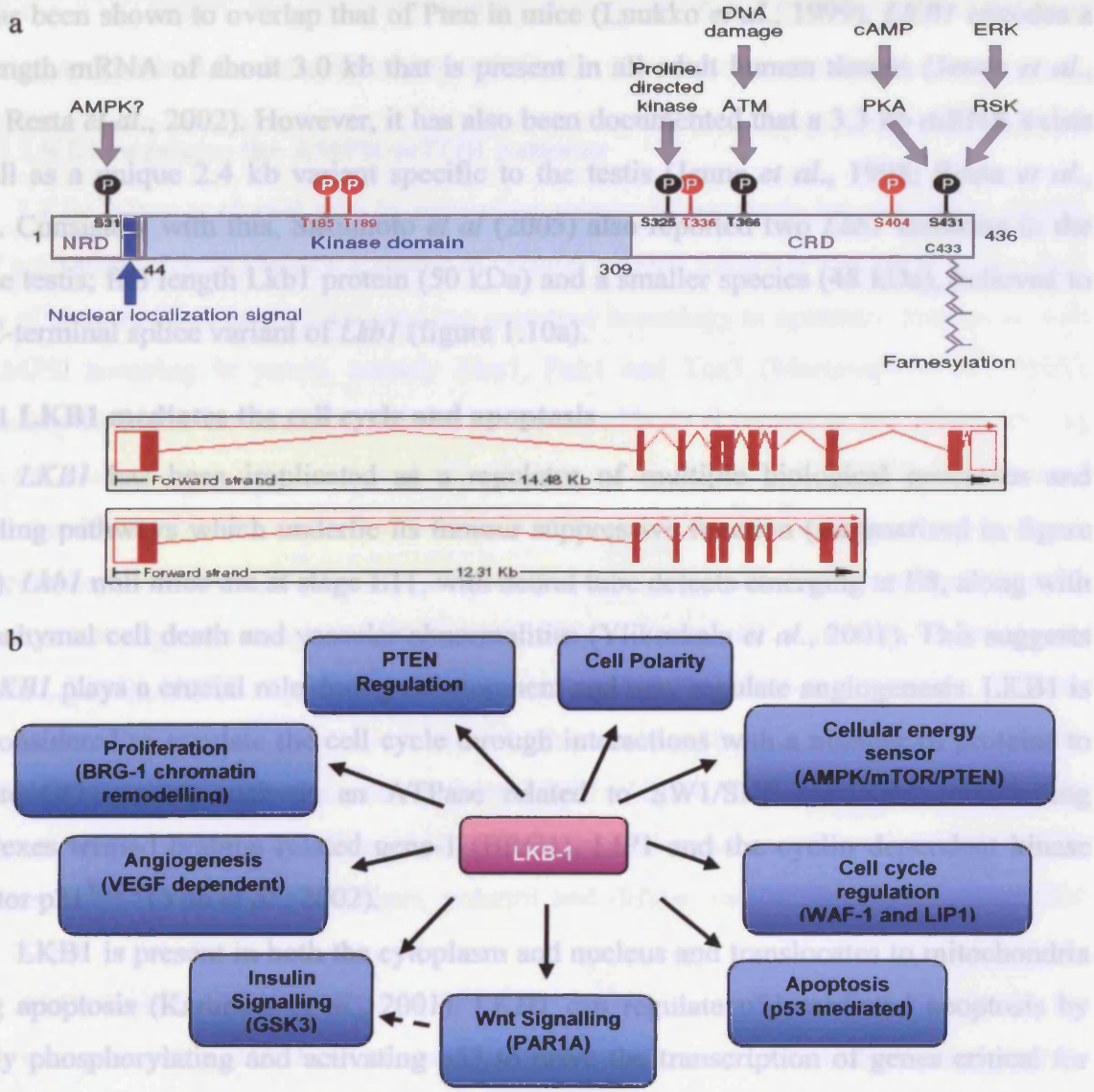


**Figure 1.10: LKB1 structure and function.** a) Schematic of mouse Lkb1 illustrating the post-translational modification sites; two N-terminal NLSs, a large conserved kinase domain containing the Thr185/189 autophosphorylation site (red) and the C-terminus where prenylation may occur at Cys433 (green). Residues Thr366, Ser404, Ser431 and Cys433 correspond to human LKB1 residues Thr363, Thr402, Ser428 and Cys430 respectively. Below, the two transcript variants of murine *Lkb1* are shown (Ensemble ENSF00000005137). Figure 1.10a is adapted from Alessi *et al* (2006). The functions LKB1 fulfils within the cell are summarised in (b).

*LKB1* is an essential gene required for normal foetal development and its expression is significantly reduced in the epithelial cells of most human and mouse adult organs (Collins *et al.*, 2000; Conde *et al.*, 2007). High levels of LKB1 expression are found in the testis, pancreas, liver, skeletal muscle, small intestine and stomach (Conde *et al.*, 2007). A low level of LKB1 expression has also been detected in the cytoplasm of prostate luminal epithelial cells in humans (Conde *et al.*, 2007). Furthermore, *Lkb1* mRNA transcript expression in the mouse correlates to the human pattern of expression (Collins *et al.*, 2000) and has been shown to overlap that of Pten in mice (Luukko *et al.*, 1999). *LKB1* encodes a full-length mRNA of about 3.0 kb that is present in all adult human tissues (Jenne *et al.*, 1998; Resta *et al.*, 2002). However, it has also been documented that a 3.3 kb mRNA exists as well as a unique 2.4 kb variant specific to the testis (Jenne *et al.*, 1998; Resta *et al.*, 2002). Consistent with this, Sakamoto *et al* (2005) also reported two *Lkb1* isoforms in the murine testis; full length Lkb1 protein (50 kDa) and a smaller species (48 kDa), believed to be a C-terminal splice variant of *Lkb1* (figure 1.10a).

#### 1.3.2.1 LKB1 mediates the cell cycle and apoptosis

*LKB1* has been implicated as a regulator of multiple biological processes and signalling pathways which underlie its tumour suppressive function (summarised in figure 1.10b). *Lkb1* null mice die at stage E11, with neural tube defects emerging at E8, along with mesenchymal cell death and vascular abnormalities (Ylikorkala *et al.*, 2001). This suggests that *LKB1* plays a crucial role during development and may regulate angiogenesis. LKB1 is also considered to regulate the cell cycle through interactions with a number of proteins to mediate G(1) arrest, such as an ATPase related to SW1/SNF chromatin-remodelling complexes termed brahma related gene-1 (BRG1), LIP1 and the cyclin dependent kinase inhibitor $p21^{WAF1}$ (Yoo *et al.*, 2002).

LKB1 is present in both the cytoplasm and nucleus and translocates to mitochondria during apoptosis (Karuman *et al.*, 2001). LKB1 can regulate p53-mediated apoptosis by directly phosphorylating and activating p53 to drive the transcription of genes critical for growth inhibition, cell senescence and apoptosis (Trotman and Pandolfi, 2003; Yoo *et al.*, 2002). LKB1 induces cell cycle G(1) arrest by phosphorylating p53 at residues Ser15 (also an AMPK target) and Ser392 (Trotman and Pandolfi, 2003; Yoo *et al.*, 2002). In its phosphorylated state, p53 is recruited directly to the p21/WAF1 promoter to initiate p21/WAF1 transcription (Zeng and Berger, 2006). Consistent with this, i*n vitro* studies have shown that LKB1 over-expression in cancer cell lines, including the G361 melanoma cells,

results in LKB1-dependent growth inhibition, owing to p53 activity and elevated levels of $p21^{WAF1}$ (Tianen *et al.*, 2002). In addition, Lkb1 expression in mice has been shown to be high at the tip of intestinal villi, where older, apoptosing epithelial cells are shed into the lumen, while Lkb1 expression in younger, proliferating cells is much lower (Karuman *et al.*, 2001). LKB1 substrates NUAK1 and NUAK2 have also been indirectly linked to apoptosis and a kinase involved in DNA damage checkpoint and p53-dependent apoptosis, termed ATM (ataxia telangiectasia mutated), has been shown to phosphorylate LKB1 at Thr366 (Katajisto *et al.*, 2007). Together, this evidence suggests that LKB1 is a key player in triggering apoptosis, a fundamental characteristic of a tumour suppressor.

#### 1.3.2.2 LKB1 regulates the AMPK/mTOR pathway

LKB1 plays a crucial role in regulating energy homeostasis by mediating AMPK (AMP activating protein kinase), a sensor of cellular energy. LKB1 is a member of the Snf1 family of kinases (Yoo *et al.*, 2002) and has sequence homology to upstream kinases to Snf1 (an AMPK homolog in yeast), namely Elm1, Pak1 and Tos3 (Marignani *et al.*, 2005), implicating LKB1 as an effective AMPK kinase (AMPKK) (Lizcano *et al.*, 2004). During low ATP conditions, LKB1 is thought to phosphorylate AMPK at Thr172, a conserved residue that lies within the activation T-loop. AMPK phosphorylation and activation results in suppression of the mTOR pathway, ultimately suppressing cell growth and proliferation to minimise energy consumption (Baas *et al.*, 2004b; Corradetti *et al.*, 2004; Spicer and Ashworth, 2004). AMPK is a highly conserved heterotrimeric kinase in eukaryotes (Lizcano *et al.*, 2004). The T-loop is conserved in >10 other protein kinases in the human genome, the majority of which are also activated by LKB1 (Figure 1.11a), (Hardie, 2005). The variety of LKB1 substrates enables this tumour suppressor to coordinate several cellular processes, such as energy metabolism, polarity and differentiation (Lizcano *et al.*, 2004; Rider, 2006).

AMP binding to AMPK is postulated to induce a conformational change in the kinase, thus presenting AMPK as a better substrate for upstream activating kinases such as LKB1. However, it has also been demonstrated that LKB1-mediated phosphorylation and activation of AMPK can be independent of the ATP:AMP ratio (Woods *et al.*, 2003) and instead, the α1 and α2 AMPK subunits are speculated to respond to energy stress levels (Shaw *et al.*, 2004). To enhance AMPK activation (up to 100-fold), LKB1 is anchored in the cytoplasm in a heterotrimeric complex with STRAD (STE20-related adaptor) and MO25 (Boudeau *et al.*, 2003), (figure 1.11b). To date, regulation of the formation and destruction

of the LKB1/STRAD/MO25 complex is not fully understood. The pseudokinase STRAD may activate LKB1 and induce its cytoplasmic translocation. In turn, STRAD is postulated to be phosphorylated by LKB1 at two distinct sites (Baas *et al.*, 2004a). Although the role of MO25 is uncertain, it is generally considered to act as a scaffolding protein, stabilising LKB1:STRAD interactions. Consistent with this, LKB1 kinase activity is diminished when MO25 is absent from the complex (Boudeau *et al.*, 2003; Hawley *et al.*, 2003). Interestingly, the AMPK phosphatases PP1γ and $PP2A_1$ have been purified with the LKB1:STRAD:MO25 complex, possibly providing a convenient route for rapid deactivation of LKB1-stimulated AMPK (Hawley *et al.*, 2003). LKB1 post-translational modifications may also be significant in regulating AMPK activity given that AMPK and LKB1 expression levels do not act in concert and LKB1 stabilisation has been shown to require interaction with heat shock protein-90 (Hsp90) (Yoo *et al.*, 2002). Further analysis of LKB1 post-translational modifications has not yet identified alternative mechanisms that can regulate the LKB1:STRAD:MO25 ternary complex. For instance, *in vitro* mutational analysis of LKB1 phosphorylation by PKA or p90RSK at Ser431 and prenylation at Cys433 did not disrupt complex formation (Boudeau *et al.*, 2003).

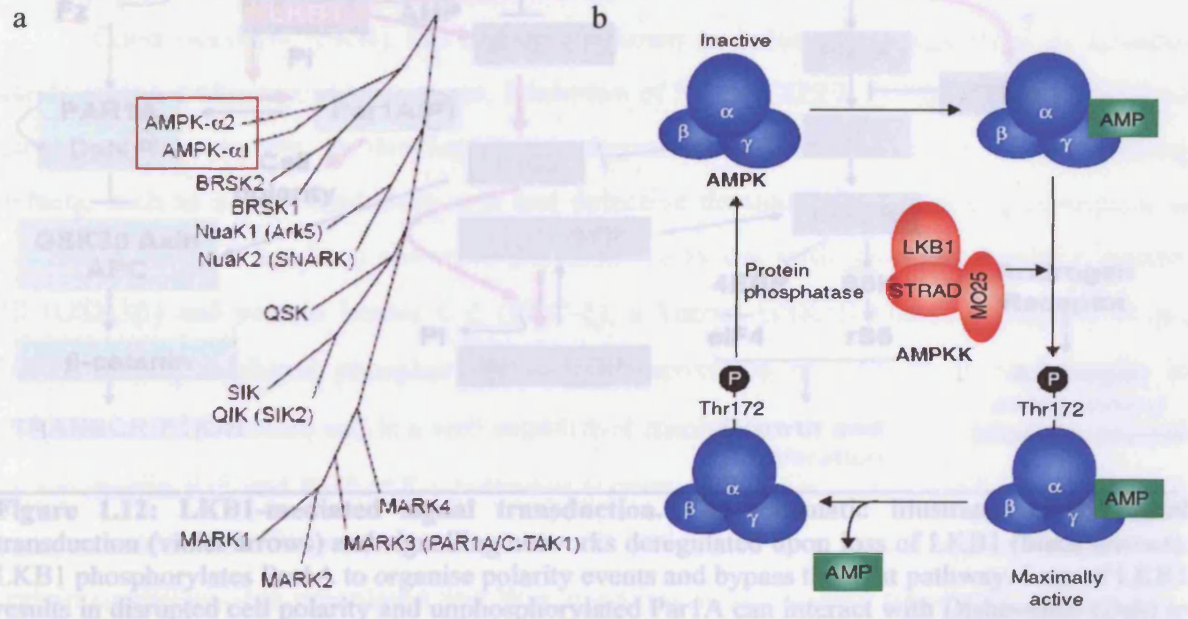


**Figure 1.11: AMPK-related kinases and LKB1-mediated AMPK regulation.** (a) Dendogram to illustrate the AMPK-related kinases; brain-specific kinases-1/2 (BRSK1/2), microtubule-affinity regulating kinases-1-4 (MARK1-4), maternal embryonic leucine zipper (MELK), AMP-regulated kinase 5 (ARK5/NUAK1), SNF1/AMPK related kinase (SNARK/NUAK2), Qin-induced kinase (QIK), QSK and salt-induced kinase (SIK). (b) Model of AMPK activation. During low energy conditions, AMP binds and allosterically activates AMPK, resulting in Thr172 phosphorylation. Maximum AMPK activity is achieved when AMPK binds the LKB1:STRAD:MO25 complex. Figures are adapted from (a) Hardie (2005) and (b) Kyriakis *at al* (2003).

mTOR (FRAP1) is a highly conserved Ser/Thr kinase that regulates protein synthesis and cell growth through multisite phosphorylation of S6K and 4E-BP1 (Sakamoto *et al.*, 2005). S6K activates its substrate p-Rps6 required for G(1) cell cycle progression and 4E-BP1 stimulates CAP-dependent translation (DeMarzo *et al.*, 2003). LKB1-mediated activation of AMPK negatively regulates the mTOR pathway (Shaw *et al.*, 2004). AMPK phosphorylates TSC2 (tuberin) to block mTOR signalling in a Rheb-dependent manner, resulting in reduced growth and proliferation during low energy circumstances (Shaw *et al.*, 2004), (figure 1.12). In high energy conditions or in an LKB1 deficient environment, the mTOR pathway is considered to be activated by extracellular stimulation of the PI3K/AKT pathway, ultimately activating TSC2. LKB1-mediated regulation of AMPK also governs other AMPK controlled events, implicating that LKB1 can regulate the down-regulation of fatty acid and cholesterol biosynthesis, as well as enhancing glucose uptake and glycolysis . Furthermore, LKB1 has been shown to regulate TGFβ signalling to prevent cell growth and proliferation by forming an LKB1:LIP1:SMAD4 ternary complex (Smith *et al.*, 2001).

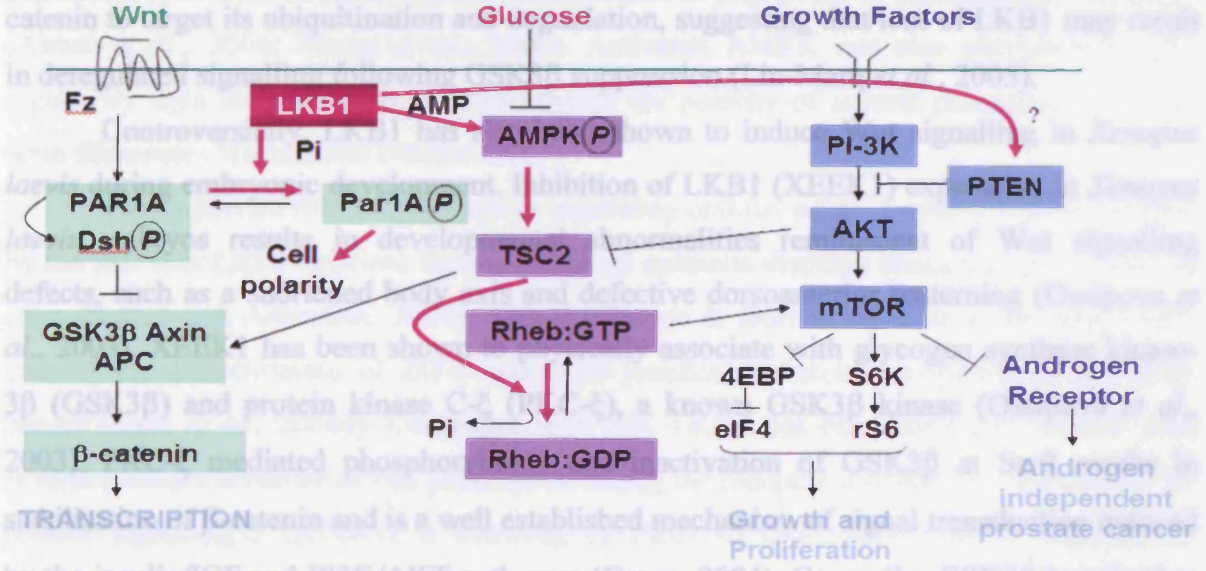


**Figure 1.12: LKB1-mediated signal transduction.** The schematic illustrates LKB1 signal transduction (violet arrows) and signalling networks deregulated upon loss of LKB1 (black arrows). LKB1 phosphorylates Par1A to organise polarity events and bypass the Wnt pathway. Loss of LKB1 results in disrupted cell polarity and unphosphorylated Par1A can interact with Dishevelled (Dsh) to trigger Wnt signalling. LKB1-mediated AMPK phosphorylation during low ATP conditions results in TSC2 phosphorylation and inactivation. TSC2 inactivation inhibits mTOR by serving as a GTPase activating protein (GAP) for the Ras-like GTPase Rheb, which is required for mTOR activation. Loss of LKB1 is postulated to elevate mTOR signalling, inducing growth and proliferation. Growth factors stimulate PI3K, resulting in AKT phosphorylation. Active AKT inhibits TSC2, allowing Rheb:GTP to activate mTOR and initiate growth and proliferation. LKB1 can interact with and phosphorylate PTEN, which is speculated to prevent AKT activation (Song *et al.*, 2007). This figure is adapted from Shaw *et al* (2004).

### 1.3.2.3 LKB1 regulates Wnt signalling

LKB1 has also been implicated in regulating the Wnt pathway. Partitioning defective proteins (PARs) share sequence homology with *LKB1* and are considered LKB1 signalling partners (Spicer *et al.*, 2003). LKB1 has been shown to regulate the Ser/Thr kinase Par1A (also termed cTAK1, MARK3 and p78) in the human cervical carcinoma cell line, HeLa S3 (Spicer *et al.*, 2003). LKB1 phosphorylation of Par1A is thought to regulate cell polarity events (Spicer *et al.*, 2003). In its unphosphorylated form, Par1A interacts with and phosphorylates Dishevelled (Dsh/Dvl) to stimulate the Wnt/β-catenin pathway (Spicer *et al.*, 2003). Consequently, LKB1 may act as a pivot, competing with Dsh for Par1A, redirecting it from Wnt signalling to organise cell polarity and prevent growth and proliferation (figure 1.12). In addition, Lin-Marq *et al* (2005) reported mutations that impair kinase activity (K78I) or alter the cellular localisation of LKB1 in HeLa cells results in diminished upregulation of several genes involved in Wnt signalling, such as WNT5B and FZD2. Furthermore, LKB1 mutants fail to activate GSK3β required to phosphorylate β-catenin to target its ubiquitination and degradation, suggesting that loss of LKB1 may result in deregulated signalling following GSK3β suppression (Lin-Marq *et al.*, 2005).

Controversially, LKB1 has also been shown to induce Wnt signalling in *Xenopus laevis* during embryonic development. Inhibition of LKB1 (XEEK1) expression in *Xenopus laevis* embryos results in developmental abnormalities reminiscent of Wnt signalling defects, such as a shortened body axis and defective dorsoanterior patterning (Ossipova *et al.*, 2003). XEEK1 has been shown to physically associate with glycogen synthase kinase-3β (GSK3β) and protein kinase C-ξ (PKC-ξ), a known GSK3β kinase (Ossipova *et al.*, 2003). PKC-ξ mediated phosphorylation and inactivation of GSK3β at Ser9 results in stabilisation of β-catenin and is a well established mechanism of signal transduction induced by the insulin/IGF and PI3K/AKT pathways (Green, 2004). Generally, GSK3β inactivation is not considered sufficient to elevate β-catenin activity or Wnt signalling, however, under certain conditions it is speculated that Wnt signalling is potentiated (Ossipova *et al.*, 2003). Indeed, two separate research groups have shown that a reduction in the affinity for GSK3β to bind to Axin may facilitate Wnt signalling in mammalian cell lines, as Axin facilitates β-catenin phosphorylation and degradation by bringing β-catenin and GSK3β together (Ding *et al.*, 2000; Yuan *et al.*, 1999). The attenuation of the apparent affinity of GSK3β for Axin has also been shown to be mediated by activated Akt in the presence of Wnt ligands (Wnt1 or Frat) (Yuan *et al.*, 1999). It is important to note that XEEK1 function may differ to that of

hLKB1 or mLkb1 owing to the fact that XEEK1 is restricted to the cytoplasm, while the human and murine homologues have been detected in the cytoplasm and nucleus (Marignani *et al.*, 2001). Alternatively, LKB1/XEEK1 might positively regulate Wnt signalling in embryos, but negatively regulate it in adult tissues (Clements and Kimelman, 2003).

### 1.3.2.4 LKB1 regulates cell polarity

LKB1 plays a crucial role in organising cell polarity using several different signal transduction cascades. To coordinate the formation of the actin cytoskeleton and tight junctions, Par1A activates Par1 homologues (MARK1-4), which phosphorylate Par3 to create binding sites for Par5 (14-3-3ξ) (Baas *et al.*, 2004b). This suggests that LKB1 regulation of Par1A not only inhibits the Wnt cascade but also drives structural organisation of the cell (Spicer *et al.*, 2003; Sun *et al.*, 2001b). Interestingly, *MARK3*$^{-/-}$ mice manifest dwarfism, reduced fertility and autoimmune disease (Hurov *et al.*, 2001) and LKB1-dependent activation of AMPK is also documented to play a role in tight junction assembly (Alessi *et al.*, 2006; Zhang *et al.*, 2006). Activated AMPK can also phosphorylate the regulatory light chain of myosin to coordinate the polarity of several processes, including actin filaments (Wodarz and Näthke, 2007).

The important role LKB1 plays in regulating cellular polarity events is demonstrated by the fact that *LKB1* deficient human intestinal epithelia displays abnormal polarisation *in vitro* (Spicer and Ashworth, 2004). This phenotype is rescued by over-expressing *LKB1*, causing the redistribution of ZO-1 and p120 junctional proteins peripheral to the brush border (Baas *et al.*, 2004a). Consistent with this, LKB1 has been shown to interact with several proteins involved in cell polarity, including the receptor-independent activator of G-protein signalling-3 (AGS-3), a homolog of PINS in *Drosophila* that is required for asymmetric neuroblast cell division (Baas *et al.*, 2004a). Furthermore, mutational analysis in the HT1080 fibrosarcoma cell line has revealed that disrupting the LKB1 ATP-binding site (K78M) or N-terminal truncation (Δ88) hinders LKB1-mediated apoptosis by microtubule disrupting agents, not DNA-damaging agents. This is consistent with the notion that LKB1 acts as a specific microtubule integrity sensor (Alessi *et al.*, 2006; Baas *et al.*, 2004b).

### 1.3.2.5 LKB1 regulates PI3K/AKT signalling

More recently, LKB1 has emerged as a regulator of PTEN stability (Mehenni *et al.*, 2005). LKB1 is speculated to bind to and phosphorylate the tumour suppressor PTEN,

causing cytoplasmic relocalisation of LKB1 (Mehenni *et al.*, 2005). *In vitro* studies have shown that LKB1 phosphorylates PTEN at S385, in combination with S380, T382 or T383 to post-translationally regulate PTEN stability (Mehenni *et al.*, 2005; Song *et al.*, 2007). However, control mechanisms that mediate PTEN stability are not well understood and should be viewed with caution (Okahara *et al.*, 2004). The fact that both LKB1 and PTEN are tumour suppressors suggests that LKB1-mediated phosphorylation of PTEN may act to confer PTEN stability, resulting in PI3K/AKT pathway inhibition to prevent cell growth and proliferation (figure 1.12). In support, Song *et al* (2007) recently reported that LKB1 is capable of mediating PTEN activation/stability, which correlated to inactivation of the survival factor AKT *in vitro* and *in vivo*.

### 1.3.3 LKB1 and its role in cancer

The revelation that LKB1 is a key participant in several essential cellular pathways provides rationale for tumourigenesis in PJS patients and other *LKB1* deficient cancers (Alessi *et al.*, 2006). Many of these processes are major players in the homeostatic control of the adult epithelium and are commonly disrupted during tumourigenesis, including regulation of the cell-cycle, energy metabolism, Wnt signalling, cell polarity, and PI3K/AKT signalling (Mehenni *et al.*, 2005; Spicer and Ashworth, 2004; Spicer *et al.*, 2003; Yoo *et al.*, 2002). The molecular events induced by *LKB1* mutation predisposing to cancer represent potential therapeutic targets and are discussed below.

Lkb1 null mice die *in utero* at stage E11, with neural tube defects emerging at E8 (Ylikorkala *et al.*, 2001). *Lkb1*$^{+/-}$ mice are viable and are prone to hamartomatous polyps of the glandular stomach (93% incidence, >20 weeks of age) and small intestinal hamartomas (31% incidence, > 50 weeks of age) (Miyoshi *et al.*, 2002). These lesions retain both the wild-type and targeted *Lkb1* alleles, suggesting *Lkb1* haploinsufficiency is sufficient to initiate gastrointestinal hamartomas in mice. To date, conditional transgenic mouse models harbouring mutated *Lkb1* in targeted tissues have revealed that LKB1 plays a critical role in the murine heart (Thomson *et al.*, 2007), skeletal muscle (Sakamoto *et al.*, 2005; Thomson *et al.*, 2007) and lung (Ji *et al.*, 2007). Inactivation of LKB1 has been found in 34% and 19% of human lung adenomas and squamous cell carcinomas respectively and is associated with the upregulation of metastasis-promoting genes (Ji *et al.*, 2007).

The disruption of the homeostatic balance between proliferation and apoptosis underlines the basis for cancer development (Hanahan and Weinberg, 2000). Aberrant LKB1-mediated regulation of G(1)cell cycle progression may cause uncontrolled cell

proliferation and induce tumour formation (Yoo *et al.*, 2002). PJS polyps devoid of LKB1 show reduced levels of apoptosis compared to normal intestinal epithelium (Karuman *et al.*, 2001). This may reflect perturbation of two separate mechanisms regulated by LKB1, namely p53-mediated apoptosis and BRG1-mediated chromatin-remodelling. Loss of heterozygosity (LOH) at 17p as well as over-expression of p53, indicative of *p53* gene mutation, has been detected in gastrointestinal adenocarcinomas associated with PJS (Gruber *et al.*, 1998). Furthermore, a human lung cancer study has shown that p53 expression is often lost concomitantly with LKB1 (Ji *et al.*, 2007) and re-introducing LKB1 into pancreatic adenocarcinomas deficient for LKB1 rescues the phenotype and elevates p53-dependent apoptosis, further demonstrating the tumour suppressive function of LKB1 (Qanungo *et al.*, 2003).

Although *p53* null mice do not develop hamartomatous polyps like *Lkb1*$^{+/-}$ mice, they do exhibit a defect in intestinal epithelial apoptosis (Karuman *et al.*, 2001). The fact that *p53* null mice do not harbour an apoptosis defect in stem cells suggests that LKB1 may participate in stress kinase pathways mediated by ASK1, JNKK and JNK (Karuman *et al.*, 2001). This provides rationale for LKB1-mediated regulation of stem cell survival in a p53-independent manner, further associating LKB1 to malignant cancer formation in the later life of PJS patients (Karuman *et al.*, 2001). In PJS patients that do not harbour an LKB1 mutation, it is feasible that the mitochondrial translocation of LKB1 to amplify apoptotic signalling by means of BCL2 family members is disrupted, ultimately reducing apoptosis (Yoo *et al.*, 2002).

LKB1 typically acts to stimulate the ATPase function of BRG1, necessary for both BRG1-dependent growth arrest and RB-induced cell cycle arrest in G(1) and S phase (Marignani *et al.*, 2001; Yoo *et al.*, 2002). Loss of LKB1-mediated BRG1 activation is considered to disrupt chromatin-remodelling complex formation, resulting in unchecked cell proliferation and tumour formation. Disrupted BRG1 interactions with other proteins including steroid hormone receptors, BRCA1 and Cyclin E may further drive tumourigenesis (Marignani *et al.*, 2001). To date, BRG1 is not known to be mutated in PJS patients (Alhopuro *et al.*, 2005), however aberrant BRG1 expression is associated with prostate cancer (Sun *et al.*, 2007), and *Brg1*$^{+/-}$ mice develop mammary carcinomas (Bultman *et al.*, 2007).

LKB1 behaves as an energy sensor through interactions with AMPK during low energy states, redirecting cellular metabolism towards ATP generation instead of energy requiring macromolecular synthesis e.g. cell division (Spicer and Ashworth, 2004). This

indicates that cells deficient for LKB1 might harbour a proliferative advantage. Consistent with this, PJS intestinal hamartomas express elevated levels of S6K1 activity and p4EBP1, indicative of hyperactivation of mTOR signalling that promotes growth and proliferation (Corradetti *et al.*, 2004; Shaw *et al.*, 2004). Rapamycin, an mTOR inhibitor is currently in phase II clinical trials for prevention of PJS and sporadic *LKB1* deficient tumours (Shaw *et al.*, 2004).

Given that vascular endothelial growth factor (*VEGF)* mRNA recruitment to polyribosomes is governed by mTOR signalling (Ylikorkala *et al.*, 2001), activation of the mTOR pathway in an LKB1 deficient environment may elevate angiogenesis, further enhancing tumour growth and assisting metastasis. Consistent with this notion, *Lkb1* null mice that are embryonic lethal exhibit vascular defects associated with elevated Vegf expression (Ylikorkala *et al.*, 2001). This evidence suggests that LKB1 plays a role in the development of the vasculature system and in the regulation of VEGF signaling. In agreement with this hypothesis, enhanced expression of LKB1 in breast cancer cells attenuates angiogenesis, invasion, and metastatic potential (Zhuang *et al.*, 2006). PJS and $Lkb1^{+/-}$ mouse tumours have also shown elevated COX-2 expression, further linking loss of LKB1 to elevated angiogenesis (Rossi *et al.*, 2002; Wei *et al.*, 2003). Consistent with this, LKB1 is speculated to interact with and phosphorylates PEA3 at Ser395, resulting in the ubiquitination and degradation of PEA3 and the transcriptional down-regulation of COX-2, ultimately preventing oncogenesis (Upadhyay *et al.*, 2006).

The Wnt signalling cascade is commonly deregulated in a number of human cancers, including PJS tumours (Miyaki *et al.*, 2000; Polakis, 2000). Loss of *LKB1* renders the AMPK-related kinase Par1A (MARK3/cTAK1) in an unphosphorylated state and can elevate Wnt signalling (figure 1.12). Activated Wnt signalling results in an elevation of Wnt target genes, such as c-Myc and CD44, which can further promote tumourigenesis (Clevers, 2006; Polakis, 2000). In addition, loss of LKB1-mediated phosphorylation of Par1A may also deregulate RAS signalling and cell polarity, which further drives neoplastic transformation of epithelial tissues (Baas *et al.*, 2004b; Wodarz and Näthke, 2007). For example, MARK3/cTAK1 has been shown to phosphorylate and inactivate the kinase suppressor of Ras (KSR) at Ser392 to suppress the MAPK pathway, which stimulates growth and proliferation (Müller *et al.*, 2001). It is speculated that loss of LKB1 might prevent MARK3/cTAK1-mediated KSR phosphorylation, leading to activated MAPK signalling and tumourigenesis.

LKB1 regulation of cell polarity is conserved in humans (Boudeau *et al.*, 2003) as well as worms and flies (Baas *et al.*, 2004b). Consistent with this, PJS hamartomas have displayed depolarisation of intestinal cells, which leads to tumour formation (Boudeau *et al.*, 2003). This process is considered to be mediated through several distinct pathways. First, phosphorylation of Par1A by LKB1 is deemed necessary for the maintenance of cell polarity (section 1.3.2.4) (Spicer and Ashworth, 2004; Spicer *et al.*, 2003). Second, PKC-ζ has been shown to elevate GSK3β phosphorylation during cell polarisation with Par-6 in an Lkb1 dependent manner in *Xenopus laevis* (Ossipova *et al.*, 2003). Connections between polarity and tumourigenesis are currently undefined, yet the location of LKB1 is believed to be important for GSK3β regulation (Ossipova *et al.*, 2003). Furthermore, Baas *et al* (2004b) suggested that PJS tumourigenesis is likely to be a result of impaired asymmetric division at the level of the epithelial stem cell.

Recently, LKB1 has been shown to interact with and phosphorylate PTEN *in vitro* and *in vivo* (Mehenni *et al.*, 2005; Song *et al.*, 2007). The implications of this event are not fully understood, although it has been speculated that LKB1 loss results in reduced PTEN function/stability, ensuing the constitutive activation of the PI3K/AKT pathway to promote tumourigenesis (section 1.3.2.5). The survival factor AKT has many downstream targets, which when activated (e.g. p-mTOR) or inactivated (e.g. p-GSK3β) stimulate cell division and differentiation (Jimenez *et al.*, 2003). Moreover, approximately 70% of PJS patients also harbour a mutation in PTEN or display loss of at least one allele of *PTEN*, a common event in many cancers (Trotman *et al.*, 2003). Lung cancer cells have also demonstrated that over-expressing LKB1 leads to cell growth suppression in a PI3K/AKT/PTEN dependent manner (Jimenez *et al.*, 2003). This evidence further implicates LKB1 exerting its tumour suppressive role through the activation or stabilisation of PTEN.

To conclude, there is currently no individual hypothesis to convincingly explain how LKB1 loss contributes to carcinogenesis. Nonetheless, LKB1 functions demonstrate clearly how morphological, biochemical and genetic events associated with *LKB1* mutation may be applied to tumourigenesis and the high cancer risk associated with PJS.

## 1.4 The proto-oncogene β-catenin

β-catenin (CTNNB1) plays a central role in transmitting Wnt signals to regulate mammalian development and cellular responses, such as growth, proliferation, polarity,

migration and differentiation. The normal cellular functions and implications of the gene in tumourigenesis are discussed in this section.

### 1.4.1 The structure and function of β-catenin

β-catenin is an 88kDa ubiquitous intracellular protein that maps to 3p22-p21.3 and consists of 16 exons (Yardy and Brewster, 2005). β-catenin contains an N-terminal domain that comprises approximately 130 amino acids, a central region of 550 amino acids and a C-terminal region of 100 amino acids (figure 1.13), (Clevers, 2006). The N-terminal region harbours a conserved set of phosphorylation sites targeted by casein kinase 1α or 1ε, CK1α/ε (Ser45) and GSK-3β (Ser33/Ser37/Thr41), as well as an α-catenin binding site (K¨lligs *et al.*, 2002). The central region contains 12 armadillo repeats (42 amino acids each) that can form complexes with cadherin adhesion molecules, axin, APC and members of the LEF/TCF-family that induce the transcription of Wnt target genes (figure 1.13) (Clevers, 2006; Kolligs *et al.*, 2002). The C-terminal carries the transactivating domain required for activation of Wnt target genes (Clevers, 2006; Kolligs *et al.*, 2002).

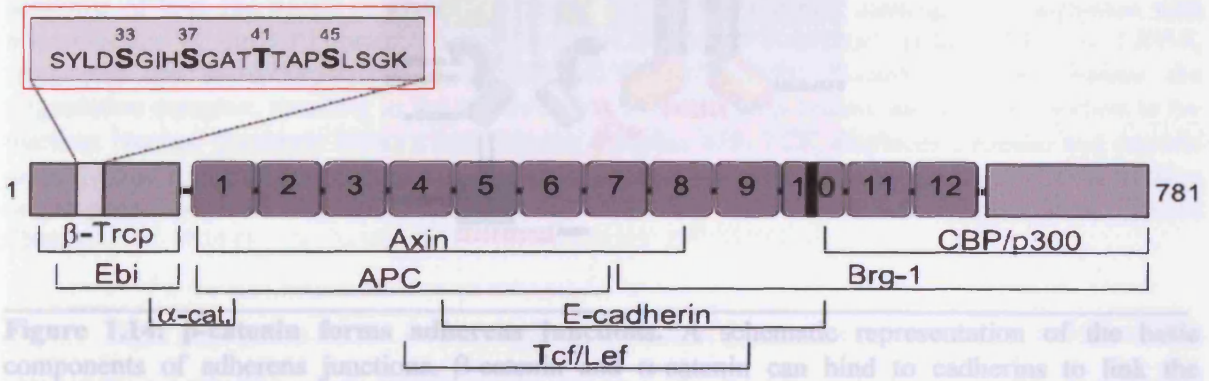


**Figure 1.13: β-catenin protein structure.** Both the N-terminal and C-terminal regions of β-catenin serve as transcriptional activators. The central part is made up of 12 highly homologous armadillo repeats (boxes 1–12), which mediate most interactions with other proteins, such as Axin, APC, Brg1, E-cadherin and Tcf/Lef. Residues Ser33, Ser37 and Thr41 are targeted by GSK3β for phosphorylation and Ser45 is phosphorylated by CKI. Mutation of one of these residues prevents degradation of β-catenin. This figure was adapted from Kolligs *et al* (2002).

β-catenin exists in three cellular pools; (a) at the membrane associated with cadherins (e.g. E-cadherin), α-catenin and other molecules involved in cell adhesion, (b) in the cytoplasm where it accumulates and (c) in the nucleus, where it translocates in response to Wnt signalling, and behaves as a transcription factor (Nollet *et al.*, 1996; Willert and Nusse, 1998; Yardy and Brewster, 2005). There are three known catenin molecules; α, β

and γ (or plakoglobin). β-catenin and γ-catenin are members of the *armadillo* family that harbour a 42-αα *arm* motif and are mammalian orthologues of *Armadillo* (*Arm*) in *Drosophila* (Nollet *et al.*, 1996). Both β-catenin and γ-catenin have been shown to bind E-cadherin to form adherens junctions while α-catenin is a vinculin-related molecule that binds to β-catenin to link β-catenin:E-cadherin complexes to actin filaments (Niessen, 2007). Adherens junctions (shown in figure 1.14) consist of two basic units, the nectin-afadin complex and the cadherin-catenin complex that are linked by interactions with actin (Niessen, 2007). Binding of β-catenin to cadherins is essential for functional adherens junctions, which are crucial for maintaining epithelial adhesion and regulation of cell growth and behaviour (Clevers, 2006).

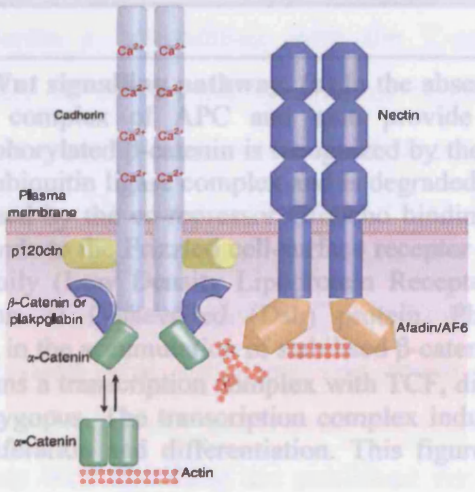


**Figure 1.14: β-catenin forms adherens junctions.** A schematic representation of the basic components of adherens junctions. β-catenin and α-catenin can bind to cadherins to link the membrane spanning cadherin to actin. Cadherin-catenin complexes can also interact with the nectin-afadin complex through actin to maintain cell-cell interactions. This figure was adapted from Niessen (2007).

β-catenin is also the central mediator of Wnt signalling. Wnt molecules are secreted extracellular glycoproteins that have key roles in directing embryonic growth and are involved in cellular processes such as migration, polarity, proliferation and cell fate specification (Yardy and Brewster, 2005). The Wnt pathway was originally described in *Drosophila* as the Wingless pathway and is highly conserved among flies, frogs, and mammals (Clevers, 2006). Currently, three different pathways are believed to be activated upon Wnt receptor activation; the canonical Wnt/β-catenin cascade, the non-canonical planar cell polarity (PCP) pathway, and the Wnt/Ca2+ pathway (Clevers, 2006). The canonical pathway is the best characterised of the three and is described in figure 1.15.

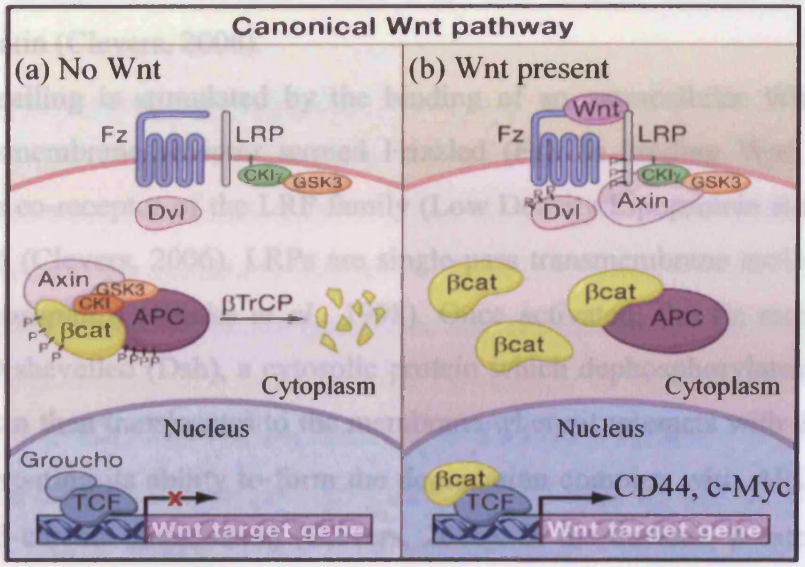


**Figure 1.15: The canonical Wnt signalling pathway.** (a) In the absence of Wnt protein secretion, the cytoplasmic degradation complex of APC and axin provide a scaffold for GSK3β to phosphorylate β-catenin. Phosphorylated β-catenin is recognized by the F box/WD repeat protein β-TrCP, a component of the E3 ubiquitin ligase complex and is degraded. In the nucleus, transcription of TCF target genes is repressed by the co-repressor Groucho binding to TCF. (b) Following the secretion of Wnt, the ligand binds to the Frizzled cell-surface receptor causing its dimerisation with a co-receptor of the LRP family (Low Density Lipoprotein Receptor), either LRP-5 or LRP-6, triggering the phosphorylation of Dishevelled (Dsh) protein. Phospho-Dsh destabilises the degradation complex, resulting in the accumulation of stabilised β-catenin and its translocation to the nucleus. Nuclear β-catenin forms a transcription complex with TCF, displaces Groucho and recruits co-activators Lgs/BCL9 and pygopus. The transcription complex induces the transcription of Wnt target genes involved in proliferation and differentiation. This figure was adapted from Clevers (2006).

Tight regulation of the free cytoplasmic pool of β-catenin is the central switch of the Wnt pathway (Kolligs *et al.*, 2002). In the absence of a Wnt ligand, the degradation complex is formed, comprised primarily of APC, GSK3β and the scaffold protein axin (figure1.15a). Diversin recruits casein kinase-1α/ε (CK1) to the degradation complex where it can phosphorylate β-catenin at Ser45, priming β-catenin for GSK3β phosphorylation at Ser33, Ser37 and Thr41 (Hagen and Vidal-Puig, 2002). This in turn initiates binding of the F-box protein h-TrCP, a component of a dedicated E3 ubiquitin ligase complex. Consequently, β-catenin is ubiquitinated and targeted for rapid destruction by the proteosome (Clevers, 2006). GSK3β also phosphorylates other members of the Wnt pathway, including Axin and APC, to regulate their stability and binding efficiency to β-catenin respectively (Kolligs *et al.*, 2002). To ensure TCF-mediated transcription is not activated in Wnt deficient

conditions, the co-repressor Groucho binds TCF and recruits histone deacetylases to condense chromatin (Clevers, 2006).

Wnt signalling is stimulated by the binding of an extracellular Wnt ligand to a seven-pass transmembrane receptor termed Frizzled (Fz). In binding Wnt, Fz receptors cooperate with a co-receptor of the LRP family (Low Density Lipoprotein Receptor) either LRP-5 or LRP-6 (Clevers, 2006). LRPs are single-pass transmembrane molecules (known as Arrow in *Drosophila*) (Glinka *et al.*, 1998). Once activated, the Fz receptors in turn phosphorylate Dishevelled (Dsh), a cytosolic protein which dephosphorylates axin (Glinka *et al.*, 1998). Axin then translocates to the membrane where it interacts with the LRP intra-cellular tail, preventing its ability to form the degradation complex with APC and GSK3β and leading to β-catenin stabilisation (Clevers, 2006). In the nucleus, β-catenin displaces Groucho from TCF and forms a heterodimer with the T-cell factor (TCF)/lymphoid enhancer factor (LEF) family of DNA binding proteins (Glinka *et al.*, 1998). Nuclear localisation of β-catenin is not currently understood and does not involve the exposure of an NLS sequence (Clevers, 2006). The β-catenin transcription factor complex drives the expression of numerous Wnt target genes including c-Myc, CD44, COX-2, c-Jun, Cyclin D1, Axin2 and SP5 (Clevers, 2006; Kolligs *et al.*, 2002; Voeller *et al.*, 1998; Yardy and Brewster, 2005). As deregulated Wnt signalling can cause cancer, it is very highly regulated. This regulation is only partially understood and additional signalling pathways and cellular factors regulating Wnt signalling are published very frequently. For example, Dickkopf (Dkk) has been shown to inhibit Wnt signaling by directly binding to LRP5/6, resulting in their internalisation and inactivation (Glinka *et al.*, 1998).

### 1.4.2 β-catenin and its role in cancer

Previous work has shown that β-catenin mutations are occasionally present in several human malignancies (Kolligs *et al.*, 2002), including the prostate (5% incidence) (Voeller *et al.*, 1998), and is over-expressed in colon cancer (Korinek *et al.*, 1997), hepatocellular cancer (Miyoshi *et al.*, 1998) and ovarian cancer (Wright *et al.*, 1999). Human disease linked to *β-catenin* stabilising mutations result in the accumulation of β-catenin in the nucleus and transcription of Wnt target genes such as c-Myc, CyclinD1 and CD44 that upregulate cell proliferation, survival and migration respectively (Clevers, 2006; Sansom *et al.*, 2004; Zhang *et al.*, 2005). Activated Wnt signalling has also been linked to

the maintenance and activation of stem cells in intestinal, epidermal and haematopoietic systems (Reya and Clevers, 2005).

*β-catenin* null mice are embryonic lethal, highlighting the vital role the proto-oncogene plays in development, particularly during axis formation (Haegel *et al.*, 1995). Over-expression of a dominant stable form of *β-catenin* using *Cre*-LoxP technology to drive transgene expression in the intestine determined a direct link between β-catenin stabilisation and Wnt activation in intestinal tumourigenesis *in vivo* (Harada *et al.*, 1999). Using the *Cre recombinase* transgene under the control of the cytokeratin 19 (*CK19*) or liver fatty acid binding protein (*Fabpl*) promoters, expression of a dominant stabilised from of β-catenin ($Catnb^{+/\Delta ex3}$) predisposed to intestinal adenomatous polyps, resembling an *APC* deficiency (Bruxvoort *et al.*, 2007; Harada *et al.*, 1999). Mutations in components of the β-catenin degradation complex have also been identified, particularly inactivation of *APC*, resulting in aberrant Wnt signalling and tumourigenesis. For example, germline inactivating mutations in the *APC* gene are associated with Familiar Adenomatous Polyposis (FAP), a hereditary condition where patients show an increased risk to colon adenomas, which display elevated nuclear β-catenin expression (Miyaki *et al.*, 2000). Using a novel inducible *AhCre* transgenic line in conjunction with a LoxP-flanked *Apc* allele to model FAP, $AhCre^{+}Apc^{fl/fl}$ mice also demonstrate elevated β-catenin nuclear translocation, concomitant with intestinal tumourigenesis (Sansom *et al.*, 2004). Furthermore, conditional transgenic mice that are deficient for *Apc* have been shown to predispose to prostate intra-epithelial neoplasia and adenocarcinoma in mice (Bierie *et al.*, 2003; Bruxvoort *et al.*, 2007; Gounari *et al.*, 2002). Together, this evidence indicates that deregulation of the Wnt pathway is a common event in the development of cancer in many tissues (Polakis, 2000).

## 1.5 The proto-oncogene Ras

Ras is a monomeric GTPase anchored at the membrane that transmits signals from the cell surface to modulate many cellular processes including transcription, translation, cell-cycle progression and apoptosis (Malumbres and Pellicer, 1998; Schubbert *et al.*, 2007). The normal cellular functions and implications of the oncogenic transformation of Ras are discussed in this section.

### 1.5.1 Structure and function of Ras

The Ras subfamily consists of three functional members: H-Ras (Harvey rat sarcoma viral oncogene homolog), N-Ras (neuroblastoma RAS viral oncogene homolog) and K-Ras (Kirsten rat sarcoma 2 viral oncogene homolog) (Schubbert *et al.*, 2007), (figure 1.16). K-Ras exists as two isoforms, 4A and 4B owing to alternative splicing at the C-terminus (Schubbert *et al.*, 2007). All four proteins are highly homologous and carry identical sequences for the first 85 amino acids where GTP and GDP bind. The γ-phosphate of GTP/GDP binds to Ras at the P-loop (phosphate binding domain, residues 10-16) and switch I and switch II regulate Ras regulator and effector binding (Schubbert *et al.*, 2007).

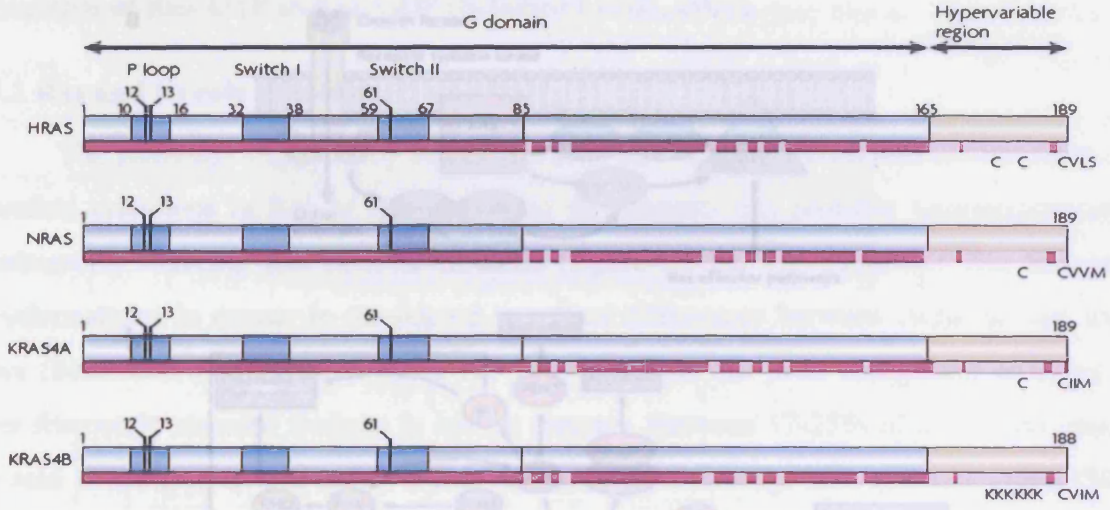


**Figure 1.16: Ras protein structure.** The four Ras isoforms HRAS, NRAS, KRAS4A and KRAS4B are highly homologous and residues 1-85 are identical, where GDP and GTP bind. The P loop (phosphate-binding loop) binds the γ-phosphate of GTP, and switch I and II regulate binding to Ras regulators and effectors. Somatic RAS mutations found in cancer frequently introduce amino-acid substitutions at positions 12 and 13 (P-loop) and 61 (switch II). The C-terminal hypervariable domain specifies membrane localization through post-translational modifications that include the farnesylation of each isoform on the C-terminal CAAX motif (CVLS, CVVM, CIIM or CVIM) and palmitoylation of key cysteines (C) on HRAS, NRAS and KRAS4A. Membrane localization of KRAS4B is facilitated by a stretch of lysines (KKKKKK) proximal to the CVIM motif. To highlight the degree of homology, conserved residues are shown in magenta and the variable residues in pink. This figure is adapted from Schubbert *et al* (2007), figure 2.

Ras proteins are small GTPases whose biological activity is catalysed by a cycle between active (GTP bound) and inactive (GDP bound) conformations (Malumbres and Pellicer, 1998). This process is triggered by growth factors binding their respective membrane-spanning receptor tyrosine kinases (RTKs), initiating RTK complex formation and subsequent activation (Malumbres and Pellicer, 1998). Once stimulated, RTKs autophosphorylate themselves at tyrosine residues within the kinase domain that lies in the cytoplasm. This elevates RTK function and creates docking sites for intracellular proteins

that carry an SH2 (Src homology 2) domain, or a PTB (phospho-tyrosine binding) domain (Schubbert *et al.*, 2007). Proteins that carry an SH2 domain include SHC (SH2-containing protein), GRB2 (growth-factor-receptor bound protein 2) and Gab (GRB2-associated binding) proteins, which when bound to an activated RTK can recruit additional proteins through their SH3 (Src homology 3) domains that bind proline-rich sequences (Malumbres and Pellicer, 1998). For example, GRB2 binds to SOS (son of sevenless), a guanidine exchange factor (GEF) that activates Ras by stimulating it to release bound GDP and exchange it for GTP (figure 1.17a). PI3K and phospholipase-Cγ may also stimulate Ras signalling by interacting with the autophosphorylated RTKs (Schubbert *et al.*, 2007).

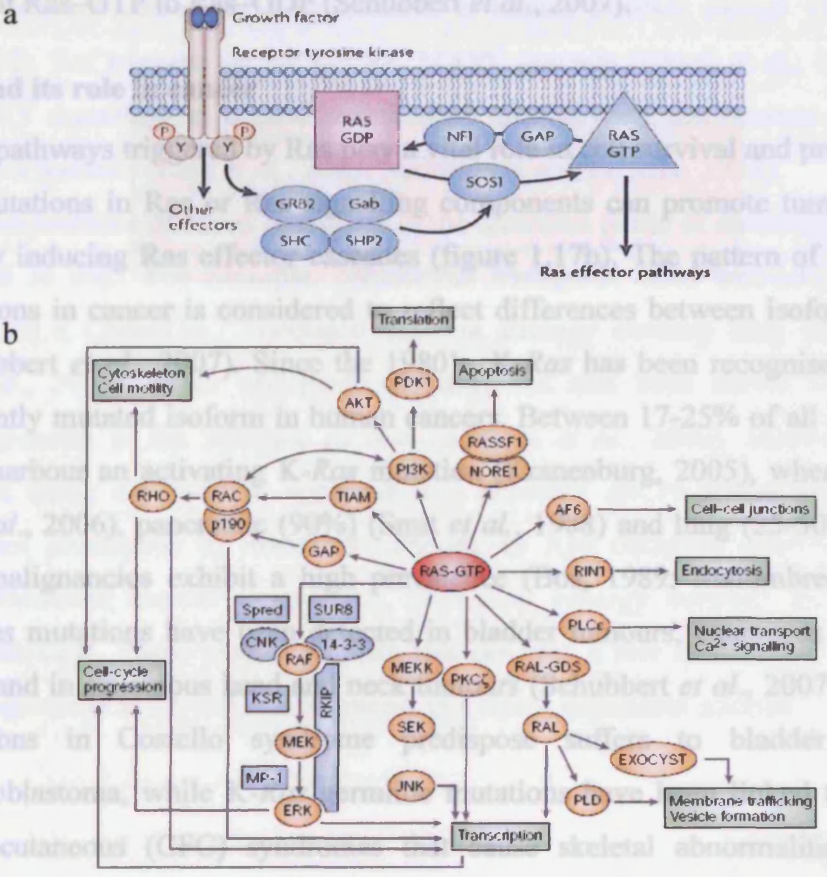


**Figure 1.17: Ras activation and effector pathways.** (a) Growth factor stimulation of a receptor tyrosine kinase results in autophosphorylation of its cytoplasmic tail at tyrosine residues that are recognised by adaptor proteins, such as Grb-2. These adaptors contain both SH2 and SH3 domains and can recruit guanine-nucleotide exchange factors (GEFs), such as SOS. SOS binds to and activates Ras by triggering a conformational change that facilitates the exchange of GDP for GTP. Ras signalling is switched off by GTPase-activating proteins (GAPs), such as NF1. The complexity of the Ras signalling is illustrated in (b). The well-characterised pathway through which Ras mediates signal transduction is the MAPK cascade. Here Ras-GTP activation of Raf, an MAPKKK, triggers MEK activation, an MAPKK that ultimately stimulates the MAPK ERK to upregulate transcription of target genes, resulting in proliferation. Figure (a) was adapted from Schubbert *et al* (2007) and (b) was adapted from Malumbres *et al* (2003).

Ras-GTP initiates numerous Ras effector pathways that ultimately drive cell growth and proliferation in response to growth factors (Malumbres and Pellicer, 1998), (figure1.17b). A crucial response is potentiation of the mitogen-activated protein kinase (MAPK) cascade, a series of serine/threonine phosphorylations mediated by Ras activation of the MAP-kinase kinase kinase, Raf. Raf phosphorylates the MAP-kinase kinase MEK which in turn triggers phosphorylation and activation of the MAP-kinase ERK, which has the ability to regulate many targets and induce cell growth, survival and proliferation (Schubbert *et al.*, 2007). To negatively regulate the Ras signalling pathway, the GTPase-activating protein (GAP) neurofibromin (NF1) binds to Ras–GTP and accelerates the conversion of Ras–GTP to Ras–GDP (Schubbert *et al.*, 2007).

### 1.5.2 Ras and its role in cancer

The pathways triggered by Ras play a vital role in cell survival and proliferation, and therefore mutations in Ras or Ras signalling components can promote tumourigenesis by continuously inducing Ras effector cascades (figure 1.17b). The pattern of Ras oncogenic transformations in cancer is considered to reflect differences between isoforms and tissue types (Schubbert *et al.*, 2007). Since the 1980's, K-*Ras* has been recognised as being the most frequently mutated isoform in human cancers. Between 17-25% of all human cancers are said to harbour an activating K-*Ras* mutation (Kranenburg, 2005), where colon (50%) (Janssen *et al.*, 2006), pancreatic (90%) (Smit *et al.*, 1988) and lung (25-50%) (Jackson *et al.*, 2001) malignancies exhibit a high prevalence (Bos, 1989; Malumbres and Pellicer, 1998). H-*Ras* mutations have been detected in bladder tumours, cutaneous squamous cell carcinomas and in squamous head and neck tumours (Schubbert *et al.*, 2007). Germline H-*Ras* mutations in Costello syndrome predispose suffers to bladder cancers and ganglioneuroblastoma, while K-*Ras* germline mutations have been linked to Noonan and Cardio-faciocutaneous (CFC) syndromes that cause skeletal abnormalities and mental retardation (Schubbert *et al.*, 2007). Finally, N-*Ras* mutations are frequent in acute leukemias (mainly of the myeloblastic cell type) and in the myelodysplastic syndromes (Malumbres and Pellicer, 1998).

Oncogenic *Ras* mutations typically cause resistance to GTPase-activating proteins (GAPs) by introducing an amino acid substitution at positions 12, 13 or 61 (Schubbert *et al.*, 2007). This results in hyperactivation of Ras, which is locked in its active (GTP bound) conformation. In general, the Ras:GAP interaction is maintained, but the ability of GAPs to catalyse GTP hydrolysis has become compromised (Schubbert *et al.*, 2007). However, *Ras*

mutations alone rarely progress towards a metastatic/invasive tumourigenic state, which is considered to require combinatorial genetic/epigenetic events (Janssen *et al.*, 2006). Consistent with this, human prostate cancer seldom manifests activating Ras mutations (Papatsoris *et al.*, 2007; Weber and Gioeli, 2004), while autocrine and paracrine factors are upregulated, suggesting that increased wild-type Ras activation can promote tumourigenesis through elevated stimulation of Ras effector pathways. In support, growth factors, such as EGF, TGFα, FGF, IGF and KGF, and their receptors, have all been found to be over-expressed in human prostate cancer (Schubbert *et al.*, 2007) and human prostate cancer cell lines (Maroni *et al.*, 2004). Deregulation of two principle Ras effectors, Raf and PI3K (a phosphatidylinositol kinase) are also common to human prostate cancer (Malumbres and Pellicer, 1998). Raf triggers the MEK/ERK MAPK cascade (Gioeli *et al.*, 1999) and PI3K regulates AKT signalling to initiate proliferation and survival and prevent apoptosis, thus driving tumourigenesis (Liao *et al.*, 2003; Malumbres and Pellicer, 1998).

The importance of K-*ras* mutations in the initiation phase of carcinogenesis has been demonstrated *in vivo*. For example, conditional transgenic mice harbouring a K-$ras^{G12V}$ mutation using a *CMV-Cre*$^{+/T}$-mediated knockin strategy develop lung adenocarcinomas (Guerra *et al.*, 2003). K-*ras* oncogenic mutation has also been shown to participate in tumour progression in the intestine *in vivo* (Sansom *et al.*, 2006). Sansom *et al* (2006) demonstrated using a Cre-LoxP approach that although *AhCre*-driven expression of K-$ras^{V12}$ did not predispose to intestinal tumours, in Apc deficient conditions, K-$ras^{GV12}$ expression enhanced tumour progression, indicating synergy between the Ras and Wnt signalling pathways. These studies indicate Ras can play a role at the onset or during later stages of progression to drive tumourigenesis in a tissue dependent manner.

## 1.6 Aims and objectives

This thesis aims to generate novel mouse models of prostate cancer using conditional transgenesis to characterise the molecular events underlying prostate tumourigenesis *in vivo*. The primary objectives to investigate the roles of Lkb1, β-catenin and K-ras in the prostate have been outlined below;

1. Use the Cre-LoxP system to develop a mouse model in which Lkb1 is absent in the prostate.
2. Characterise the phenotype of Lkb1 deficiency in the mouse prostate using immunohistochemistry and to confirm deregulation of Lkb1-mediated pathways.
3. Investigate the cooperativity between Lkb1 loss and Wnt signalling activation by conditionally activating β-catenin and deleting Lkb1 within the mouse prostate.
4. Study the synergistic relationship between Ras and Wnt signalling using Cre-LoxP technology to express activated K-ras and β-catenin in the mouse prostate.

A floxed Lkb1 allele (Sakamoto *et al.*, 2005), combined with a prostate-specific Cre-recombinase (Ireland *et al.*, 2004; Wu *et al.*, 2001) will allow removal of Lkb1 in the prostate epithelium. LKB1 plays a key role in suppressing the oncogenic nature of the mTOR, PI3K/AKT and Wnt signalling pathways that drive proliferation, cellular polarity and survival (Alessi *et al.*, 2006; Hardie, 2005; Spicer *et al.*, 2003). Deletion of Lkb1 should consequently deregulate these pathways to facilitate tumourigenesis by disrupting cellular polarity and elevating growth and proliferation of the prostate epithelial cells.

Spicer *et al* (2003) showed that LKB1 can phosphorylate PAR1A *in vitro* to suppress Wnt signalling and coordinate cellular polarity. To investigate the effects of Lkb1 loss and activated Wnt signalling in the mouse prostate I will use a prostate-specific Cre-recombinase to drive conditional deletion of Lkb1 and dominant stabilisation of β-catenin simultaneously in the same mouse. Given Lkb1's role in suppressing the Wnt pathway, it is predicted that upregulated Wnt signalling and loss of cellular polarity in an Lkb1 deficient environment will accelerate tumour progression. This experiment is designed to provide an insight into the molecular mechanisms employed by Lkb1 to prevent tumour formation in the prostate.

The multi-step nature of tumourigenesis has been demonstrated in many mouse models, whereby the synergistic relationship between Ras and Wnt signalling facilitates

tumour progression (Hanahan and Weinberg, 2000). Synchronous activation of Ras and Wnt signalling has been shown to cooperate in colorectal (Janssen *et al.*, 2006; Li *et al.*, 2005), intestinal (Sansom *et al.*, 2006), kidney (Sansom *et al.*, 2006), mammary (Jang *et al.*, 2006) and liver (Harada *et al.*, 2004) tumours in mice. Conditional activation of β-catenin and K-ras in the murine prostate will be used to investigate the cooperativity of Wnt and Ras signalling pathways in the development and progression of prostate tumourigenesis. Given the role of these pathways in cell survival, growth, proliferation and their convergence in upregulating Wnt target genes such as c-Myc and COX-2, compound mutants are expected to accelerate the progression of the disease (Araki *et al.*, 2003; He *et al.*, 1998; Kerkhoff *et al.*, 1998).

# Chapter 2: Experimental procedures

All laboratory reagents and supplier details are detailed in Appendix 1.

## 2.1. Mouse colonies

Mice harbouring the *p450 Cyp1a1 Cre Recombinase* (*AhCre)* transgene on the C57BL6 background were supplied by Doug Winton (Ireland *et al.*, 2004) and the B6.D2-Tg(Pbsn-Cre)4Prb (*PBCre*) strain was supplied by MMHCC Repository (NCI Frederick) to direct transgene expression to the prostate. The *Lkb1*-floxed deletion model was constructed and supplied by Alan Ashworth (Sakamoto *et al.*, 2005) and the constitutively active *β-catenin* strain was developed by Makoto M. Taketo (Harada *et al.*, 1999). Transgenic mice carrying an activating mutation in K-ras (termed K-$ras^{V12}$) were derived via a knockin strategy by Mariano Barbacid (Guerra *et al.*, 2003). All mice were fed the Harlan standard diet (scientific diet services) and water provided *al libitum*. All animal studies and breeding were carried out under a UK Home Office project licence.

### 2.1.1 Induction of the *AhCre* promoter

*AhCre* activity was induced by 4 i.p. injections of 80 mg/kg β-naphthoflavone within 24 hours and tissue harvested 7 days later. β-naphthoflavone was prepared by dissolving 1 g β-naphthoflavone in 100 ml corn oil (Sigma) at 99°C in a water bath whilst stirring occasionally for 1 h. Aliquots were prepared and stored at -20°C. Prior to injection, aliquots were defrosted at 65°C for 10-15 min.

## 2.2 Genotyping

Mice were genotyped by PCR using DNA extracted from tail biopsies at weaning age (four weeks old), using anaesthetic. Genotypes were re-confirmed at death.

### 2.2.1 DNA isolation and purification

Using the PureGene DNA isolation system (Gentra), 2-3 mm tail biopsy was lysed with 10 μl Proteinase K and 500 μl cell lysis solution overnight at 37°C. 200 μl of protein precipitation buffer was added and samples spun (10 min, 14,000 rpm). The S/N was transferred to a fresh tube with 500 μl propan-2-ol and spun (15 min, 14,000 rpm). The S/N

was removed and the pellet air-dried for 10 min before re-suspending in 500 µl nuclease-free water. Samples typically contained 50-100 ng/µl.

### 2.2.2 Genotyping PCR

**Primer design:** Primer sequences were designed by 'Primer 3' software (Whitehead Institute), unless previously described (Table 2.1) and blast searched using 'Ensembl' to check the specificity. Oligonucleotides were ordered from 'Sigma Aldrich'.

**Table 2.1: Genotyping primers**

| Primer Name | Sequence (5'-3') | Product size (bp) |
|---|---|---|
| AhCre (Ireland *et al.*, 2004) | CreB = ATTGCCCCTGTTTCACTATC<br>AHC = CCTGACTAGCATGGCGATAC | 1200 |
| β-catenin (Primer 3) | Ctnnb1 = CTGCGTGGACAATGGCTACT<br>Ctnnb2 = TCCATCAGGTCAGCTGTAAAAA | WT = 324<br>HOM = 500 |
| β-catenin recombined (Harada *et al.*, 1999) | AS5 = ACGTGTGGCAAGTTCCGTCATCC<br>GF2 = GGTAGGTGAAGCTCAGCGCAG | WT = 900<br>Rec = 700 |
| Cre/LacZ (Ireland *et al.*, 2004) | CreA = TGACCGTACACCAAAATTTG<br>CreB = ATTGCCCCTGTTTCACTATC<br>LacZA = CTGGCGTTACCCAACTTAAT<br>LacZB = ATAACTGCCGTCACTCCAAC | Cre = 1000<br>LacZ = 500 |
| K-ras$^{LSLV12}$ (Guerra *et al.*, 2003) | 510 = AGGGTAGGTGTTGGGATAGC<br>3Ex1 = CTCAGTCATTTTCAGCA<br>103rev-2 = CTGTCCTTTACTGAAGGCTC | WT = 403<br>Floxed = 621<br>Rec = 669 |
| Lkb1 (Primer 3) | Lkb1f = GATTTCCGCCAGCTGATTGA<br>Lkb1r = AGTGTGACCCCAGCTGACCA | WT = 320<br>Floxed = 280 |
| Lkb1 recombined (Primer 3) | Lkb1A = CAGAATCACATCCCCTGGTT<br>Lkb1B = TTCCCCTCCTCCTGCTAGAT | Rec = 500 |
| Pten (Suzuki *et al.*, 2001) | Pten1 = CTCCTCTACTCCATTCTTCCC<br>Pten2 = ACTCCCACCAATGAACAAAC | WT = 228<br>HOM = 335 |

**Genotyping PCR protocols:** PCR reactions were performed in a 96-well plate with PicTaq (Cancer Research UK), PlatinumTaq (Invitrogen) or GoTaq (Promega) DNA polymerases, depending on the primer set (Table 2.2). Details for a single 50 µl reaction are provided below for each polymerase.

**PicTaq:** 2 µl DNA, 37 µl nuclease-free water, 5 µl 5x PicTaq PCR Buffer (1.21 g Tris and 3.72 g KCl in 100 ml nuclease-free water at pH 8.3 and filtered through a 0.2 µl filter prior to use), 5 µl 25 mM $MgCl_2$, 0.4 µl 25 mM dNTPs, 0.4 µl PicTaq, 0.1 µl of each primer (100 µM).

**PlatinumTaq:** 2 µl DNA, 37.2 µl nuclease-free water, 5 µl 10x PlatinumTaq buffer, 5 µl 25 mM $MgCl_2$, 0.4 µl 25 mM dNTPs, 0.2 µl PlatinumTaq, 0.1 µl of each primer (100 µM). **GoTaq:** 2 µl DNA, 32.2 µl nuclease-free water, 10 µl 5x GoTaq Flexi Buffer, 5 µl 25 mM $MgCl_2$, 0.4 µl 25 mM dNTPs, 0.2 µl GoTaq, 0.1 µl of each primer (100 µM).

**Standard PCR protocol:**

(1) 94°C for 2.5 min, (2) 94°C for 30 sec, (3) 60°C for 30 sec, (4) 72°C for 1 min, (5) Repeat step 2 – 4 for 34 cycles, (6) 72°C for 5 min, (7) END (14°C hold).

Alterations for specific primers are outlined in Table 2.2.

**Table 2.2 PCR protocols**

| Primer Name | DNA Polymerase | Alterations to PCR protocol steps |
|---|---|---|
| AhCre | PicTaq | Standard |
| β-catenin | GoTaq | (6) 72°C for 10 min |
| β-catenin recombined | GoTaq | (3) 60°C for 1.5 min<br>(4) 72°C for 5 min<br>(6) 72°C for 10 min |
| Cre/LacZ | Platinum Taq | Standard |
| K-ras$^{LSLV12}$ | PicTaq | Standard |
| Lkb1 | GoTaq | Standard |
| Lkb1 recombined | GoTaq | Standard |
| Pten | PicTaq | (1) 95°C for 2 min<br>(2) 95°C for 1 min<br>(3) 58°C for 1 min |

**Gel Electrophoresis:** To detect PCR products, 5µl of loading dye was added to each sample and 20 µl run on a 2% agarose TBE gel containing 15 µl ethidium bromide/200 ml (except β-catenin recombined PCR which was run on a 1% agarose TBE gel). Electrophoresis was run at 100 V for 30 min in 1x TBE running buffer and PCR fragments were detected using a UV light box.

## 2.3 Tissue preparations

### 2.3.1 Tissue harvesting

The genitourinary (GU) tract and liver, lung, stomach, kidney, spleen, pancreas, salivary gland and small intestine were harvested using a micro-dissection kit. Small

intestine samples were prepared by removing waste from the gut by flushing it with water using a syringe. 3x 1 cm sections were cut 10 cm from proximal end, and wrapped together longitudinally and parallel to each other in surgical tape to form a bundle. All samples were fixed in neutral buffered 10% formalin fixative (Sigma) on ice for a maximum of 24 hours to allow cross-polymerisation to occur within the tissue. Samples were then embedded in paraffin wax immediately using an automated tissue processor (Leica TP1050) or transferred to 70% ethanol at 4°C for short-term storage prior to processing. Sections were cut (5-10 μm thick) onto poly-L-lysine coated slides using a Leica RM2135 microtome. Samples adhered to the slides on a hot plate (15-30 min) and then in an oven at 45°C for a minimum of 24 hours prior to histological procedures. Frozen samples were snap frozen in liquid nitrogen in tubes which were stored at -80°C until use. Cryosections (10-15 μm thick) were prepared by embedding samples in OCT (Lamb) on cork discs and slides were stored at -80°C until use.

## 2.4 Immunohistochemistry

Before commencing immunohistochemistry (IHC) and staining procedures, formalin-fixed, paraffin-embedded sections were de-waxed and rehydrated in a fume hood in the following; 2x 5 min Xylene, 2x 2 min 100% EtOH, 1x 2 min 95% EtOH, 1x 2 min 70% EtOH and a 5 min wash in $dH_2O$. Dehydration in preparation for mounting followed this protocol in reverse. For each antibody, tissue sections of known positive and negative control samples were included and the Lambda Phosphatase Kit (#P0753, NEB) was employed according to manufacturer's instructions to confirm the specificity of phosphorylated antibodies. Briefly 100 μl of control solution (10 μl 10x buffer, 10 μl 10x $MnCl_2$ in 80 μl nuclease-free water) or Lambda phosphatase solution (10 μl 10x buffer, 10 μl 10x $MnCl_2$, 4 μl Lambda enzyme in 76 μl nuclease-free water) was applied to control slides following the peroxidase block. Slides were covered in paraffin to prevent evaporation, incubated at 37°C for 2 h and washed 3x 5 min in the wash buffer before resuming the original protocol. Treating sections with Lambda phosphatase removes all phosphate groups at serine, threonine and tyrosine residues.

### 2.4.1 Primary antibodies

Primary antibodies employed are listed in Table 2.3 which indicates the supplier, concentration and protocol required. Primary (and secondary) antibody dilutions were prepared in 10% normal serum diluted in the wash buffer (unless stated otherwise).

**Table 2.3 Primary antibodies**

| Antibody | Host | Supplier | Dilution | Method |
|---|---|---|---|---|
| p-Akt (Ser 473) | Rabbit | Cell Signalling Technology #9277 | 1:50 | 2 |
| p-AMPK (Thr 172) | Rabbit | Cell Signalling Technology #2531 | 1:50 | 2 |
| Androgen Receptor | Rabbit | Labvision NeoMarkers #RB-1358 | 1:100 | 1 |
| β-catenin | Mouse | Transduction Laboratories #C19220 | 1:200 | 6 |
| Caspase-3 | Rabbit | R&D #AF835 | 1:750 | 1 |
| CD44 | Rat | Pharmingen #550538 | 1:50 | 4 |
| Chromogranin A/B | Rabbit | Abcam #ab8205 | 1:100 | 1 |
| CK2α | Rabbit | QED Bioscience Inc #11040-25 | 1:300 | 2 |
| COX2 | Rabbit | Labvision Neomarkers #RB-9072 | 1:200 | 2 |
| E-cadherin | Mouse | Transduction Laboratories #610182 | 1:100 | 4 |
| p-ERK1/2 (Thr202/Tyr204) | Rabbit | Cell Signalling Technology #4376 | 1:100 | 2 |
| Foxa1 | Mouse | Seven Hills Bioreagents #2F83 | 1:800 | 4 |
| p-Gsk3β (Ser9) | Rabbit | Cell Signalling Technology #9336 | 1:50 | 2 |
| Keratin 5 | Rabbit | Covance #PRB-160P | 1:1000 | 2 |
| Keratin 8 | Chicken | Abcam #ab14053 | 1:500 | 5 |
| Keratin 14 | Rabbit | Covance #PRB-155P | 1:500 | 2 |
| Keratin 18 | Mouse | Progen, #61525 | 1:50 | 4 |
| Ki-67 | Mouse | Vector Laboratories #VP-K452 | 1:20 | 4 |
| p63 | Mouse | Neomarkers #MS-1081 | 1:50 | 3 |
| p-MEK1/2 (Ser221) | Rabbit | Cell Signalling Technology #2338 | 1:75 | 2 |
| p-mTOR (Ser2448) | Rabbit | Cell Signalling Technology #2976 | 1:100 | 2 |
| c-Myc | Rabbit | Santa Cruz #SC-764 | 1:200 | 7 |
| p-PDK1 (Ser241) | Rabbit | Abcam #ab32800 | 1:100 | 2 |
| Pten | Rabbit | Cell Signalling Technology #9559 | 1:100 | 2 |
| p-PTEN (S380/T382/383) | Rabbit | Cell Signalling Technology #9554 | 1:25 | 2 |
| p-Rps6 (Ser240/244) | Rabbit | Cell Signalling Technology #2215 | 1:200 | 2 |
| p-S6K (Thr 421/424) | Rabbit | Cell Signalling Technology #9204 | 1:200 | 2 |
| ZO-1 | Rabbit | Zymed, Invitrogen #40-2300 | 1:20 | 8 |

### 2.4.2 Immunohistochemistry protocols

**Method 1: Rabbit polyclonal primary antibodies (Envision)**

Antigen unmasking was achieved by microwaving for 10 min in 1x citrate buffer (pH 6.0) (#AP-9003-500, Labvision). Slides were cooled for 30 min, rinsed in $dH_2O$ and incubated for 20 min in $H_2O_2$ solution (Rabbit Envision Kit, DAKO #K4010) to block

endogenous peroxidase activity. Slides were washed (3x 5 min) in TBS/Tween (0.1%) and incubated in 10% normal goat serum (DAKO) for 40 min to eliminate background staining. The rabbit polyclonal primary antibody was added for 2 h at room temperature and any excess washed off TBS/Tween (0.1%). Detection of the primary antibody was achieved by the horseradish peroxidase (HRP)-conjugated polymer (Rabbit Envision Kit, DAKO) for 1 hour and washed in TBS/Tween (0.1%) to remove excess polymer. HRP was detected by applying Diaminobenzidine (DAB) solution (#K3467, DAKO) according to manufacturer's instructions for 2-10 minutes until a brown product developed. Slides were counterstained with Meyer's haematoxylin for 30-60 sec, rinsed in running water and dehydrated before being mounted with DPX.

**Method 2: Rabbit polyclonal (Biotin)**

Antigen unmasking was achieved by microwaving for 15 min in 1x citrate buffer (pH 6.0) (#AP-9003-500, Labvision). Slides were cooled for 30 min prior to blocking endogenous peroxidase activity with 1.5% $H_2O_2$ (Sigma) in $dH_2O$ for 20 min. Sections were washed in TBS/Tween (0.1%) and incubated in 10% normal goat serum (DAKO) for 40 min to eliminate background staining. The rabbit polyclonal primary antibody was applied o/n at 4°C and slides washed thoroughly in TBS/Tween (0.1%) the next day. To detect the primary antibody, the goat-anti-rabbit biotin conjugated secondary antibody (#E0432, DAKO) was applied, 1:200 for 30 min. Slides were washed in TBS/Tween (0.1%) and Biotin-HRP labelled for 30 min using the Vectastain ABC-HRP conjugate (Standard Vectastain Kit, #PK6100). Sections were washed in TBS/Tween (0.1%) and stained with DAB solution (#K3467, DAKO) according to the manufacturer's instructions to produce a brown product. Slides were counterstained with Meyer's haematoxylin for 30-60 sec, rinsed in running water and dehydrated before being mounted with DPX.

**Method 3: Mouse monoclonal (Envision)**

Antigen unmasking was achieved by microwaving for 10 min in 1x citrate buffer (pH 6.0) (#AP-9003-500, Labvision). Slides were cooled for 30 min, rinsed in $dH_2O$ and incubated for 20 min using the Mouse Envision Kit $H_2O_2$ solution (DAKO #K4006) according to manufacturer's instructions. Slides were washed (3x 5 min) in TBS/Tween (0.1%) and incubated in 10% normal rabbit serum for 40 min to eliminate background staining prior to incubating with the mouse monoclonal primary antibody for 2 h at room

temperature. To detect the primary antibody, sections were incubated with the HRP-conjugated polymer (Mouse Envision Kit) for 1 h and washed in TBS/Tween (0.1%). Sections were stained with DAB solution (#K3467, DAKO) according to the manufacturer's instructions to produce a brown product. Slides were counterstained with Meyer's haematoxylin for 30-60 sec, rinsed in running water and dehydrated before being mounted with DPX.

**Method 4: Mouse/Rat polyclonal (Biotin)**

Antigen unmasking was achieved by microwaving for 15 min in 1x citrate buffer (pH 6.0) (#AP-9003-500, Labvision). Slides were cooled for 30 min prior to endogenous peroxidase activity blocking with 1.5% $H_2O_2$ (Sigma) in $dH_2O$ for 20 min. Sections were washed in TBS/Tween (0.1%) and incubated in 10% normal rabbit serum (DAKO) for 40 min to eliminate background staining. The mouse primary antibody (or Rat for anti-CD44) was applied o/n at 4°C and slides were washed thoroughly in TBS/Tween (0.1%) the next day. To detect the primary antibody, slides were incubated with the rabbit-anti-mouse biotin conjugated secondary antibody (#E0464, DAKO) or for CD44, the rabbit-anti-rat (#E0468, DAKO) biotin conjugated secondary antibody, 1:200 for 30 min. Sections were washed in TBS/Tween (0.1%) and Biotin-HRP labelled by incubating with the Vectastain ABC-HRP conjugate (Standard Vectastain Kit, #PK6100) for 30 min. Sections were washed in TBS/Tween (0.1%) and stained with DAB solution (#K3467, DAKO) according to the manufacturer's instructions to produce a brown product. Slides were counterstained with Meyer's haematoxylin for 30-60 sec, rinsed in running water and dehydrated before being mounted with DPX.

**Method 5: Chicken polyclonal (Biotin)**

Antigen unmasking was achieved by microwaving for 15 min in 1x citrate buffer (pH 6.0) (#AP-9003-500, Labvision). Slides were cooled for 30 min prior to endogenous peroxidase activity blocking with 1.5% $H_2O_2$ (Sigma) in $dH_2O$ for 20 min. Sections were washed in TBS/Tween (0.1%) and incubated in 10% normal rabbit serum (DAKO) for 40 min to eliminate background staining. The chicken polyclonal primary antibody was applied o/n at 4°C and slides were washed thoroughly in TBS/Tween (0.1%) the next day. To detect the primary antibody, slides were incubated with the rabbit-anti-chicken (#12-341, Upstate) HRP-conjugated secondary antibody, 1:200 for 30 min prior washing in TBS/Tween (0.1%)

and stained with DAB solution (#K3467, DAKO) according to the manufacturer's instructions to produce a brown product. Slides were counterstained with Meyer's haematoxylin for 30-60 sec, rinsed in running water and dehydrated before being mounted with DPX.

**Method 6: β-catenin immunohistochemistry**

To remove endogenous peroxidase activity, slides were incubated with fresh 1.5% $H_2O_2$ (Sigma) prepared in peroxidase block solution (2.08 g citric acid, 5.38 g DiSodium Hydrogen Phosphate-2-hydrate and 0.5 g Sodium Azide in 500 ml $dH_2O$) for 40 min and washed in PBS. Antigen unmasking was achieved by boiling for 50 min in 30 ml antigen retrieval solution (24.2 g Tris and 1.86 g EDTA in 100 ml $dH_2O$, pH 8) diluted in 1.5 L $dH_2O$. Slides were cooled for 1 h hour and washed in PBS. To prevent endogenous staining, sections were blocked for 30 min in 1% BSA (Sigma, #A4503) in PBS. Slides were incubated o/n at 4°C with the mouse monoclonal β-catenin antibody (diluted 1:300 in 1% BSA). Sections were washed in PBS and incubated with the HRP-conjugated polymer (Mouse Envision Kit, DAKO #K4006) for 1 h to detect the primary antibody, washed in PBS and DAB solution (#K3467, DAKO) applied for 1-2 min according to the manufacturer's instructions to detect positive cells. Sections were counterstained with haematoxylin for 30-60 sec, rinsed in running water, dehydrated and mounted with DPX.

**Method 7: c-Myc immunohistochemistry**

To remove endogenous peroxidase activity, slides were incubated with fresh 1.5% $H_2O_2$ (Sigma) prepared in peroxidase block solution (2.08 g citric acid, 5.38 g DiSodium Hydrogen Phosphate-2-hydrate and 0.5 g Sodium Azide in 500 ml $dH_2O$) for 40 min and washed in tap water. Antigen unmasking was achieved by microwaving sections for 15 min in antigen retrieval buffer (1.21 g Tris and 0.186 g EDTA in I L $dH_2O$, pH 9). Slides were cooled for 1 h hour and washed in tap water. To prevent endogenous staining, sections were blocked for 30 min in 1% BSA (Sigma, #A4503) in PBS. Slides were incubated o/n at 4°C with the rabbit polyclonal c-Myc antibody (diluted 1:200 in 1% BSA/PBS). Sections were washed in tap water and incubated with the HRP-conjugated secondary antibody, anti-rabbit Powervision solution (Immunotech) for 30 min to detect the primary antibody, washed in tap water and DAB solution (#K3467, DAKO) applied for 1-2 min according to the

manufacturer's instructions to detect positive cells. Sections were counterstained with haematoxylin for 30-60 sec, rinsed in running water, dehydrated and mounted with DPX.

**Method 8: ZO-1 immunofluorescence**

Cryosections (10-15 μm thick) were warmed to room temperature and washed in PBS to remove the OCT embedding medium. Slides were treated with 3 drops of "Digest-All" pepsin solution (Zymed #00-3009) and covered with strips of paraffin to prevent evaporation during incubation at 37°C for 5-10 min. Slides were washed in PBS and incubated in 10% normal goat serum (DAKO) for 30 min to prevent endogenous staining. The ZO-1 (N-term) rabbit polyclonal primary antibody (Zymed, Invitrogen #40-2300) was applied at 1:20 dilution o/n at 4°C. Sections were washed in PBS and incubated with 1:200 AlexaFluor-488 goat-anti-rabbit secondary antibody (Molecular probes #A24922) for 1 h in the dark. Sections were washed in PBS and mounted with Vectashield HardSet + DAPI mounting medium (Vector Laboratories #H-1500). Using a confocal microscope DAPI staining of nuclei appeared blue while ZO-1 positive tight-junctions were green.

### 2.4.3 Scoring

The percentage of p63, Ki-67, Foxa1 and AR positive cells (detected by immunohistochemistry) was calculated by counting the total positive and negative cells from 20 acini, or in tumours 20 random 2500 $\mu m^2$ regions (determined by a grid using the "AnalySIS" software (Olympus Soft Imaging System GMBH) at 40x magnification). A minimum of 1000 cells/mouse were counted (n = 3). The average score for each genotype at each time point underwent statistical analysis using the non-parametric Mann Whitney test (95% confidence interval) to assess any significant difference between genotypes. P-values $<0.05$ represent a significant difference between data sets. Statistical analysis was carried out using MiniTab software.

A running mean is the ongoing calculation of a statistic, using progressively more of the available data values. This process starts with a single value and continues to include all data values in the order that they are supplied. An example of a running mean chart is shown in figure 2.1, where the percentage of proliferative cells has been determined by counting Ki-67 positive and negative cells in *wild-type* adult prostate acini (n = 20 per mouse). The chart indicates scoring 20 acini is sufficient to generate a stabilised estimate of the percentage of Ki-67 positive cells within the prostate.

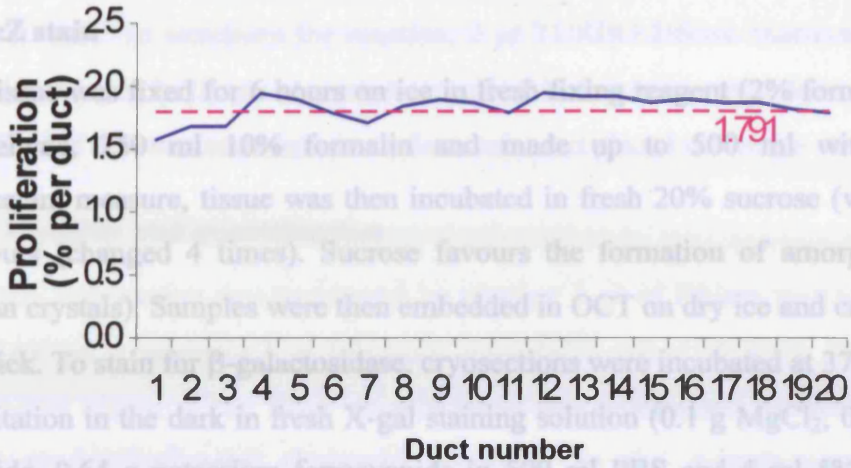


**Figure 2.1: Running mean plot of Ki-67 positive cells in *wild-type* adult prostate epithelium.** Plot demonstrates the generation of a running mean where the percentage of proliferating cells labelled with Ki-67 were counted in 20 difference acini of an adult *wild-type* male. The running percentage of Ki-67 positive cells is shown in blue, while the average number of Ki-67 positive cells is in pink, representing 1.791%.

## 2.5 Histological tissue stains

Staining procedures were performed following de-waxing and rehydration of formalin-fixed, paraffin-embedded sections (unless stated otherwise). Once staining procedures were completed, slides were rinsed in running water for 5 min and dehydrated and cleared in xylene prior to mounting in DPX (see section 2.4).

### 2.5.1 Cresyl violet acetate stain

Cresyl violet acetate solution was prepared by dissolving cresyl violet powder (Sigma #C1791) 1% w/v in ACS grade 100% EtOH and left at room temperature under constant agitation for 3 hours or overnight. The solution was filtered through a 0.2 µM filter unit prior to use. Frozen sections were rinsed in nuclease-free water to remove OCT embedding medium and stained for 20 sec in cresyl violet acetate solution. Slides were dehydrated by rinsing for 1 min in 70% EtOH and 1 min in 100% EtOH. Stained sections were used immediately for LCMD where the nuclei appear blue/dark purple.

### 2.5.2 Haematoxylin and eosin stain

For histological analysis, slides were immersed in Meyer's Haematoxylin (Lamb, #170-D) for 1 min and rinsed in water for 5 min, prior to being counterstained in 1% aqueous Eosin (Lamb, 100-D) for 30 sec.

### 2.5.3 LacZ stain

Tissue was fixed for 6 hours on ice in fresh fixing reagent (2% formaldehyde, 0.2% glutaraldehyde, 250 ml 10% formalin and made up to 500 ml with PBS). As a cryoprotectant measure, tissue was then incubated in fresh 20% sucrose (w/v) solution for 24-28 hours (changed 4 times). Sucrose favours the formation of amorphous ice (solid rather than crystals). Samples were then embedded in OCT on dry ice and cryosectioned 10-15 μm thick. To stain for β-galactosidase, cryosections were incubated at 37°C for 1-3 hours under agitation in the dark in fresh X-gal staining solution (0.1 g $MgCl_2$, 0.48 g potassium ferricyanide, 0.64 g potassium ferrocyanide in 500 ml PBS and 4 ml 5% X-gal in DMF (Promega) was added before use). Sections were washed in PBS and lightly counterstained with 0.1% nuclear fast red (see section 2.5.1) for 1 min.

## 2.6 Harvesting RNA and qRT-PCR

### 2.6.1 RNA isolation

Tissue was harvested, snap-frozen in liquid nitrogen and stored at -80°C for short-term storage or placed in 3 ml RNA Later solution (Sigma #R0901) at -80°C for long-term storage. Samples were thawed in 2 ml lysing matrix tubes (Q-Biogene #6913-500) containing 1 ml TRIzol reagent (Invitrogen #15596-026). This reagent contains lysis buffer and phenol to destroy proteins. Tissue was homogenised at 5600 rpm for 2x 25 sec using the Stretton Scientific Homogeniser and then centrifuged (13,000 rpm for 10 min at 4°C). The S/N was transferred to 200 μl chloroform and incubated on ice for 15 min to remove the phenol. Samples were then centrifuged (13,000 rpm for 15 min at 4°C) and the S/N transferred to 600 μl propan-2-ol and incubated o/n at 4°C to precipitate the RNA. Following precipitation, samples were centrifuged (13,000 rpm for 15 min at 4°C) and the pellet washed with 500 μl chilled 100% EtOH. Samples were centrifuged (13,000 rpm for 10 min at 4°C) and the S/N discarded. The pellet was air-dried for 5 min, re-suspended in 50-100 μl nuclease-free water by heating at 65°C for 10 min. Samples were placed immediately on ice or at -80°C for long-term storage.

### 2.6.2 DNase treatment

To eliminate DNA contamination, DNAse treatment was carried out using the Ambion TURBO kit (#1907) according to the manufacturer's instructions. Briefly, 20 μl of total RNA was mixed with 2 μl TURBO buffer and 1 μl DNase enzyme and incubated at

37°C for 30 min. To terminate the reaction, 2 µl TURBO DNase Inactivator solution was added and incubated for 2 min at room temperature before being spun down (10,000 rpm for 2 min). 20 µl of S/N was transferred to a fresh tube and placed on ice (or stored at 4°C).

### 2.6.3 RNA quality and quantification

RNA degradation was monitored by running 1 µl of DNase treated RNA on a 1% agarose TAE gel (containing 1 µl Ethidium bromide/25 ml) at 50 V for 30 min in 1x TAE running buffer (figure 2.2a). RNA quantification was determined by using the Nanodrop ND-1000 spectrophotometer (Labtech) according to the manufacturer's instructions. Samples were discarded if the 260/280 ratio was not within the range 1.8-2.0 (figure 2.2b).

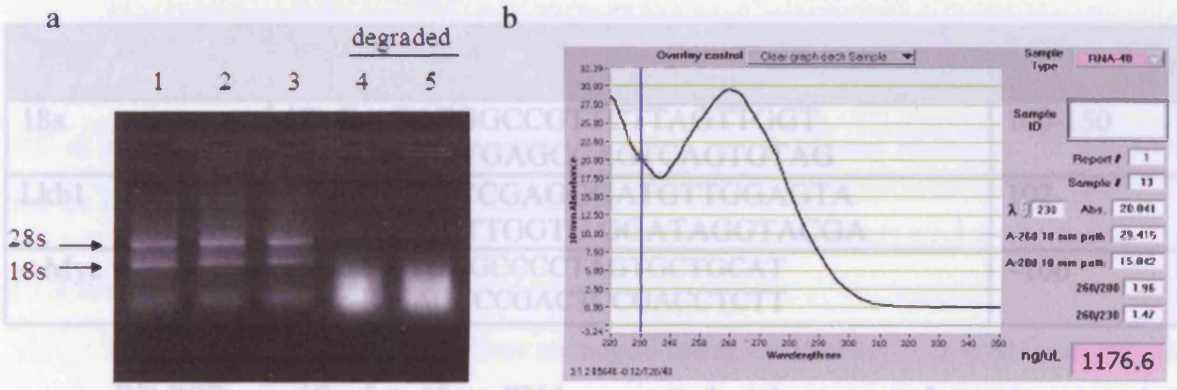


**Figure 2.2: Determining the quality of RNA samples.** Samples were run on a 1% TAE gel to check for degradation (a). Lanes 1-3 represent good quality RNA while lanes 4 and 5 show degraded RNA. Mammalian 28S and 18S rRNAs are approximately 5 kb and 2kb in size. The 260/280 ratio was checked using the Nanodrop ND-1000 spectrophotometer (b). Any samples that were either degraded on the gel or were not within the 260/280 ratio range of 1.8-2.0 were discarded.

### 2.6.4 Reverse transcription

To convert RNA into cDNA (1µg/20µl) reverse transcription was carried out using the Invitrogen Superscript II Kit (#18064071, Invitrogen). Briefly, samples of 1 µg RNA in 9 µl nuclease-free water (Sigma) were prepared and heated in a thermocycler at 70°C for 10 min. Samples were cooled to 42°C before adding 10 µl of master mix (2 µl DNp6 (100 ng/µl), 4 µl 5x Buffer, 2 µl 0.1 M DTT, 0.4 µl 25 mM dNTPs (Sigma), 0.5 µl RNaseIN Plus (Promega, #N2611), 1.1 µl $dH_2O$). Samples were incubated for 2-3 min at 42°C, placed on ice whilst adding 1 µl Superscript II and incubated at 42 °C for 1 h. To inactivate the reaction, samples were heated to 70°C for 15 min and placed on ice (or stored at -20°C) until use. Controls were prepared in a similar manner except the master mix added

contained 2.1 µl $H_2O$ and no Superscript II was added. To check for contamination, controls underwent normal PCR and were run on a 2% TBE agarose gel.

### 2.6.5 qRT-PCR

Duplicate qRT-PCR reactions were performed using the Chromo4 real time detector (MJ Research) and the DyNAmo HS SYBR Green qPCR kit (#F-410L, GRI). Primers were designed to exon-exon boundaries (to eliminate DNA contamination) using "Primer 3" online software and their specificity was checked using an "Ensembl" blast search. Sequences are shown in Table 2.4.

**Table 2.4: qRT-PCR primers**

| Primer Name | Sequence (5'-3') | Product size (bp) |
|---|---|---|
| 18s | 18s-F = CATGGCCGTTCTTAGTTGGT<br>18s-R = CGCTGAGCCAGTCAGTGTAG | 100-150 |
| Lkb1 | Lkb1-F = CTCCGAGGGATGTTGGAGTA<br>Lkb1-R = GCTTGGTG GGATAGGTACGA | 102 |
| c-Myc | cMyc-F = TGAGCCCCTAGTGCTGCAT<br>cMyc-R = AGCCCGACTCCGACCTCTT | ~100 |

qRT-PCR specific for *18s* mRNA was employed as an endogenous control to normalise for differences in RNA quantites between samples. 2.5 µl of forward and reverse primer mixes (10 µM each) were added into the 96-well plate (white) and 22.5 µl of the master-mix added (7 µl cDNA (1 µg/200 µl), 3 µl nuclease-free water and 12.5 µl DyNAmo Hot Start SYBR green (#F-410L, GRI). qRT-PCR was run at 95°C for 15 min, 40 cycles of 95°C for 30 sec, 60°C for 30 sec, 72°C for 30 sec and 82°C for 30 sec. The 82°C step helps to eliminate primer-dimer formation. A melting curve was recorded at 53 - 95°C every 0.5°C to check for the presence of primer dimers and to confirm all samples generated the same product (i.e. same Tm). Fold change between samples was calculated using the $2^{\wedge-\Delta\Delta Ct}$ method previously described (Livak and Schmittgen, 2001). To double-check for contamination and primer-dimers, 5 µl of the qRT-PCR product was also run on a 2% agarose TBE gel.

## 2.7 Electron microscopy

### 2.7.1 Preparation of electron microscopy samples

Electron Microscopy was performed with the assistance of Antony Hann (Electron Microscopy Service, Cardiff University) as described previously (Maunsbach and Bjorn, 1999). Briefly, tissue was fixed for 2 h at 4°C in 2.5% (v/v) glutaraldehyde buffered with 0.1 M Sorensen phosphate buffer (pH 7.4). Samples were washed 2x 10 minutes in PBS to remove excess glutaraldehyde and post-fixed for 1 h at 4°C in 1% osmium tetroxide solution (1% osmium tetroxide in 0.1 M phosphate buffer). Infiltration occurred o/n in 1:1 mixture of propylene oxide and resin araldite CY212 and samples were embedded for 2 days at 60°C in pure araldite. Samples were washed 5 min in PBS and 4x 15 min $ddH_2O$ to remove free osmium. To stain samples, they were incubated for 45 min in 0.5% uranyl acetate (1 ml 2% uranyl acetate in 3 ml $dH_2O$) and washed in $ddH_2O$ prior to dehydrating at 4°C in a graded series of ethanol concentrations (30, 50, 70, 90 and 100%) for 15 min each and 2x 10 min changes of pure propylene oxide.

### 2.7.2 Electron microscopy

The resin polymerised block was sectioned using the Reichert Ultracut E microtome (Leica, UK) to produce 1.5 μm thick sections and stained with toluidine blue (1 g toluidine blue and 1 g borax in 100 ml $dH_2O$, filtered prior to use). Slides were rinsed with water, dried on a hot plate and viewed under a light microscope. If the section was of interest then samples were prepared for electron microscopy.

Sections were cut 0.9 μm thick using the Reichert Ultracut E microtome (Leica, UK) and collected on a pioloform-coated copper grid. Sections were stained with 2% uranyl acetate (2 g uranyl acetate in 100 ml $dH_2O$) for 10 min and then 5 min in Reynold lead citrate (prepared by shaking in 1.33 g lead nitrate and 1.76 g sodium citrate in 30 ml $CO_2$-free $dH_2O$ for 30 minutes, adding 8 ml of 1M NaOH and 12 ml of $dH_2O$ and spinning down before use). Samples were then examined using a transmission electron microscope (Phillips EM 208).

## 2.8 Laser Capture Microdissection (LCMD)

### 2.8.1 Tissue preparation for LCMD

Snap-frozen tissue was embedded in OCT on dry ice and cryosectioned (15 μm thick) onto polyethylene naphthol membrane-coated glass slides (PALM, #415101-4401-000) and air-dried before proceeding (or stored at -80°C). Slides were washed in nuclease-free water for 1 min to remove the OCT and stained for 15 sec with 1% cresyl violet acetate (section 2.5.2). Slides were quickly dehydrated in 75% EtOH and 100% EtOH for 1 min each.

### 2.8.2 DNA isolation of LCMD tissue

The total time taken to complete LCMD for each sample was restricted to no more than 30 min (to prevent heat degradation of the tissue) using the PALM laser capture microdissection equipment (PALM, Germany). Approximately 1-1.5 x $10^6$ $\mu m^2$ of target tissue was catapulted into a 0.2 ml PALM adhesive cap (#415101-4400-245) and visualised using a dissecting microscope before isolating DNA with the QIAamp DNA Micro Kit (#56304, Qiagen) according to manufacturer's instructions. Briefly, samples were incubated o/n at room temperature upside down with 30 μl ATL lysis buffer and 10 μl Proteinase K. Samples were spun in a microcentrifuge (max. speed for 1 min) and 40 μl AL buffer and 40 μl 100% EtOH added. Samples were spun (max. speed for 5-10 sec) and incubated at 65°C in a water bath for 10 min. Samples were spun (max. speed for 1 min) and transferred to a spin column and spun (13,000 rpm for 1 min), retaining the DNA on the column membrane. The column membrane was washed with 500 μl AW1 buffer and tubes spun (13,000 rpm for 1 min) and re-washed with 500 μl AW2 buffer. Samples were centrifuged twice more (13,000 rpm, 3 min) and DNA collected into a fresh 1.5 ml tube by incubating the membrane with 20 μl nuclease-free water for 10 min and centrifuging (13,000 rpm for 2 min). DNA (2 μl) was quantified using the Nanodrop ND-1000 spectrophotometer (Labtech) and concentrations ranged between 5-25 ng/μl.

### 2.8.3 DNA amplification and ethanol precipitation

To amplify LCMD DNA to a quantity suitable for PCR, the Genomiphi DNA amplification kit from Amersham (#25-6600-00) was employed according to the manufacturer's instructions. Briefly, 1-2 μl DNA and 9 μl sample buffer was incubated for 3 min at 95°C in a water bath and placed on ice for 2 h. 1 μl enzyme and 9 μl reaction buffer

was added to each sample and incubated in a thermocycler at 30°C for 16-18 hours followed by an inactivation step at 65°C for 10 min. DNA was ethanol precipitated (recommended by Amersham) by adding 20 µl nuclease-free water, 4 µl clean up buffer (0.5 ml 1.5 M NaAc, pH 9.5 and 0.5 ml 0.5 M EDTA) and 100 µl 100% EtOH. Samples were spun (12,000 rpm for 15 min), the S/N discarded and the pellet washed with 400 µl 70% EtOH. Samples were spun (12,000 rpm for 2 min), the S/N removed and the pellet air-dried for 5 min before re-suspending in 20 µl nuclease-free water.

### 2.8.4 LCMD PCR

The log phase for each primer set was determined by running PCRs at 15, 20, 25, 30 and 35 amplification cycles, running the products on a 2% agarose TBE gel and checking for band saturation. LCMD DNA was quantified using the Nanodrop ND-1000 spectrophotometer (Labtech) and 50 ng/µl dilutions prepared. PCR reactions were carried out according to section 2.2.2, except the cycle number for each primer set was reduced to 25 cycles (confirmed to be within the log phase). To calculate the recombination percentage within the prostate, PCR products were run on a 2% gel and the intensity of the bands (n = 6) were measured using densitometry software (Bio-Rad).

## 2.9 *In situ* hybridisation

### 2.9.1 Generation of the probe

The *Lkb1* full length cDNA clone inserted in the *pYX-Asc* vector (1.69 kb) was obtained from RZPD, Germany (#IRAVp968E05123D). The clone was cultured in *E.coli* strain DH10B TonA on selective agar containing 0.05 mg/ml ampicillin. DNA was purified using the QIAprep Spin Mini prep kit (Qiagen, #27104) according to manufacturer's instructions. To confirm plasmid orientation and to verify construct validity DNA was sequenced from both T3 and T7 RNA polymerase binding sites by the DNA Sequencing Core (Molecular Biology Unit, Cardiff University. The T3 primer (5'-AARRAACCCTCACTAAAGGG-3') and the T7 primer (5'-TAATACGACTCACTAA AGGG-3') were provided by Dr. Rosalind John (Cardiff University). Sequencing determined the 5'-end of the *Lkb1* insert begins at T7 and confirmed 100% identity of the *Lkb1* insert with the NCBI Sequence (accession number BC052379). Single restriction digests using *Eco*RI (#R0101S, NEB) and *Not*I (#R0189S, NEB) determined the linear plasmid to be 3.2 kb and a double digest revealed the *Lkb1* insert was 1.6 kb by running the

samples on a 1% agarose TBE gel. Restriction digests were carried out in a thermocycler according to the manufacturer's instructions at 37°C o/n. Large quantities of the *Lkb1* insert were acquired by using the HiPure Plasmid DNA kit (#K2100-03, Invitrogen) according to the manufacturer's instructions. To generate templates, 20 µg of the purified DNA was linearised with either *Eco*R1 (Anti-sense) or *Not*1 (Sense) and DNA phenol chloroform extracted and ethanol precipitated. To verify linearization, 0.5 µl was run on a 1% agarose TBE gel (expected size = 3.2 kb). Anti-sense and sense RNA probes were then obtained by *in vitro* transcription of the template (1 µg/µl) using T3 (anti-sense) and T7 (sense) RNA polymerases (#1031163 and #881767, Roche). Probes were DNase treated and labelled using the DIG RNA labelling kit (BM 1175025, Roche) according to the manufacturer's instructions. Probes were run on a 1% agarose TBE gel to ensure the correct size and to check that degradation had not occurred. Aliquots of 10 µl were stored at -80°C in hybridisation buffer (2.5 ml 20x SSC (Sigma, S6639), 5 ml formamide (Sigma, #47671), 0.5 ml 20% SDS, 50 µl 10 mg/ml Heparin (Sigma, #H4784), 50 µl 10 mg/ml calf liver tRNA (Sigma, R4752-100N) in 10 ml DEPC $H_2O$).

### 2.9.2 *In situ* hybridisation

*In situ* hybridisation was performed in glassware baked o/n at 175°C and using DEPC-treated $H_2O$ (RNase-free) for preparation of all solutions as described previously (Kikyo *et al.*, 1997). Briefly, 5-10 µm thick sections from formalin-fixed, paraffin-embedded sections (stored at 4°C) were de-waxed in 2x 10 min fresh xylene and re-hydrated in a graded series of ethanol (2x 100, 95, 85, 75, 50 and 30%) for 1 min each. Sections were washed with 1x saline and 1x PBS, 5 min each. To inactivate endogenous alkaline phosphatase activity, sections were incubated in 6% hydrogen peroxidase block (25 ml 10x PBS, 50 ml 30% $H_2O_2$ and 175 ml DEPC $H_2O$) for 30 min. Sections were then fixed on ice for 15 min in 4% paraformaldehyde, washed with 1x PBS and treated with Proteinase K solution (12.5 ml 1 M Tris pH8, 2.5 ml 0.5 M EDTA pH8, 250 µl 20 mg/ml Proteinase K in 250 ml DEPC $H_2O$) for 5 min to increase the signal. Slides were post-fixed in 4% paraformaldehyde for 5 min and to prevent non-specific binding and incubated for 10 min in TEA HCl/acetic anhydride solution (25 ml 1 M Triethanolamine hydrochloride (Sigma), 225 ml DEPC $H_2O$ and 0.63 ml acetic anhydride (Sigma)). Slides were washed in 1x PBS and 1x saline (5 min each) and de-hydrated in a graded series of EtOH (30, 50, 70, 85, 95 and 2x 100%), 30 sec each. Hybridisation buffer was heated to 80°C and the probe added

immediately before use (1:50). Slides were air-dried for 30 min and hybridized with 200 µl of probe solution per slide o/n at 65°C in a water bath. Slides were covered with parafilm to prevent evaporation and placed in an air-tight container to prevent them from drying out. Sections were washed 1x 15 min in 5x SSC to remove excess probe and then washed 3x 30 min at 65°C in solution 1 (200 ml formamide, 100 ml 20x SSC, 40 ml 10% SDS and 60 ml DEPC $H_2O$). Slides were incubated at room temperature in solution II (200 ml formamide, 10 ml 1 M TrisHCl, pH7.5, 1 ml Tween 20 made up to 1 L with DEPC $H_2O$) 3x 10 min, 1x 45 min at 37°C (containing 10 mg/ml RNase A) and 1x 10 min at room temperature. Slides were washed with solution III (200 ml formamide, 40 ml 20x SSC and 160 ml DEPC $H_2O$) 2x 30 min at 65°C and 2x 5 min PBS washes prior to blocking with 10% sheep serum (X0503, DAKO) at room temperature for 3 h. Meanwhile, the alkaline phosphatase-conjugated anti-digoxigenin (DIG) antibody (#11327723, Roche), 1:500, was pre-absorbed at 4°C for 3 h (in 500 µl 1x PBS containing 3 mg embryo powder and 10 µl 50% sheep serum) to prevent non-specific binding and spun at 4°C for 5 min, 14,000 rpm. The S/N was transferred to a fresh tube and made up to 2 ml with 1% sheep serum. Slides were incubated with 200 µl of the anti-DIG antibody overnight at 4°C in the dark. Slides were washed 3x 5 min and 3x 30 min in PBT (1x PBS in DEPC $H_2O$ and 0.1% Tween 20) and then preconditioned with 3x 5 min washes in NTMT solution (5 ml 5 M NaCl, 25 ml 1 M TrisHCl, pH9.5, 12.5 ml 1 M $MgCl_2$, 0.25 ml Tween 20, 0.25 ml 2 M Levamisole (Sigma, #L9756) made up to 250 ml with DEPC $H_2O$). Levamisole acts to remove endogenous alkaline phosphatase activity. Alkaline phosphatase activity was detected by using BM purple AP (Roche) according to the manufacturer's instructions (for 8-24 hrs in the dark) until a purple colour developed. Slides were then washed 3x 5 min in PBT, 30 min in DEPC $H_2O$ and lightly counterstained using Eosin. Sections were air-dried and mounted using the aqueous mounting medium VectaMount AQ (#H5501, Vector Labs).

# Chapter 3: Lkb1 deficiency causes prostate neoplasia

## 3.1 Introduction

### 3.1.1 LKB1 is expressed at low levels in the prostate

LKB1 (STK11) is a 60 kDa serine threonine kinase that was originally identified as a tumour suppressor in Peutz-Jeghers Syndrome (PJS) (Alessi *et al.*, 2006). Multiple germline mutations of *LKB1* that abrogate enzymatic function in PJS patients predispose hamartomas in the small intestine and a number of extra-intestinal cancers including those of the reproductive system (Yoo *et al.*, 2002). Collins *et al* (2000) documented the expression of *Lkb1* mRNA in the mouse, illustrating the importance of this gene in a variety of different tissues. High *Lkb1* expression was detected in the liver, testis, skeletal muscle and small intestine, while a moderate level of *Lkb1* mRNA transcript was also detected in the prostate (figure 3.1) (Collins *et al.*, 2000).

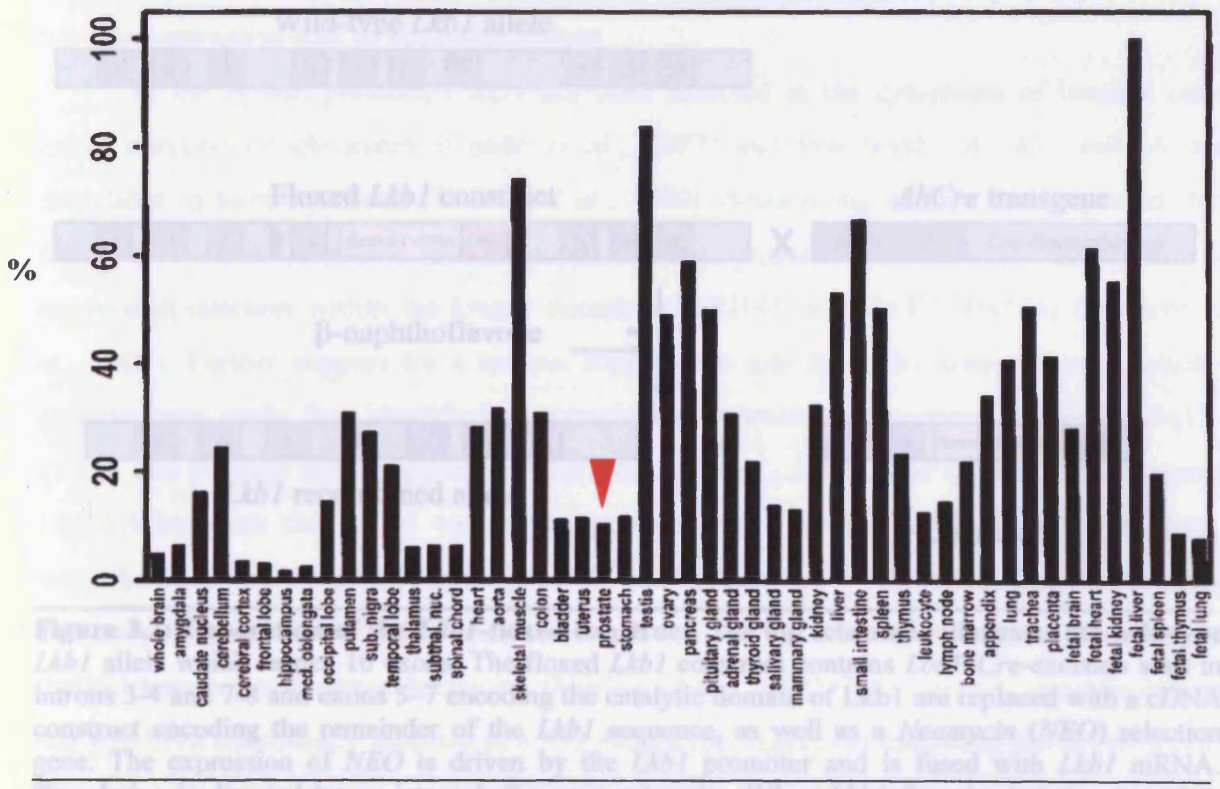


**Figure 3.1: *Lkb1* mRNA expression in mice.** This figure demonstrates adult and foetal mRNA levels of *Lkb1* normalised to foetal liver tissue (100%). An RNA master blot was probed with the *Lkb1* anti-sense probe and hybridization was observed in all tissues and brain regions examined, with the highest levels in skeletal muscle, testis, small intestine and foetal liver. Moderate *Lkb1* mRNA levels in the prostate (red arrow head). This figure was adapted from Collins *et al* (2000).

### 3.1.2 Derivation of *AhCre*$^{+}$*Lkb1*$^{fl/fl}$ mice to study Lkb1 function in the small intestine

To investigate the role of Lkb1 specifically within the small intestine, Shorning *et al* (2008, under review) exploited the *p450 Cyp1a1*-driven *Cre-Recombinase* transgene (termed *AhCre*), controlled by xenobiotic promoter induction (Ireland *et al.*, 2004), in conjunction with a *LoxP*-flanked (floxed) *Lkb1* construct (Sakamoto *et al.*, 2005) to generate *AhCre*$^{+}$*Lkb1*$^{fl/fl}$ mice (figure 3.2). Importantly, this system allows *Lkb1* to be monitored at several expression levels owing to the hypomorphic nature of the *Lkb1* floxed construct. Sakamoto *et al* (2005) assessed the hypomorphic nature of un-induced *Cre*$^{-}$*Lkb1*$^{fl/fl}$ mice to show that Lkb1 protein expression and activity is reduced 5-10 fold in the tissues analysed (testis, skeletal muscle, heart, liver and kidney). *Cre*$^{-}$*Lkb1*$^{+/fl}$ mice showed a 2-fold reduction in Lkb1 expression and activity (Sakamoto *et al.*, 2005). Shorning *et al* (2008, under review) determined that intestinal *Lkb1* transcript levels are 2-fold down in *Cre*$^{-}$*Lkb1*$^{fl/fl}$ mice and 30-fold down in *AhCre*$^{+}$*Lkb1*$^{fl/fl}$ mice following xenobiotic induction of the *Ah* (*Cyp1A1)* promoter compared to *wild-type* mice.

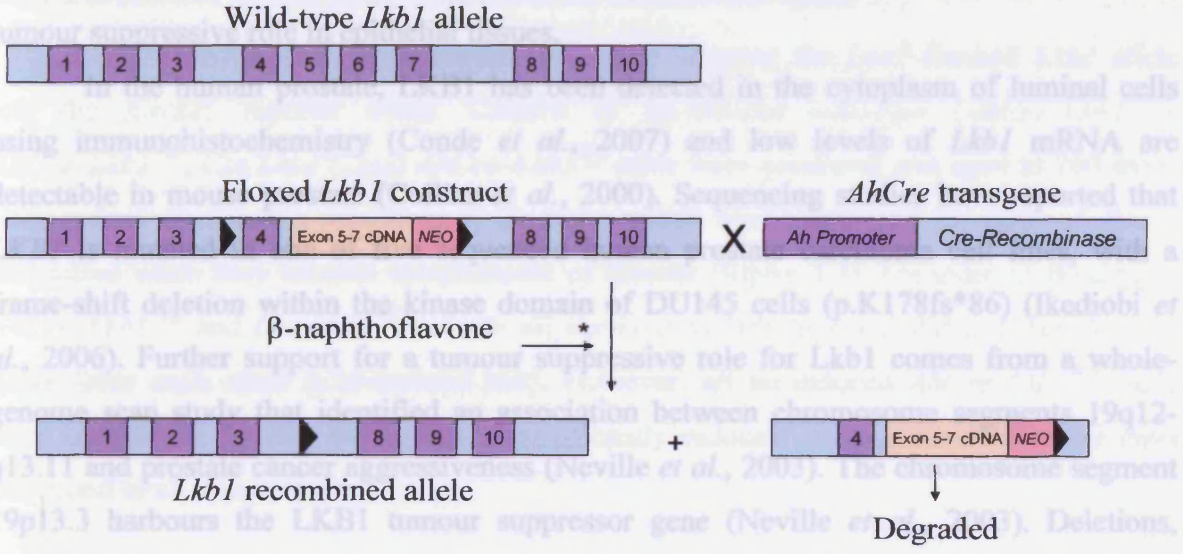


**Figure 3.2: Generation of the *Lkb1*-floxed construct.** The top schematic illustrates the wild-type *Lkb1* allele which carries 10 exons. The floxed *Lkb1* construct contains *LoxP Cre*-excision sites in introns 3-4 and 7-8 and exons 5–7 encoding the catalytic domain of Lkb1 are replaced with a cDNA construct encoding the remainder of the *Lkb1* sequence, as well as a *Neomycin* (*NEO*) selection gene. The expression of *NEO* is driven by the *Lkb1* promoter and is fused with *Lkb1* mRNA. Translation is directed by an internal ribosome entry site. When *Lkb1* floxed mice are crossed to mice harbouring the *AhCre* transgene, exons 4–7 of the *Lkb1* gene are deleted through action of the *Cre recombinase*, thereby ablating functional expression of Lkb1. Activity of the *AhCre*-transgene can be induced by xenobiotics such as β-naphthoflavone or by endogenous activation of the *Ah* promoter(Ireland *et al.*, 2004). This figure is based on Sakamoto *et al* (2005).

*AhCre*$^{+}$*Lkb1*$^{fl/fl}$ mice induced with the xenobiotic β-naphthoflavone showed *Cre*-mediated deletion of *Lkb1* in the small intestine (Shorning *et al.*, 2007). The pattern of recombination was confirmed using the surrogate marker LacZ in the Rosa26 reporter system (Soriano, 1999), detailed in Section 1.2.4. Induced *AhCre*$^{+}$*Lkb1*$^{fl/fl}$ mice demonstrated proliferation of absorptive enterocyte lineages in the small intestine, resulting in their apoptosis, in conjunction with expansion of the secretory cell population that manifested aberrant secretory functions (Shorning *et al.*, 2007). It was during the course of these studies that a prostate phenotype became apparent in un-induced mice, suggesting spontaneous activation of the *AhCre* transgene occurs in prostate epithelium.

### 3.1.3 Lkb1 plays a role in the prostate

There is currently little in the literature to directly link *LKB1* mutation with human or murine prostate neoplasia. However, somatic *LKB1* mutations have been observed in human lung cancer and inactivation of *Lkb1* has been shown to predispose to lung tumourigenesis in the mouse (Ji *et al.*, 2007). This suggests that Lkb1 may have a broad tumour suppressive role in epithelial tissues.

In the human prostate, LKB1 has been detected in the cytoplasm of luminal cells using immunohistochemistry (Conde *et al.*, 2007) and low levels of *Lkb1* mRNA are detectable in mouse prostate (Collins *et al.*, 2000). Sequencing studies have reported that *LKB1* is mutated in one of five sequenced human prostate carcinoma cell lines, with a frame-shift deletion within the kinase domain of DU145 cells (p.K178fs*86) (Ikediobi *et al.*, 2006). Further support for a tumour suppressive role for Lkb1 comes from a whole-genome scan study that identified an association between chromosome segments 19q12-q13.11 and prostate cancer aggressiveness (Neville *et al.*, 2003). The chromosome segment 19p13.3 harbours the LKB1 tumour suppressor gene (Neville *et al.*, 2003). Deletions, amplifications and structural rearrangements of Chromosome 19 have also been reported in a variety of tumours including pancreatic adenocarcinomas, both benign and anaplastic thyroid tumours and stomach cancers (Neville *et al.*, 2003). Interestingly, prostate cancer has also been anecdotally reported in a PJS patient (66 years old) following the development of colon cancer (Boardman *et al.*, 1998). The presence of prostate cancer in PJS patients is not a frequent occurrence, possibly as a consequence of the normal age of onset of disease. Prostate cancer is typically diagnosed in the 7$^{th}$ decade of life, while PJS patients have an average life-span of 57 years (Yoo *et al.*, 2002).

## 3.2 Aim

The objective of this chapter is to determine the expression pattern of the tumour suppressor *Lkb1* in the mouse GU tract and to investigate the possible link between loss of *Lkb1* and prostate tumourigenesis using the un-induced *AhCre*$^{+}$*Lkb1*$^{fl/fl}$ conditional transgenic mouse model. Cohorts were analysed histologically and by immunohistochemistry. Un-induced *AhCre*-mediated recombination and excision of the *Lkb1* targeted allele in the prostate was determined by LacZ staining in mice harbouring both the *AhCre* transgene and the Rosa26 reporter locus. PCR amplification of the recombined allele on prostate DNA isolated by laser-capture microdissection and an *in situ* hybridisation that detects *Lkb1* mRNA transcripts was also employed to assay recombination and *Lkb1* expression in the mouse GU tract.

## 3.3 Results

### 3.3.1 Un-induced *AhCre*$^{+}$*Lkb1*$^{fl/fl}$ mice have a reduced life-span

*AhCre*$^{+}$ mice were inter-crossed with mice carrying the *LoxP*-flanked *Lkb1* allele and the *Rosa26* reporter allele. Cohorts of un-induced *wild-type* (*AhCre*$^{+}$*Lkb1*$^{+/+}$), *AhCre*$^{+}$*Lkb1*$^{+/fl}$, *Cre*$^{-}$*Lkb1*$^{fl/fl}$ and *AhCre*$^{+}$*Lkb1*$^{fl/fl}$ mice were generated and aged to 200 days. Each cohort contained a minimum of 20 males which were monitored for signs of illness and killed when they became symptomatic of disease (figure 3.3). Un-induced *Wild-type*, *AhCre*$^{+}$*Lkb1*$^{+/fl}$ and *Cre*$^{-}$*Lkb1*$^{fl/fl}$ cohorts all survived to 200 days and did not significantly differ from each other (Chi-squared test). However, all un-induced *AhCre*$^{+}$*Lkb1*$^{fl/fl}$ male mice became ill by 200 days, with a significantly reduced average survival of 83 days compared to all other cohorts.

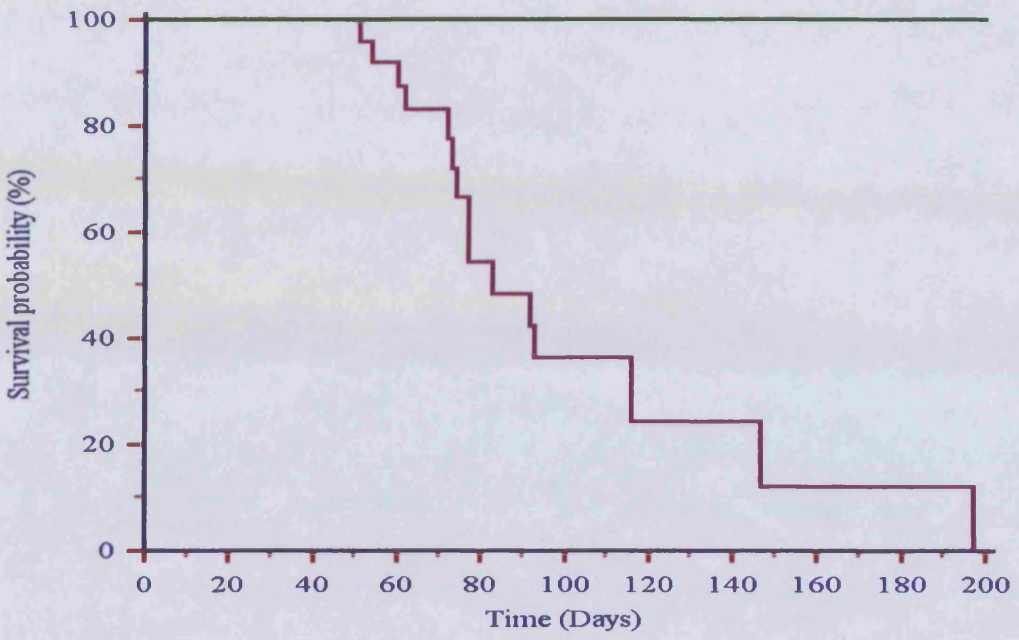


**Figure 3.3: Un-induced *AhCre$^{+}$Lkb1$^{fl/fl}$* male mice display reduced longevity.** A Kaplan-Meier plot of the un-induced *wild-type* (n = 26), *AhCre$^{+}$Lkb1$^{+/fl}$* (n = 41), *Cre$^{-}$Lkb1$^{fl/fl}$* (n = 20) cohorts all represented in green and un-induced *AhCre$^{+}$Lkb1$^{fl/fl}$* mice (n = 26) illustrated in purple. Un-induced *AhCre$^{+}$Lkb1$^{fl/fl}$* mice show decreased longevity, with 100% of the cohort not surviving past 200 days. Chi-squared tests confirmed un-induced *AhCre$^{+}$Lkb1$^{fl/fl}$* mice exhibit a significantly reduced average survival of 83 days compared to un-induced *wild-type* ($p < 0.0001$, $\chi^2 = 39.85$), *AhCre$^{+}$Lkb1$^{+/fl}$* ($p < 0.0001$, $\chi^2 = 59.01$) and *Cre$^{-}$Lkb1$^{fl/fl}$* ($p < 0.0001$, $\chi^2 = 31.97$) cohorts. Statistical analysis was carried out using a Chi-squared test using "MiniTab" software.

### 3.3.2 Un-induced *AhCre$^{+}$Lkb1$^{fl/fl}$* mice develop multiple GU tract phenotypes

Histological analysis of the genitourinary (GU) tract is summarised in Table 3.1. No gross phenotype was observed in un-induced *wild-type* (n = 21) and *AhCre$^{+}$Lkb1$^{+/fl}$* (n = 18) mice aged to 200 days. The un-induced *AhCre$^{+}$Lkb1$^{fl/fl}$* cohort (n = 18) was predisposed to a number of GU tract phenotypes. The anterior prostate from un-induced *AhCre$^{+}$Lkb1$^{fl/fl}$* mice between 2-4 months of age revealed foci of atypical hyperplasia (AH) with 100% incidence. Progression to high-grade prostate intra-epithelial neoplasia (HG-PIN) was also observed (83% incidence), predominantly in the proximal region of the duct. Neoplastic lesions were observed as early as 8 weeks when mice became sick. Dorsolateral and ventral lobes displayed a less severe phenotype, where cells exhibited nuclear atypia associated with focal epithelial hyperplasia with 61% and 56% incidence respectively. These mice were also prone to an interstitial immune infiltrate throughout the GU tract (100% incidence), which in 33% of the cohort obstructed the prostate lumen (resembling prostatitis). Additional male accessory glands other than the prostate also manifested aberrant architecture in the un-

induced *AhCre*$^{+}$*Lkb1*$^{fl/fl}$ cohort. Hyperplastic bulbourethral gland (BUG) cysts were observed with 100% incidence and a subset of the cohort also developed urethral hyperplasia (39%) and seminal vesicle squamous metaplasia (11%). Furthermore, both un-induced *Cre*$^{-}$*Lkb1*$^{fl/fl}$ (n = 19) and *AhCre*$^{+}$*Lkb1*$^{fl/fl}$ cohorts were infertile with 100% incidence, corresponding to a previous study (Sakamoto *et al.*, 2005).

**Table 3.1 Phenotype incidence in un-induced *AhCre*-mediated *Lkb1* deficient transgenic mice**

| Genotype / Phenotype | *Wild-type* (n=21) | *AhCre*$^{+}$*Lkb1*$^{+/fl}$ (n=18) | *Cre*$^{-}$*Lkb1*$^{fl/fl}$ (n =19) | *AhCre*$^{+}$*Lkb1*$^{fl/fl}$ (n=18) |
|---|---|---|---|---|
| Anterior AH | 0 | 0 | 0 | 18 (100%) |
| Anterior PIN | 0 | 0 | 0 | 15 (83%) |
| Dorsolateral AH | 0 | 0 | 0 | 11 (61%) |
| Ventral AH | 0 | 0 | 0 | 10 (56%) |
| Inflammation | 0 | 0 | 0 | 18 (100%) |
| Prostatitis | 0 | 0 | 0 | 6 (33%) |
| Bulbourethral gland cyst | 0 | 0 | 0 | 18 (100%) |
| Urethral hyperplasia | 0 | 0 | 0 | 7 (39%) |
| Seminal vesicle squamous metaplasia | 0 | 0 | 0 | 2 (11%) |
| Infertile | 0 | 0 | 19 (100%) | 18 (100%) |

### 3.3.3 Un-induced *AhCre*$^{+}$*Lkb1*$^{fl/fl}$ mice are predisposed to prostate neoplasia

Histological analysis of the genitourinary (GU) tract was in accordance with the consensus report from the Bar Harbor meeting of the mouse models of human cancer consortium prostate pathology committee (Shappell *et al.*, 2004) and confirmed by Prof. Collins (urology consultant histopathologist, Bristol Royal Infirmary).

Un-induced control anterior prostate (*Cre*$^{-}$*Lkb1*$^{fl/fl}$) demonstrates normal single-layered, ordered branching of the prostate epithelium that project into the lumen and show normal secretory function at 200 days (figure 3.4a-b). Un-induced *AhCre*$^{+}$*Lkb1*$^{fl/fl}$ demonstrated AH and PIN lesions at terminal end-points. Characteristic of hyperplasia, tufts of cells demonstrating aberrant architecture of the acini have accumulated within the lumen, displaying loss of cellular polarity, mitotic bodies and cytological atypia, including prominent nucleoli and nuclear enlargement (figure 3.4c-d).

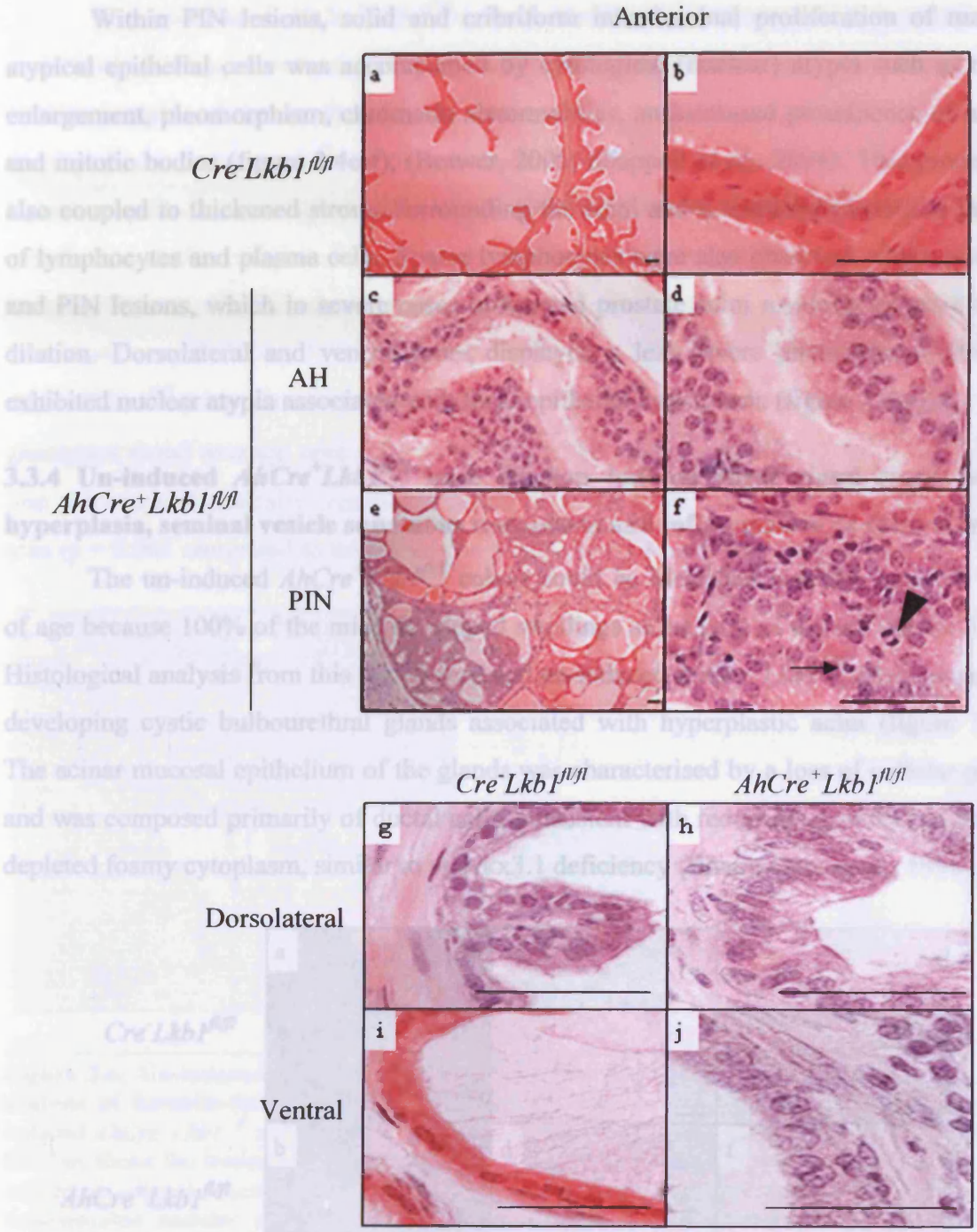


**Figure 3.4: Un-induced A*hCre*-mediated deletion of *Lkb1* predisposes to PIN.** Histological analysis of H&E stained formalin-fixed, paraffin-embedded tissue from un-induced *Cre⁻Lkb1$^{fl/fl}$* and *AhCre⁺Lkb1$^{fl/fl}$* mice aged 2-7 months. Un-induced *Cre⁻Lkb1$^{fl/fl}$* anterior prostate at low (a) and high magnification (b) shows ordered architecture of normal epithelium. Atypical hyperplasia in the un-induced *AhCre⁺Lkb1$^{fl/fl}$* mutants illustrates tufting of luminal cells and cytological atypia (c-d). Progression to PIN was observed in 83% of the cohort, demonstrating cribriform architecture (e), apoptosis (arrow) and cytological atypia, such as enlarged nuclei and mitosis (arrow head) (f). Dorsolateral (g-h) and ventral (i-j) prostate lobes exhibited hyperplasia in association with nuclear atypia in the un-induced *AhCre⁺Lkb1$^{fl/fl}$* cohort. Images were taken at low power (20x) or high power (40x) magnification and scale bars represent 50 μm.

Within PIN lesions, solid and cribriform intra-luminal proliferation of markedly atypical epithelial cells was accompanied by cytological (nuclear) atypia such as nuclear enlargement, pleomorphism, chromatin abnormalities, an increased prominence of nucleoli and mitotic bodies (figure 3.4e-f), (Brawer, 2005; Shappell *et al.*, 2004). This process was also coupled to thickened stroma surrounding the acini and a scattered interstitial infiltrate of lymphocytes and plasma cells. Sparse lymphocytes were also observed within some AH and PIN lesions, which in severe cases obstructed prostate acini resulting in gross tubular dilation. Dorsolateral and ventral lobes displayed a less severe phenotype, where cells exhibited nuclear atypia associated with focal epithelial hyperplasia (figure 3.4g-j).

### 3.3.4 Un-induced *AhCre*$^{+}$*Lkb1*$^{fl/fl}$ mice develop bulbourethral gland cysts, urethra hyperplasia, seminal vesicle squamous metaplasia and inflammation of the GU tract

The un-induced *AhCre*$^{+}$*Lkb1*$^{fl/fl}$ cohort could be identified visually from 6-8 weeks of age because 100% of the mice developed swellings at the base of the tail (figure 3.5a-b). Histological analysis from this region revealed un-induced *AhCre*$^{+}$*Lkb1*$^{fl/fl}$ mice are prone to developing cystic bulbourethral glands associated with hyperplastic acini (figure 3.5c-f). The acinar mucosal epithelium of the glands was characterised by a loss of cellular polarity and was composed primarily of ductal cells, consistent with reduced secretory function and depleted foamy cytoplasm, similar to an Nkx3.1 deficiency (Bhatia-Gaur *et al.*, 1999).

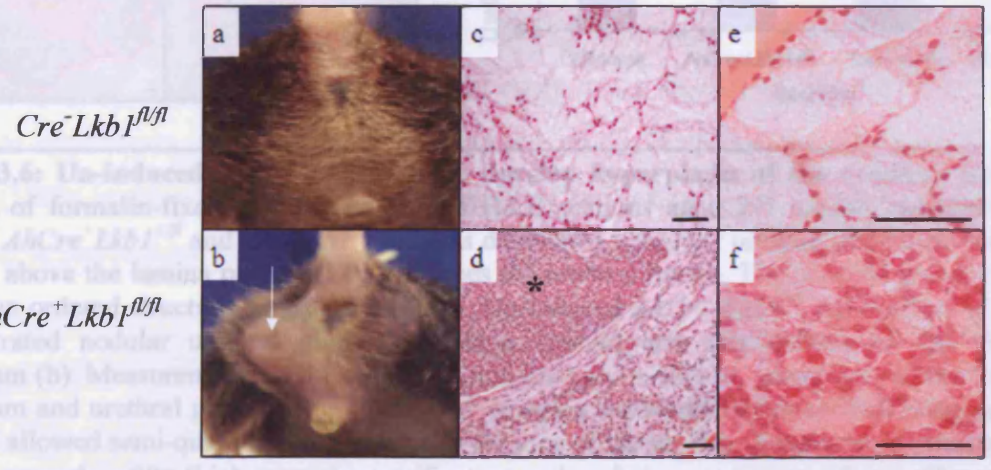


**Figure 3.5: Un-induced *AhCre*$^{+}$*Lkb1*$^{fl/fl}$ mice develop bulbourethral gland cysts.** Compared to control cohorts (a), un-induced *AhCre*$^{+}$*Lkb1*$^{fl/fl}$ mice developed bulbourethral gland cysts at the base of the tail (b) by 6-8 weeks of age. Histological analysis of formalin-fixed, paraffin-embedded H&E sections revealed ordered acini in control cohorts (c and e) while un-induced *AhCre*$^{+}$*Lkb1*$^{fl/fl}$ mice demonstrated chronic infection (*) (d), reduced secretory function and over populated acini (f). Histology images were taken at 20x (low) and 40x (high) magnification and scale bars represent 50 μm.

The un-induced *AhCre*$^{+}$*Lkb1*$^{fl/fl}$ cohort manifested urethral gland hyperplasia (39% incidence). *Wild-type* urethral glands typically form a narrow layer between the muscle and lamina propria of the urethra (figure 3.6a), while un-induced *AhCre*$^{+}$*Lkb1*$^{fl/fl}$ mutants displayed nodular hyperplasia of the membranous urethra transitional epithelium within the lamina propria. In conjunction with this, cytological atypia and proliferation of the urethral glands was evident (figure 3.6b). Using the "Analysis" imaging software (Olympus Soft Imaging System, GMBH, demonstrated in figure 3.6c-d) the area of the urethral gland and transitional epithelium in un-induced *wild-type*, *Cre*$^{-}$*Lkb1*$^{fl/fl}$, *AhCre*$^{+}$*Lkb1*$^{+/fl}$ and *AhCre*$^{+}$*Lkb1*$^{fl/fl}$ mice was determined (average area 4.87 x $10^6$ $\mu m^2$). Compared to all other genotypes (total average area 1.27 x $10^6$ $\mu m^2$), the un-induced *AhCre*$^{+}$*Lkb1*$^{fl/fl}$ transgenic line showed a statistically significant 3-fold increase in the urethral gland and epithelium area ($p = 0.001$ compared to un-induced *wild-type* mice, Mann Whitney), (figure 3.6e).

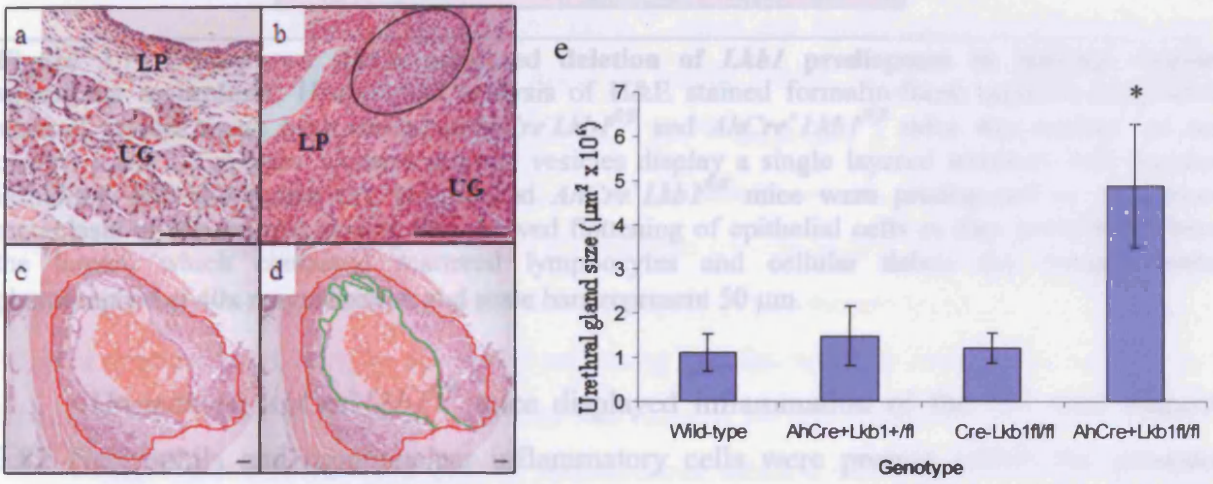


**Figure 3.6: Un-induced *AhCre*$^{+}$*Lkb1*$^{fl/fl}$ mice develop hyperplasia of the urethra.** Histological analysis of formalin-fixed, paraffin-embedded H&E sections aged 2-7 months revealed that un-induced *AhCre*$^{+}$*Lkb1*$^{+/fl}$ and *Cre*$^{-}$*Lkb1*$^{fl/fl}$ cohorts developed *wild-type* urethral transitional epithelium that lies above the lamina propria (LP) and faces the urethral lumen. The urethral glands (UG) also exhibit an ordered structure beneath the LP (a). Un-induced *AhCre*$^{+}$*Lkb1*$^{fl/fl}$ mice taken at end point demonstrated nodular urethral gland hyperplasia (circle) and proliferation of the transitional epithelium (b). Measurements of the outside (c, red line) and inside (d, green line) of the transitional epithelium and urethral glands using "Analysis" imaging software (Olympus Soft Imaging System, GMBH) allowed semi-quantitative estimates of the area of the urethra. Images were photographed at 4x (low power) or 20x (high power) magnification and scale bars represent 50 μm. The area of the urethra for each genotype is plotted in (e), indicating a 3-fold increase in the un-induced *AhCre*$^{+}$*Lkb1*$^{fl/fl}$ cohort ($n = 8$). Statistical analysis was performed using the non-parametric Mann Witney test (MiniTab Software, 95% confidence interval) revealing a significant difference between *AhCre*$^{+}$*Lkb1*$^{fl/fl}$ mutants (*) compared to un-induced *wild-type* ($p = 0.0011$, $n = 8$), *AhCre*$^{+}$*Lkb1*$^{+/fl}$ ($p = 0.0029$, $n = 7$) and *Cre*$^{-}$*Lkb1*$^{fl/fl}$ ($p = 0.0019$, $n = 9$) mice. Error bars represent standard deviation.

A small proportion of the un-induced *AhCre*$^{+}$*Lkb1*$^{fl/fl}$ cohort also developed seminal vesicle squamous metaplasia (11% incidence). The seminal vesicle typically functions to store sperm in male adults. Un-induced *Wild-type*, *AhCre*$^{+}$*Lkb1*$^{+/fl}$ and *Cre*$^{-}$*Lkb1*$^{fl/fl}$ mice all displayed normal single-layered branched architecture (figure 3.7a). Seminal vesicle squamous metaplasia in un-induced *AhCre*$^{+}$*Lkb1*$^{fl/fl}$ deficient mice comprised of proliferation of the transitional epithelium into the lumen and flattening of the epithelial cells (figure 3.7b).

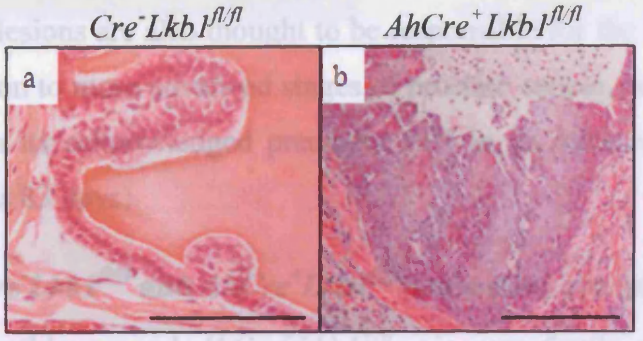


**Figure 3.7: Un-induced *AhCre*-mediated deletion of *Lkb1* predisposes to seminal vesicle squamous metaplasia.** Histological analysis of H&E stained formalin-fixed, paraffin-embedded seminal vesicle tissue from un-induced *Cre*$^{-}$*Lkb1*$^{fl/fl}$ and *AhCre*$^{+}$*Lkb1*$^{fl/fl}$ mice was carried out on cohorts aged 2-7 months. Control seminal vesicles display a single layered structure with regular infoldings into the lumen (a). Un-induced *AhCre*$^{+}$*Lkb1*$^{fl/fl}$ mice were predisposed to squamous metaplasia of the seminal vesicle that showed flattening of epithelial cells as they proliferated into the lumen, which contained scattered lymphocytes and cellular debris (b). Images were photographed at 40x magnification and scale bars represent 50 μm.

Un-induced *AhCre*$^{+}$*Lkb1*$^{fl/fl}$ mice displayed inflammation of the GU tract (figure 3.8). Neutrophils and mononuclear inflammatory cells were present within the prostate glandular epithelium, the lumen of the prostate gland (33% incidence) and the prostatic stroma (100% incidence). The infection resembled both chronic prostatitis and cystic lesions observed in the bulbourethral glands.

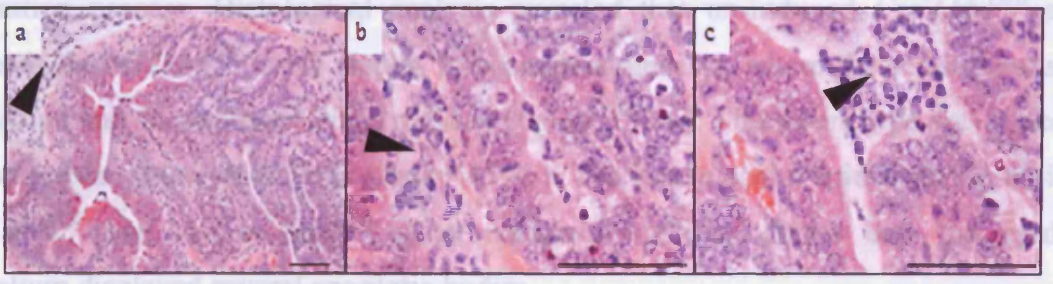


**Figure 3.8: Un-induced *AhCre*$^{+}$*Lkb1*$^{fl/fl}$ male mice develop GU tract inflammation.** Formalin-fixed, paraffin-embedded H&E sections from un-induced *AhCre*$^{+}$*Lkb1*$^{fl/fl}$ anterior prostate aged 2-7 months. Immune infiltrate was observed in the interstitium (a-b) and inside prostate acini, resembling prostatitis (c). Images were taken at 20x (low power) and 40x (high power) magnification and scale bars represent 50 μm. Arrowheads indicate immune cell infiltration.

It is important to note that areas devoid of inflammation still exhibited hyperplasia and PIN (shown in figure 3.4). This indicates that PIN is not likely to be a consequence of reactive hyperplasia caused by inflammation (termed proliferative inflammatory atrophy or PIA), which occurs in approximately 20% of human prostate cancers (DeMarzo *et al.*, 1999). Indeed, the PIN lesions are considered to reflect *Lkb1* loss in the prostate epithelium and it is speculated that the development/disruption of cystic bulbourethral glands in un-induced $AhCre^{+}Lkb1^{fl/fl}$ mice is the cause of an aggressive inflammatory response within the GU tract. The BUG lesions are also thought to be responsible for the reduced life-span, thus preventing progression to more advanced stages of prostate cancer, such as adenocarcinoma and metastasis, from its acknowledged precursor PIN in un-induced $AhCre^{+}Lkb1^{fl/fl}$ mice (average survival was 83 days).

### 3.3.5 Un-induced $Cre^{-}Lkb1^{fl/fl}$ and $AhCre^{+}Lkb1^{fl/fl}$ male mice are infertile

Un-induced *wild-type* and $AhCre^{+}Lkb1^{+/fl}$ mice are fertile while un-induced $Cre^{-}Lkb1^{fl/fl}$ and $AhCre^{+}Lkb1^{fl/fl}$ adult male mice are sterile (100% incidence). Male infertility has been reported previously in un-induced $Cre^{-}Lkb1^{fl/fl}$ mice and is considered to reflect the hypomorphic nature of the *Lkb1* floxed allele (Sakamoto *et al.*, 2005). Sakamoto *et al* (2005) reported that in addition to the 50 kDa protein corresponding to full length Lkb1, the LKB1 antibody employed in an immunoblot analysis of the mouse testis also recognised a 48 kDa species. Interestingly, the faster migrating species was not detected in un-induced $Cre^{-}Lkb1^{fl/fl}$ mice, while the 50 kDa species was reduced 10-fold (Sakamoto *et al.*, 2005).

The testis consists of a coil of seminiferous tubules, the site of spermatogenesis (figure 3.9a). The epididymis is split into four compartments consisting of the initial segment, caput (head), corpus (body) and cauda (tail) (figure 3.9b) and forms a coiled structure that surrounds the testis. Sperm pass through the epididymis to complete the maturation process. Histological analysis revealed that un-induced $Cre^{-}Lkb1^{fl/fl}$ and un-induced $AhCre^{+}Lkb1^{fl/fl}$ testes display hypospermatogenesis, where the seminiferous tubule epithelium and spermatogenesis is reduced (figure 3.9c-e). This phenotype was concomitant with aspermia in the epididymis (figure 3.9f-q). The lumen of the epididymis in un-induced $Cre^{-}Lkb1^{fl/fl}$ and $AhCre^{+}Lkb1^{fl/fl}$ mice contained cellular debris and the epididymal epithelium displayed several apoptotic bodies.

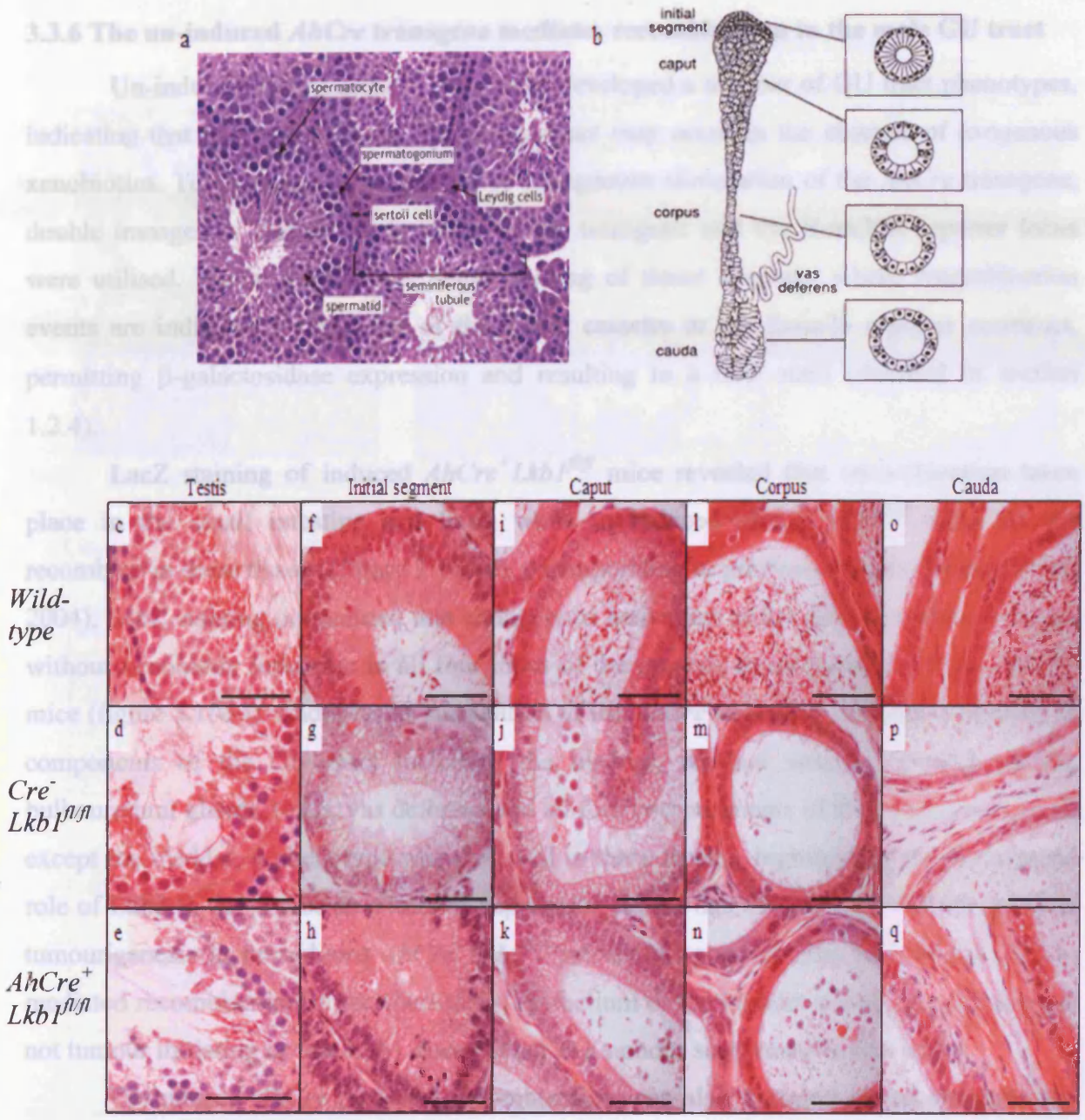


**Figure 3.9: Un-induced *Cre⁻Lkb1$^{fl/fl}$* and *AhCre⁺Lkb1$^{fl/fl}$* males are infertile.** (a) Illustrates the ultrastructure of the seminiferous tubules that comprise the mouse testis. (b) Depicts the four major compartments of the murine epididymis; initial segment, caput, corpus and cauda. Formalin-fixed, paraffin-embedded H&E stained sections from adult male mice aged 2-7 months were analysed. Un-induced *wild-type* testis (c) illustrates normal spermatogenesis and seminiferous tubule epithelium consisting of many layers of spermatogenesis. Un-induced *Cre⁻Lkb1$^{fl/fl}$* and *AhCre⁺Lkb1$^{fl/fl}$* cohorts both demonstrated hypospermatogenesis and a decrease in the epithelial layer of the seminiferous tubule (d-e). Un-induced *wild-type* epididymis compartments all contain maturing sperm in the lumen while un-induced *Cre⁻Lkb1$^{fl/fl}$* and *AhCre⁺Lkb1$^{fl/fl}$* cohorts are devoid of sperm and cellular debris is present (f-q). All images were taken at 40x magnification and scale bars represent 50 μm. Figure (a) is adapted from "The Mouse Histology Atlas" (http://www.deltagen.com/target/histologyatlas/HistologyAtlas.html) and (b) is adapted from "The Androgen Society" (http://www.androlgysociety.com).

### 3.3.6 The un-induced *AhCre* transgene mediates recombination in the male GU tract

Un-induced *AhCre*$^{+}$*Lkb1*$^{fl/fl}$ male mice developed a number of GU tract phenotypes, indicating that expression of the *AhCre* construct may occur in the absence of exogenous xenobiotics. To characterise the pattern of endogenous stimulation of the *AhCre* transgene, double transgenics harbouring both the *AhCre* transgene and the Rosa26R reporter locus were utilised. Figure 3.10 shows X-gal staining of tissue sections, where recombination events are indicated by excision of the STOP cassette in the Rosa26 reporter construct, permitting β-galactosidase expression and resulting in a blue stain (detailed in section 1.2.4).

LacZ staining of induced *AhCre*$^{+}$*Lkb1*$^{fl/fl}$ mice revealed that recombination takes place in the small intestine and liver, while un-induced *AhCre*$^{+}$*Lkb1*$^{fl/fl}$ mice do not recombine in these tissues (figure 3.10a-d), corresponding to previous studies (Ireland *et al.*, 2004). LacZ staining determined that endogenous activation of the *AhCre* construct occurs without xenobiotic induction in all four lobes of the prostate in un-induced *AhCre*$^{+}$*Lkb1*$^{fl/fl}$ mice (figure 3.10e-j). Endogenous stimulation of the *AhCre* transgene was also identified in components of the GU tract including the bladder, seminal vesicle, urethral glands, bulbourethral glands, testis, vas deferens and all four compartments of the epididymis. In all except the bladder, a phenotype was observed in these tissues, highlighting the widespread role of Lkb1 in the mouse as a tumour suppressor. Given that the bladder was not prone to tumourigenesis in un-induced *AhCre*$^{+}$*Lkb1*$^{fl/fl}$ mice, it is possible that un-induced *AhCre*-mediated recombination in the transitional epithelium of the bladder occurs in cells that are not tumour initiating or that Lkb1 does not act as a tumour suppressor in this tissue.

Un-induced *AhCre*-mediated recombination was also detected in the stomach and kidney of un-induced *AhCre*$^{+}$*Lkb1*$^{fl/fl}$ mice (figure 3.10d, m and n). Indeed, un-induced *AhCre*$^{+}$ transgenic mice homozygous for a conditional *Apc* allele (*AhCre*$^{+}$*Apc*$^{fl/fl}$) have previously been shown to develop renal carcinoma (Sansom *et al.*, 2005). Here, histological analysis revealed no gross phenotype in the kidney or stomach in *AhCre*$^{+}$*Lkb1*$^{fl/fl}$ mice aged 2-7 months.

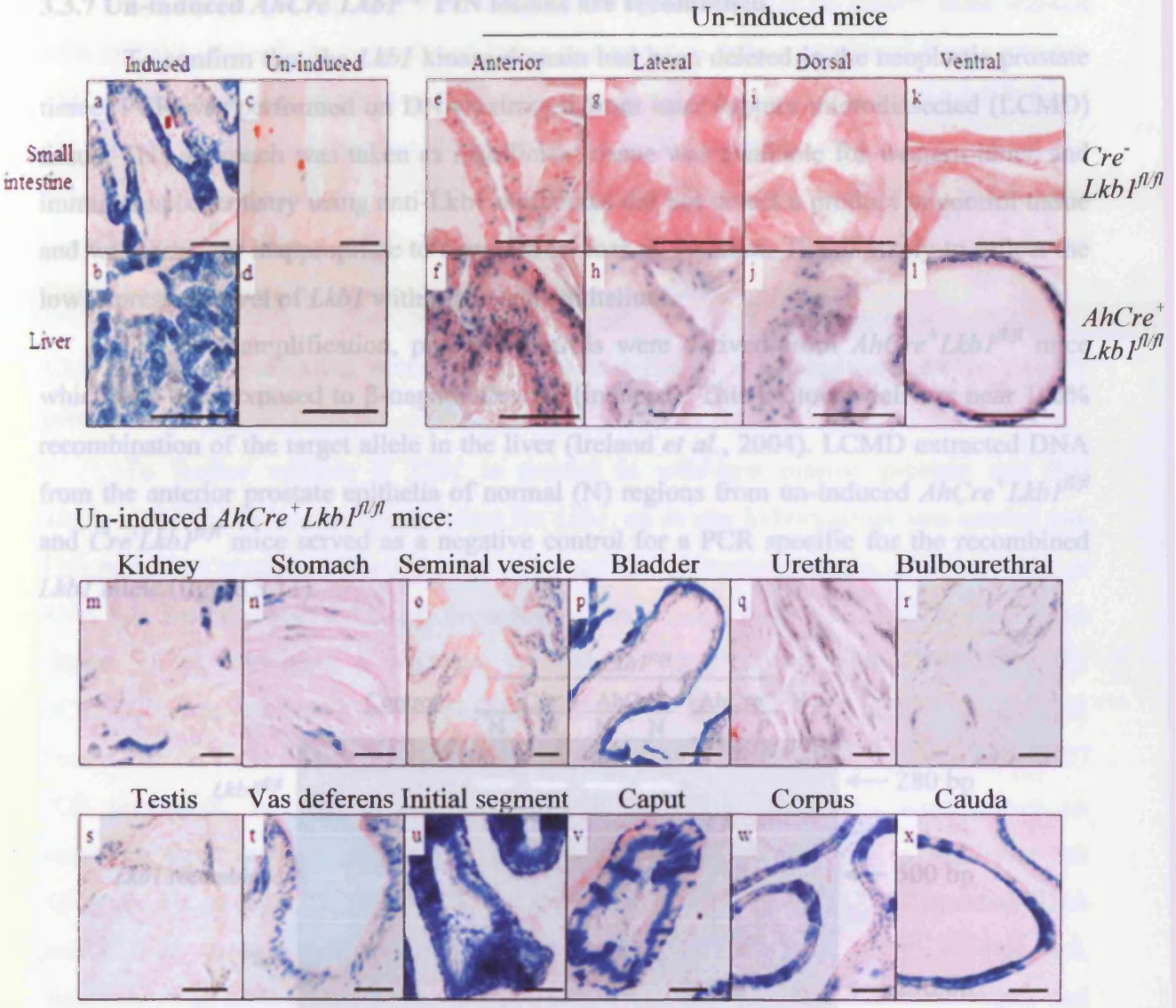


**Figure 3.10: Un-induced *AhCre*-mediated recombination of *Lkb1* occurs within the GU tract.** Tissue from adult transgenic mice (aged 2-4 months) was harvested for the detection of *Ah* driven *Cre recombinase* activity using X-gal staining (blue stain). *AhCre*$^{+}$ *Lkb1*$^{fl/fl}$ positive controls were exposed to four daily i.p injections of β-naphthoflavone (80 mg/kg) and harvested 6 days later. This strategy of induction has been reported to be sufficient for near 100% recombination in the small intestine (a) and liver (b), (Ireland *et al.*, 2004). Un-induced controls were negative (c-d). Cross-sections from un-induced *Cre*$^{-}$*Lkb1*$^{fl/fl}$ and un-induced *AhCre*$^{+}$ *Lkb1*$^{fl/fl}$ anterior (e-f) lateral (g-h), dorsal (i-j) and ventral (k-l) prostate lobes revealed that endogenous activation of the *AhCre* construct occurs in all four lobes. Punctate staining shown in (e) is attributable to endogenous β-lactamase activity. *AhCre*-mediated recombination was also detected in un-induced *AhCre*$^{+}$ *Lkb1*$^{fl/fl}$ kidney (m), stomach (n), seminal vesicle (o), bladder (p), urethral glands (q), bulbourethral glands (r), testis (s), vas deferens (t), and the epididymis initial segment (u), caput (head) (v), corpus (body) (w) and cauda (tail) (x). This indicates that a wide variety of tissues are capable of activating expression of the *AhCre* construct without xenobiotic stimulation. Images were photographed at 20x (a and c) or 40x magnification (b, d-x) and scale bars represent 50 μm.

### 3.3.7 Un-induced *AhCre*$^{+}$*Lkb1*$^{fl/fl}$ PIN lesions are recombined

To confirm that the *Lkb1* kinase domain had been deleted in the neoplastic prostate tissue, PCR was performed on DNA extracted from laser capture microdissected (LCMD) tissue. This approach was taken as insufficient tissue was available for western blots, and immunohistochemistry using anti-Lkb1 antibodies did not detect a product in control tissue and was therefore inappropriate to demonstrate loss of function. This is likely to reflect the low expression level of *Lkb1* within prostate epithelium.

For PCR amplification, positive controls were derived from *AhCre*$^{+}$*Lkb1*$^{fl/fl}$ mice which had been exposed to β-naphthoflavone (induced). This protocol delivers near 100% recombination of the target allele in the liver (Ireland *et al.*, 2004). LCMD extracted DNA from the anterior prostate epithelia of normal (N) regions from un-induced *AhCre*$^{+}$*Lkb1*$^{fl/fl}$ and *Cre*$^{-}$*Lkb1*$^{fl/fl}$ mice served as a negative control for a PCR specific for the recombined *Lkb1* allele (figure 3.11).

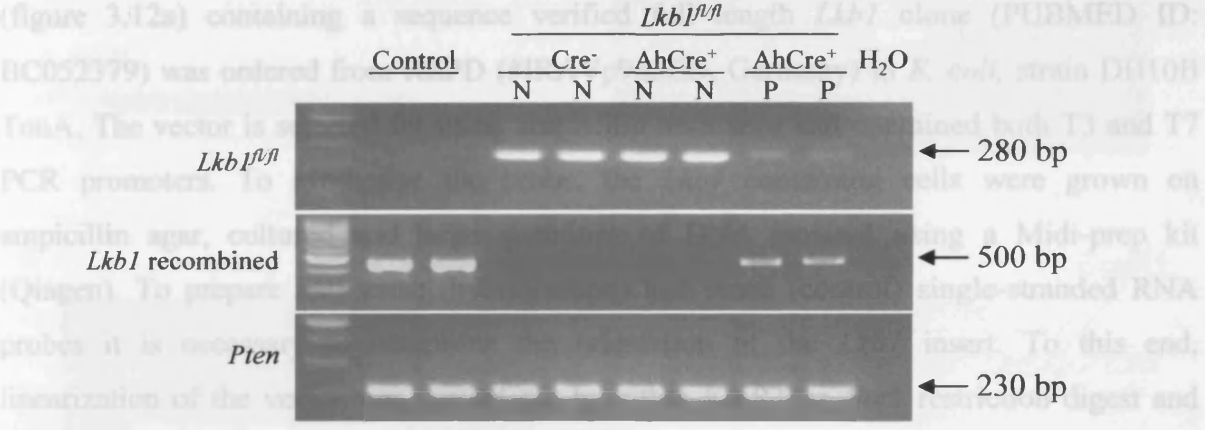


**Figure 3.11: Un-induced *AhCre*$^{+}$*Lkb1*$^{fl/fl}$ PIN lesions are recombined.** Using laser capture microdissection, DNA was isolated from anterior prostate lobes of un-induced *Cre*$^{-}$*Lkb1*$^{fl/fl}$ and both normal (N) and PIN (P) lesions from un-induced *AhCre*$^{+}$*Lkb1*$^{fl/fl}$ mice and underwent PCR analysis (a). Induced *AhCre*$^{+}$*Lkb1*$^{fl/fl}$ liver was used as a positive control, where mice were exposed to four daily i.p injections of β-naphthoflavone (80 mg/kg) and harvested 6 days later, reported to be sufficient for near 100% recombination (Ireland *et al.*, 2004). LCMD extracted DNA from 2 mice was run on a gel (although n = 6 for each genotype). The top gel shows the product for the un-recombined *LoxP*-flanked *Lkb1* allele (280 bp), revealing none in the induced positive control, a strong band in *Cre*$^{-}$*Lkb1*$^{fl/fl}$ and *AhCre*$^{+}$*Lkb1*$^{fl/fl}$ normal (N) un-induced samples and reduced levels in un-induced *AhCre*$^{+}$*Lkb1*$^{fl/fl}$ PIN lesions (P). Densitometry suggested that compared to material from un-induced *Cre*$^{-}$*Lkb1*$^{fl/fl}$ mice there was an 87% reduction in the level of the un-recombined allele in PIN material. The middle gel shows results for the *Lkb1* recombined allele (500 bp), with a strong band in the positive control and a weaker band in the PIN material, reflecting 64% recombination compared to the control. Un-induced *Cre*$^{-}$*Lkb1*$^{fl/fl}$ negative controls showed no recombination. The lower gel shows a PCR for *Pten*, employed as a loading control (230 bp).

Densitometry of anterior PIN lesions from un-induced *AhCre*$^{+}$*Lkb1*$^{fl/fl}$ mice showed 64% of *Lkb1* alleles to be recombined (when compared to fully recombined liver controls). This correlated with a marked reduction in the level of the un-recombined *LoxP*-flanked *Lkb1* allele (87%). The fact that recombination was below 100% presumably reflects the observed stromal content in the PIN lesions. These observations establish that recombination of the *LoxP*-flanked *Lkb1* allele is associated with PIN, but cannot discriminate between the hypomorphism and haploinsufficiency of *Lkb1*.

### 3.3.8 *In situ* hybridisation determined *Lkb1* is deficient in un-induced *AhCre*$^{+}$*Lkb1*$^{fl/fl}$ prostate

To further validate if *Lkb1* is present in *wild-type* murine prostate and that *AhCre*$^{+}$*Lkb1*$^{fl/fl}$ PIN lesions are deficient for *Lkb1*, an *in situ* hybridisation was carried out. This procedure requires a labelled complementary strand, termed a probe, of either DNA or RNA that hybridises to the target sequence within a tissue section. The pYX-Asc vector (figure 3.12a) containing a sequence verified full length *Lkb1* clone (PUBMED ID: BC052379) was ordered from RZPD (#IRAVp968ED, Germany) in *E. coli,* strain DH10B TonA. The vector is selected for using ampicillin resistance and contained both T3 and T7 PCR promoters. To synthesise the probe, the *Lkb1* containing cells were grown on ampicillin agar, cultured and large quantities of DNA isolated using a Midi-prep kit (Qiagen). To prepare anti-sense (hybridisation) and sense (control) single-stranded RNA probes it is necessary to determine the orientation of the *Lkb1* insert. To this end, linearization of the vector was carried out by either *Eco*R1 or *Not*1 restriction digest and primers to T3 or T7 promoters within the vector were used to initiate sequencing (figure 3.12b-c). Sequencing analysis (carried out by the DNA sequencing core, Cardiff University) determined that the T7 primer is at the 3'-end of the *Lkb1* insert, allowing the insert to be transcribed from linearised DNA using the appropriate polymerase (i.e. T7 for anti-sense and T3 for sense probes) and DIG labelled. A double restriction digest using *Eco*RI and *Not*1 confirmed the size of the insert as 1.7 kb and only fully digested samples were chosen for RNA probe generation and DIG labelling (figure 3.12d-e).

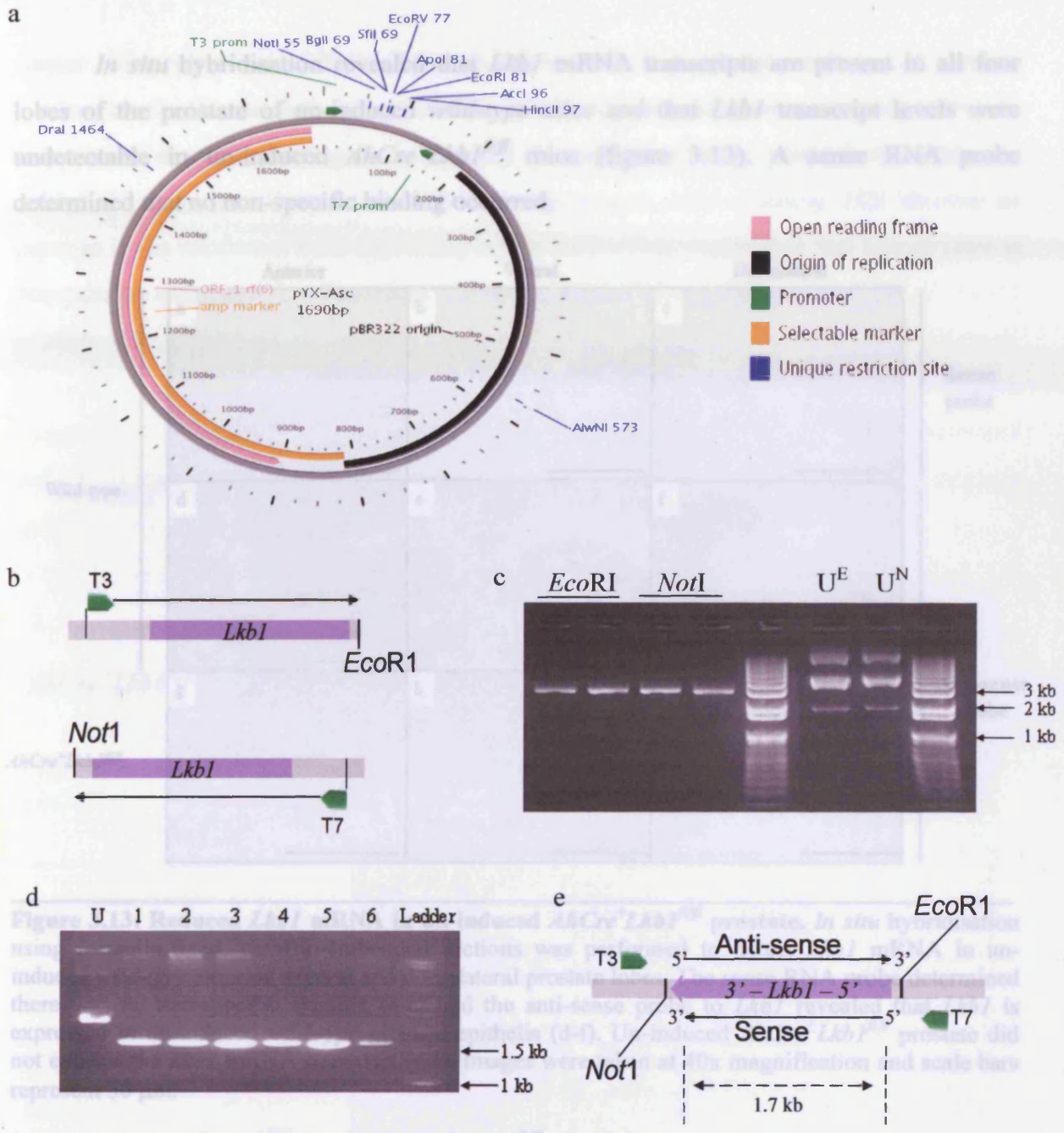


**Figure 3.12: Probe preparation for *Lkb1* specific *in situ* hybridisation.** The Qiagen Midi-prep kit was used to prepare large scale production of the pYX-Asc vector, 1.69 kb (a) carrying a full length *Lkb1* clone (1.7 kb, PubMed ID: BC052379) ordered from RZPD (IRAVp968E05123D, Germany). The vector was successfully linearised using *Eco*R1 (b, top) or *Not*1 (b, bottom) restriction enzymes and samples were run on a 1% agarose gel producing a band 3.4 kb in size. $U^E$ and $U^N$ represent undigested controls for *Eco*RI and *Not*I digests respectively (c). A double restriction digest using *Eco*RI and *Not*I restriction enzymes determined the insert size to be 1.7 kb, the same as the vector, where U represents an undigested sample and lanes 1-6 represent double digest samples (d). The 1 kb ladder shown in (c) is the 1 kb Plus DNA Ladder (Invitrogen) and the Standard 1 kb Ladder (Promega) is shown in (d). Linearised DNA was sequenced using PCR primers specific to the T3 promoter for *Eco*R1 digested DNA and the T7 promoter for *Not*I digested DNA (carried out by the DNA Sequencing Core, Cardiff University) to confirm sequence orientation and identity. The orientation of the insert determined the anti-sense and sense templates (e). The pYX-Asc vector map in (a) was adapted from the RZPD website.

*In situ* hybridisation revealed that *Lkb1* mRNA transcripts are present in all four lobes of the prostate of un-induced *wild-type* mice and that *Lkb1* transcript levels were undetectable in un-induced *AhCre*$^{+}$*Lkb1*$^{fl/fl}$ mice (figure 3.13). A sense RNA probe determined that no non-specific binding occurred.

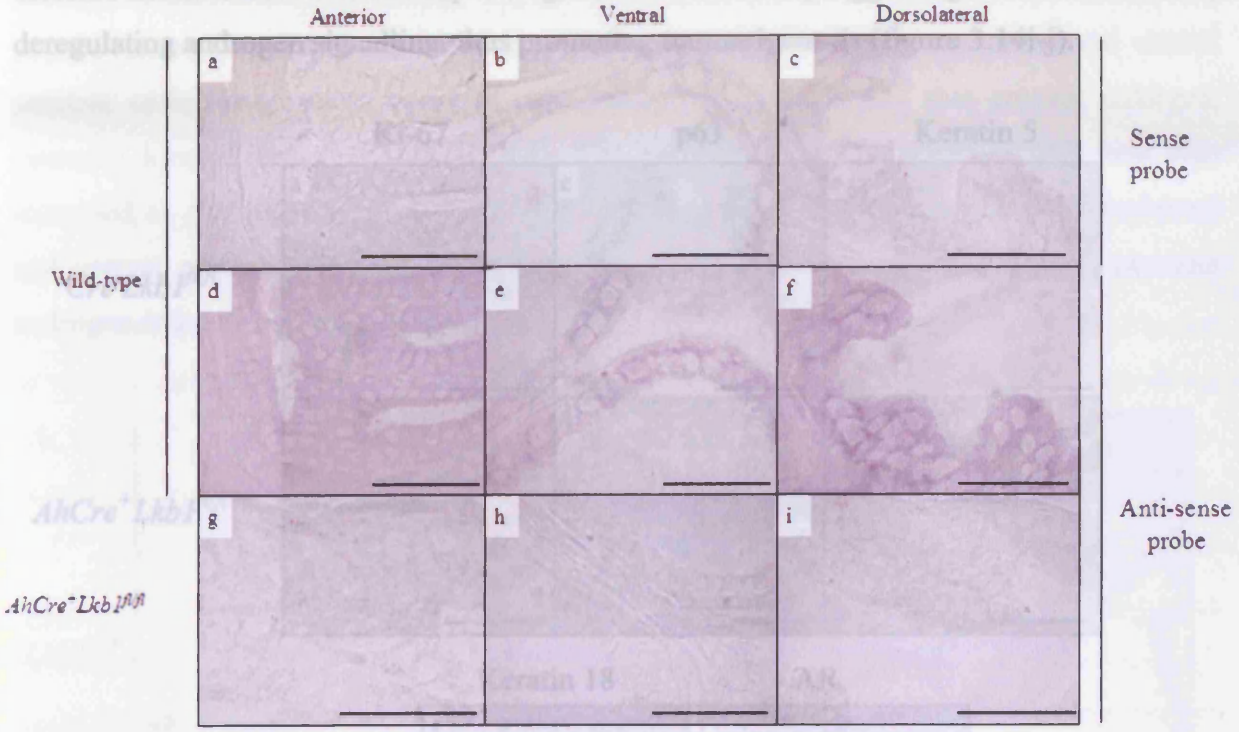


**Figure 3.13: Reduced *Lkb1* mRNA in un-induced *AhCre*$^{+}$*Lkb1*$^{fl/fl}$ prostate.** *In situ* hybridisation using formalin-fixed, paraffin-embedded sections was performed to detect *Lkb1* mRNA in un-induced *wild-type* anterior, ventral and dorsolateral prostate lobes. The sense RNA probe determined there was no non-specific staining (a-c) and the anti-sense probe to *Lkb1* revealed that *Lkb1* is expressed in un-induced *wild-type* prostate epithelia (d-f). Un-induced *AhCre*$^{+}$*Lkb1*$^{fl/fl}$ prostate did not express the *Lkb1* mRNA transcript (g-i). Images were taken at 40x magnification and scale bars represent 50 μm.

### 3.3.9 Analysing the un-induced *AhCre*$^{+}$*Lkb1*$^{fl/fl}$ prostate phenotype

To further characterise the anterior prostate lesions at a molecular level, immunohistochemistry was performed. The proliferation marker, Ki-67, was rarely expressed in un-induced control (*Cre*$^{-}$*Lkb1*$^{fl/fl}$) anterior prostate epithelium, however it was significantly elevated in epithelial cells throughout the acini of un-induced *AhCre*$^{+}$*Lkb1*$^{fl/fl}$ mice (figure 3.14a-b). Basal cells were detected using antibodies against p63 and Keratin-5 in the epithelial lining of anterior acini (Shappell *et al.*, 2004), indicating a marked accumulation and clustering of these cells within PIN foci (figure 3.14c-f). Keratin-18, an epithelial tumour marker (Shappell *et al.*, 2004), is not highly expressed in control anterior acini epithelium while PIN lesions showed elevated expression, mimicking human prostate

cancer (Shappell *et al.*, 2004), (figure 3.14g-h). AR is a pivotal mediator of prostate carcinogenesis (Isaacs and Isaacs, 2004). AR activation and downstream signalling in response to engaging androgens is required for prostate growth, particularly within the epithelial population (Prins *et al.*, 1991). In agreement, *Lkb1* deficient PIN showed an increase in the number of cells expressing AR in the nucleus, suggesting that loss of Lkb1 is deregulating androgen signalling, thus promoting tumourigenesis (figure 3.14i-j).

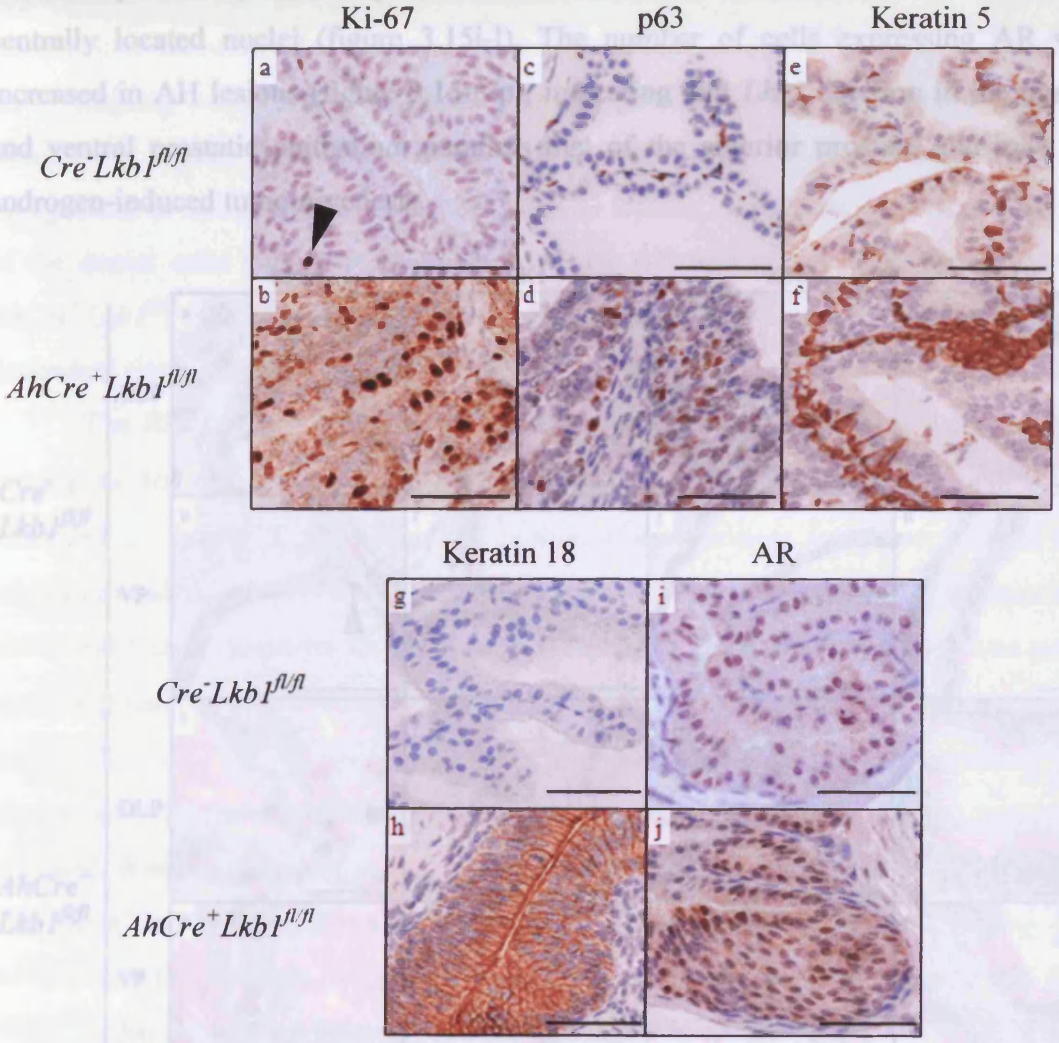


**Figure 3.14: Characterisation of *Lkb1* deficient prostate intra-epithelial neoplasia.** Immunohistochemical analysis of the anterior prostate of un-induced control ($Cre^{-}Lkb1^{fl/fl}$) and un-induced $AhCre^{+}Lkb1^{fl/fl}$ mice (aged 2-7 months) revealed an increase in proliferation using an anti-Ki-67 antibody (a-b), arrow head indicates a homeostatic level of proliferation in normal anterior prostate epithelium. Basal cell clustering was determined by monitoring p63 (c-d) and Keratin-5 (e-f) expression, which were over-expressed in neoplastic lesions. The luminal cell marker Keratin-18 is elevated in PIN foci (g-h) as is the androgen receptor (AR), suggesting deregulation of androgen signalling within neoplastic lesions (i-j). Images were taken at 40x magnification and the scale bars represent 50 μm.

3.3.10 Analysis of dorsolateral and ventral lobe atypical hyperplasia (AH) revealed that the proliferation marker, Ki-67 (Shappell *et al.*, 2004) was elevated in hyperplastic foci compared to control sections (figure 3.15a-d). Using an anti-Keratin-5 antibody, basal cell clustering in hyperplastic lesions was detected, particularly in the dorsolateral lobe (figure 3.15e-h). Immunohistochemistry to detect Keratin-18 determined the luminal cell population has become disorganised in un-induced *AhCre*$^{+}$*Lkb1*$^{fl/fl}$ dorsolateral and ventral prostate epithelium, where layers of cells have arisen in AH foci that contain enlarged, centrally located nuclei (figure 3.15i-l). The number of cells expressing AR was also increased in AH lesions (figure 3.15m-p), indicating that *Lkb1* deletion in the dorsolateral and ventral prostatic epithelium parallels that of the anterior prostate and may promote androgen-induced tumourigenesis.

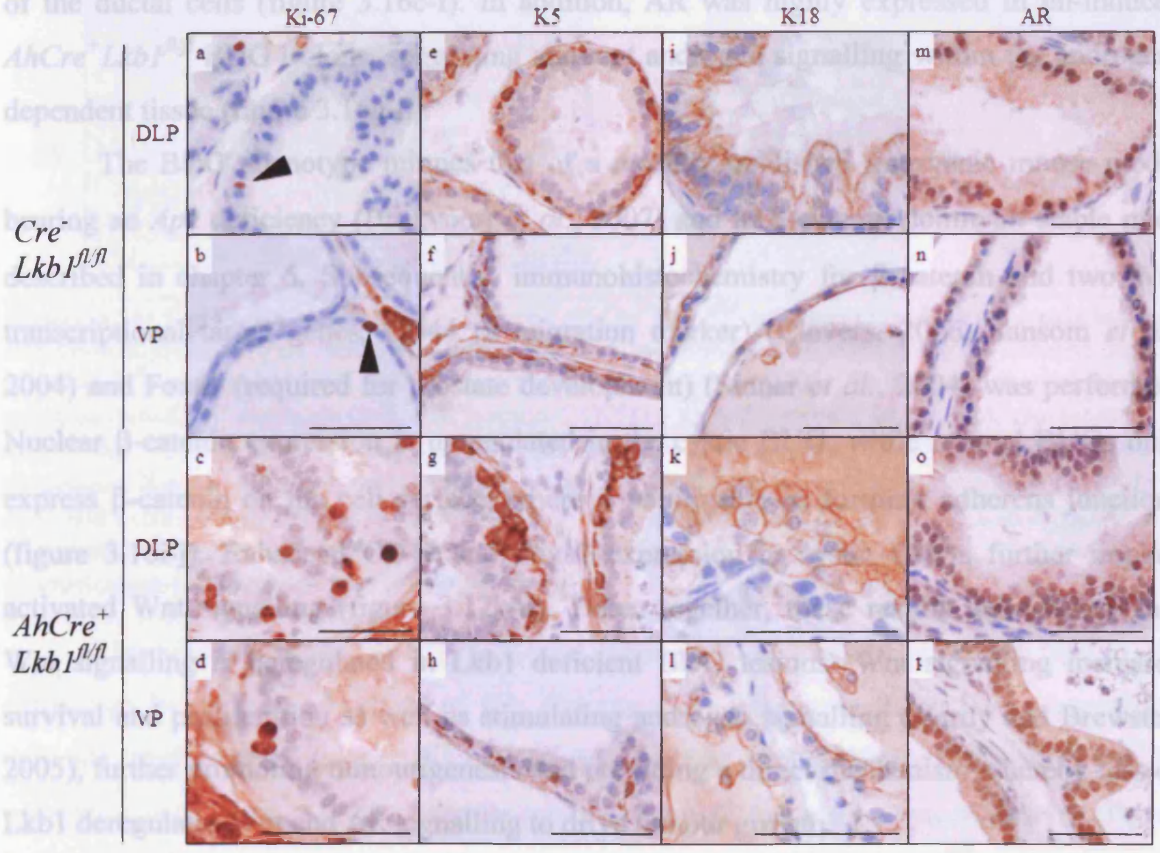


**Figure 3.15: Characterisation of atypical hyperplasia in the dorsolateral and ventral lobes of *Lkb1* deficient mice.** Immunohistochemistry of 10% formalin-fixed, paraffin-embedded sections from un-induced control (*Cre*$^{-}$*Lkb1*$^{fl/fl}$) and un-induced *AhCre*$^{+}$*Lkb1*$^{fl/fl}$ mice aged 2-7 months revealed an increase in proliferation using an anti-Ki-67 antibody in both the dorsolateral (DLP) and ventral (VP) lobes (a-d). Arrowheads indicate a basal level of proliferation in normal epithelium. Basal cell clustering was detected in hyperplastic foci by monitoring Keratin-5 expression (e-h). The luminal cell marker Keratin-18 was expressed in control prostate epithelium and was upregulated in Lkb1 deficient AH foci (i-l). AR was upregulated in hyperplastic lesions, suggesting deregulation of androgen signalling (m-p). Images were taken at 40x magnification and scale bars represent 50 μm.

### 3.3.10 Characterisation of un-induced *AhCre*$^{+}$*Lkb1*$^{fl/fl}$ bulbourethral gland, urethra and seminal vesicle lesions

Un-induced *AhCre*-mediated recombination of the floxed *Lkb1* transgene also occurred in the bulbourethral gland (BUG), urethra and seminal vesicle (figure 3.10). These tissues displayed abnormalities that were characterised further by means of immunohistochemistry. Firstly, un-induced *AhCre*$^{+}$*Lkb1*$^{fl/fl}$ mice were predisposed to hyperplasia of the BUG in association with the development of cystic lesions. Immunohistochemistry determined that un-induced *AhCre*$^{+}$*Lkb1*$^{fl/fl}$ BUGs exhibited elevated Ki-67 staining within the hyperplastic ductal cells and immune infiltrate, indicating these lesions are highly proliferative (figure 3.16a-b). Keratin-5 and Keratin-18 were also upregulated in un-induced *AhCre*$^{+}$*Lkb1*$^{fl/fl}$ BUG lesions, consistent with transdifferentiation of the ductal cells (figure 3.16c-f). In addition, AR was highly expressed in un-induced *AhCre*$^{+}$*Lkb1*$^{fl/fl}$ BUG lesions, suggesting aberrant androgen signalling within the androgen-dependent tissue (figure 3.16g-h).

The BUG phenotype mimics that of a recently published transgenic mouse model bearing an *Apc* deficiency (Bruxvoort *et al.*, 2007) and in β-catenin dominant stable mice described in chapter 5. Subsequently, immunohistochemistry for β-catenin and two Wnt transcriptional target genes, CD44 (a migration marker) (Clevers, 2006; Sansom *et al.*, 2004) and Foxa1 (required for prostate development) (Sinner *et al.*, 2004) was performed. Nuclear β-catenin expression is upregulated in the cystic BUG, while normal BUGs only express β-catenin on the cell surface, where it participates in forming adherens junctions (figure 3.16i-j). Enhanced CD44 and Foxa1 expression in cystic BUGs further implies activated Wnt signalling (figure 3.12k-n). Taken together, these results demonstrate that Wnt signalling is deregulated in Lkb1 deficient BUG lesions. Wnt signalling increases survival and proliferation as well as stimulating androgen signalling (Yardy and Brewster, 2005), further promoting tumourigenesis and providing a direct mechanism whereby loss of Lkb1 deregulates Wnt and AR signalling to drive tumour growth.

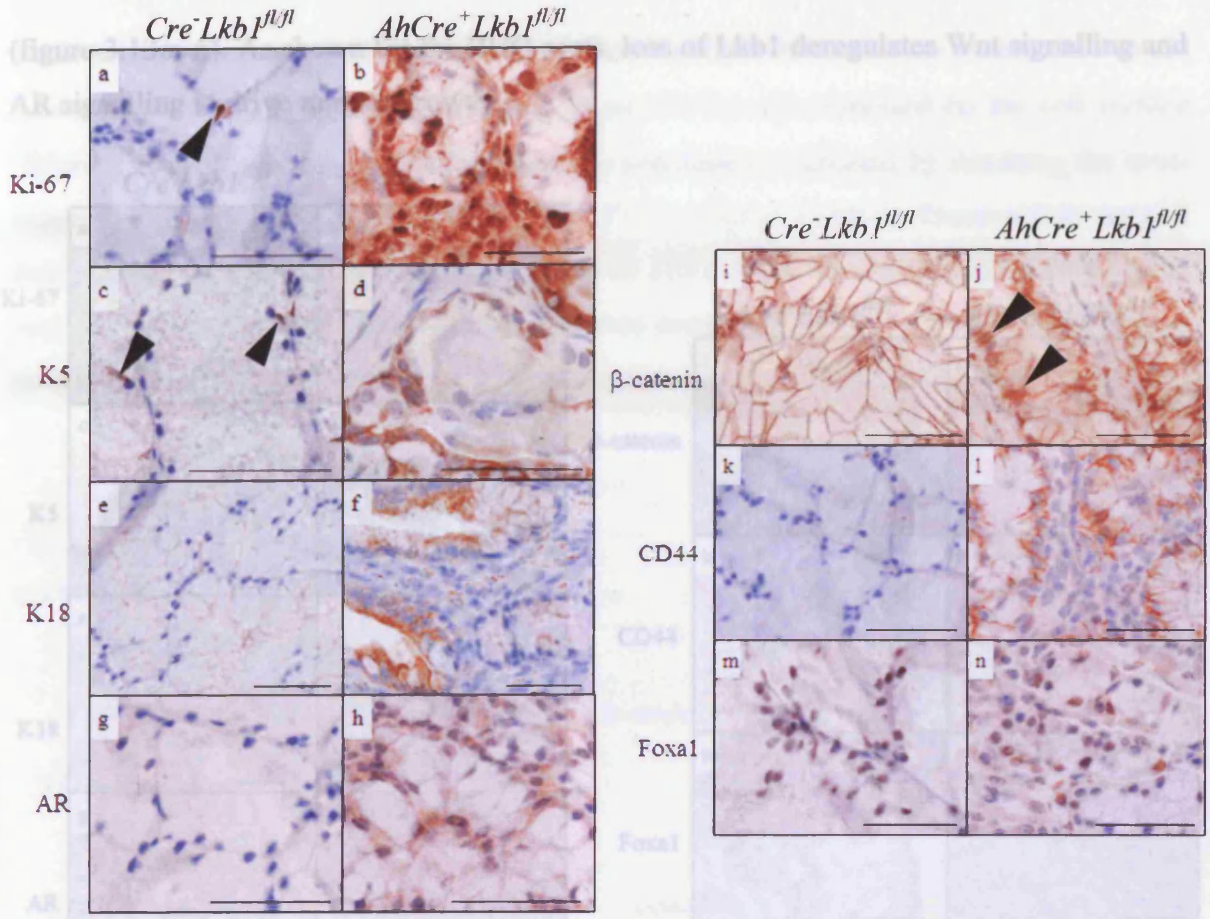


**Figure 3.16: Characterisation of un-induced *AhCre⁺Lkb1^fl/fl* bulbourethral gland cystic lesions.** Immunohistochemistry of 10% formalin-fixed, paraffin-embedded sections from un-induced control (*Cre⁻Lkb1^fl/fl*) and un-induced *AhCre⁺Lkb1^fl/fl* mice (aged 2-7 months). An increase in proliferation, using an anti-Ki-67 antibody (a-b) and Keratin-5 (K5) (c-d) was detected in the BUG ductal cells of un-induced *AhCre⁺Lkb1^fl/fl* mice. Arrowheads indicate a basal level of proliferation and K5 expression. Keratin-18 (K18) (e-f), AR (g-h), and Wnt signalling components, β-catenin (i-j), CD44 (k-l) and Foxa1 (m-n) were also upregulated in Lkb1 deficient BUGs. This evidence suggests that BUG tumourigenesis might be driven by aberrant Wnt and AR signalling. Images were taken at 40x magnification and the scale bars represent 50 μm.

Un-induced *AhCre⁺Lkb1^fl/fl* mice were predisposed to urethral gland and transitional epithelium hyperplasia. Analysis of this phenotype by immunohistochemistry determined that the proliferation marker Ki-67 (figure 3.17a-b) and Keratin-5 (figure 3.17c-d) expression is elevated in urethral lesions while Keratin-18 expression was not altered (figure 3.17e-f). Androgen receptor is highly expressed in un-induced *Cre⁻Lkb1^fl/fl* control urethral transitional epithelium and this level of expression was maintained in the un-induced *AhCre⁺Lkb1^fl/fl* hyperplastic lesions (figure 3.17g-h). Further investigation determined that urethral tumourigenesis is associated with an increase in the nuclear localisation of β-catenin, suggesting Wnt signalling is active in this tissue (figure 3.17i-j). Consistent with this, Wnt transcriptional targets CD44 (figure 3.17k-l) and Foxa1 were also over expressed

(figure 3.13m-n). As shown for the BUG cysts, loss of Lkb1 deregulates Wnt signalling and AR signalling to drive tumour growth.

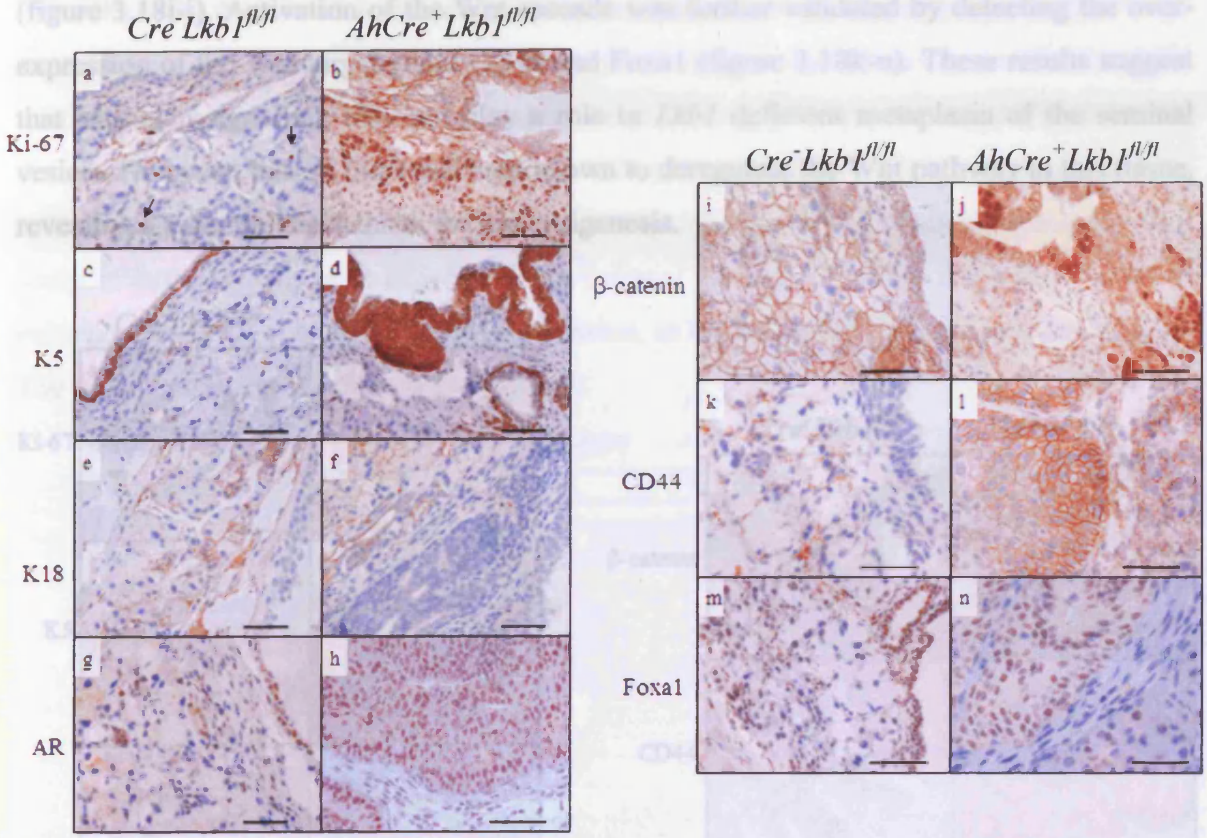


**Figure 3.17: Characterisation of un-induced *AhCre⁺Lkb1fl/fl* urethral gland and transitional epithelium hyperplasia.** Immunohistochemistry of 10% formalin-fixed, paraffin-embedded sections from un-induced control (*Cre⁻Lkb1fl/fl*) and un-induced *AhCre⁺Lkb1fl/fl* mice aged 2-7 months revealed an increase in proliferation of the un-induced *AhCre⁺Lkb1fl/fl* urethral glands and transitional epithelium using an anti-Ki-67 antibody (a-b). The arrow in (a) indicates a basal level of proliferation in the urethra. Keratin-5 (K5) is located in the basal layer of the transitional epithelium that is 1-2 cells thick in control tissue (c). In un-induced *AhCre⁺Lkb1fl/fl* hyperplastic foci, K5 is expressed continuously throughout hyperplastic foci, some 4-8 cells thick (d). Keratin-18 (K18) is expressed within the urethral glands (e) and expression was not altered in un-induced *AhCre⁺Lkb1fl/fl* urethral lesions (f). AR is highly expressed in control transitional epithelium, and the number of cells expressing AR in hyperplastic lesions was increased (g-h). Wnt signalling components, β-catenin (i-j), CD44 (k-l) and Foxa1 (m-n) were all upregulated in urethral tumours. Images were taken at 40x magnification and scale bars represent 50 μm.

Seminal vesicle squamous metaplasia occurred with 11% incidence in un-induced *AhCre⁺Lkb1fl/fl* mice. Immunohistochemistry determined that tumours over-expressed the proliferation marker Ki-67 (figure 3.18a-b) as well as Keratin-5 and Keratin-18 (figure 3.18c-f). Nuclear AR was also upregulated in control and tumour tissue (figure 3.18g-h), possibly reflecting the fact that seminal vesicle growth is regulated by androgens.

Immunohistochemistry for β-catenin revealed that nuclear translocation is increased in the lesions compared to control tissue, where β-catenin is only expressed on the cell surface (figure 3.18i-j). Activation of the Wnt cascade was further validated by detecting the over-expression of the Wnt target genes CD44 and Foxa1 (figure 3.18k-n). These results suggest that androgen signalling may not play a role in *Lkb1* deficient metaplasia of the seminal vesicle. However, loss of Lkb1 has been shown to deregulate the Wnt pathway in this tissue, revealing a potential mechanism for tumourigenesis.

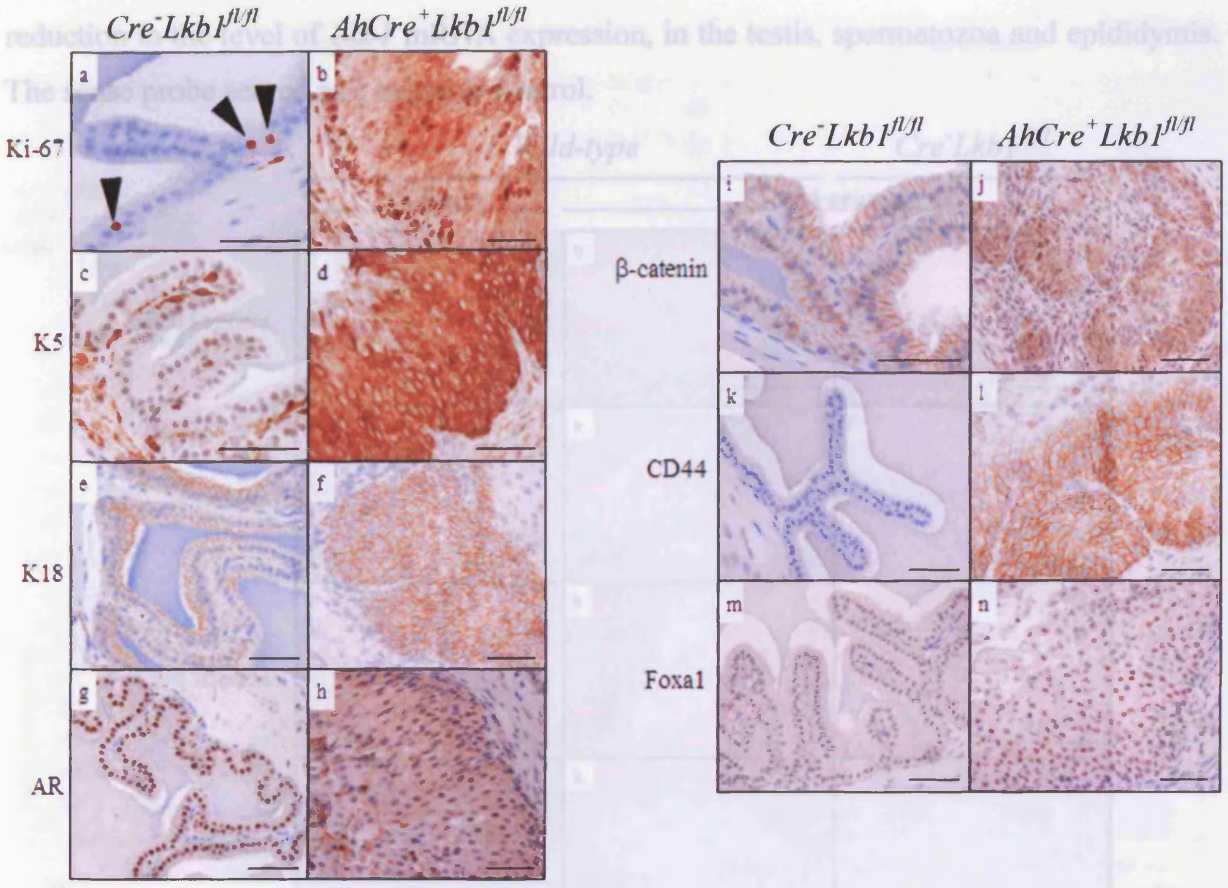


**Figure 3.18: Characterisation of seminal vesicle squamous metaplasia in un-induced *AhCre⁺Lkb1fl/fl* mice.** Immunohistochemistry of 10% formalin-fixed, paraffin-embedded sections from un-induced mice aged 2-7 months revealed that cells expressing Ki-67 (a-b), Keratin-5 (K5) (c-d), Keratin-18 (K18) (e-f), and AR (g-h) were all elevated in seminal vesicle squamous metaplasia. Increased expression of nuclear β-catenin (i-j) indicated aberrant Wnt signalling in lesions. Downstream transcriptional targets of the Wnt pathway were also upregulated, namely CD44 (k-l) and Foxa1 (m-n), indicating that the Wnt cascade is activated in Lkb1 deficient seminal vesicle squamous metaplasia. Images were taken at 40x magnification and scale bars represent 50 μm.

### 3.3.11 Characterising male sterility in un-induced *Cre⁻Lkb1$^{fl/fl}$* mice

Histology studies of the testis and epididymis from male cohorts determined infertility to be associated with reduced *Lkb1* expression in both un-induced *Cre⁻Lkb1$^{fl/fl}$* and un-induced *AhCre⁺Lkb1$^{fl/fl}$* male mice (figure 3.9). *In situ* hybridisation specific for *Lkb1* mRNA determined that *Lkb1* is expressed in all four compartments of the epididymis and in the seminiferous tubules of the testis in *wild-type* mice (figure 3.19). Interestingly, the spermatozoa also highly express the *Lkb1* transcript, correlating to an immunohistochemical study in humans (Conde *et al.*, 2007). Un-induced *Cre⁻Lkb1$^{fl/fl}$* mice displayed a marked reduction in the level of *Lkb1* mRNA expression, in the testis, spermatozoa and epididymis. The sense probe served as a negative control.

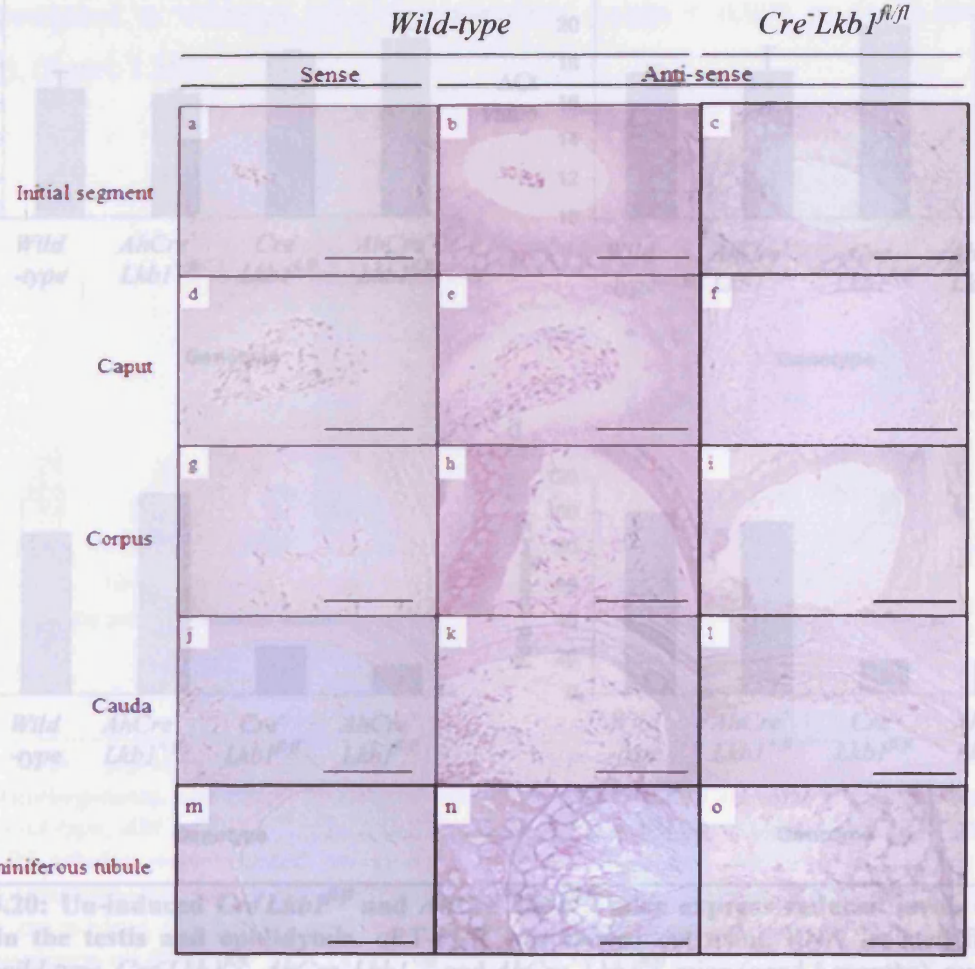


**Figure 3.19: Un-induced *Cre⁻Lkb1$^{fl/fl}$* testis and epididymis have reduced *Lkb1* mRNA transcripts.** *In situ* hybridisation was carried out using probes described in section 3.3.8 on formalin-fixed, paraffin embedded sections (aged 5 months). Un-induced *wild-type* prostate displayed *Lkb1* mRNA in all four compartments of the epididymis, seminiferous tubule epithelium, Leydig cells and spermatozoa, which was markedly reduced in un-induced *Cre⁻Lkb1$^{fl/fl}$* mice. The sense probe confirmed no un-specific binding occurred. Images were taken at 40x magnification and scale bars represent 50 μm.

A reduction in *Lkb1* mRNA transcript levels in un-induced *Cre⁻Lkb1$^{fl/fl}$* and un-induced *AhCre⁺Lkb1$^{fl/fl}$* testis and epididymis was further confirmed by means of qRT-PCR (figure 3.20). *Lkb1* mRNA levels in the testis were significantly decreased in *Cre⁻Lkb1$^{fl/fl}$* hypomorphic mice and *AhCre⁺Lkb1$^{fl/fl}$* mice (70% and 82% respectively) compared to *wild-type* and *AhCre⁺Lkb1$^{+/fl}$* testis ($p = 0.0404$, Mann Whitney), (figure 3.20a-b). The epididymis also demonstrated a significant reduction in *Lkb1* mRNA levels in *Cre⁻Lkb1$^{fl/fl}$* and *AhCre⁺Lkb1$^{fl/fl}$* mice (82% and 81% respectively) compared to control cohorts ($p = 0.0404$, Mann Whitney test), (figure 3.20c-d).

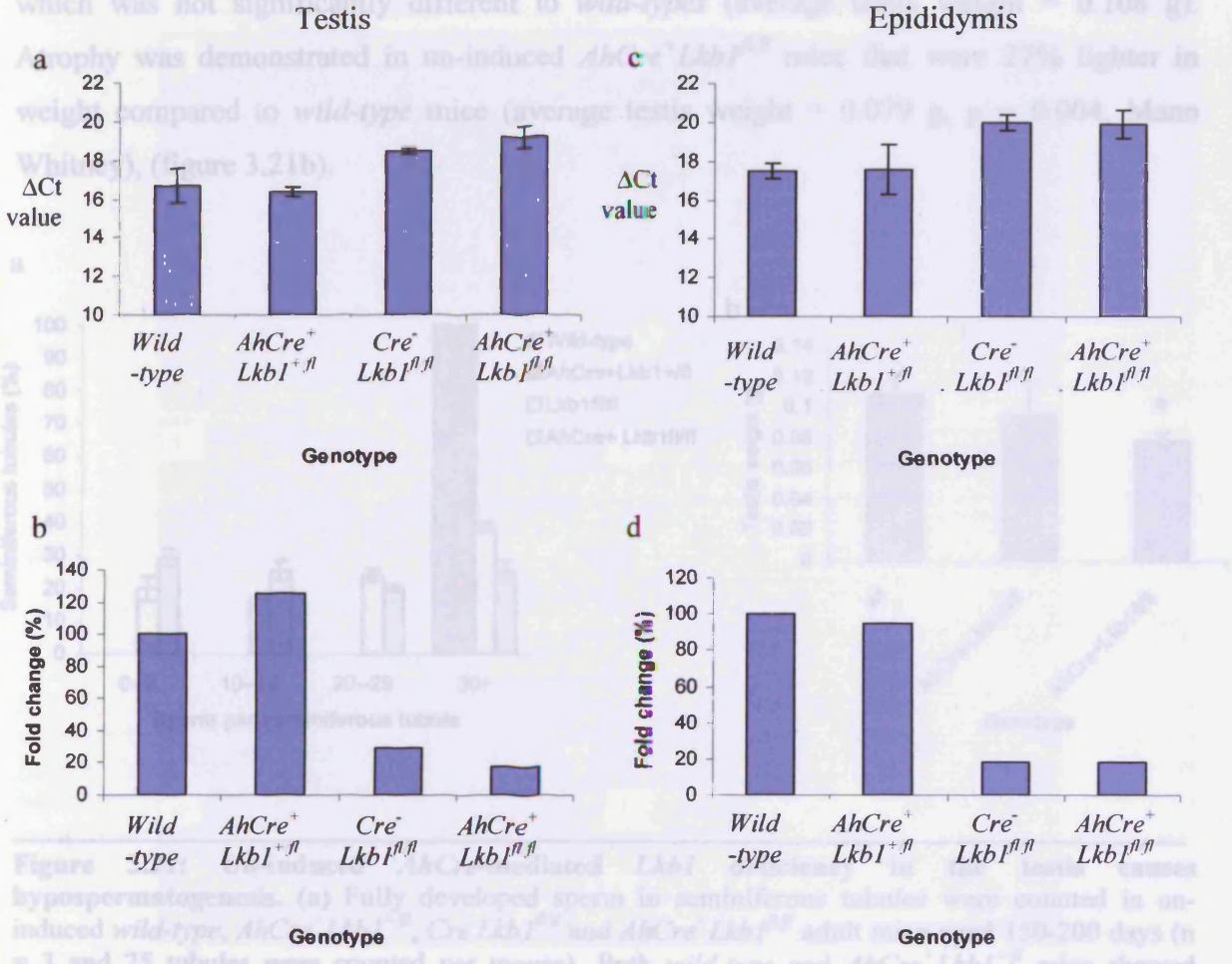


**Figure 3.20: Un-induced *Cre⁻Lkb1$^{fl/fl}$* and *AhCre⁺Lkb1$^{fl/fl}$* mice express reduced levels of *Lkb1* mRNA in the testis and epididymis.** qRT-PCR was carried out using RNA isolated from un-induced *wild-type*, *Cre⁻Lkb1$^{fl/fl}$*, *AhCre⁺Lkb1$^{+/fl}$* and *AhCre⁺Lkb1$^{fl/fl}$* mice (aged 5 months), revealing a reduction in the testis (a-b) and epididymis (c-d) within *Cre⁻Lkb1$^{fl/fl}$* and *AhCre⁺Lkb1$^{fl/fl}$* mice (n = 3). Normalised Ct (ΔCt) values confirmed that *Cre⁻Lkb1$^{fl/fl}$* and *AhCre⁺Lkb1$^{fl/fl}$* mice display a significant reduction in *Lkb1* mRNA levels in the testis (a) and epididymis (c) compared to *wild-type* and *AhCre⁺Lkb1$^{+/fl}$* cohorts ($p = 0.0404$ and $p = 0.0404$ respectively). The level of *Lkb1* mRNA in the hypomorph testis and epididymis was not significantly different to *AhCre⁺Lkb1$^{fl/fl}$* mice ($p = 0.0952$ and $p = 0.065$ respectively). Error bars represent standard deviation and statistical analysis was carried out using a non-parametric Mann Whitney test using "MiniTab" software (95% confidence interval).

To further characterise male sterility, sperm production in the testis was determined by scoring fully developed spermatozoa within the seminiferous tubules (figure 3.21a). Un-induced *wild-type* and un-induced *AhCre*$^{+}$*Lkb1*$^{+/fl}$ mice displayed >30 spermatozoa in 100% of the seminiferous tubules scored (25 per mouse, n = 3). Scoring un-induced *Cre*$^{-}$*Lkb1*$^{fl/fl}$ and *AhCre*$^{+}$*Lkb1*$^{fl/fl}$ cohorts revealed that 62% and 75% of the seminiferous tubules contained less than 30 spermatozoa respectively, indicative of hypospermatogenesis and infertility. Analysis of testis weight determined that atrophy of the organ had not occurred in un-induced *Cre*$^{-}$*Lkb1*$^{fl/fl}$ mice (average testis weight = 0.096 g, p = 0.3176, Mann Whitney), which was not significantly different to *wild-types* (average testis weight = 0.108 g). Atrophy was demonstrated in un-induced *AhCre*$^{+}$*Lkb1*$^{fl/fl}$ mice that were 27% lighter in weight compared to *wild-type* mice (average testis weight = 0.079 g, p = 0.004, Mann Whitney), (figure 3.21b).

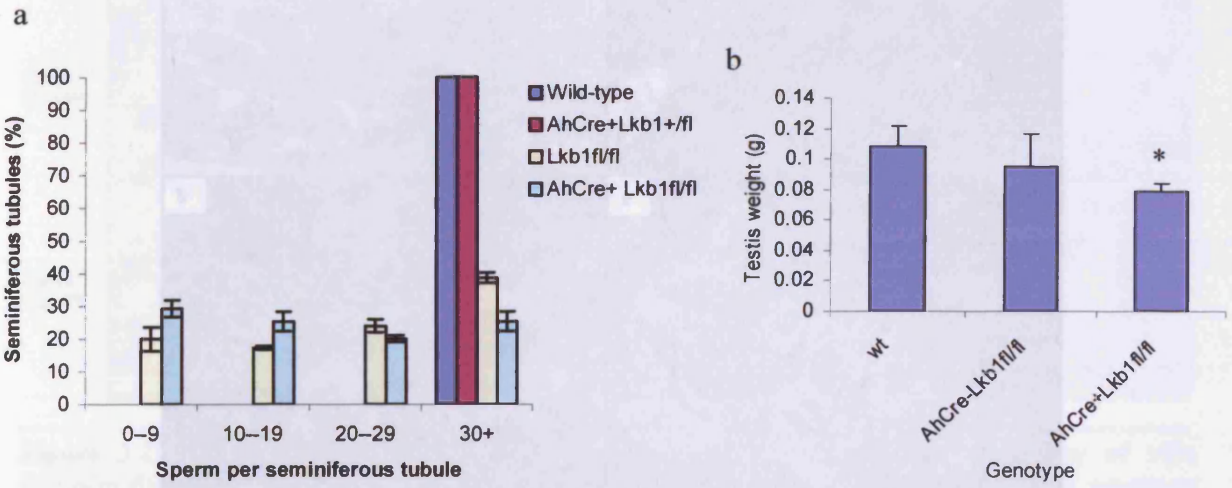


**Figure 3.21: Un-induced *AhCre*-mediated *Lkb1* deficiency in the testis causes hypospermatogenesis.** (a) Fully developed sperm in seminiferous tubules were counted in un-induced *wild-type*, *AhCre*$^{+}$*Lkb1*$^{+/fl}$, *Cre*$^{-}$*Lkb1*$^{fl/fl}$ and *AhCre*$^{+}$*Lkb1*$^{fl/fl}$ adult mice aged 150-200 days (n = 3 and 25 tubules were counted per mouse). Both *wild-type* and *AhCre*$^{+}$*Lkb1*$^{+/fl}$ mice showed normal spermatogenesis, where all seminiferous tubules scored contained >30 spermatozoa. Sperm counts in un-induced *Cre*$^{-}$*Lkb1*$^{fl/fl}$ and *AhCre*$^{+}$*Lkb1*$^{fl/fl}$ cohorts revealed hypospermatogenesis with <30 spermatozoa in 62% and 75% of the seminiferous tubules respectively. (b) Testicle weights revealed *AhCre*$^{+}$*Lkb1*$^{fl/fl}$ deficient testes (n = 5) were 27% lighter compared to *wild-types* (n = 12, p = 0.004), but not the hypomorphs (p = 0.0603). This indicates acute testicular atrophy in the conditional knockouts. Error bars represent standard deviation and statistical analysis was carried out using a non-parametric Mann Whitney test using "MiniTab" software (95% confidence interval).

Hypospermatogenesis was investigated further by means of electron microscopy (figure 3.22). Micrographs revealed that control seminiferous epithelium displays ordered architecture (figure 3.22a-b) and normal spermatozoa production (figure 3.22c). Un-induced *Cre⁻Lkb1*$^{fl/fl}$ mice demonstrate loss of cell polarity and apoptosis during spermatogenesis (figure 3.22d), along with phagocytosis of dysfunctional sperm (figure 3.22e). Abnormal sperm development (figures 3.22f and g) is considered to reflect the hypomorphic nature of the *Lkb1* floxed allele.

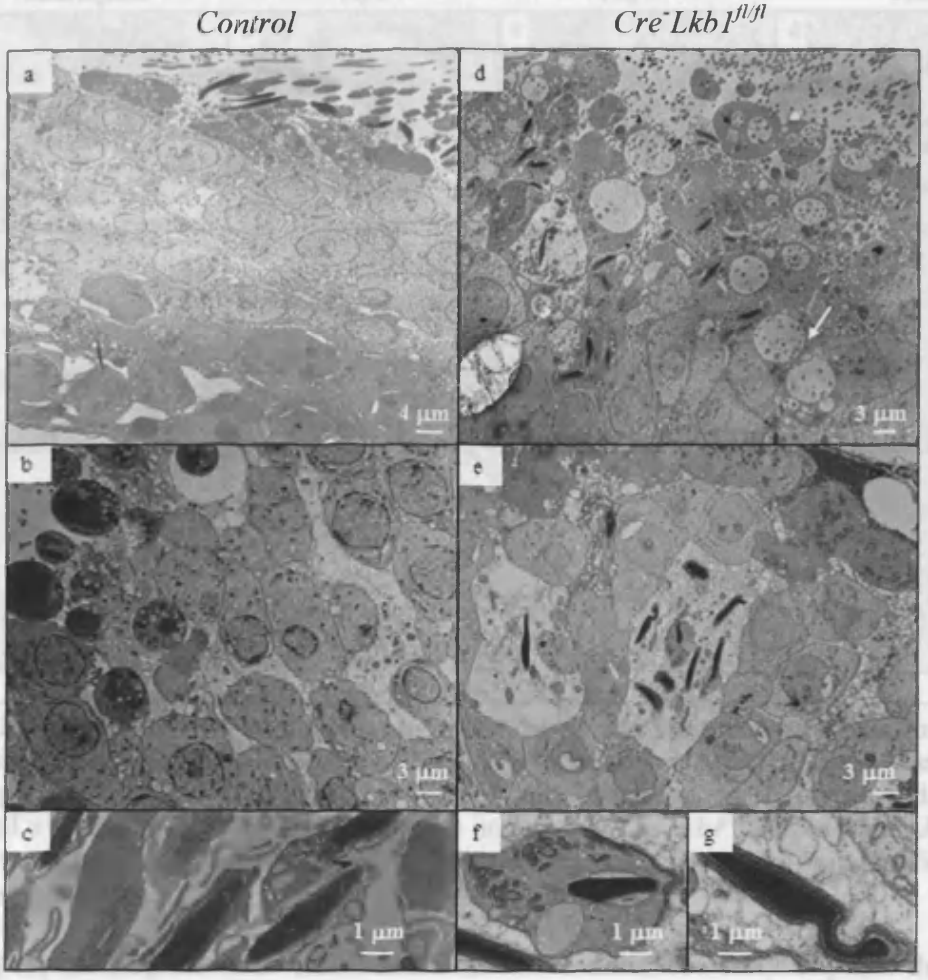


**Figure 3.22: Morphology of *Lkb1* deficient testis.** Micrographs of un-induced control (*AhCre⁺Lkb1*$^{+/fl}$) and un-induced *Cre⁻Lkb1*$^{fl/fl}$ seminiferous tubule epithelium (aged 5 months) show ordered spermatogenesis in control tissue (a-b) and normal spermatozoa (c). In *Cre⁻Lkb1*$^{fl/fl}$ testis, cell architecture is disrupted indicating loss of cell polarity and many apoptotic cells are present (arrow) (d). *Cre⁻Lkb1*$^{fl/fl}$ abnormal sperm appear to be undergoing phagocytosis (e). Abnormal sperm are depicted at high power in (f) and (g) where the tail has not formed properly (f) or the head is bent (g). Micrographs were taken using the transmission electron microscope (Phillips EM 208).

Transport of spermatozoa through the coils of the epididymis is necessary for sperm maturation and motility (Rankin *et al.*, 1992). The fact that the epididymis tubules were not dilated indicates that the epididymis is not obstructed in un-induced $Cre^{-}Lkb1^{fl/fl}$ or un-induced $AhCre^{+}Lkb1^{fl/fl}$ mice. Spermatozoa debris and macrophages are present in the lumen of the tubules and apoptotic bodies were evident in epididymis epithelium. Detection of the apoptosis marker, Caspase-3 (apoptosis-related cysteine peptidase, CP322) revealed a dramatic increase in the number of apoptotic cells in $Cre^{-}Lkb1^{fl/fl}$ epididymis (figure 3.23).

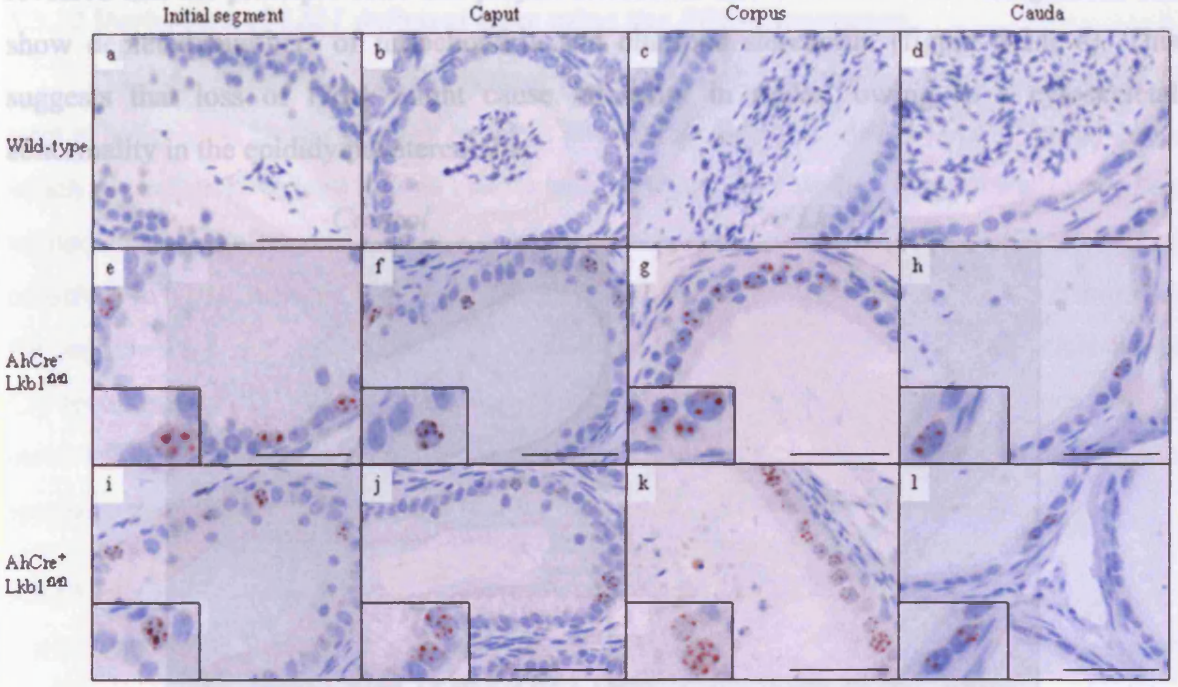


**Figure 3.23: *Lkb1* deficient epididymis is highly apoptotic.** Immunohistochemistry of 10% formalin-fixed, paraffin-embedded sections from mice aged 2-7 months to detect the apoptosis marker Caspase-3. Un-induced *wild-type* epididymis (initial segment, caput, corpus and cauda) all demonstrated a negligible level of apoptosis while un-induced $Cre^{-}Lkb1^{fl/fl}$ and $AhCre^{+}Lkb1^{fl/fl}$ mice showed elevated levels of Caspase-3 positive cells. Images were taken at 40x magnification and scale bars represent 50 μm.

Hypospermatogenesis in Lkb1 deficient testes does not fully explain the lack of spermatozoa in the epididymis. There are several potential scenarios currently acknowledged to cause infertility (Rankin *et al.*, 1992), these include; (a) loss of polarity of the stereocilia lining the epididymis, thus preventing normal passage of the sperm through the lumen, (b) abnormal sperm maturation, (c) deregulated hormone secretion from stereocilia required for sperm maturation or (d) loss of motility. Loss of motility is highly probable considering Lkb1 plays a role in both energy metabolism and cell polarity (Yoo *et al.*, 2002) and that *Lkb1* mRNA is expressed in spermatozoa in mice (figure 3.19) and

humans (Conde *et al.*, 2007). Nonetheless, mature sperm were not detected in the epididymis where the spermatozoa complete the maturation process and gain the ability to become motile. Preliminary sperm motility assays did not detect mature sperm in the epididymis, only cellular debris (data not shown). To further investigate the cause of aspermia in the epididymis, a morphological investigation using electron microscopy was carried out. Control epididymis displayed ordered architecture of the epithelium and stereocilia (figure 3.24a-b). Micrographs of the un-induced *Cre⁻Lkb1* deficient epididymis revealed that the principle cells that project stereocilia into the lumen are disorganised and show depleted numbers of mitochondria and clumped stereocilia (figure 3.24c-d). This suggests that loss of Lkb1 might cause infertility in males, owing to a cytoskeletal abnormality in the epididymal stereocilia.

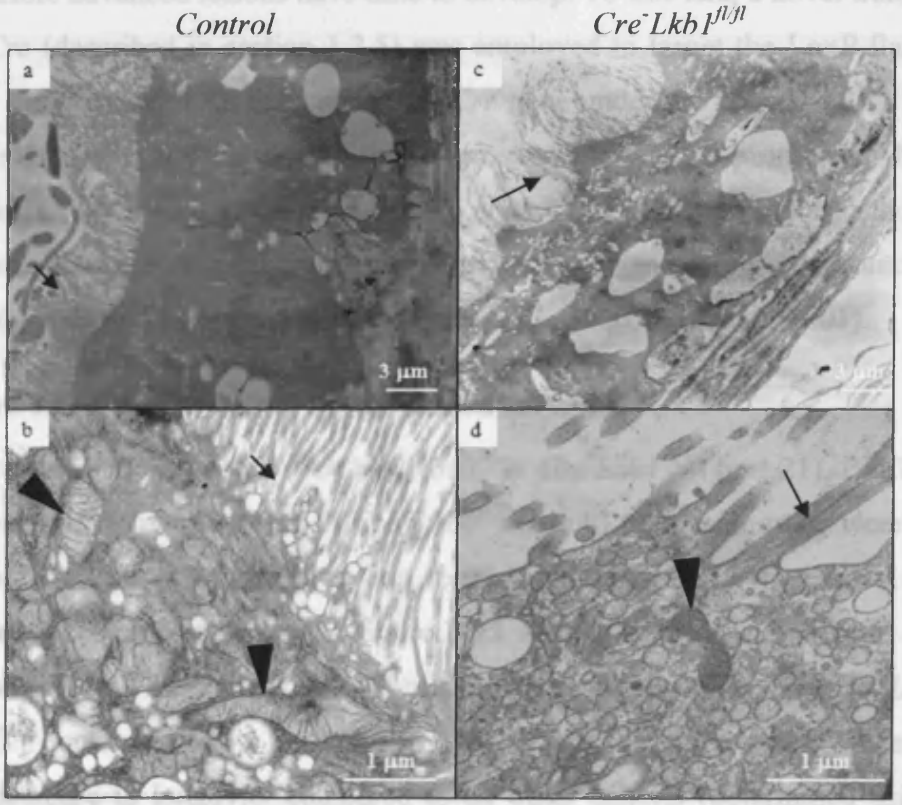


**Figure 3.24: Morphology of Lkb1 deficient epididymis.** Electron micrographs were taken from un-induced control (*AhCre⁺Lkb1⁺/fl*) and un-induced *Cre⁻Lkb1fl/fl* caput epididymis (aged 5 months). Control epididymal epithelium demonstrated ordered architecture with a smooth apical surface which projects stereocilia (arrow) into the lumen (a). The stereocilia are supported by many mitochondria (arrow heads) to provide energy for their movement (b). Lkb1 deficient epididymis manifested aberrant architecture where the apical surface appears to have lost cellular polarity and the stereocilia appear clumped together (c). High magnification of the stereocilia revealed a reduction in mitochondria and a disruption in the coordination of the stereocilia from the apical surface of the principle cells of the epididymal epithelium (d). Arrowheads indicate mitochondria and arrows point to stereocilia. Micrographs were taken using the transmission electron microscope (Phillips EM 208).

Together, these data suggest that infertility in Lkb1 deficient mice is likely to be caused by hypospermatogenesis, abnormal development of sperm in the testis, as well as loss of cellular polarity, apoptosis and aberrant stereocilia formation in the epididymis epithelium (figure 3.22-3.24). This is in keeping with Lkb1 being responsible for microtubule integrity (Karuman *et al.*, 2001). Disruption of stereocilia might prevent sperm transport through the coils and could disrupt secretion and absorption of epididymal proteins required for maturation, such as MEP7-10 (Rankin *et al.*, 1992).

### 3.3.12 Derivation of *Lkb1* deficient mice using the *PBCre* transgene

The development of bulbourethral gland cysts and interstitial infection of the GU tract is believed to be the primary cause of reduced longevity in $AhCre^{+}Lkb1^{fl/fl}$ male mice, which die before advanced lesions have time to develop. To this end, a novel transgenic line termed *PBCre* (described in section 1.2.5) was employed to target the LoxP-flanked *Lkb1* construct to the prostate. This line carries the *Cre* gene under the control of the composite PB promoter, $ARR_2PB$, a derivative of the rat prostate-specific *PB* promoter, which drives *Cre* recombinase expression in the prostate (Wu *et al.*, 2001). This promoter is thought to be more efficient than the original minimal *PB* promoter or the large *PB* promoter and is spontaneously activated by androgens (Maddison *et al.*, 2000; Wu *et al.*, 2001).

### 3.3.13 $PBCre^{+}Lkb1^{fl/fl}$ mice do not show reduced survival

Cohorts of male *wild-type* ($PBCre^{+}Lkb1^{+/+}$ *or* $Cre^{-}Lkb1^{+/+}$) (n = 21), $PBCre^{+}Lkb1^{+/fl}$ (n = 14), $Cre^{-}Lkb1^{fl/fl}$ (n = 12), and $PBCre^{+}Lkb1^{fl/fl}$ (n = 8) transgenic mice were generated and aged to 500 days or sacrificed owing to ill health (or tumour burden >1 cm). The Kaplan-Meier survival plot shown in figure 3.25 compares the survival rates of *PBCre* cohorts harbouring the LoxP-flanked *Lkb1* allele with aged, un-induced $AhCre^{+}Lkb1^{+/fl}$ and $AhCre^{+}Lkb1^{fl/fl}$ cohorts. Only un-induced $AhCre^{+}Lkb1^{fl/fl}$ mice show a statistically significant decrease in longevity compared to all other cohorts (determined using a Chi-squared test) and the aged $Cre^{-}Lkb1^{fl/fl}$, $PBCre^{+}Lkb1^{+/fl}$ and $PBCre^{+}Lkb1^{fl/fl}$ cohorts exhibited survival rates similar to the *wild-type* mice.

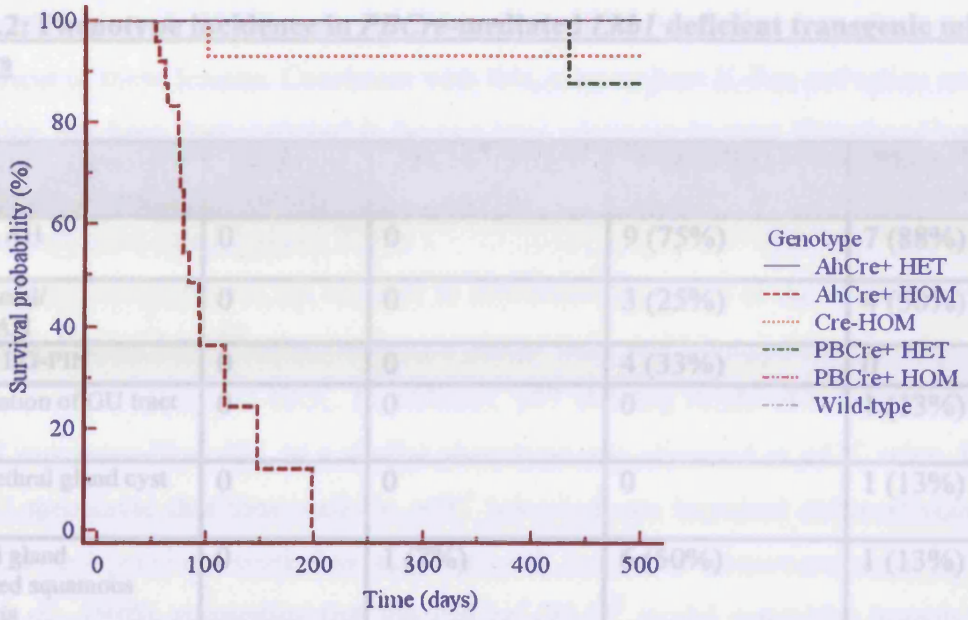


**Figure 3.25: Un-induced *AhCre$^+$Lkb1$^{fl/fl}$* male mice display reduced longevity compared to *PBCre$^+$Lkb1$^{fl/fl}$* mice.** (a) Kaplan-Meier plot of *wild-type* (n = 14), un-induced *AhCre$^+$Lkb1$^{+/fl}$* (n = 13), un-induced *AhCre$^+$Lkb1$^{fl/fl}$* (n = 26), *Cre$^-$Lkb1$^{fl/fl}$* (n = 12), *PBCre$^+$Lkb1$^{+/fl}$* (n = 14) and *PBCre$^+$Lkb1$^{fl/fl}$* (n = 8) mice aged to 500 days or sacrificed when sick. Only un-induced *AhCre$^+$Lkb1$^{fl/fl}$* mice demonstrate decreased longevity, with 100% of the cohort not surviving past 200 days. Chi-squared tests confirmed un-induced *AhCre$^+$Lkb1$^{fl/fl}$* mice exhibit a significantly reduced average survival of 83 days compared to *wild-types* ($p = 0.000$, $\chi^2 = 65.42$), *Cre$^-$Lkb1$^{fl/fl}$* ($p = 0.000$, $\chi^2 = 29.43$) and *PBCre$^+$Lkb1$^{fl/fl}$* ($p = 0.000$, $\chi^2 = 20.46$) cohorts. Chi-squared tests were performed using MiniTab software and the Kaplan-Meier survival curve was generated using 'MedCalc' software.

### 3.3.14 *PBCre$^+$Lkb1$^{fl/fl}$* mice develop multiple GU tract phenotypes

Histological analysis of H&E sections from all cohorts aged 500 days determined several GU tract phenotypes were predisposed in *Cre$^-$* and *PBCre$^+$* Lkb1 deficient mice (Table 3.2). Inflammation of the GU tract was only observed in a single mouse of the *PBCre$^+$Lkb1$^{fl/fl}$* cohort that also harboured a BUG cyst, further linking the co-incident development of these two phenotypes that were frequently observed in un-induced *AhCre$^+$Lkb1$^{fl/fl}$* mice.

**Table 3.2: Phenotype incidence in *PBCre*-mediated *Lkb1* deficient transgenic mice at 500 days**

| Phenotype \ Genotype | *Wild-type* (n=21) | *PBCre*$^{+}$*Lkb1*$^{+/fl}$ (n=14) | *PBCre*$^{-}$*Lkb1*$^{fl/fl}$ (n=12) | *PBCre*$^{+}$*Lkb1*$^{fl/fl}$ (n=8) |
|---|---|---|---|---|
| Anterior AH | 0 | 0 | 9 (75%) | 7 (88%) |
| Dorsolateral/ Ventral AH | 0 | 0 | 3 (25%) | 4 (50%) |
| Anterior LG-PIN | 0 | 0 | 4 (33%) | 0 |
| Inflammation of GU tract | 0 | 0 | 0 | 1 (13%) |
| Bulbourethral gland cyst | 0 | 0 | 0 | 1 (13%) |
| Preputial gland keratinised squamous metaplasia | 0 | 1 (7%) | 6 (50%) | 1 (13%) |
| Seminal vesicle squamous metaplasia | 0 | 0 | 0 | 1 (13%) |
| Infertile | 0 | 0 | 12 (100%) | 8 (100%) |
| Stomach hamartoma | 0 | 3 (21%) | 4 (33%) | 3 (38%) |
| Kidney abnormalities | 0 | 6 (42%) | 4 (33%) | 8 (100%) |

### 3.3.15 *PBCre*$^{+}$*Lkb1*$^{fl/fl}$ mice develop prostate atypical hyperplasia

Histological analysis of *PBCre* cohorts aged to 500 days determined that both *Cre*$^{-}$*Lkb1*$^{fl/fl}$ and *PBCre*$^{+}$*Lkb1*$^{fl/fl}$ mice were predisposed to a prostate phenotype, while control (*PBCre*$^{+}$*Lkb1*$^{+/fl}$) prostate showed normal duct architecture (figure 3.26a-c). *Cre*$^{-}$*Lkb1*$^{fl/fl}$ mice aged to 500 days displayed atypical hyperplasia (AH) in the anterior, dorsolateral and ventral lobes of the prostate (75%, 25% and 25% incidence respectively), which progressed to LG-PIN in the anterior prostate with 33% incidence. LG-PIN foci displayed cribriform structures and cytological atypia, resembling the *AhCre*$^{+}$*Lkb1*$^{fl/fl}$ model (figure 3.26d-f). This phenotype was not observed in *Cre*$^{-}$*Lkb1*$^{fl/fl}$ mice that were only aged to 200 days however, differences in strain, background and cellular stress levels may also play a role.

*PBCre*$^{+}$*Lkb1*$^{fl/fl}$ mice developed anterior, dorsolateral and ventral AH foci with 88%, 50% and 50% incidence respectively and progression to PIN was not observed (figure 3.26g-i). AH lesions in *PBCre*$^{+}$*Lkb1*$^{fl/fl}$ mice also demonstrated a high number of apoptotic bodies. Interestingly, epithelium of the anterior lobe also exhibited large cytoplasmic vacuoles that contained basal and compressed nuclei (figure 3.26g). This phenotype resembles mucinous metaplasia observed in *PBCre*$^{+}$ mice bearing an H-*Ras* activating

mutation (Scherl *et al.*, 2004), suggesting that aberrant Ras signalling may play a role in the development of these lesions. Consistent with this, concomitant K-Ras activation and LKB1 inactivation has been demonstrated in human lung adenocarcinomas (Sanchez-Cespedes *et al.*, 2002), and a recent mouse lung cancer model has shown cooperativity between K-ras activation and Lkb1 loss (Ji *et al.*, 2007).

Further investigations are required to determine the nature of the mucinous-like cells observed in *PBCre*$^{+}$*Lkb1*$^{fl/fl}$ mice, such as a mucin stain and immunohistochemistry of Ras effectors, such as MEK and ERK. In addition, p63 staining might also help to define the observed mucinous-like cells, as a similar phenotype was observed in *p63*$^{-/-}$ mice. Kurita *et al* (2004) speculated that these cells in *p63*$^{-/-}$ mice indicate impaired differentiation of the basal cells and previous work has also reported mucinous adenocarcinoma in humans (Odom *et al.*, 1986), suggesting that the *PBCre*$^{+}$*Lkb1*$^{fl/fl}$ model resembles human prostate pathology.

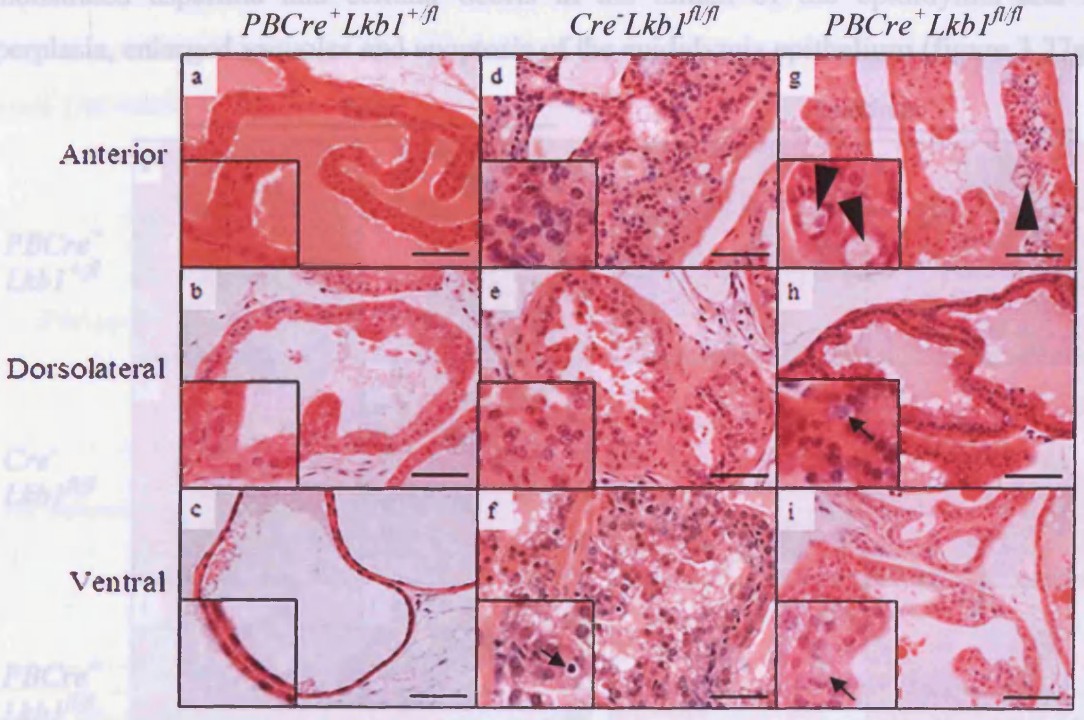


**Figure 3.26: *PBCre*-mediated deletion of *Lkb1* causes prostate atypical hyperplasia.** Histological analysis of formalin-fixed, paraffin-embedded H&E stained prostate sections from control (*PBCre*$^{+}$*Lkb1*$^{+/fl}$) (a-c), *Cre*$^{-}$*Lkb1*$^{fl/fl}$ (d-f) and *PBCre*$^{+}$*Lkb1*$^{fl/fl}$ (g-i) mice (aged 500 days). *Cre*$^{-}$*Lkb1*$^{fl/fl}$ anterior prostate developed LG-PIN (d) while the dorsolateral and ventral lobes developed AH (e-f). *PBCre*$^{+}$*Lkb1*$^{fl/fl}$ mice were predisposed to AH of all four prostate lobes (g-i) and cells containing large cytoplasmic vacuoles (mucinous-like cells) were observed in the anterior lobe (arrowheads). Images were taken at 40x magnification and scale bars represent 50 μm.

### 3.3.16 *PBCre*$^{+}$*Lkb1*$^{fl/fl}$ male mice are infertile

Histological analysis of *PBCre*$^{+}$*Lkb1*$^{+/fl}$ testis (aged 500 days) revealed normal seminiferous tubule epithelium architecture and spermatogenesis (figure 3.27a-b). *Cre*$^{-}$ *Lkb1*$^{fl/fl}$ and *PBCre*$^{+}$*Lkb1*$^{fl/fl}$ male cohorts were infertile (100% incidence), resembling the *AhCre* transgenic line (section 3.3.5). Hypospermatogenesis was observed in *Cre*$^{-}$*Lkb1*$^{fl/fl}$ mice at 500 days (figure 3.27c-d), consistent with that described for *Cre*$^{-}$*Lkb1*$^{fl/fl}$ testis at 200 days and un-induced *AhCre*$^{+}$*Lkb1*$^{fl/fl}$ mice (figure 3.9). *PBCre*$^{+}$*Lkb1*$^{fl/fl}$ mice demonstrated Sertoli-cell-only syndrome (SCOS) with 100% incidence, where the seminiferous tubule epithelium is comprised solely from the Sertoli cells (figure 3.27e-f). Interestingly, PJS patients develop testicular tumours of Sertoli-cell origin, providing a direct link between the transgenic model and the human disease (Westerman and Wilson, 1999). *PBCre*$^{+}$*Lkb1*$^{+/fl}$ mice displayed normal epididymis epithelium with abundant sperm in the lumen undergoing maturation (figure 3.27g-h). *Cre*$^{-}$*Lkb1*$^{fl/fl}$ and *PBCre*$^{+}$*Lkb1*$^{fl/fl}$ mice aged to 500 days demonstrated aspermia and cellular debris in the lumen of the epididymis and focal hyperplasia, enlarged vacuoles and apoptosis of the epididymis epithelium (figure 3.27g-l).

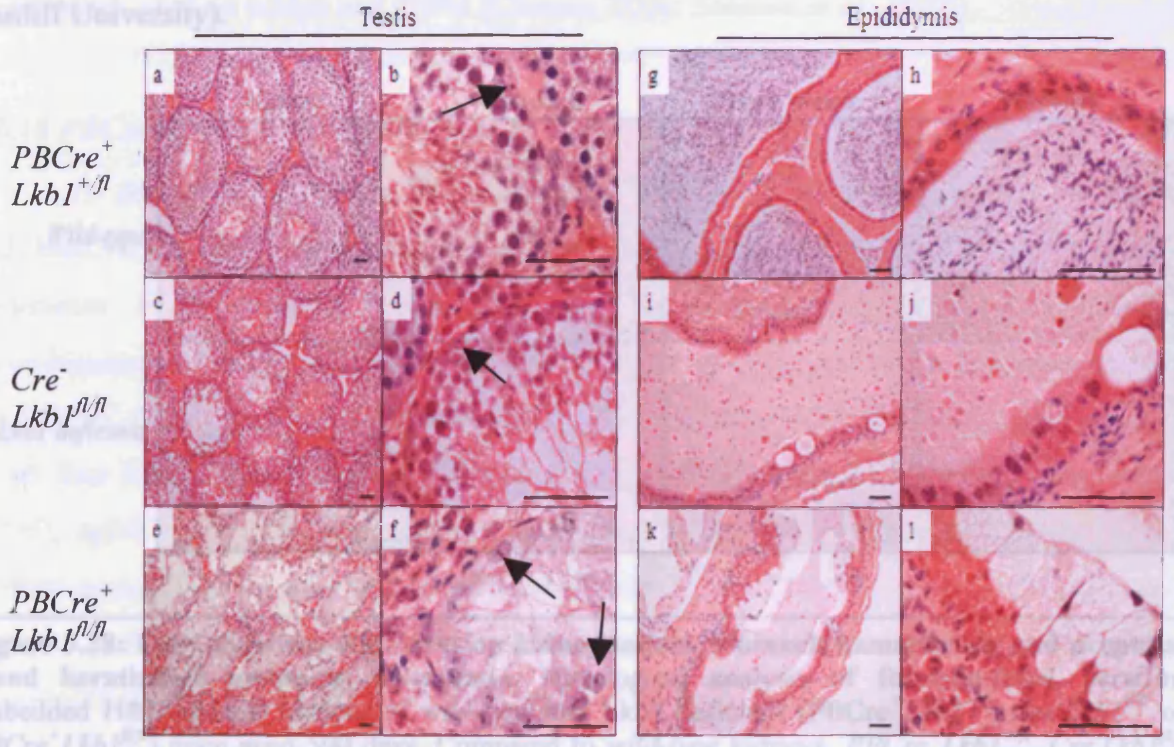


**Figure 3.27: Lkb1 deficient mice are infertile and *PBCre*-mediated recombination predisposes to Sertoli-cell-only syndrome.** Histological analysis of formalin-fixed, paraffin-embedded H&E stained sections of *PBCre*$^{+}$*Lkb1*$^{+/fl}$, *Cre*$^{-}$*Lkb1*$^{fl/fl}$ and *PBCre*$^{+}$*Lkb1*$^{fl/fl}$ testis and epididymis (caput shown) aged 500 days. Arrows indicate Sertoli cells, showing the enlarged, circular nuclei in SCOS lesions compared to the smaller, triangular nuclei of normal testis. Images were taken at 40x magnification and scale bars represent 50 μm.

### 3.3.17 *PBCre*$^{+}$ *Lkb1* deficient mice develop kidney lesions, stomach hamartomas and preputial gland squamous metaplasia

Histological analysis of *PBCre* cohorts aged to 500 days determined that *PBCre*$^{+}$*Lkb1*$^{+/fl}$, *Cre*$^{-}$*Lkb1*$^{fl/fl}$ and *PBCre*$^{+}$*Lkb1*$^{fl/fl}$ mice were predisposed to several non-prostatic lesions (figure 3.28). *PBCre*$^{+}$*Lkb1*$^{+/fl}$, *Cre*$^{-}$*Lkb1*$^{fl/fl}$ and *PBCre*$^{+}$*Lkb1*$^{fl/fl}$ mice developed kidney abnormalities (42%, 33% and 100% incidence respectively) that consisted of gross fatty deposits and epithelial neoplasms (figure 3.28b). In the small neoplasms, dilated tubules contained epithelial cells that varied in size and showed enlarged nuclei. This phenotype resembled oncocytomas in humans and preneoplastic tubuli in *p53* null mice that were also heterozygous for Wilms' Tumour 1 (*Wt1*) (Menke *et al.*, 2003). Further renal analysis (such as urine and plasma albumin levels to detect renal failure) is required to define the aberrant kidney physiology observed in *Lkb1* deficient mice. The presence of the fatty deposits has been observed previously in long-term *AhCre*$^{+}$*Lkb1*$^{+/fl}$ mice (induced with β-naphthoflavone) and is reported to share similarities with glycogen storage diseases (J Zabkiewicz, Ph.D. thesis, *In vivo* modelling of tumour suppressor gene function, 2005, Cardiff University).

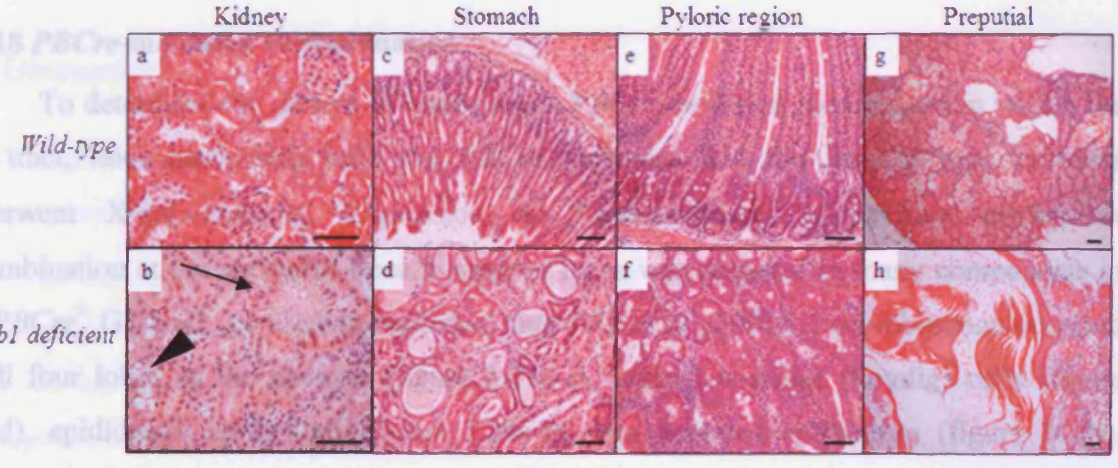


**Figure 3.28: Lkb1 deficient mice develop kidney lesions, stomach hamartomas and preputial gland keratinised squamous metaplasia.** Histological analysis of formalin-fixed, paraffin-embedded H&E stained sections of *wild-type* and Lkb1 deficient (PBCre$^{+}$*Lkb1*$^{+/fl}$, *Cre*$^{-}$*Lkb1*$^{fl/fl}$ or *PBCre*$^{+}$*Lkb1*$^{fl/fl}$) mice aged 500 days. Compared to *wild-type* kidneys, *PBCre*$^{+}$*Lkb1*$^{+/fl}$, *Cre*$^{-}$*Lkb1*$^{fl/fl}$ and *PBCre*$^{+}$*Lkb1*$^{fl/fl}$ mice developed lesions that demonstrated small epithelial neoplasms (arrow) and deposits resembling fat (arrowhead) (b). In addition hamartomas in the stomach and pyloric region were also observed with a relatively high frequency (c-f). In comparison to *wild-type* mice, Lkb1 deficient cohorts manifested keratin pearl formation in association with squamous metaplasia within the preputial gland, which also appeared dilated (g-h). Images were taken at 40x magnification and scale bars represent 50 μm.

Hamartomas of the stomach and pyloric region were detected in *PBCre*$^{+}$*Lkb1*$^{+/fl}$, *Cre*$^{-}$*Lkb1*$^{fl/fl}$ and *PBCre*$^{+}$*Lkb1*$^{fl/fl}$ mice (21%, 33% and 38% incidence respectively) aged to 500 days (figure 3.28c-f). This is consistent with PJS patients that are predisposed to hamartomatous polyps and carcinomas throughout the gastrointestinal tract with a 93% risk (Giardiello *et al.*, 1987). In addition, heterozygous, *Lkb1*$^{+/-}$ knockout mice also develop PJS symptoms, predominantly gastrointestinal hamartomatous polyposis, directly resembling the human disorder (Miyoshi *et al.*, 2002).

The preputial gland is androgen regulated and functions to produce olfactory substances. *PBCre*$^{+}$*Lkb1*$^{+/fl}$, *Cre*$^{-}$*Lkb1*$^{fl/fl}$ and *PBCre*$^{+}$*Lkb1*$^{fl/fl}$ mice aged to 500 days were also predisposed to keratinised squamous metaplasia of the preputial gland (7%, 50% and 13% respectively), shown in figure 3.28g-h. Preputial gland keratinised squamous metaplasia has been previously demonstrated in mice expressing a dominant stable form of β-catenin (Gounari *et al.*, 2002). This data suggests that Lkb1 plays a role in preventing tumourigenesis in the preputial gland and that Lkb1 loss in this gland results in deregulated Wnt signalling, which ultimately drives tumourigenesis by upregulating oncogenic Wnt target genes, such as c-Myc and CD44 (Clevers, 2006; Sansom *et al.*, 2004).

### 3.3.18 *PBCre*-mediated recombination

To determine the pattern of endogenous *PBCre*-mediated recombination within the GU tract, mice harbouring both the *PBCre* transgene and the Rosa26 reporter locus underwent X-gal staining. Expression of β-galactosidase, a positive marker of recombination at the surrogate Rosa26 reporter locus was detected in many components of the *PBCre*$^{+}$ GU tract, paralleling published data (Wu *et al.*, 2001). Recombination occurred in all four lobes of the prostate (figure 3.29a-c), testis interstitial (Leydig) cells (figure 3.29d), epididymis epithelium (figure 3.29e-h), vas deferens epithelium (figure 3.29i), urethral gland (figure 3.29j) and the stomach (figure 3.29k). Notably, no recombination was detected in the kidney, bladder, liver or transitional epithelium of the urethra, in contrast to un-induced mice expressing the *AhCre* transgene (figure 3.10).

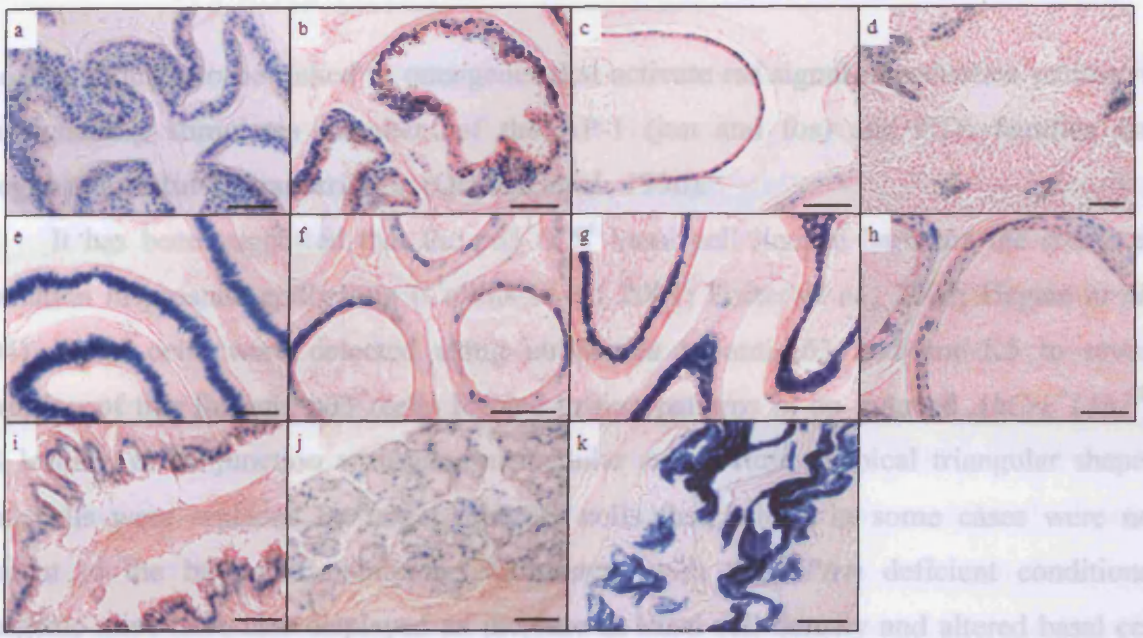


**Figure 3.29: The *PBCre* construct mediates recombination within the GU tract.** Tissue from adult male *PBCre*$^{+}$*Rosa26R*$^{+}$ transgenic mice (aged 12 months) underwent LacZ staining to determine the profile of *PBCre*-mediated recombination, where recombination events are represented by a blue stain. Recombination was detected in the anterior (a), dorsolateral (b) and ventral (c) prostate lobes as well as the interstitial (Leydig) cells of the testis (d) and the epithelium of epididymal compartments; initial segment (e), caput (f), corpus (g), and cauda (h). The epithelium of the vas deferens (i), urethral gland (j) and the stomach (k) were also positive for recombination. Images were photographed at 40x magnification and scale bars represent 50 μm.

## 3.4 Discussion

### 3.4.1 Un-induced *AhCre*$^{+}$*Lkb1*$^{fl/fl}$ mice develop prostate neoplasia, mimicking aspects of human prostate cancer

In this chapter, I have shown that the tumour suppressor Lkb1 plays a role in the onset and progression of prostate cancer using a conditional transgenic approach. Loss of Lkb1 in un-induced *AhCre*$^{+}$*Lkb1*$^{fl/fl}$ mice significantly reduced male longevity and predisposed to prostate AH that progressed to PIN in the anterior lobe (within 2-4 months), which resembled aspects of human prostate cancer. Immunohistochemical analysis of Lkb1 deficient PIN showed that the proliferation marker Ki-67 is upregulated in PIN lesions, correlating with both human and mouse PIN studies (Chin and Reiter, 2004). PIN lesions also displayed elevated levels of Keratin-18, suggesting that Lkb1 deficient PIN parallels human prostate cancer in the expression of a clinically relevant biomarker (Bostwick *et al.*, 1996; Shappell *et al.*, 2004). Keratin-18 is widely used to aid detection and identification of tumours owing to the fact that it is persistently expressed in tumour cells derived from simple (single-layered) epithelia (Oshima *et al.*, 1996). Continual Keratin-18 expression in

lesions is thought to be linked to oncogenes that activate ras signal transduction pathways. Ras signalling stimulates members of the AP-1 (jun and fos) and ETS families that upregulate Keratin-18 transcription (Oshima *et al.*, 1996).

It has been suggested that the $p63^+/K5^+$ basal cell lineage harbours the stem cell population in prostate epithelium (Collins *et al.*, 2001; Foster *et al.*, 2002; Uzgare *et al.*, 2004). Basal cells were detected using antibodies to anti-p63 and anti-K5 to reveal expansion of this lineage. $p63^+$ cells formed tufting patterns in un-induced $AhCre^+Lkb1^{fl/fl}$ PIN lesions, in conjunction with aberrant cellular architecture. Typical triangular shaped basal cells were replaced by larger, circular cells that, which in some cases were not adjacent to the basement membrane. Consistent with this, *Pten* deficient conditional transgenic mice have also displayed an increase in basal cell density and altered basal cell morphology and localisation, believed to represent expansion of the transit-amplifying zone (Wang *et al.*, 2006b). This may be confirmed by carrying out double-labelling of p63 and a transit-amplifying cell marker such as PSCA (Tran *et al.*, 2002) or c-MET (Van-Leenders *et al.*, 2002). Wang *et al* (2006) reported that the expansion of a prostate stem/progenitor-like subpopulation in $PBCre^+Pten^{fl/fl}$ mice is concomitant with basal cell proliferation and these cells expressed p63, Sca-1 and Bcl-2. Furthermore, qRT-PCR analysis of $Sca\text{-}1^+$ cells sorted by FACS displayed elevated ΔNp63, AR and keratin 5 transcript levels, while TAp63 mRNA levels were reduced (Wang *et al.*, 2006b). This suggests that expression levels of the p63 isoforms may direct the differentiation status of the basal cell population and that Pten loss can promote stem cell self renewal in the prostate, which has been shown previously in neural stem cells (Groszer *et al.*, 2006).

The trans-activating TAp63 form is considered to inhibit terminal differentiation while the non-trans-activating form ΔNp63α/β isoforms are common to adult prostate epithelium and stimulate terminal differentiation (Kurita *et al.*, 2004). Consequently, the phenotype observed in Lkb1 deficient prostate may reflect differential regulation of p63 isoforms in oncogenesis, as TAp63 and ΔNp63 are transcribed from different promoters (Park *et al.*, 2000). Interestingly, elevated p63 expression has also recently been observed in lung tumours from mice bearing *Lkb1* inactivation (Ji *et al.*, 2007). Taken together, this evidence suggests that Lkb1 may regulate basal cell differentiation and that loss of Lkb1 in un-induced $AhCre^+Lkb1^{fl/fl}$ mice may result in the expansion of the prostate stem/progenitor cell population.

In an attempt to identify tumour initiating cells within un-induced *AhCre*$^{+}$*Lkb1*$^{fl/fl}$ PIN lesions, immunohistochemistry to detect the stem cell marker CD133 was carried out (Tsujimura *et al.*, 2007). Positive nuclear CD133 staining was widely observed throughout malignant prostate epithelium, suggestive of non-specific staining. To address this hypothesis further, FACS analysis of *AhCre*$^{+}$*Lkb1*$^{fl/fl}$ PIN lesions to detect stem cell markers, such as Sca-1 and CD133, along with subsequent *in vitro* and *in vivo* analysis would be necessary (Tsujimura *et al.*, 2007; Xin *et al.*, 2005).

Anti-androgen hormone therapy is commonly undertaken to treat prostate cancer patients (Isaacs and Isaacs, 2004). Un-induced *AhCre*$^{+}$*Lkb1*$^{fl/fl}$ mice exhibited elevated levels of AR in PIN foci, suggesting tumourigenesis is probably androgen-dependent, especially considering the early stage of progression. However, this cannot be unequivocally determined without modifying the circulating level of androgens either chemically or by castration. It is speculated that these lesions would regress following androgen ablation, demonstrating androgen-dependent prostate neoplasia.

A human prostate cancer study using a tissue microarray was not possible during the time course of this project. Preliminary analysis of human prostate RNA revealed that *Lkb1* mRNA transcript levels are not significantly altered in benign prostatic hyperplasia (BPH) compared to adenocarcinomas, irrespective of tumour grade (figure 3.30). However, this might reflect the fact that Lkb1 loss is considered to play a role in cancer initiation or the cellular heterogeneity of prostate cancer. To address this, qRT-PCR to detect the level of *Lkb1* in normal prostate samples is required.

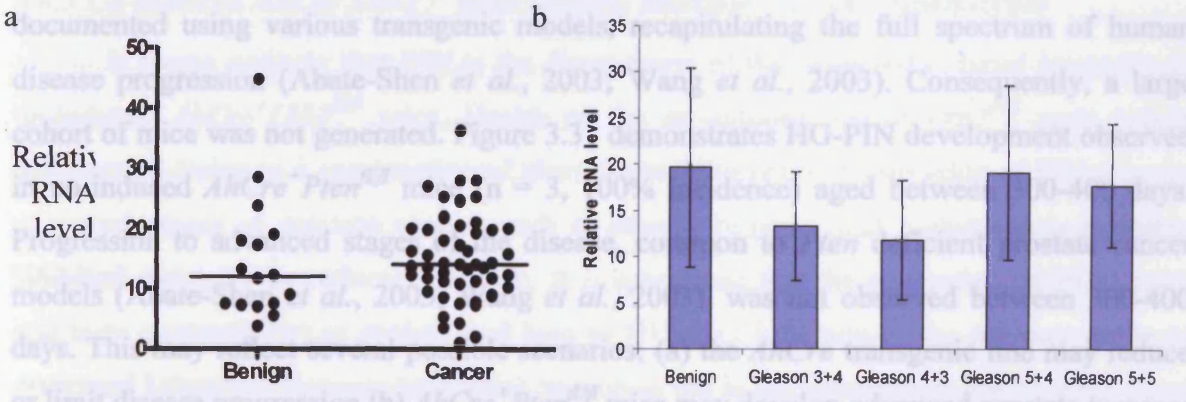


**Figure 3.30: *LKB1* mRNA expression in human prostate cancer.** (a) qRT-PCR was performed on LCMD human RNA using *Lkb1* specific primers to amplify the *Lkb1* transcript. Figure (a) was prepared by Caroline Pennington (University of East Anglia, UK). (b) Comparing benign samples (n = 16) with Gleason grades 3+4 (n=19), 4+3 (n=4), 5+4 (n=5) and 5+5 (n=5) determined there was no statistical significant difference associated with tumour aggression (p = 0.0621, p = 0.1444, p = 0.5, p = 0.4756 respectively) (b). Statistical analysis was carried out using the non-parametric Mann Whitney test (95% confidence interval) using "MiniTab" software.

### 3.4.2 The *AhCre* transgene drives spontaneous recombination events in the prostate

In un-induced mice, LacZ staining revealed that *AhCre* mediates recombination in all four lobes of the prostate, reflecting endogenous activity of the *Ah* promoter. β-galactosidase expression identified a mosaic recombination pattern, suggesting the *AhCre* transgene might target a subpopulation of cells residing in the prostate epithelium. The pattern of recombination may also reflect the differences in the genetic background of the mice, cellular stress levels or the extent of GU tract infection. Considering that recombination was observed in all four lobes of the prostate, it is surprising that the advanced lesions (HG-PIN) were restricted to the anterior prostate. The biochemical properties of each lobe are not completely understood and may play a role in determining the penetrance of the phenotype. The fact that *Lkb1* deficiency did not result in PIN with 100% incidence suggests that PIN lesions were not observed owing to the plane of sectioning. Furthermore, factors additional to *Lkb1* loss may be required to facilitate tumourigenic progression from hyperplasia to neoplasia, such as cellular stress or the genetic background. Spontaneous activity of the *Cyp1a1* (*Ah*) promoter within the prostate may be a result of endogenous *Ah* receptor transcription factors and the receptors co-factor *ARNT* (Campbell *et al.*, 1996). Furthermore, pervious work has shown that Wnt signalling may regulate *Cyp1a1* expression, following the discovery of three consensus TCF binding sites in the *Ah* receptor promoter (Chesire *et al.*, 2004).

Un-induced $AhCre^{+}Pten^{fl/fl}$ mice also developed HG-PIN, with similar phenotypic elements to that of the $AhCre^{+}Lkb1^{fl/fl}$ mice. *Pten* deficiency in the prostate has been well documented using various transgenic models, recapitulating the full spectrum of human disease progression (Abate-Shen *et al.*, 2003; Wang *et al.*, 2003). Consequently, a large cohort of mice was not generated. Figure 3.31 demonstrates HG-PIN development observed in un-induced $AhCre^{+}Pten^{fl/fl}$ mice (n = 3, 100% incidence) aged between 300-400 days. Progression to advanced stages of the disease, common to *Pten* deficient prostate cancer models (Abate-Shen *et al.*, 2003; Wang *et al.*, 2003), was not observed between 300-400 days. This may reflect several possible scenarios; (a) the *AhCre* transgenic line may reduce or limit disease progression (b) $AhCre^{+}Pten^{fl/fl}$ mice may develop advanced prostate tumours upon aging or (c) differences in genetic background, strain and cellular stress play a role in generating invasive prostate lesions.

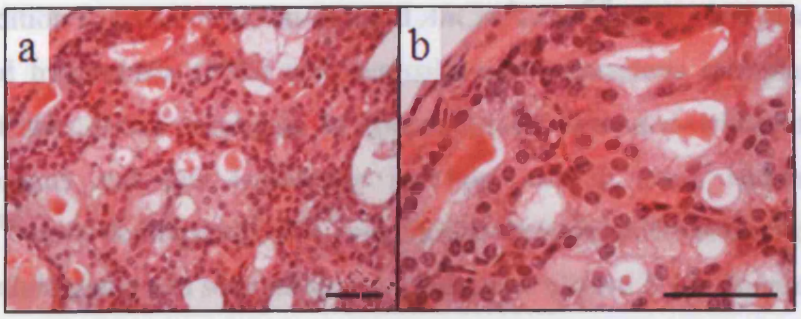


**Figure 3.31: *AhCre*$^{+}$*Pten*$^{fl/fl}$ mice develop neoplasia.** Histological analysis of formalin-fixed, paraffin-embedded H&E sections revealed *AhCre*-mediated recombination in un-induced *AhCre*$^{+}$*Pten*$^{fl/fl}$ mice results in HG-PIN (n = 3, aged 300-400 days). Images were taken at (a) 20x (low power) and (b) 40x (high power) magnification and the scale bars represent 50 μm.

It remains possible that the prostate phenotype and additional GU tract disorders observed in *AhCre*$^{+}$*Lkb1*$^{fl/fl}$ mice might be a consequence of un-induced *AhCre*-mediated recombination in a non-GU tract organ. Un-induced *AhCre*-mediated recombination has been reported previously in the kidney (Sansom *et al.*, 2005), in accordance with previous *AhCre* studies (Ireland *et al.*, 2004). Consistent with this, the Rosa26 reporter identified a low level of *AhCre*-mediated recombination in the kidney, stomach and bladder of un-induced *AhCre*$^{+}$*Lkb1*$^{fl/fl}$ mice (figure 3.10). However, histological analysis of these organs did not detect any gross phenotype, suggesting that endogenous spontaneous recombination of the *AhCre* construct in non-prostatic organs (except the BUG cyst) is not responsible for prostate tumourigenesis in this model.

### 3.4.3 Un-induced *AhCre*$^{+}$*Lkb1*$^{fl/fl}$ mice develop multiple GU tract phenotypes

It seems unlikely that PIN is the direct cause of the observed reduced longevity in un-induced *AhCre*$^{+}$*Lkb1*$^{fl/fl}$ mice. Health of the un-induced *AhCre*$^{+}$*Lkb1*$^{fl/fl}$ male cohort deteriorated owing to a combination of phenotypes. Ultimately, progression of PIN to more advanced stages of prostate cancer, such as adenocarcinoma and metastasis is probably inhibited owing to the reduced life-span. It is speculated that the generation of BUG cysts and their susceptibility to rupture and lead to GU tract infection is the primary cause of decreased longevity. Immune infiltration was observed in the interstitium and in some cases obstructing prostate acini, resembling prostatitis. Consistent with this, not all PIN lesions were associated with infection (figure 3.4). Bulbourethral disorders in association with GU tract infection have also been demonstrated in other murine prostate models, indicating that prostate tumourigenesis may predispose to cystic BUG hyperplasia (Abate-Shen *et al.*, 2003; Bhatia-Gaur *et al.*, 1999; Dunker and Aumuller, 2002).

In addition to BUG cysts, un-induced *AhCre*$^{+}$*Lkb1*$^{fl/fl}$ mice were also predisposed to urethral gland hyperplasia (39%) and seminal vesicle squamous metaplasia (11%). This suggests that the *AhCre* transgene is spontaneously activated within these androgen-dependent organs and this hypothesis is supported by LacZ staining. Un-induced *AhCre*$^{+}$*Lkb1*$^{fl/fl}$ mice demonstrated *AhCre*-mediated recombination of the Rosa26 reporter in the BUG, urethral gland and seminal vesicle epithelium (figure 3.10). Immunohistochemical characterisation of these lesions showed an increased level of proliferation and Wnt signalling, which is frequently deregulated in many organs to drive tumour formation and progression (Clevers, 2006). This presents a direct mechanism whereby Lkb1 loss deregulates the Wnt pathway to promote tumourigenesis (refer to section 1.3.3). Consistent with this, mice expressing a dominant stable form of β-catenin under the control of the *MMTV-LTR-Cre* construct resulted in proliferation of the urethral glands in association with inflammation (Bierie *et al.*, 2003), closely resembling the *AhCre*$^{+}$*Lkb1*$^{fl/fl}$ phenotype. Furthermore, BUG cysts also demonstrated AR over-expression which may be linked to elevated β-catenin nuclear translocation (Yardy and Brewster, 2005). As detailed in Chapter 5, BUG lesions are frequent in mice bearing an activating β-catenin mutation, using the *PBCre* transgenic line to drive transgene expression.

### 3.4.4 *Lkb1* deficiency leads to male sterility

Lkb1 has been implicated in proliferation, cell cycle regulation and polarity events (Alessi *et al.*, 2006). All these are required for the homeostasis of adult epithelium and spermatogenesis. High levels of *Lkb1* mRNA have been detected in human seminiferous tubules using *in situ* hybridisation (Rowan *et al.*, 2000) and Conde *et al* (2007) have demonstrated that LKB1 is present in the cytoplasm of Sertoli cells, spermatids and spermatozoa and its expression mimics phospho-Acetyl CoA carboxylase, p-ACC (an AMPK target). Together, this suggests that Lkb1 may play a tumour suppressive role within the testis. Interestingly, PJS patients are predisposed to testicular cancer, particularly a rare disorder termed Sertoli cell only syndrome (SCOC), (Rowan *et al.*, 2000). Mutational screening of 28 testicular tumours by single-strand conformation polymorphism analysis revealed 4% of tumours carried a heterozygous *LKB1* missense type variant, in which glycine 163 was changed to aspartic acid (within exon 4 of the kinase domain), (Rowan *et al.*, 2000). This change was absent in the DNA of normal tissue. Together, these findings suggest that somatic mutations of LKB1 are not frequent in colorectal and testicular cancer

(Avizienyte *et al.*, 1998). However, this study does not account for any possible epigenetic inactivation of the gene.

Male un-induced $Cre^{-}Lkb1^{fl/fl}$ and $AhCre^{+}Lkb1^{fl/fl}$ mice were sterile and demonstrated hypospermatogenesis and abnormal sperm production. *In situ* hybridisation and qRT-PCR to detect mRNA showed a dramatic decrease in testicular and epipdidymal *Lkb1* transcript levels in $Cre^{-}Lkb1^{fl/fl}$ mice (70% and 81% respectively). This reflects the hypomorphic nature of the LoxP-flanked *Lkb1* allele and suggests a role for Lkb1 within these tissues. *PBCre*-mediated *Lkb1* deficiency in the testis predisposed to non-obstructive Sertoli-cell-only syndrome (SCOS) in $PBCre^{+}Lkb1^{fl/fl}$ mice at 500 days, resembling PJS patients. The fact that SCOS was not observed in un-induced $AhCre^{+}Lkb1^{fl/fl}$ or hypomorphic $Cre^{-}Lkb1^{fl/fl}$ mice (at 200 and 500 days), suggests that SCOS observed in $PBCre^{+}Lkb1^{fl/fl}$ mice could reflect a further reduction in the level of *Lkb1* mRNA in $PBCre^{+}Lkb1^{fl/fl}$ testis or that *AhCre* and *PBCre* transgenes target different cells within the testis. However, we cannot rule out the possibility that *PBCre*-mediated recombination results in Lkb1 loss in an unidentified tissue or that the genetic background and cellular stress levels, which could also predispose to SCOS.

The fact that un-induced $Cre^{-}Lkb1^{fl/fl}$, $AhCre^{+}Lkb1^{fl/fl}$ and $PBCre^{+}Lkb1^{fl/fl}$ mice demonstrated mature spermatids in some normally composed seminiferous tubules indicates that the observed phenotype is likely to be caused by impairment of early germ cell proliferation or survival, and not a specific block during sperm maturation (i.e. maturation arrest) (Behr *et al.*, 2007).

There is little in the literature to link Lkb1 loss to male infertility however, several potential scenarios exist and are discussed below. First, Lkb1 plays a role in regulating both the PI3K and mTOR signalling pathways (Alessi *et al.*, 2006) and previous work has shown that the stem cell factor (SCF)/c-kit system can regulate germ cell proliferation, meiosis, and apoptosis through the PI3K/AKT/p70S6K pathway, which is inhibited by the mTOR inhibitor Rapamycin (Feng *et al.*, 2000). Immunohistochemistry do detect active Akt and mTOR would determine whether deregulation of the PI3K/AKT and mTOR pathways plays a part in *Lkb1* deficient hypospermatogenesis. Preliminary analysis determined a decrease in p-mTOR expression in $Lkb1^{fl/fl}$ seminiferous tubules (not shown).

Second, Lkb1 loss in $PBCre^{+}Lkb1^{fl/fl}$ testis may predispose to infertility by deregulating the paracrine-mediated production of inhibin in Sertoli cells. Inhibin ($\alpha$ or $\beta$) is a gonadal glycoprotein hormone that is stimulated by FSH and functions to negatively

regulate the release of FSH in the pituitary (Pineau *et al.*, 1990). Loss of Lkb1 has been shown to play a role in Sertoli cell tumours in PJS patients, where inhibin-α is upregulated in parallel with a reduction in FSH, LH and testosterone levels in the blood (Lefevre *et al.*, 2006). Detecting FSH, LH and testosterone serum levels and determining whether *PBCre* recombination occurs in the hypothalamus, anterior pituitary or adrenal cortex may provide insights into the mechanisms leading to male infertility in the $PBCre^{+}Lkb1^{fl/fl}$ model.

Third, Lkb1 is known to mediate cellular polarity events (Alessi *et al.*, 2006; Baas *et al.*, 2004b) (section 1.3.2), subsequently loss of *Lkb1* may disrupt the adhesion of proteins participating in adherens (cadherin-catenin), tight (zonula occludens) and gap (connexins) junctions required during spermatogenesis (Pointisa *et al.*, 2005). In particular, Connexin 43 (Cx43) has been identified to play a key role in specific spermatogenic steps and Cx43 null mice (which are embryonic lethal) display a 50% reduction in primordial germ cells and exhibit abnormal proliferation and differentiation of germ cells derived from the foetal testis (Pointisa *et al.*, 2005).

Immunohistochemical analysis showed that expression of the tight junction protein ZO-1, which coincidentally binds Cx43 (Fink *et al.*, 2006), is decreased in $Cre^{-}Lkb1^{fl/fl}$ testis compared to *wild-type* mice (figure 3.32a-b). This suggests that Lkb1 regulates ZO-1 expression in the testis, which could account for the observed defect in spermatogenesis in *Lkb1* deficient mice. Consistent with this notion, LKB1 expression has been shown to rescue depolarisation of LKB1 deficient intestinal cells by redistributing ZO-1 to the brush border (Baas *et al.*, 2004a).

Aberrant ZO-1 expression in human testicular carcinoma in situ (CIS), the non-invasive precursor of most human testicular germ cell tumours, has been shown to disrupt the blood-testis barrier (Fink *et al.*, 2006), (figure 3.32c). The blood-testis barrier divides the seminiferous epithelium into a basal compartment and an adluminal compartment and this barrier is regulated by an array of signalling networks including TGFβ, occluding, PKA and PKC (Lui *et al.*, 2003). The basal compartment contains spermatogonial and preleptotene spermatocytes, which can access blood-borne circulating molecules (Fink *et al.*, 2006). All other germ cells are contained in the adluminal compartment, an immune-free environment maintained by the Sertoli cells that is required to protect post-meiotic germ cells and is essential for spermatogenesis (Fink *et al.*, 2006). Preleptotene and leptotene spermatocytes must translocate from the basal to the adluminal compartment to develop into spermatids (Lui *et al.*, 2003). Together, this evidence suggests that Lkb1 loss disrupts the formation of

ZO-1 tight-junctions, which may result in disruption of the blood-testis barrier to predispose to impaired maturation of the Sertoli cells and hypospermatogenesis.

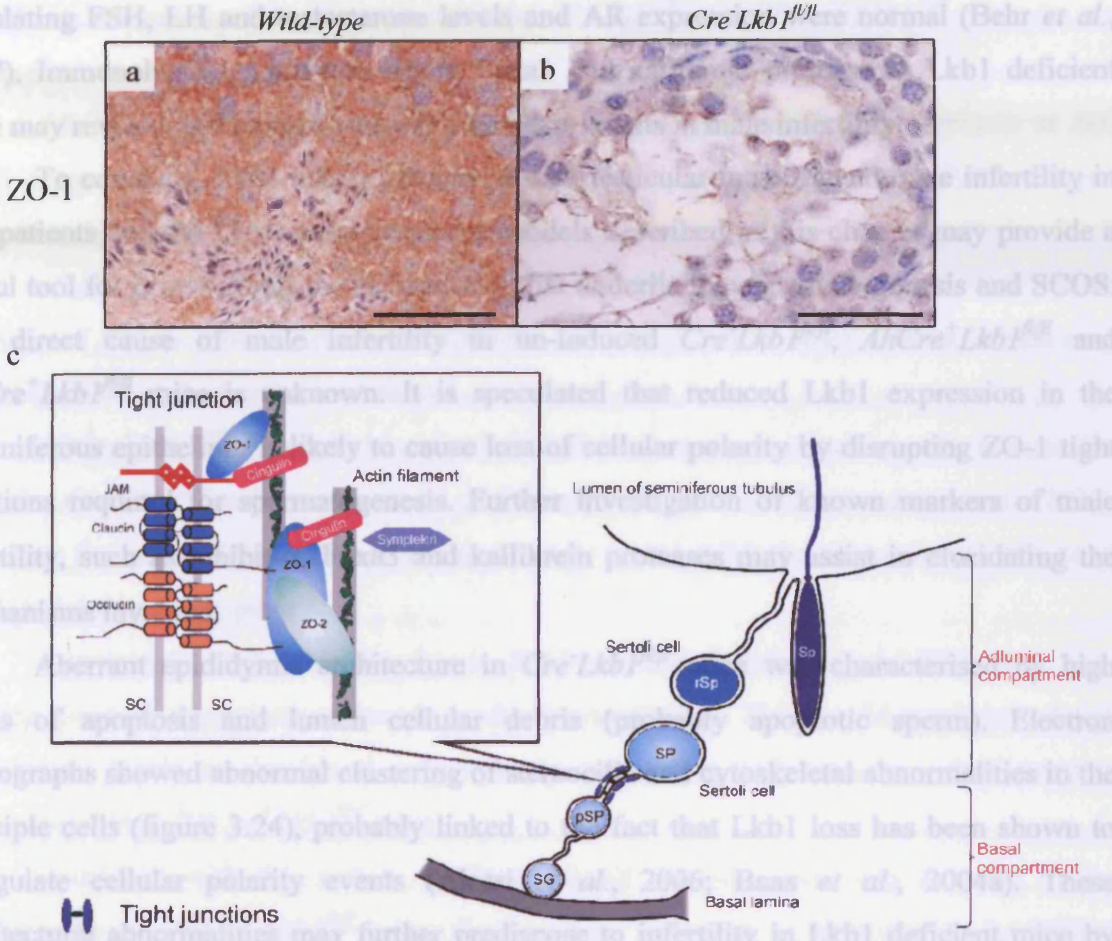


**Figure 3.32: Cellular polarity is lost in un-induced *Cre⁻Lkb1$^{fl/fl}$* seminiferous tubules.** Immunohistochemistry of formalin-fixed, paraffin-embedded testis sections (aged 2-7 months) revealed ZO-1 is expressed in wild-type seminiferous tubules undergoing spermatogenesis (a) and shows a marked in un-induced *Cre⁻Lkb1$^{fl/fl}$* mice (b). Images were taken at 40x magnification and the scale bars represent 50 µm. (c) Schematic of the tight-junction structure in the seminiferous epithelium. ZO-1 forms tight junctions between adjacent Sertoli cells (SC) near the basal lamina, constituting the blood–testis barrier and separating the seminiferous epithelium into the basal and adluminal compartments. SG, spermatogonium; pSP, preleptotene/leptotene spermatocyte; SP, pachytene spermatocyte; rSp, round spermatid; Sp, elongated spermatid; JAM, junctional adhesion molecules. Figure (c) was adapted from Fink *et al* (2006).

Finally, previous work has shown that haploinsufficiency of *Foxa3* predisposes to SCOS, resembling *PBCre⁺Lkb1$^{fl/fl}$* mice (Behr *et al.*, 2007). Foxa3 is a forkhead box transcription factor that is expressed in the liver and testis and plays a vital role in organ development and metabolism (Behr *et al.*, 2007; Friedman and Kaestner, 2006). *Foxa3* deficient SCOS displays aberrant Sertoli cell maintenance, which might be a consequence of increased testicular kallikrein proteases that are capable of disrupting the local

communication between the Leydig cells and the cells of the seminiferous tubules. Importantly, paracrine hormone signalling was not altered in *Foxa3* deficient mice, as circulating FSH, LH and testosterone levels and AR expression were normal (Behr *et al.*, 2007). Immunohistochemistry to detect Foxa3 and kallikrein protease in Lkb1 deficient mice may reveal a mechanism whereby Lkb1 loss results in male infertility.

To conclude, Lkb1 loss is associated with testicular tumours and male infertility in PJS patients and the Lkb1 deficient mouse models described in this chapter may provide a useful tool for investigating the mechanisms that underlie hypospermatogenesis and SCOS. The direct cause of male infertility in un-induced $Cre^{-}Lkb1^{fl/fl}$, $AhCre^{+}Lkb1^{fl/fl}$ and $PBCre^{+}Lkb1^{fl/fl}$ mice is unknown. It is speculated that reduced Lkb1 expression in the seminiferous epithelium is likely to cause loss of cellular polarity by disrupting ZO-1 tight junctions required for spermatogenesis. Further investigation of known markers of male infertility, such as inhibit-α, Foxa3 and kallikrein proteases may assist in elucidating the mechanisms involved.

Aberrant epididymis architecture in $Cre^{-}Lkb1^{fl/fl}$ mice was characterised by high levels of apoptosis and lumen cellular debris (probably apoptotic sperm). Electron micrographs showed abnormal clustering of stereocilia and cytoskeletal abnormalities in the principle cells (figure 3.24), probably linked to the fact that Lkb1 loss has been shown to deregulate cellular polarity events (Alessi *et al.*, 2006; Baas *et al.*, 2004a). These architectural abnormalities may further predispose to infertility in Lkb1 deficient mice by preventing any mature sperm that are produced in the testes from passing through the epididymal coils or leading to defective secretion of hormones/factors required for maturation of spermatozoa (Taboga *et al.*, 1999).

### 3.4.5 *PBCre*-mediated *Lkb1* loss causes prostate hyperplasia

Lkb1 deletion at the onset of prostate tumourigenesis and progression to PIN was driven using the *AhCre* transgene to mediate recombination of *Lkb1*-floxed alleles. However, as a consequence of the reduced longevity, it was not possible to age the animals beyond 200 days to determine whether Lkb1 loss could drive progression to advanced stages of the disease. In an attempt to overcome this difficulty, the well characterised *PBCre* transgenic line was exploited. Indeed, $PBCre^{+}Lkb1^{+/fl}$, $Cre^{-}Lkb1^{fl/fl}$ and $PBCre^{+}Lkb1^{fl/fl}$ cohorts displayed survival rates comparable to *wild-type* mice of 500 days.

Un-induced $Cre^{-}Lkb1^{fl/fl}$ mice developed LG-PIN lesions demonstrating that hypomorphic deletion of Lkb1 induces PIN in the prostate at 500 days. This phenotype was

enhanced to HG-PIN in un-induced *AhCre*$^{+}$*Lkb1*$^{fl/fl}$ mice, in which endogenous expression of *Cre* drives recombination, resulting in additional loss of Lkb1 in the prostate. The level of Lkb1 is critical for this phenotype as *AhCre*$^{+}$*Lkb1*$^{+/fl}$ *and PBCre*$^{+}$*Lkb1*$^{+/fl}$ mice do not develop prostate lesions.

*PBCre*$^{+}$*Lkb1*$^{fl/fl}$ mice exhibited a reduced phenotype (atypical hyperplasia at 500 days) compared to LG-PIN observed in *Cre*$^{-}$*Lkb1*$^{fl/fl}$ mice. This suggests that *PBCre* targets recombination to cells in which deficiency of Lkb1 does not induce PIN, or cells in which Lkb1 deficiency actually inhibits tumourigenesis. It is also important to note that cohort numbers of *PBCre*$^{+}$*Lkb1*$^{fl/fl}$ mice are relatively low compared to other cohorts, which may reflect the phenotype incidence observed.

*PBCre*$^{+}$*Lkb1*$^{fl/fl}$ mice will have loss of Lkb1 in the tumour initiating cells in common with the *Cre*$^{-}$*Lkb1*$^{fl/fl}$ mice, as well as additional cells mediated by endogenous *PBCre*. Therefore the loss of Lkb1 in these additional cells must inhibit the tumourigenic effects of Lkb1 deficiency in the prostate.

A potential mechanism for this is *PBCre*-mediated deletion of LKB1 in a non-prostate tissue that regulates androgen production/synthesis. This would result in reduced testosterone levels in the blood, subsequently preventing androgen-dependent prostate tumourigenesis in *PBCre*$^{+}$*Lkb1*$^{fl/fl}$ mice.

Consistent with this notion, *PBCre*-mediated recombination was detected in the Leydig cells of *PBCre*$^{+}$*Lkb1*$^{fl/fl}$ mice, that produce androgen in response to luteinising hormone (LH) and follicle stimulating hormone (FSH), predisposing to Sertoli-cell-only syndrome (SCOS). In support of this model, SCOS has been shown to reduce testosterone levels in humans (Kim and Lee, 1987), however, assays of circulating levels of LH, FSH and testosterone in *PBCre*$^{+}$*Lkb1*$^{fl/fl}$ mice are required to validate this hypothesis.

Importantly, *PBCre*-mediated deletion of other genes, such as *Pten*, have been shown to predispose to prostate cancer (Kasper, 2005; Wang *et al.*, 2003; Wang *et al.*, 2006b). This suggests two potential mechanisms, either that Lkb1 deficiency causes tumourigenesis in a different subset of cancer initiating cells to Pten, or alternatively, that loss of Pten in the *PBCre* targeted cells does not have the same tumour suppressing effect that loss of Lkb1 does in the same cells.

To conclude, deficiency of Lkb1 either by hypomorphic deletion or endogenous *AhCre* activity results in PIN. However, loss of Lkb1 by endogenous *PBCre* does not result in PIN, suggesting that loss of Lkb1 in some cells can actually inhibit tumourigenesis.

### 3.4.6 *PBCre*-mediated *Lkb1* loss causes multiple phenotypes

The fact that the un-induced *AhCre*$^{+}$*Lkb1*$^{fl/fl}$ cohort showed a significantly reduced life-span compared to the *PBCre*$^{+}$*Lkb1*$^{fl/fl}$ cohort is considered to reflect the lack of BUG cyst development in *PBCre*$^{+}$*Lkb1*$^{fl/fl}$ transgenic mice. A single mouse in the *PBCre*$^{+}$*Lkb1*$^{fl/fl}$ cohort that developed a small BUG cyst (< 1 cm) also displayed infection of the GU tract interstitium and prostate acini (at 500 days), providing evidence to link the two phenotypes. Infection was not observed in any other members of the *PBCre*$^{+}$*Lkb1*$^{fl/fl}$ cohort.

A number of other non-prostatic tumours were also observed in *PBCre*$^{+}$Lkb1 deficient mice. Preputial keratinised squamous metaplasia developed in *PBCre*$^{+}$*Lkb1*$^{+/fl}$, *PBCre*$^{-}$*Lkb1*$^{fl/fl}$ and *PBCre*$^{+}$*Lkb1*$^{fl/fl}$ cohorts (7%, 50% and 13% respectively), indicating that the *PB* promoter drives recombination in this sebaceous, androgen-regulated gland. A similar phenotype has been observed in mice expressing a dominant stable form of β-catenin under control of the *MMTV-LTR-Cre* construct (Bierie *et al.*, 2003), suggesting that aberrant Wnt signalling may play a role.

*PBCre*$^{+}$*Lkb1*$^{+/fl}$ mice displayed keratinised squamous metaplasia of the preputial gland, stomach hamartomas and kidney abnormalities, despite no evidence for *PBCre*-mediated recombination in these tissues. This implicates the hypomorphic nature of the LoxP-flanked *Lkb1* allele in the predisposition to these unexpected phenotypes. Consistent with this, the frequency of these lesions increased in mice homozygous for the *Lkb1* transgene (displayed in Table 3.2).

In parallel with un-induced *AhCre*$^{+}$*Lkb1*$^{fl/fl}$ mice, seminal vesicle squamous metaplasia was observed in the *PBCre*$^{+}$*Lkb1*$^{fl/fl}$ cohort (13% incidence). However, LacZ staining showed that the *PBCre* construct does not drive recombination in the seminal vesicle epithelium, unlike un-induced *AhCre*-mediated recombination (figure 3.10o). Consequently, in a *PBCre* setting, development of seminal vesicle squamous metaplasia might not be directly associated with loss of *Lkb1*, but could reflect alterations in the stroma and paracrine signalling molecules caused by adjacent prostate lesions. Alternatively, seminal vesicle tumours observed in *PBCre*$^{+}$*Lkb1*$^{fl/fl}$ mice may simply arise as a consequence of the hypomorphic nature of the *Lkb1* transgene.

*PBCre*$^{+}$*Lkb1*$^{+/fl}$, *PBCre*$^{-}$*Lkb1*$^{fl/fl}$ and *PBCre*$^{+}$*Lkb1*$^{fl/fl}$ cohorts aged to 500 days were also predisposed to kidney lesions (42%, 33% and 100% incidence) and stomach hamartomas (21%, 33% and 38%). No recombination was detected in the kidney and although LacZ staining did reveal recombination in the forestomach, this region of the

stomach was not predisposed to tumourigenesis and could in fact reflect endogenous β-lactamase activity causing a false-positive. This evidence suggests that the hypomorphic floxed-*Lkb1* allele might be sufficient to drive the formation of kidney lesions and stomach hamartomas. To address this, qRT-PCR would determine whether there is a reduction in the level of *Lkb1* mRNA transcription in these tissues.

Interestingly, the phenotypes observed in aged *PBCre*$^{+}$*Lkb1*$^{+/fl}$, *PBCre*$^{-}$*Lkb1*$^{fl/fl}$ and *PBCre*$^{+}$*Lkb1*$^{fl/fl}$ cohorts resemble that of PJS patients (Giardiello *et al.*, 1987), namely stomach and pyloric hamartomas and Sertoli-cell-only syndrome. Consistent with this model, a similar phenotype has been shown in *Lkb1*$^{+/-}$ mice (>20 weeks) considered to be linked to *Lkb1* gene haploinsufficiency, that is, without LOH (Miyoshi *et al.*, 2002). These data suggest a link between loss of Lkb1 and PJS.

## 3.5 Summary

Despite the high incidence of prostate cancer in the Western World, the paucity of animal models has constrained details of the molecular events predisposing the initiation and progression to carcinoma and metastasis of the disease. To address this, I have developed a mouse model in which the prostate is deficient in the tumour suppressor *Lkb1*. Loss of this gene in the mouse prostate predisposes to PIN. This is the first demonstration of a link between Lkb1 deficiency and prostate neoplasia. Furthermore, Lkb1 may also function to suppress tumourigenesis in a variety of male accessory organs including the bulbourethral glands, urethral glands, seminal vesicle, epididymis and testis. Importantly, this model may also provide insights into the development of male infertility associated with Sertoli-cell-only syndrome. Chapter 4 shall explore the deregulated molecular mechanisms incurred by an *Lkb1* functional mutation in prostate epithelium.

# Chapter 4: Investigating the molecular mechanisms underlying *Lkb1* deficient PIN

## 4.1 Introduction

To further investigate the mechanism underlying the predisposition to prostate neoplasia in un-induced *AhCre*$^{+}$*Lkb1*$^{fl/fl}$ mice, three Lkb1-mediated pathways will be investigated; (a) the AMPK/mTOR pathway, (b) Wnt signalling and (c) the PI3K/Pten/Akt cascade (detailed in section 1.3). To date, there is little published data to support a direct role for AMPK deregulation in prostate tumourigenesis (Lee *et al.*, 2006). However, aberrant Wnt signalling and deregulated PI3K/Pten/Akt signalling are common events in human prostate cancer (Sun *et al.*, 2001a; Yardy and Brewster, 2005). All Lkb1 deficient mice in this chapter are aged, un-induced *AhCre*$^{+}$*Lkb1*$^{fl/fl}$ mice. *Wild-type* or un-induced *Cre*$^{-}$ *Lkb1*$^{fl/fl}$ mice, that displayed normal prostate tissue at 200 days, were used as controls.

## 4.2 Aim

The objective of this chapter is to carry out immunohistochemical analysis of un-induced *AhCre*$^{+}$*Lkb1*$^{fl/fl}$ deficient PIN lesions to determine whether Lkb1 related signalling pathways have been deregulated to drive prostate tumourigenesis, such as the AMPK/mTOR pathway, Wnt signalling and the PI3K/PTEN/AKT cascade.

## 4.3 Results

### 4.3.1 mTOR signalling is suppressed in un-induced *AhCre*$^{+}$*Lkb1*$^{fl/fl}$ PIN

To establish on a molecular level whether loss of *Lkb1* deregulates mTOR signalling in *AhCre*$^{+}$*Lkb1*$^{fl/fl}$ PIN foci, immunohistochemistry was performed to detect active p-AMPKα, p-mTOR, p-S6K (ribosomal protein S6 kinase, 70kDa, RSK), a p-mTOR downstream target and its substrate p-Rps6 (ribosomal protein S6) (figure 4.1). Compared to control mice (*wild-type* and *Cre*$^{-}$*Lkb1*$^{fl/fl}$ mice, 200 days old), cytoplasmic p-AMPKα expression increased significantly in *AhCre*$^{+}$*Lkb1*$^{fl/fl}$ PIN foci (figure 4.1a-c). Lambda phosphatase treatment (that dephosphorylates proteins) was used to determine the extent of any non-specific staining following anti-p-AMPKα immunohistochemistry, which was observed weakly at the apical surface of the epithelium (figure 4.1d). Similar controls for other antibodies used did not identify any non-specific staining (figure 4.1h, l and p).

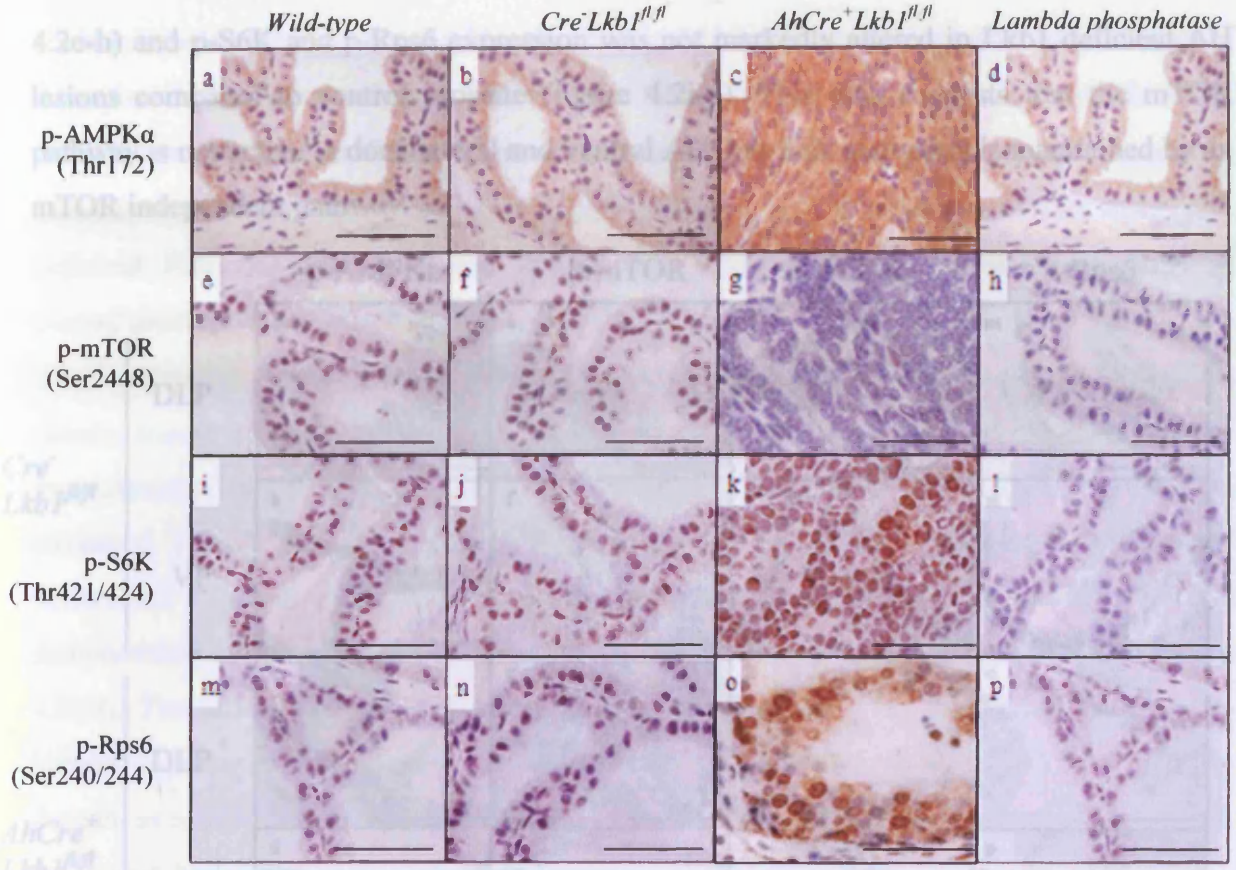


**Figure 4.1: The mTOR pathway is suppressed in Lkb1 deficient PIN.** Formalin-fixed, paraffin-embedded anterior prostate tissue sections from *wild-type*, *Cre⁻Lkb1$^{fl/fl}$* and *AhCre⁺Lkb1$^{fl/fl}$* mice aged 2-7 months underwent immunohistochemistry to detect p-AMPKα (a-d), p-mTOR (e-h), p-S6K (i-l) and p-Rps6 (m-p). Lkb1 deficient PIN lesions displayed elevated p-AMPKα throughout the cytoplasm while p-mTOR nuclear expression is lost. The mTOR downstream target p-S6K and its substrate p-Rps6 were depleted in PIN foci. Lambda phosphatase was used as a control to detect non-specific phosphate binding of each antibody (d, h, l and p) according to the Cell Signalling Technology protocol. Images were taken at 40x magnification and scale bars represent 50 μm.

AMPK activation stimulates TSC2 to prevent mTOR phosphorylation and activation by restricting Rheb to its GDP conformation (Alessi *et al.*, 2006). Nuclear p-mTOR expression is lost in PIN foci while control mice displayed nuclear p-mTOR in a subset of basal and luminal cells (figure 4.1e-g). Inconsistent with a decrease in mTOR expression, the mTOR target p-S6K (figure 4.1i-k) and its substrate p-Rps6 (figure 4.1m-o) were elevated in PIN lesions. This data suggests that S6K is activated via an mTOR independent mechanism in PIN lesions.

Further investigation into the mTOR pathway in *AhCre⁺Lkb1$^{fl/fl}$* dorsolateral and ventral prostate atypical hyperplasia (AH) revealed p-AMPKα was highly expressed in the cytoplasm of dorsolateral and ventral prostate lobes in control and Lkb1 deficient mice (figure 4.2a-d). However, nuclear expression of p-mTOR was detected at a low level in *Cre⁻Lkb1$^{fl/fl}$* dorsolateral and ventral lobes and was absent in *AhCre⁺Lkb1$^{fl/fl}$* AH lesions (figure

4.2e-h) and p-S6K and p-Rps6 expression was not markedly altered in Lkb1 deficient AH lesions compared to control prostate (figure 4.2i-p). This data suggests that the mTOR pathway is not active in dorsolateral and ventral AH, but S6K activation is maintained by an mTOR independent pathway.

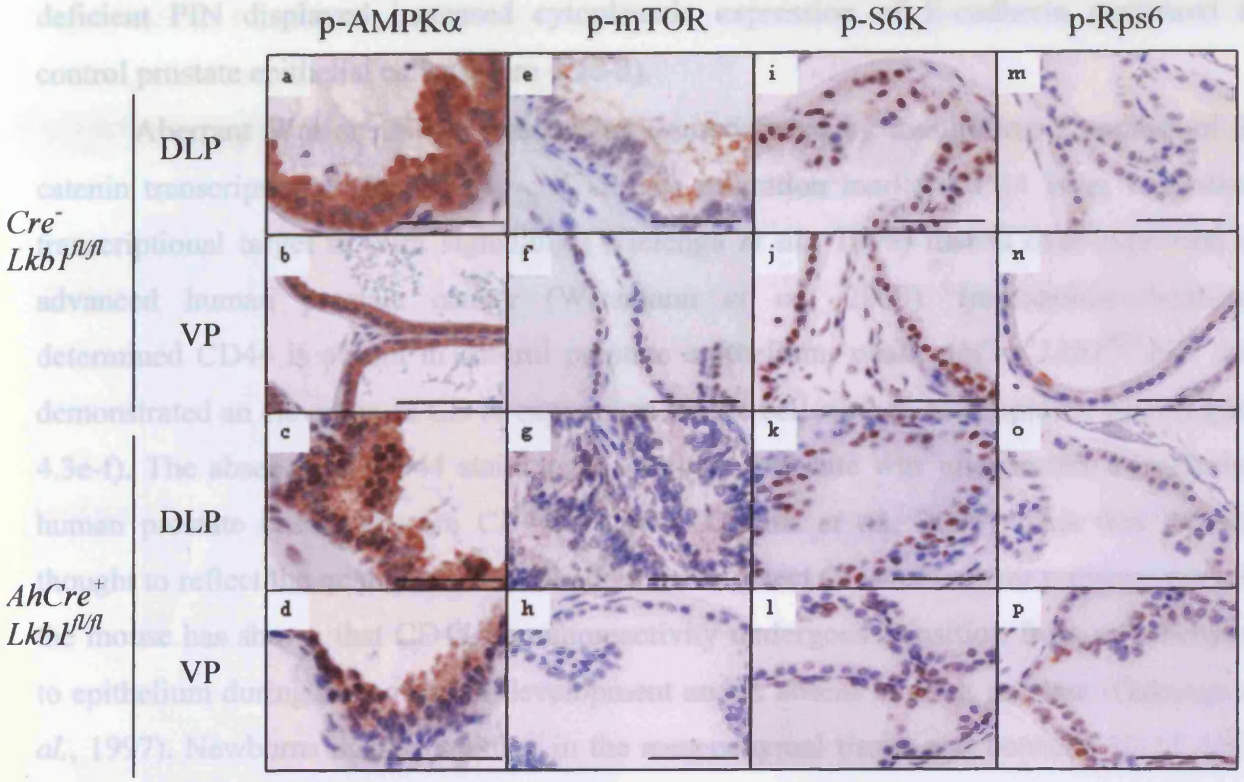


**Figure 4.2: The mTOR pathway is suppressed in Lkb1 deficient AH lesions.** Formalin-fixed, paraffin-embedded dorsolateral (DLP) and ventral (VP) prostate tissue sections from *Cre⁻Lkb1$^{fl/fl}$* and *AhCre⁺Lkb1$^{fl/fl}$* mice (aged 2-7 months) were stained for p-AMPKα (a-d), p-mTOR (e-h), p-S6K (i-l) and p-Rps6 (m-p) to reveal no marked changes in p-AMPKα expression, while p-mTOR nuclear expression was lost. p-S6K and p-Rps6 expression was not altered in Lkb1 deficient lesions. Images were photographed at 40x magnification and scale bars represent 50 μm.

### 4.3.2 Wnt signalling is deregulated in un-induced *AhCre⁺Lkb1$^{fl/fl}$* PIN

To investigate whether Wnt signalling was deregulated in Lkb1 deficient PIN lesions, the expression of a number of Wnt signalling components and downstream transcriptional targets were monitored using immunohistochemistry (figure 4.3). Lkb1 has previously been shown to mediate Par1A to regulate both the Wnt cascade and cellular polarity (Spicer *et al.*, 2003). *Wild-type* and *Cre⁻Lkb1$^{fl/fl}$* prostate epithelial cells predominantly express β-catenin at the cell surface membrane where it binds catenins to form adherens junctions (figure 4.3a). β-catenin was rarely observed in the nucleus where it associates with transcription factors to regulate Wnt target genes. However, β-catenin

nuclear translocalisation was highly elevated in Lkb1 deficient neoplastic cells indicating activation of the Wnt pathway (figure 4.3b). Recently, E-cadherin cytoplasmic relocation from the membrane has been linked to β-catenin switching from its structural role to a transcription factor that transmits Wnt signals (Li *et al.*, 2007b). Consistent with this, Lkb1 deficient PIN displayed increased cytoplasmic expression of E-cadherin compared to control prostate epithelial cells (figure 4.3c-d).

Aberrant Wnt signalling was further demonstrated by monitoring a number of β-catenin transcriptional targets. The cell surface migration marker CD44 is an immediate transcriptional target of Wnt signalling (Wielenga *et al.*, 1999) that is over-expressed in advanced human prostate cancer (Wissmann *et al.*, 2003). Immunohistochemistry determined CD44 is absent in control prostate epithelium, while $AhCre^{+}Lkb1^{fl/fl}$ PIN foci demonstrated an elevation in CD44 expression on the cell surface of neoplastic cells (figure 4.3e-f). The absence of CD44 staining in *wild-type* prostate was unexpected, considering human prostate basal cells are CD44 positive (Collins *et al.*, 2005). This was initially thought to reflect the quality of the antibody used to detect CD44, however previous work in the mouse has shown that CD44 immunoreactivity undergoes transition from mesenchyme to epithelium during the course of development and is absent in adult prostate (Gakunga *et al.*, 1997). Newborns display staining in the mesenchymal tissue and between 10-15 days, strong staining was detected in the epithelial membrane while staining in the mesenchyme was reduced. At 30 days no CD44 immunostaining was evident (Gakunga *et al.*, 1997). These results are suggestive of the significant role played by hyaluronan-CD44 interactions in mediating androgen-induced prostatic growth and morphogenesis (Gakunga *et al.*, 1997).

Activation of the Wnt pathway was further demonstrated by immunohistochemistry to detect Foxa1, a Forkhead box factor involved in prostate development that acts as AR co-activator (Gao *et al.*, 2003). Wnt signalling drives transcription of Sox17, which in turn induces Foxa1 transcription (Sinner *et al.*, 2004). Foxa1 was markedly elevated in Lkb1 deficient PIN lesions compared to control prostate epithelium. Counting the percentage of positive Foxa1 nuclei in prostate epithelium revealed a significant increase in Foxa1 staining in Lkb1 deficient PIN lesions (92% positivity) compared to control epithelium (39% positivity) (figure 4.3e). This data supports the LADY model system (described in section 1.2.3) where PIN lesions over-expressed Foxa1 (Mirosevich *et al.*, 2005).

Upregulated Wnt signalling was also demonstrated by detecting inactivation of glycogen synthase kinase 3β (GSK3β). GSK3β phosphorylates β-catenin at Ser33, Ser37

and Thr41 to target it for ubiquitin-mediated degradation (section 1.4.1). Inactivation of Gsk3β at Ser9 subsequently results in β-catenin nuclear translocation and upregulation of Wnt target genes (Clevers, 2006). Immunohistochemistry to detect inactive p-Gsk3β (Ser9) revealed that it is expressed at a low level in the cytoplasm of control epithelium and is highly elevated in PIN lesions (figure 4.3j-k). Together, this evidence further implies Lkb1 loss results in activated Wnt signalling.

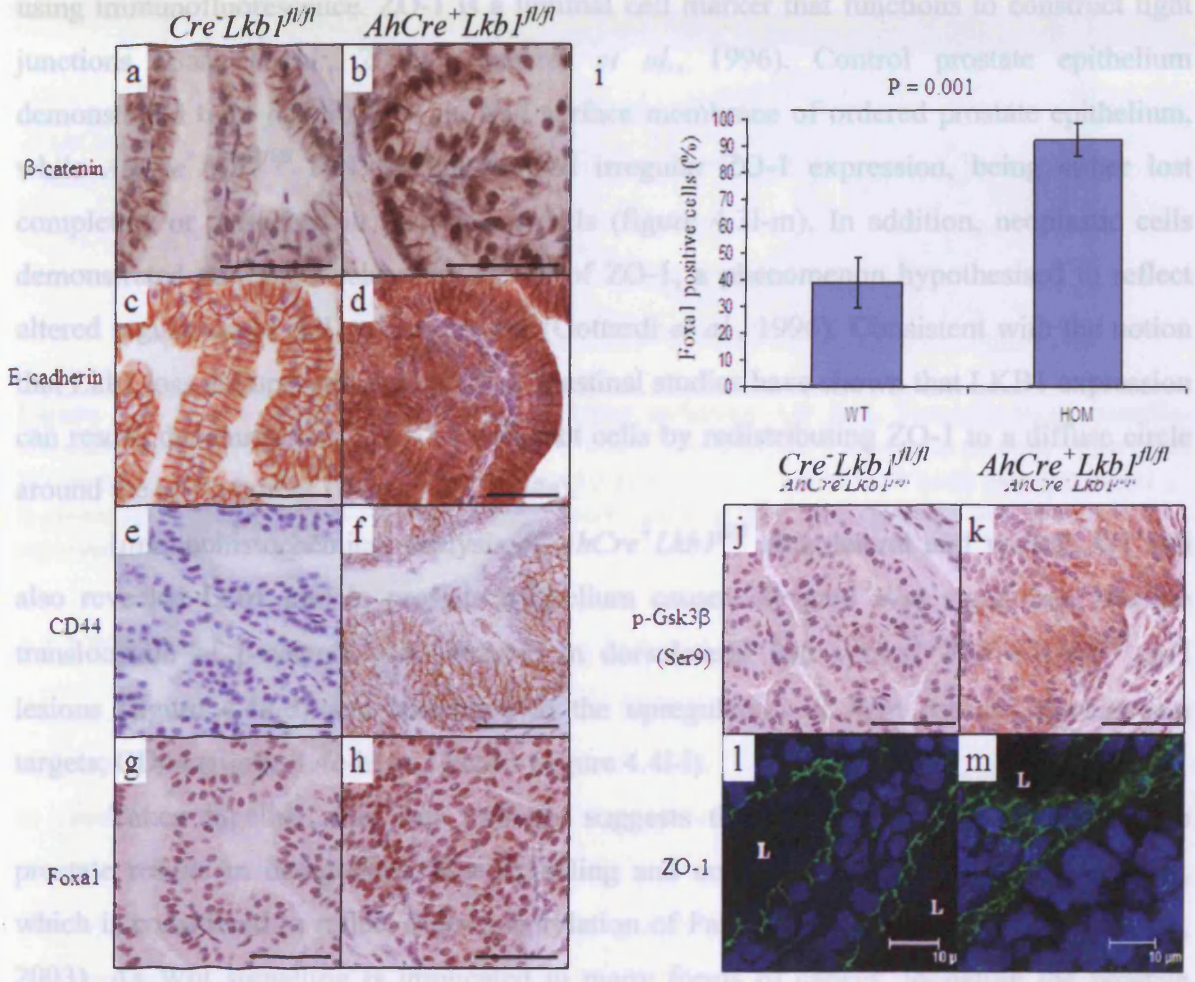


**Figure 4.3: Wnt signalling is activated in Lkb1 deficient PIN.** Formalin-fixed, paraffin-embedded anterior prostate tissue sections from *Cre⁻Lkb1$^{fl/fl}$* and *AhCre⁺Lkb1$^{fl/fl}$* mice (aged 2-7 months) were stained for Wnt signalling components; β-catenin (a-b), E-cadherin (c-d), CD44 (e-f), Foxa1 (g-h) and p-Gsk3β (j-k). All components were all elevated in *AhCre⁺Lkb1$^{fl/fl}$* PIN, indicating Wnt signalling is deregulated. Photographs were taken at 40x magnification and scale bars represent 50 µm. (i) Scoring positive Foxa1 nuclear expression within control (WT) and *AhCre⁺Lkb1$^{fl/fl}$* prostate epithelium revealed a 53% increase in Foxa1 nuclear expression levels in PIN foci ($p = 0.001$, $n = 3$). Error bars represent standard deviation and statistical analysis was carried out using the non-parametric Mann Whitney test using "MiniTab" software. Immunofluorescence to detect the tight junction protein ZO-1 revealed control prostate epithelium exhibits ordered cellular polarity, while *AhCre⁺Lkb1$^{fl/fl}$* PIN lesions display aberrant ZO-1 surface expression and punctate nuclear accumulation, suggesting loss of polarity (l-m). Confocal images were taken at 63x magnification and scale bars represent 10 µm.

In addition to activating the Wnt pathway, loss of Lkb1-mediated Par1A phosphorylation is speculated to disrupt cellular polarity (Spicer *et al.*, 2003). Cell polarity is critical for epithelial formation and function and loss of cellular polarity is a hallmark of cancer, where decreased cell-cell attachments lead to abnormal architecture of the tissue and facilitates malignant progression (Wodarz and Näthke, 2007). Potential loss of cellular polarity in Lkb1 deficient tumours was assessed by staining for zona-occludens-1 (ZO-1) using immunofluorescence. ZO-1 is a luminal cell marker that functions to construct tight junctions (Baas *et al.*, 2004a; Gottardi *et al.*, 1996). Control prostate epithelium demonstrated tight junctions on the cell surface membrane of ordered prostate epithelium, while $AhCre^{+}Lkb1^{fl/fl}$ PIN lesions showed irregular ZO-1 expression, being either lost completely or perturbed in a subset of cells (figure 4.3l-m). In addition, neoplastic cells demonstrated punctate nuclear expression of ZO-1, a phenomenon hypothesised to reflect altered regulation of cell polarity events (Gottardi *et al.*, 1996). Consistent with the notion that Lkb1 loss disrupts cellular polarity, intestinal studies have shown that LKB1 expression can rescue depolarisation of LKB1 deficient cells by redistributing ZO-1 to a diffuse circle around the brush border (Baas *et al.*, 2004a).

Immunohistochemical analysis of $AhCre^{+}Lkb1^{fl/fl}$ dorsolateral and ventral AH foci also revealed Lkb1 loss in prostate epithelium causes elevated Wnt signalling. Nuclear translocation of β-catenin was detected in dorsolateral and ventral $AhCre^{+}Lkb1^{fl/fl}$ AH lesions (figure 4.4a-d) and correlated to the upregulation of Wnt cascade downstream targets; CD44 (figure 4.4e-h) and Foxa1 (figure 4.4i-l).

Taken together, this data strongly suggests that Lkb1 deficiency in the mouse prostate results in deregulated Wnt signalling and concomitant loss of cellular polarity, which is considered to reflect dephosphorylation of Par1A (MARK3/cTAK) (Spicer *et al.*, 2003). As Wnt signalling is implicated in many forms of cancer, including the prostate (Yardy and Brewster, 2005), this data provides a model in which Lkb1 loss stimulates the oncogenic effects of the Wnt signalling pathway, which includes elevated AR signalling (Yardy and Brewster, 2005).

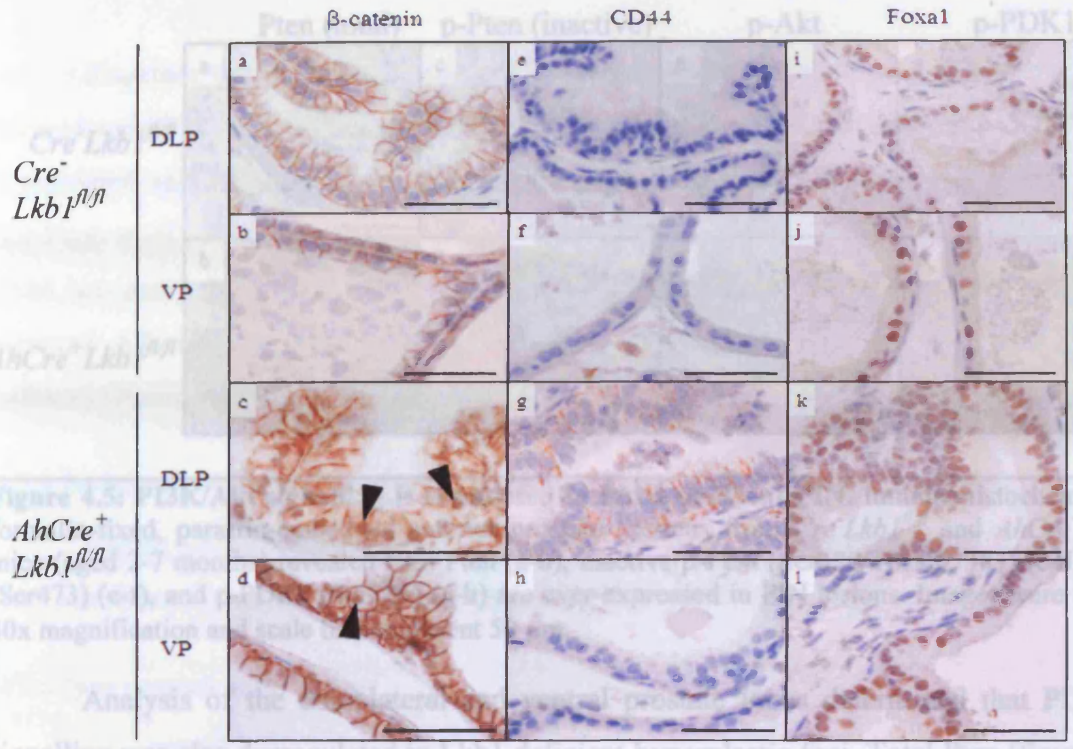


**Figure 4.4: Wnt signalling is activated in Lkb1 deficient AH foci.** Formalin-fixed, paraffin-embedded sections from *Cre⁻Lkb1$^{fl/fl}$* and *AhCre⁺Lkb1$^{fl/fl}$* dorsolateral and ventral prostate lobes (aged 2-7 months) were stained with antibodies to anti-β-catenin (a-d), anti-CD44 (e-h) and anti-Foxa1 (i-l) revealing aberrant Wnt signalling. Images were taken at 40x magnification and the scale bars represent 50 μm.

### 4.3.3 PI3K/Akt signalling is activated in un-induced *AhCre⁺Lkb1$^{fl/fl}$* PIN

Lkb1 has been shown to regulate the PI3K/AKT pathway by directly interacting with and phosphorylating PTEN (Mehenni *et al.*, 2005; Song *et al.*, 2007). PTEN functions to prevent PI3K/AKT signalling, which drives growth, differentiation, proliferation and recently, PTEN has been shown to interact with AR to promote AR degradation (Lin *et al.*, 2004b). To determine whether the PI3K/Akt pathway is deregulated upon loss of Lkb1, immunohistochemistry was carried out using an antibody directed against total Pten (figure 4.5a-b) and one that only recognises inactive/phosphorylated (Ser380/385 and Thr382) p-Pten (figure 4.5c-d). Total and inactive Pten are over-expressed in Lkb1 deficient PIN (figure 4.5a-d). This data implicates that although total Pten expression is elevated, it is phosphorylated at sites known to reduce Pten function/stability. Consistent with reduced Pten activity, *AhCre⁺Lkb1$^{fl/fl}$* mice also exhibited increased activation of p-Akt (figure 4.5e-f) and p-PDK1 (figure 4.5g-h) within PIN foci, demonstrating activation of the PI3K/Akt pathway in Lkb1 deficient PIN.

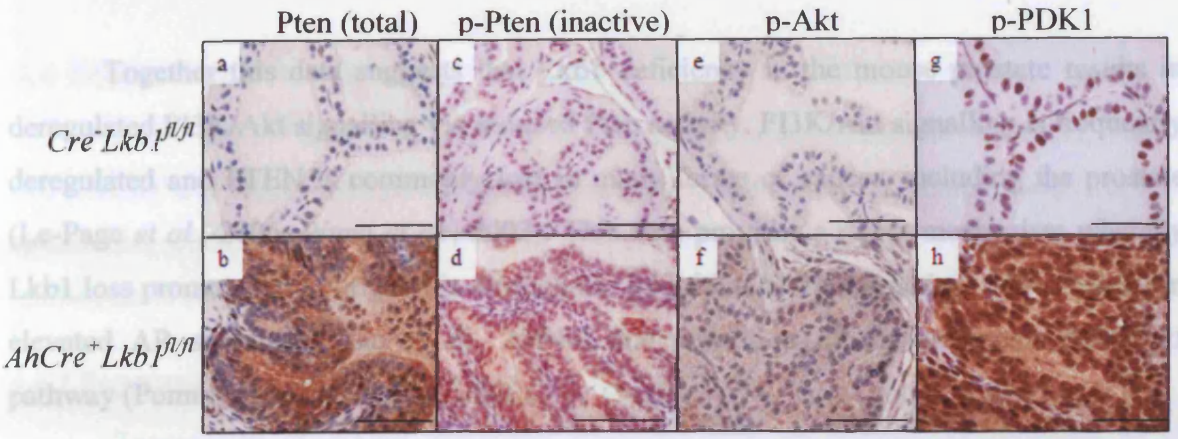


**Figure 4.5: PI3K/Akt signalling is stimulated in Lkb1 deficient PIN.** Immunohistochemistry of formalin-fixed, paraffin-embedded anterior prostate sections from *Cre⁻Lkb1$^{fl/fl}$* and *AhCre⁺Lkb1$^{fl/fl}$* mice (aged 2-7 months) revealed total Pten (a-b), inactive p-Pten (Ser380/Thr382/383) (c-d), p-Akt (Ser473) (e-f), and p-PDK1 (Ser241) (g-h) are over-expressed in PIN lesions. Images were taken at 40x magnification and scale bars represent 50 μm.

Analysis of the dorsolateral and ventral prostate lobes determined that PI3K/Akt signalling was also dysregulated in Lkb1 deficient hyperplastic foci. Total Pten (figure 4.6a-d), inactive p-Pten (figure 4.6e-h) and p-Akt (figure 4.6i-l) were all over-expressed in the cytoplasm of Lkb1 deficient dorsolateral and ventral prostate epithelium and activated p-PDK1 expression was increased in the nucleus and cytoplasm (figure 4.6m-p).

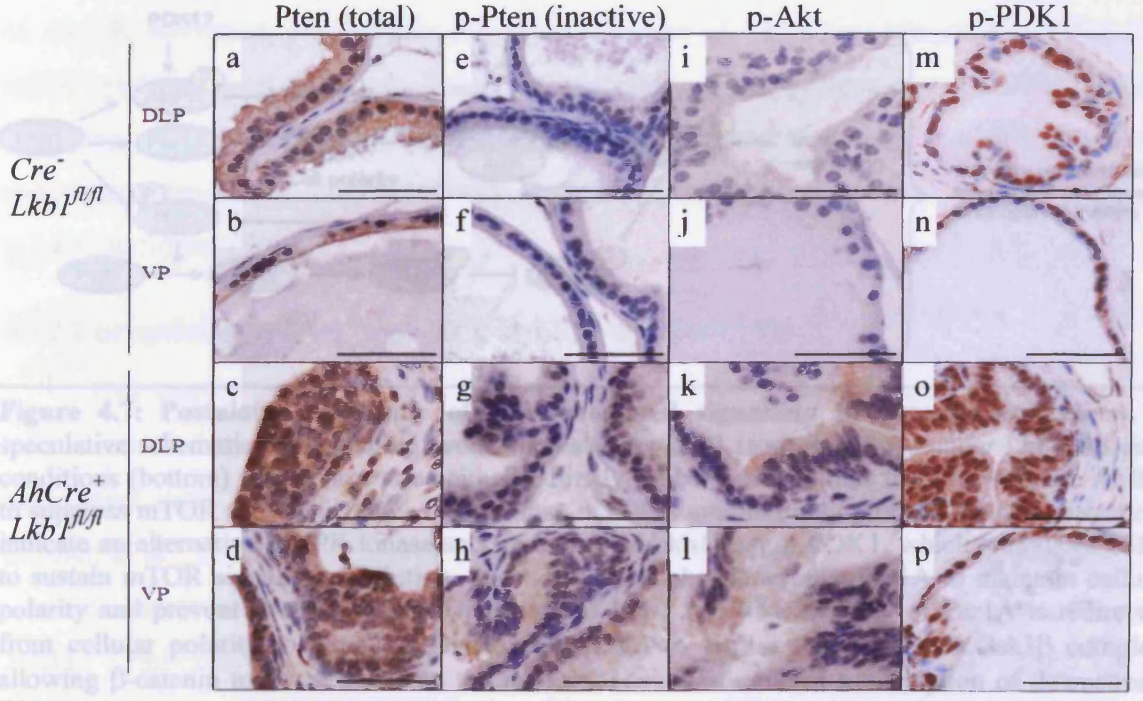


**Figure 4.6: The PI3K/Akt signalling cascade is stimulated in Lkb1 deficient AH foci.** Immunohistochemistry of formalin-fixed, paraffin-embedded dorsolateral (DLP) and ventral (VP) prostate sections from control (*Cre⁻Lkb1$^{fl/fl}$*) and *AhCre⁺Lkb1$^{fl/fl}$* mice (aged 2-7 months) revealed total Pten (a-d), inactive p-Pten (Ser380/Thr382/383) (e-h), p-Akt (Ser473) (i-l), and p-PDK1 (Ser241) (m-p) are all over-expressed in DLP and VP hyperplastic foci. Images were taken at 40x magnification and scale bars represent 50 μm.

Together this data suggests that Lkb1 deficiency in the mouse prostate results in deregulated PI3K/Akt signalling via reduced Pten activity. PI3K/Akt signalling is frequently deregulated and PTEN is commonly lost in many forms of cancer, including the prostate (Le-Page *et al.*, 2006; Wang *et al.*, 2003). This data provides a direct mechanism whereby Lkb1 loss promotes tumourigenesis through the inhibition of Pten function, which results in elevated AR signalling (Lin *et al.*, 2004b) and activation of the oncogenic PI3K/Akt pathway (Pommery and Henichart, 2005).

### 4.3.4 Insights into the molecular mechanism that causes PIN upon *Lkb1* loss

Figure 4.7 illustrates a speculative schematic for signalling events mediated by Lkb1 (top) and those under Lkb1 deficient conditions (bottom) within prostatic epithelia.

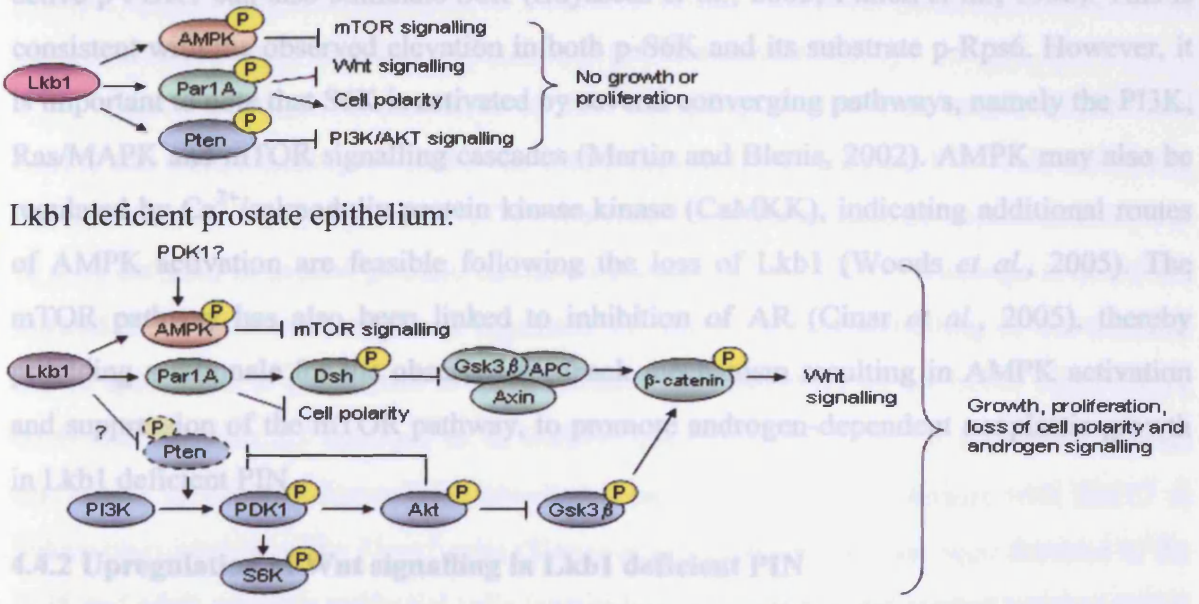


**Figure 4.7: Postulated schematic of Lkb1-mediated signalling in prostate epithelium.** A speculative schematic for signalling events mediated by Lkb1 (top) and those under Lkb1 deficient conditions (bottom) within prostatic epithelia. Firstly, Lkb1 typically acts to phosphorylate AMPK to suppress mTOR signalling. Once Lkb1 is lost, mTOR signalling may proceed. Our investigations indicate an alternative AMPK kinase acts on behalf of Lkb1 (e.g. p-PDK1, which stimulates S6K), to sustain mTOR signalling inhibition. Secondly, Lkb1 phosphorylates Par1A to maintain cellular polarity and prevent Wnt signalling. Upon loss of Lkb1 function, the role of Par1A is redirected from cellular polarity to stimulate Dishevelled (Dsh) to inhibit the APC:Axin:Gsk3β complex, allowing β-catenin to translocate into the nucleus. Here it stimulates transcription of downstream Wnt target genes and induces growth and proliferation as well as androgen signalling (Yardy and Brewster, 2005). Finally, although the role of Lkb1 interaction and phosphorylation of Pten is still undefined, our data suggests that Lkb1 maintains Pten stability, inhibiting Akt activation. In the absence of Lkb1, we observed inactivation of Pten function, a common precursor to prostate cancer. Pten loss results in activated Akt and ultimately results in p-Gsk3β expression, which can act to maintain Wnt signalling and drive tumourigenesis.

## 4.4 Discussion

*AhCre*$^{+}$*Lkb1*$^{fl/fl}$ anterior PIN exhibited elevated Wnt and PI3K/Akt signalling, loss of cell polarity and suppression of the mTOR pathway within the neoplastic epithelial cells. A speculative schematic of events occurring in the presence and absence of Lkb1 in prostate epithelium is depicted in figure 4.7.

### 4.4.1 Suppression of mTOR signalling in Lkb1 deficient PIN

Suppression of mTOR signalling coincides with an unexpected elevation of p-AMPKα in PIN and AH lesions. It is feasible that either Lkb1 does not regulate AMPK within adult prostate tissue or that an alternative AMPKK compensates for the loss of *Lkb1*, resulting in suppression of the mTOR pathway. Our data suggests PDK1 as a likely candidate for such a role (Zou *et al.*, 2003) and consistent with this, others have shown that active p-PDK1 can also stimulate S6K (Bayascas *et al.*, 2005; Pullen *et al.*, 1998). This is consistent with the observed elevation in both p-S6K and its substrate p-Rps6. However, it is important to note that S6K is activated by several converging pathways, namely the PI3K, Ras/MAPK and mTOR signalling cascades (Martin and Blenis, 2002). AMPK may also be regulated by $Ca^{2+}$/calmodulin protein kinase kinase (CaMKK), indicating additional routes of AMPK activation are feasible following the loss of Lkb1 (Woods *et al.*, 2005). The mTOR pathway has also been linked to inhibition of AR (Cinar *et al.*, 2005), thereby providing a rationale for the observed feedback mechanism resulting in AMPK activation and suppression of the mTOR pathway, to promote androgen-dependent neoplastic growth in Lkb1 deficient PIN.

### 4.4.2 Upregulation of Wnt signalling in Lkb1 deficient PIN

Our results from the *AhCre*$^{+}$*Lkb1*$^{fl/fl}$ mice parallel those of previous studies which have monitored the effects of aberrant Wnt signalling in the prostate, demonstrating an association with prostate tumourigenesis (Bierie *et al.*, 2003; Bruxvoort *et al.*, 2007; Gounari *et al.*, 2002). Lkb1 loss of function has been reported to reduce phosphorylation of a microtubule-associated protein for tau termed Par1A (cTAK1, MARK3), (Spicer *et al.*, 2003). Unphosphorylated Par1A results in phosphorylation of Dishevelled (Dsh), propagating the translocation of β-catenin into the nucleus to initiate transcription of Wnt target genes, concomitant with the disruption of Par1A-mediated cellular polarity events (Spicer *et al.*, 2003). This gives a direct mechanism whereby Lkb1 loss may lead to activated Wnt signalling and disrupt cellular polarity. Furthermore, Lkb1 loss was shown to

deregulate E-cadherin expression (figure 4.3d), which may further promote the loss of cellular polarity in *AhCre*$^{+}$*Lkb1*$^{fl/fl}$ PIN lesions.

Lkb1 deficient tissues have been previously shown to lose cell polarity, particularly in the intestine (Spicer and Ashworth, 2004) and the Lkb1 C-terminus exerts an essential function in the control of cell polarity (and AMPK regulation) (Forcet *et al.*, 2005). Lkb1 has been shown to regulate the cell polarity of intestinal epithelial cells, which display aberrant expression of the tight-junctional protein ZO-1 in Lkb1 deficient conditions (Baas *et al.*, 2004a; Baas *et al.*, 2004b). Consistent with this, ZO-1 expression is depleted in *AhCre*$^{+}$*Lkb1*$^{fl/fl}$ neoplastic cells, suggesting that loss of cellular polarity in Lkb1 deficient PIN is a consequence of disrupted tight junctions (figure 4.3m). This evidence also parallels that observed in Lkb1 deficient murine testicles (described in section 3.4.4). Unfortunately, attempts to determine whether the observed loss of cellular polarity in Lkb1 deficient prostate epithelium involves loss of Par1A (cTAK, MARK3) phosphorylation, using immunohistochemistry to detect p-cTAK have not been successful.

Over-expression of a number of Wnt signalling downstream targets (CD44 and Foxa1) and components (p-GSK3β) was determined in Lkb1 deficient PIN foci, facilitating tumour formation and progression. CD44 is a type-1 transmembrane glycoprotein known to be a be elevated in human prostate cancer (Wissmann *et al.*, 2003). Wielenga *et al* (1999) showed that *CD44* transcription is regulated by β-catenin/Tcf4 signalling in the intestine and is speculated to participate in the generation and turn-over of epithelial cells. Foxa1 (HNF-3α) has recently emerged as an indirect transcriptional target of β-catenin. Animal cap assays in *Xenopus laevis* have revealed β-catenin physically interacts with Sox17 to induce transcription of the *Foxa1* gene (Sinner *et al.*, 2004). Foxa1 has been detected in the UGS and adult prostatic epithelial cells (particularly the anterior and ventral prostate lobes) where it is speculated to direct morphogenesis and cell differentiation, further establishing a potential role in prostate tumourigenesis (Besnard *et al.*, 2004). Foxa1 may also govern androgen signalling by binding regions adjacent to androgen response elements (AREs) to facilitate androgen-regulated prostatic gene expression (Gao *et al.*, 2003; Mirosevich *et al.*, 2005; Yu *et al.*, 2005). Consistent with this, *in vitro* studies have documented β-catenin can interact directly with AR (Truica *et al.*, 2000) and β-catenin accumulation during prostate cancer has been shown to permit β-catenin to behave as a transcriptional co-regulator of AR (Yardy and Brewster, 2005). Consequently, AR over-expression in *AhCre*$^{+}$*Lkb1*$^{fl/fl}$ PIN may be a direct consequence of activated Wnt signalling.

*AhCre*$^{+}$*Lkb1*$^{fl/fl}$ PIN resembles aspects of transgenic mice expressing either a dominant form of β-catenin or Apc loss in the prostate, under the control of the *MMTV-LTR-Cre* or *PBCre* constructs respectively (Bierie *et al.*, 2003; Bruxvoort *et al.*, 2007; Gounari *et al.*, 2002), although the overall phenotype is significantly less severe in the *AhCre*$^{+}$*Lkb1*$^{fl/fl}$ model. The discrepancy in severity probably reflects differences in gene function (between *Lkb1* and *Apc/β-catenin*) within the prostate; but may also reflect differences in the experimental approaches used, such as the pattern of *Cre*-mediated recombination. It is also important to note that elevated β-catenin/Wnt signalling has also been shown to increase Ah receptor transcript and protein expression, which regulates *Cyp1a1 p450* (*Ah*) expression (Chesire *et al.*, 2004). This suggests that activation of Wnt signalling could further enhance *Cre*-mediated recombination events.

Taken together, these results suggest that Lkb1 loss predisposes to prostate neoplasia in the mouse through the deregulation of cellular polarity events (as determined by aberrant ZO-1 expression) and concomitant with elevated β-catenin nuclear translocation, which upregulates Wnt targets to further promote tumourigenesis.

### 4.4.3 Elevated PI3K/Akt signalling in *Lkb1* deficient PIN

The observed progression of AH to PIN in *AhCre*$^{+}$*Lkb1*$^{fl/fl}$ shares phenotypic characteristics with *Pten* deficient mice (Di Cristofano *et al.*, 2001; Di Cristofano *et al.*, 1998; Wang *et al.*, 2003), although again being somewhat less severe. Loss of *Pten* results in AH which predisposes to PIN that has been shown to progress into carcinoma and metastasis in *PBCre*$^{+}$*Pten*$^{fl/fl}$ mice (Wang *et al.*, 2003). *Pten* deficient tumourigenesis is positively correlated with the over-expression of p-PDK1, p-Akt and its downstream targets, such as p-Gsk3β (Wang *et al.*, 2003). *Lkb1* mutant mice mimic this pattern and the elevation of both total Pten and inactive Pten was previously observed in the TRAMP model (detailed in section 1.2.3) (Shukla *et al.*, 2005). Together, this suggests that loss of Lkb1 impairs Pten function, possibly as a consequence of directly interacting with and regulating Pten stability (Mehenni *et al.*, 2005), leading to enhanced PDK-1 and Akt activity and ultimately predisposing to PIN. This is consistent with recent *in vitro* studies that have shown LKB1-mediated phosphorylation of PTEN results in PTEN stabilisation (Mehenni *et al.*, 2005; Song *et al.*, 2007). In addition, an *in vitro* study in LNCaP cells has reported that PTEN can repress androgen signalling through the PI3K/Akt pathway and can directly interact with AR to sequester it in the cytoplasm, thus preventing AR protein degradation and

suppression of AR transactivation and apoptosis (Lin *et al.*, 2004b). Consequently, in the absence of PTEN function, AR signalling is considered to be deregulated and can contribute to androgen-dependent tumour formation. However, it is important to note that elevated PTEN expression induces cell death, indicating that the results from these experiments (carried out using dying LNCaP cells) should be viewed with caution. Furthermore, PI3K/Akt signalling is reported to stimulate androgen signalling through Gsk3β inhibition and β-catenin accumulation (Sharma *et al.*, 2002). Aberrant PI3K/Akt signalling also provides a direct mechanism for deregulation of the Wnt pathway. Active p-Akt can phosphorylate and inactivate Gsk3β, which maintains Wnt signalling by inhibiting ubiquitin-mediated degradation of β-catenin (Al-Khouri *et al.*, 2005; Green, 2004). Had more time been available it would have been interesting to see whether downstream AR signalling targets (such as PSA) are upregulated and to confirm that PIN lesions are androgen dependent by carrying out an androgen ablation study.

Casein kinase II (CK2) is a protein kinase frequently upregulated in human prostate cancer and plays key roles in cell growth, proliferation and survival (Laramas *et al.*, 2007). Among its many cellular activities (including Nkx3.1 activation) it functions to regulate PTEN stability (Laramas *et al.*, 2007). Post-translational modifications of PTEN are not well understood and should be viewed with caution, however CK2 has been shown by independent research groups to phosphorylate residues S380, T382 and T383 and predominantly S370 and S385 to regulate PTEN stability/activity (Al-Khouri *et al.*, 2005; Mehenni *et al.*, 2005). To further investigate the inactivation of Pten in Lkb1 deficient PIN lesions, expression levels of CK2 were monitored (figure 4.8). Immunohistochemistry demonstrated that CK2 is not expressed in control prostate epithelium but is significantly elevated in Lkb1 deficient tumours, consistent with the observed inactivation of Pten. This presents an additional mechanism whereby PTEN might be phosphorylated and subsequently inactivated by upregulated CK2, leading to PDK1 and Akt activation.

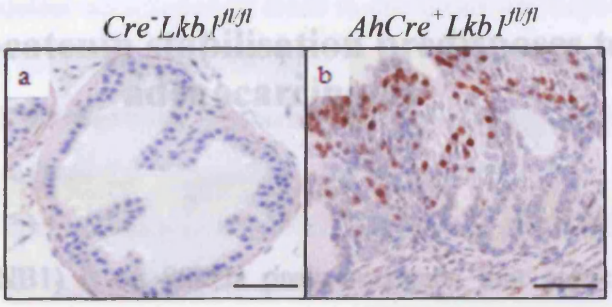


**Figure 4.8: Analysis of CK2 expression in Lkb1 deficient PIN.** Immunohistochemistry of formalin-fixed, paraffin-embedded dorsolateral and ventral prostate sections from *Cre⁻Lkb1$^{fl/fl}$* and *AhCre⁺Lkb1$^{fl/fl}$* mice (aged 2-7 months) revealed that CK2 is absent in control tissue (a) and over-expressed in the nuclei of Lkb1 deficient neoplastic cells (b). Images were taken at 40x magnification and scale bars represent 50 μm.

To conclude, these data suggest that loss of Lkb1 in the prostate causes neoplastic transformation, owing to the loss of Pten activity, which ultimately results in tumourigenesis by stimulating the oncogenic effects of the PI3K/Akt signalling pathway. It is speculated that elevated CK2 expression may play a role in mediating this process by phosphorylating and inactivating Pten. The fact that p-PDK1 is upregulated, provides a direct mechanism for the observed suppression of the mTOR pathway and elevated levels of p-S6K.

## 4.5 Summary

To conclude, Lkb1 deficiency predisposes to anterior prostate neoplasia by deregulating Lkb1-mediated signalling pathways. PIN lesions demonstrated aberrant Wnt and PI3K/Akt pathways that may cooperate to modulate apoptosis, loss of cell polarity, migration, proliferation and androgen signalling, the combined consequence of which is to facilitate neoplastic tumour formation. Consistent with this phenotype, Lkb1 deficiency mirrors aspects of both PTEN loss and hyperactivation of the Wnt pathway. Although AMPK is activated by Lkb1, an unexpected increase in p-AMPK was detected in Lkb1 deficient neoplastic prostate epithelial cells in parallel with suppression of the mTOR pathway. It is speculated that inhibition of the mTOR pathway may be the direct result of a negative feedback mechanism whereby AMPK is activated by an alternate AMPKK to Lkb1, such as PDK1 or CaMKK. In agreement with this hypothesis, p-PDK1 expression was elevated in PIN lesions and corresponds to the observed S6K activation. Mechanisms for such deregulation and pathway cross-talk have been illustrated in figure 4.7.

# Chapter 5: β-catenin stabilisation predisposes to prostate adenocarcinoma

## 5.1 Introduction

β-catenin (CTNNB1) is an 88kDa proto-oncogene that participates in adherens junctions and Wnt signalling (discussed in section 1.4). Aberrant Wnt signalling is emerging as a key event in the development of prostate cancer, possibly as a direct consequence of its role in regulating AR transcriptional activity (Yardy and Brewster, 2005). Consistent with this, *AhCre*$^{+}$*Lkb1*$^{fl/fl}$ prostate intra-epithelial neoplasia demonstrated elevated Wnt signalling (chapter 4). To address the genetic basis for prostate cancer in Lkb1 deficient mice, a novel model of prostate cancer was generated where the *PBCre* transgenic line was used to drive recombination of both the *Lkb1* floxed transgene (Sakamoto *et al.*, 2005) and a dominant stabilised form of *β-catenin* (Harada *et al.*, 1999).

### 5.1.1 β-catenin and prostate cancer

Approximately 5-7% of human prostate cancers harbour an activating β-catenin mutation within the regulatory region (Voeller *et al.*, 1998) and inactivating mutations in *APC* and *hTRCP1* (also known as *BTRC*), which prevent the degradation of β-catenin, have also been detected in human prostate cancer (Gerstein *et al.*, 2002). In addition, human tissue microarray studies have shown that 50% of early and 80% of metastatic prostate cancer samples display β-catenin nuclear localisation, indicating active Wnt signalling (DeLaTaille *et al.*, 2003).

β-catenin is known to stimulate the transcription of AR target genes and androgen ablation/regeneration experiments have shown that β-catenin accumulates in the nuclei of testosterone-restored animals, suggesting that β-catenin may play a role in androgen-induced prostate regeneration (Chesire *et al.*, 2002). In addition, Cheshire et al (2002) also observed that transient β-catenin over-expression enhances AR-mediated transcription of two natural target gene promoters in six prostate cancer cell lines *in vitro* (Chesire *et al.*, 2002). AR co-activators and co-repressors contain LXXLL motifs that mediate their binding to AR (Truica *et al.*, 2000). β-catenin harbours five LXXLL motifs within the armadillo repeat region that are postulated to facilitate β-catenin:AR interactions (Truica *et al.*, 2000). Evidence for β-catenin as an AR receptor co-activator has been demonstrated *in*

*vitro*, where β-catenin nuclear accumulation leads to enhanced AR-dependent transcription, including transcriptional activity of the AR gene itself (Terry *et al.*, 2006; Truica *et al.*, 2000; Yang *et al.*, 2006). Furthermore, β-catenin may alter the ligand specificity of the AR and has been shown to relieve the repression of anti-androgens, thus contributing to the progression of prostate cancer (Truica *et al.*, 2000; Verras and Sun, 2006).

Regulation of the Wnt signalling pathway, and therefore AR signalling, is a complex process that to date is not well defined. GSK3β plays a dual role in cells, linking the regulation of Wnt pathway to AR signalling and is itself regulated by PI3K/AKT signalling (Terry *et al.*, 2006). Gsk3β has recently been shown to act as a negative regulator of AR-mediated transcription through direct interactions with AR (Wang *et al.*, 2004a). PI3K/AKT signalling has also been shown to be mediated by androgen signalling via GSK3β phosphorylation, permitting nuclear translocation of β-catenin and augmenting AR activity (Sharma *et al.*, 2002). An indirect mechanism for β-catenin activation of AR signalling involves β-catenin-mediated transcription of Sox-17, a HMG box transcription factor that directly triggers Foxa1 mRNA expression (Sinner *et al.*, 2004). Foxal is required during prostate development (Mirosevich *et al.*, 2005) and has recently emerged as an AR signalling component (Gao *et al.*, 2003; Yu *et al.*, 2005).

β-catenin can also down-regulate the metastasis suppressor gene *KAI1*, whose expression is frequently decreased in metastatic prostate cancer (Kim *et al.*, 2005; Reya and Clevers, 2005). β-catenin and the reptin chromatin remodelling complex are thought to act in concert with histone deacetylases to antagonise the Tip60-pontin co-activator complex, which is required to activate transcription of *NF-κB* genes, including *KAI1*. Ultimately, β-catenin-reptin complexes prevent the Tip60-pontin co-activator complex from binding to the *KAI1* promoter, suppressing *KAI1* expression and promoting tumourigenesis (Kim *et al.*, 2005).

### 5.1.2 Wnt signalling and mouse models of prostate cancer

Mouse models have demonstrated that aberrant Wnt signalling causes prostate tumourigenesis but have been limited in terms of progression. Gounari *et al* (2002) derived mice bearing a dominant stabilised form of β-catenin in the prostate, using the *MMTV-LTR-Cre* construct to drive transgene expression (detailed in section 5.1.3). PIN-like lesions manifested keratinised squamous metaplasia by 10 weeks of age and demonstrated upregulation of AR and the Wnt target c-Myc (Gounari *et al.*, 2002). These mice also

displayed hair follicle cysts, urethral hyperplasia, odontomas and keratinised squamous metaplasia of the salivary, preputial, hardarian and mammary glands indicating β-catenin plays a role in widespread epithelial tumours (Gounari *et al.*, 2002). Mice were aged to 5 months and no evidence for further disease progression, invasion or metastasis was observed. Bierie *et al* (2003) also characterised the dominant stabilised β-catenin model in *MMTV-LTR-Cre* transgenic mice, determining epithelial hyperplasia and extensive trans-differentiation into epidermal-like structures that expressed keratin 1 and 6, filaggrin, loricrin and involucrin. These mice were not viable past 3 months, which hindered studies of late stage progression. Ventral prostate transplants to mammary fat pads were necessary for further progression to squamous metaplasia and neoplastic transformation (Bierie *et al.*, 2003). Discrepancies in the phenotype observed in these two transgenic models are thought to reflect subtleties in strain background.

More recently, Bruxvoort *et al* (2007) derived mice bearing biallelic inactivation of the *Apc* gene using the *PBCre* transgenic line to drive activation of the Wnt pathway in the prostate. *Apc* loss was coupled with increased β-catenin expression in the nucleus, suggesting deregulation of the Wnt signalling pathway. Hyperplasia was observed at 4.5 weeks and progressed to prostate carcinoma by 7 months, which castration experiments revealed were androgen independent (Bruxvoort *et al.*, 2007). No evidence for metastasis was observed, despite 30% of the mice developing hepatomas and tumour derived lymphadenopathy of the lumbar lymph nodes (Bruxvoort *et al.*, 2007).

### 5.1.3 Derivation of a dominant stable *β-catenin* isoform

Using Cre-LoxP technology, Harada *et al* (1999) developed a conditional, activated form of β-catenin to study the role of deregulated Wnt signalling within the intestine during tumourigenesis and progression *in vivo*. Here, exon 3 (amino acids 5-80) of the *β-catenin* gene is followed by a PGK-NEO cassette and is sandwiched between two LoxP sites, termed $Catnb^{lox(ex3)}$ (Harada *et al.*, 1999), (figure 5.1). Following Cre-mediated recombination, exon 3 is excised resulting in the loss of the highly conserved Ser33, Ser37 and Thr41 residues that are phosphorylated by GSK3β to target β-catenin for ubiquitin-mediated degradation (Harada *et al.*, 1999). This ultimately generates a dominant stable form of the gene that is constitutively active.

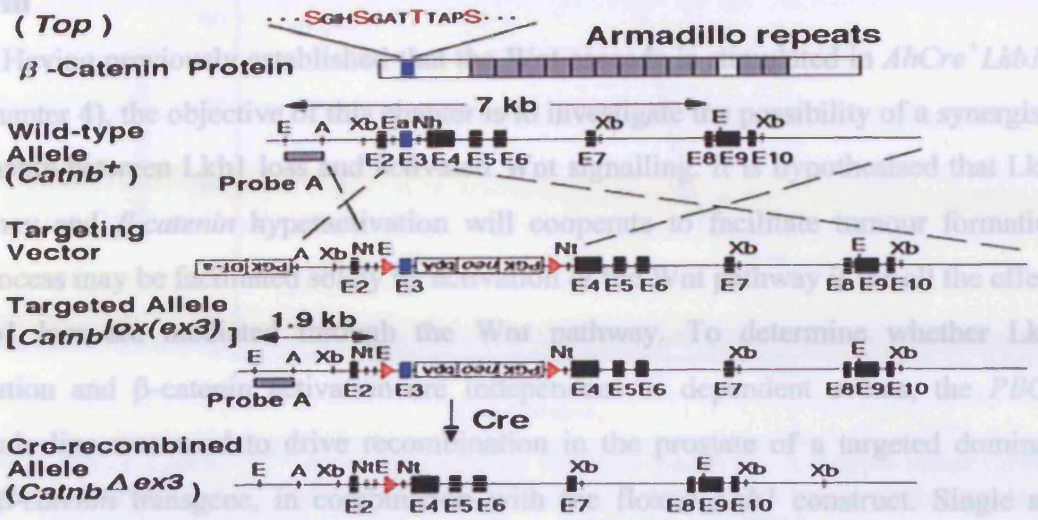


**Figure 5.1: Construction of dominant stabilised form of β-catenin using the Cre-LoxP system.** From top to bottom, structures show β-catenin protein (phosphorylation sites in red), the *wild-type* allele (*Catnb*$^{+}$), the targeting vector, targeted allele (*Catnb*$^{lox(ex3)}$) and the recombined allele (*Catnb*$^{\Delta ex3}$) respectively. Red arrows indicate the LoxP sites flanking exon 3 that carries the GSK3β phosphorylation site. Figure is adapted from Harada *et al* (1999).

Using the promoter regions of either cytokeratin 19 (*CK19*) or rat liver fatty acid binding protein (*Fabpl*) to drive Cre-recombinase expression, Harada *et al* (1999) targeted transgene expression to intestinal and colonic epithelia. Mice were predisposed to numerous intestinal adenomatous polyps and some colonic microadenomas (emerging ~2 weeks after birth), demonstrating that activation of the Wnt pathway in the gut results in tumourigenesis (Harada *et al.*, 1999). To date, the dominant stable *β-catenin* transgene has been widely exploited in several different tissues to reveal direct experimental evidence for elevated Wnt signalling in cancer. These include colorectal neoplasms, hepatocarcinogenesis, hair follicle tumours, mammary carcinomas and keratinised squamous metaplasia of the prostate and preputial gland (Bierie *et al.*, 2003; Gounari *et al.*, 2002; Harada *et al.*, 2004; Harada *et al.*, 1999).

## 5.2 Aim

Having previously established that the Wnt cascade is stimulated in *AhCre*$^{+}$*Lkb1*$^{fl/fl}$ PIN (chapter 4), the objective of this chapter is to investigate the possibility of a synergistic relationship between Lkb1 loss and activated Wnt signalling. It is hypothesised that Lkb1 deficiency and *β-catenin* hyperactivation will cooperate to facilitate tumour formation. This process may be facilitated solely by activation of the Wnt pathway if the all the effects of Lkb1 loss are mediated through the Wnt pathway. To determine whether Lkb1 inactivation and β-catenin activation are independent or dependent events, the *PBCre* transgenic line was used to drive recombination in the prostate of a targeted dominant stable *β-catenin* transgene, in combination with the floxed *Lkb1* construct. Single and double mutant cohorts were analysed histologically and the underlying molecular events that led to prostate adenocarcinomas were investigated using immunohistochemistry.

## 5.3 Results

### 5.3.1 *PBCre*$^{+}$*Catnb*$^{+/lox(ex3)}$ male mice have a reduced life-span

*PBCre* transgenic mice were inter-crossed with mice bearing one LoxP-flanked *β-catenin* allele (shown in figure 5.1) and one wild-type *β-catenin* allele. Male cohorts of *wild-type* (*PBCre*$^{+}$*Catnb*$^{+/+}$ or *Cre*$^{-}$*Catnb*$^{+/+}$), control (*Cre*$^{-}$*Catnb*$^{+/lox3(ex3)}$) and mutant (*PBCre*$^{+}$*Catnb*$^{+/lox(ex3)}$) mice were aged and monitored for signs of disease. Mice were harvested when they became symptomatic of disease or at specified time points (100, 200 and 500 days). Each long-term cohort contained a minimum of 15 males while earlier time points allocated to monitor progression were smaller (n = 6). All members of the *wild-type* and *Cre*$^{-}$*Catnb*$^{+/lox(ex3)}$ cohorts survived to 500 days while a Chi-squared test determined the average survival of the *PBCre*$^{+}$*Catnb*$^{+/lox(ex3)}$ cohort was significantly reduced to 417 days as mice became sick ($\chi^2 = 34.56$, $p = 0.000$). Only 22% of the mutant males survived to the 500 day endpoint.

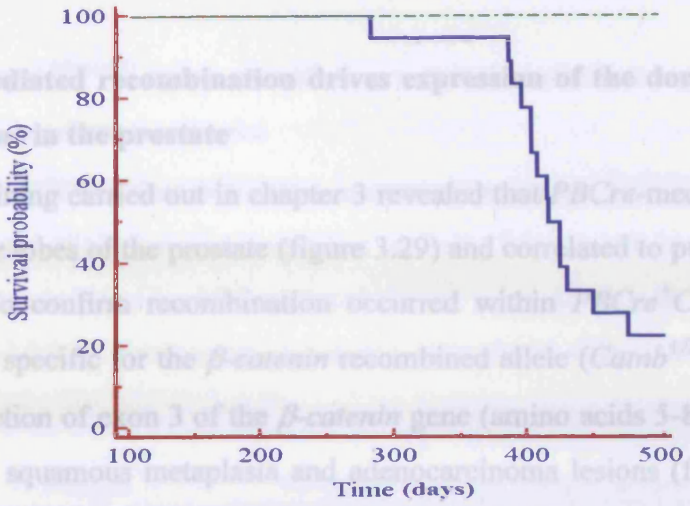


**Figure 5.2: *PBCre$^{+}$Catnb$^{+/lox(ex3)}$* male mice display reduced longevity.** A Kaplan-Meier survival curve where *wild-type* (n = 32) and *Cre$^{-}$Catnb$^{+/lox3(ex3)}$* (n = 15) cohorts are represented in green and the *PBCre$^{+}$Catnb$^{+/lox(ex3)}$* cohort (n = 18) is in blue. *PBCre$^{+}$Catnb$^{+/lox(ex3)}$* mice show decreased longevity, with only 22% of the cohort living till the endpoint of 500 days. Chi-squared tests confirmed *PBCre$^{+}$Catnb$^{+/lox(ex3)}$* mice exhibit a significantly reduced average survival of 417 days compared to *wild-type* and *PBCre$^{-}$Catnb$^{+/lox3(ex3)}$* cohorts ($\chi^2 = 34.56$, $p = 0.000$). Statistical analysis was carried out by a Chi-squared test using 'MiniTab' software and the Kaplan-Meier plot was generated using 'MedCalc' software.

### 5.3.2 *PBCre$^{+}$Catnb$^{+/lox(ex3)}$* mice are predisposed to multiple GU tract phenotypes

Histological analysis of H&E sections from all cohorts aged to 100 (n = 6), 200 (n = 6) and 500 days (or end point, n = 18) determined *PBCre$^{+}$Catnb$^{+/lox(ex3)}$* mice were predisposed to multiple GU tract tumours, while *wild-type* (n = 32) and control (n = 15) cohorts were normal (Table 5.1).

**Table 5.1 Phenotype incidence in *PBCre$^{+}$Catnb$^{+/lox(ex3)}$* mice**

| Genotype / Phenotype | *Wild-type* (500 d) | *Cre$^{-}$ Catnb$^{+}$ lox(ex3)* (500 d) | *PBCre$^{+}$ Catnb$^{+}$ lox(ex3)* (100 d) | *PBCre$^{+}$ Catnb$^{+}$ lox(ex3)* (200 d) | *PBCre$^{+}$ Catnb$^{+}$ lox(ex3)* (End point) |
|---|---|---|---|---|---|
| Prostate HG-PIN and keratinised squamous metaplasia | 0% | 0% | 100% | 100% | 0% |
| Prostate adenocarcinoma | 0% | 0% | 0% | 100% | 100% |
| Bulbourethral gland keratinised squamous metaplasia | 0% | 0% | 100% | 100% | 100% |
| Preputial gland keratinised squamous metaplasia | 0% | 0% | 67% (4 mice) | 100% | 100% |
| Urethra keratinised squamous metaplasia | 0% | 0% | 0% | 17% (1 mouse) | 28% (5 mice) |

### 5.3.3 *PBCre*-mediated recombination drives expression of the dominant stabilised *β-catenin* transgene in the prostate

LacZ staining carried out in chapter 3 revealed that *PBCre*-mediated recombination occurs in all four lobes of the prostate (figure 3.29) and correlated to published reports (Wu *et al.*, 2001). To confirm recombination occurred within $PBCre^{+}Catnb^{+/lox(ex3)}$ prostate tumours, a PCR specific for the *β-catenin* recombined allele ($Catnb^{+/\Delta ex3}$) was carried out. Monoallelic deletion of exon 3 of the *β-catenin* gene (amino acids 5-80) was confirmed in both keratinised squamous metaplasia and adenocarcinoma lesions (figure 5.3a). In *wild-type* prostate epithelium, β-catenin expression is predominantly found at the cell surface to form adherens junctions and is rarely detected in the nucleus (figure 5.3b). All $PBCre^{+}$ *β-catenin*$^{+/\Delta ex3}$ lesions (squamous metaplasia and adenocarcinoma) demonstrated increased β-catenin nuclear localisation where it can regulate transcription of Wnt target genes (figure 5.3c-e). Together this data indicates *β-catenin* oncogenic transformation occurred in $PBCre^{+}Catnb^{+/\Delta ex3}$ prostate lesions.

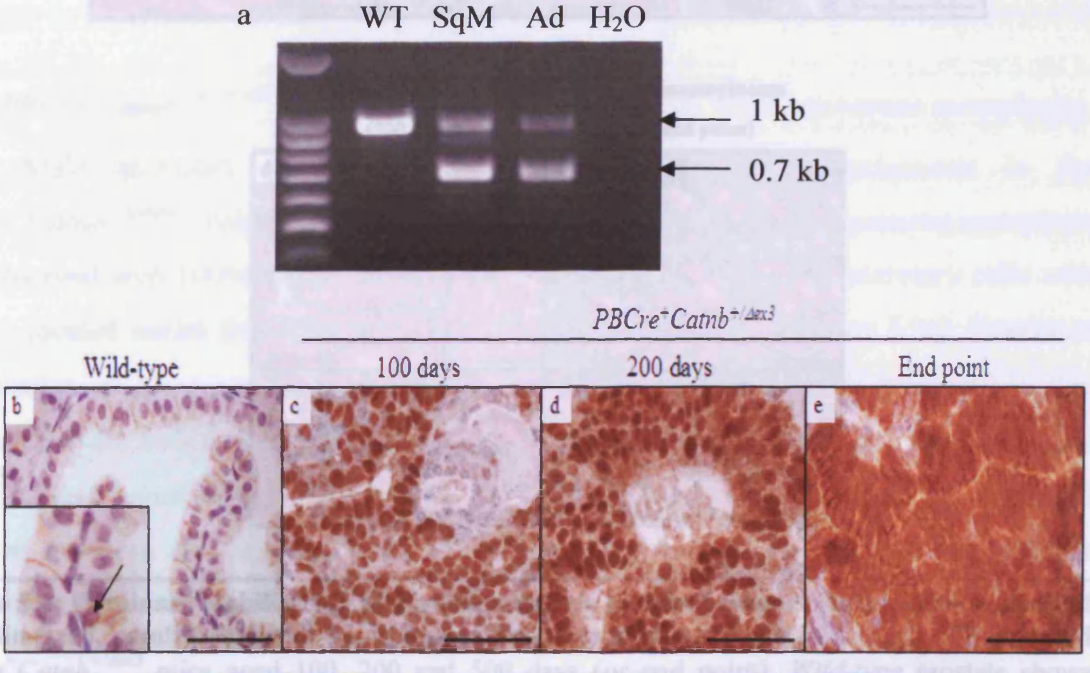


**Figure 5.3: β-catenin is constitutively active in $PBCre^{+}Catnb^{+/\Delta ex3}$ prostate tumours.** DNA isolated from anterior prostate lobes of *wild-type* mice (aged 500 days) and squamous metaplasia and adenocarcinoma lesions of $PBCre^{+}Catnb^{+/lox(ex3)}$ mice underwent *β-catenin* recombined PCR analysis (a). *Wild-type* (WT) prostate displayed the wild-type *β-catenin* allele (1 kb) while squamous metaplasia (SqM) and adenocarcinomas (Ad) expressed one *WT* allele and one *β-catenin* recombined allele (0.7kb). Immunohistochemistry to detect β-catenin in *wild-type* (b) and $PBCre^{+}Catnb^{+/lox(ex3)}$ mice aged 100 days (c), 200 days (d) and at end point (e) revealed elevated nuclear β-catenin expression in prostate lesions. Images were taken at 40x magnification and scale bars represent 50 μm.

### 5.3.4 *PBCre*$^{+}$*Catnb*$^{+/lox(ex3)}$ mice manifest prostate keratinised squamous metaplasia that progressed to adenocarcinoma

*Wild-type* (*PBCre*$^{+}$*Catnb*$^{+/+}$) and control (*Cre*$^{-}$*Catnb*$^{+/lox(ex3)}$) mice demonstrated normal architecture of all four prostate lobes (anterior lobe shown in figure 5.4a). By day 100, all four prostate lobes in *PBCre*$^{+}$*Catnb*$^{+/lox(ex3)}$ mice developed a diffuse, aggressive HG-PIN that exhibited keratinised squamous metaplasia with 100% incidence (figure 5.4b).

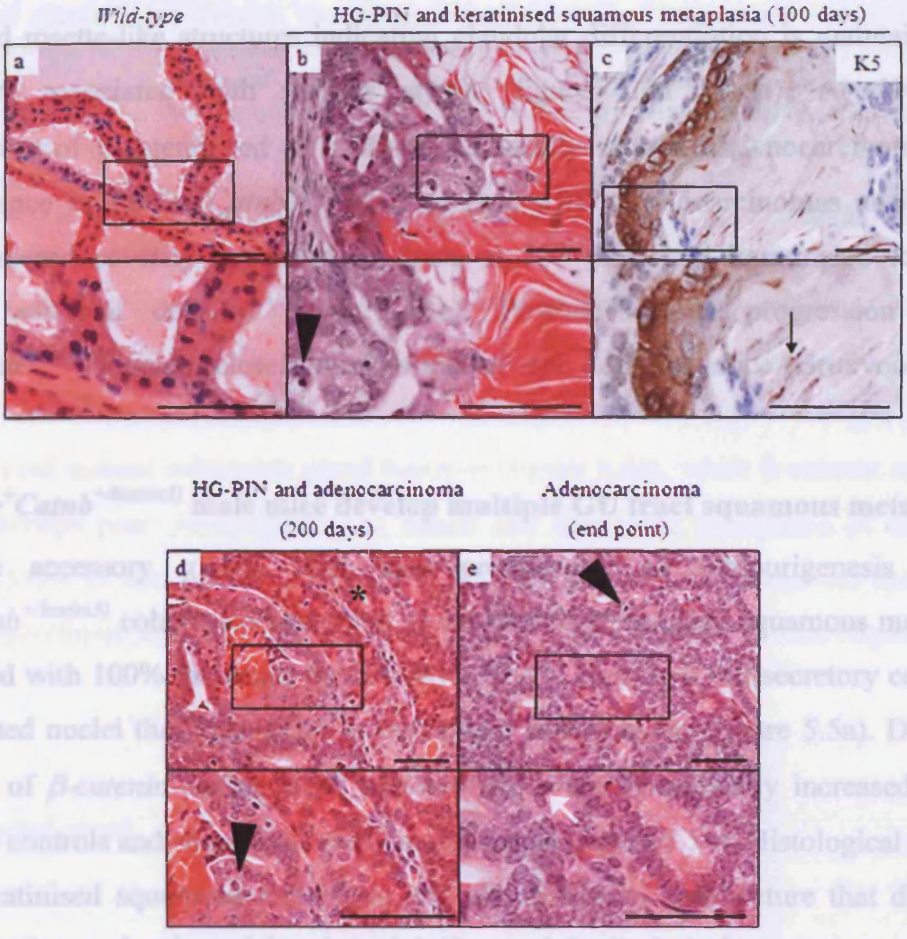


**Figure 5.4: Dominant stabilisation of *β-catenin* causes prostate cancer.** Histological analysis of formalin-fixed, paraffin-embedded H&E stained sections from *wild-type* mice aged 500 days and *PBCre*$^{+}$*Catnb*$^{+/\Delta ex3}$ mice aged 100, 200 and 500 days (or end point). *Wild-type* prostate shows ordered single-layered branched intra-luminal projections (a). Dominant stabilisation of *β-catenin* resulted in HG-PIN-like lesions that manifested keratinised squamous metaplasia at 100 days (b). The insert in (b) indicates apoptotic cells (arrow head) within metaplastic foci. Keratin pearl formations stained positively for Keratin-5 and the arrow represents a positively stained keratinocyte (c). At day 200, HG-PIN lesions and keratinised squamous metaplastic foci were present in addition to the development of adenocarcinoma that formed rosette (*) structures (d). End point mice manifested diffuse and locally invasive adenocarcinomas associated with mitosis (white arrow) and apoptosis (black arrow head). All images were taken at 40x magnification and scale bars represent 50 μm.

Lesions demonstrated nuclear atypia, apoptotic bodies, mitosis, angiogenesis, keratin pearl formation, extensive over-crowding of the lumen as multi-cellular disorganised layers form and metaplastic foci, surrounded by thick muscle walls. Keratin was detected by anti-keratin-5 immunohistochemistry staining that also labels the basal cell population (figure 5.4c). Staining for epidermal differentiation markers, such as loricrin, involucrin and fillagrin would further validate keratinisation and squamous metaplasia.

At 200 days, the *PBCre*$^{+}$*Catnb*$^{+/lox(ex3)}$ cohort (n = 6) was predisposed to lesions of keratinised squamous metaplasia and adenocarcinoma with 100% incidence (figure 5.3d). Cells formed rosette-like structures indicating glandular differentiation is maintained and lesions were associated with nuclear atypia (figure 5.4d insert). At 500 days, hyperactivation of β-catenin led to diffuse and locally invasive adenocarcinomas with 100% incidence in *PBCre*$^{+}$*Catnb*$^{+/lox(ex3)}$ mice (n = 18). Adenocarcinomas at 500 days showed increased severity compared to those at 200 days and keratinised squamous metaplasia was not detected (figure 5.4e). Prostate cancer progression in the *PBCre*$^{+}$*Catnb*$^{+/lox(ex3)}$ model closely mirrors that of *Apc* deficient mice (Bruxvoort *et al.*, 2007).

### 5.3.5 *PBCre*$^{+}$*Catnb*$^{+/lox(ex3)}$ male mice develop multiple GU tract squamous metaplasias

Male accessory glands were also predisposed to tumourigenesis in the *PBCre*$^{+}$*Catnb*$^{+/lox(ex3)}$ cohort. Bulbourethral gland (BUG) keratinised squamous metaplasia was observed with 100% incidence by 100 days. BUGs consist of tall secretory cells with basally located nuclei that form acini in the tubular coiled gland (figure 5.5a). Dominant stabilisation of *β-catenin* caused BUG tumours that were dramatically increased in size compared to controls and showed elevated angiogenesis (figure 5.5b). Histological analysis revealed keratinised squamous metaplasia and aberrant acini architecture that displayed reduced secretion and enlarged basal nuclei (figure 5.5c-d). It is important to note that these lesions did not demonstrate any immune cell infiltrate and were histologically distinct to the hyperplastic BUG cysts predisposed in *AhCre*$^{+}$*Lkb1*$^{fl/fl}$ mice (section 3.3.4).

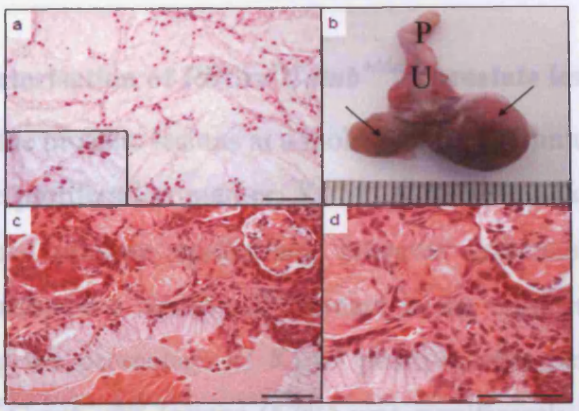


**Figure 5.5: *PBCre$^{+}$Catnb$^{+/lox(ex3)}$* mice develop keratinised squamous metaplasia of the bulbourethral gland.** H&E staining was performed on formalin-fixed, paraffin-embedded *wild-type* tissue sections at 100 days illustrating normal duct architecture and secretory function (a). *PBCre$^{+}$Catnb$^{+/lox(ex3)}$* mice displayed enlarged bulbourethral glands (arrows), adjacent to the distal urethra (U) where it joins the penis (P) (b), taken at 500 days and the ruler indicates 1 mm. H&E staining of *PBCre$^{+}$Catnb$^{+/lox(ex3)}$* bulbourethral gland at low (c) and high magnifications (d) revealed squamous metaplasia and aberrant ductal cells and secretory function at 100 days. Images were taken at 20x (low power) and 40x (high power) magnification and scale bars represent 50 μm.

Keratinised squamous metaplasia of the preputial gland and urethra was observed at 100 days (67% and 0% incidence respectively), 200 days (100% and 17% incidence respectively) and at end point (100% and 28% incidence respectively). *Wild-type* preputial glands displayed normal sebaceous gland function (figure 5.6a), while β-catenin activation resulted in keratin pearl formation in the lumen and squamous metaplasia of the ductal cells (figure 5.6b). A similar phenotype was observed in the urethra transitional epithelium, where acini developed squamous metaplasia and the lumen contained keratin (figure 5.6d).

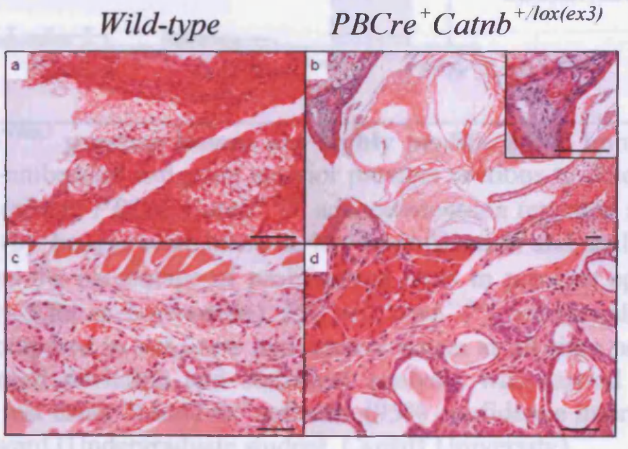


**Figure 5.6: *PBCre$^{+}$Catnb$^{+/lox(ex3)}$* mice develop preputial gland and urethra keratinised squamous metaplasia.** *Wild-type* preputial gland exhibits normal ductal architecture and secretory function (a) while *PBCre$^{+}$Catnb$^{+/lox(ex3)}$* mice display keratinised squamous metaplasia (b). Flattening of cells is clearly seen in (b). *Wild-type* urethra is shown in (c) and keratinised squamous metaplasia of *PBCre$^{+}$Catnb$^{+/lox(ex3)}$* urethra is illustrated in (d). Keratin is clearly identifiable in acini formed within the urethral transitional epithelium. Images were taken at 20x (low power) and 40x (high power) magnification and scale bars represent 50 μm. All mice were 200 days old.

### 5.3.6 Molecular characterisation of *PBCre*$^{+}$*Catnb*$^{+/\Delta ex3}$ prostate lesions

To characterise the prostate lesions at a molecular level, immunohistochemistry was performed to detect the proliferation marker, Ki-67. A basal level of Ki-67 positive cells was observed in control prostate epithelium, however dominant stabilised β-catenin prostate tumours demonstrated a significant increase in the number of proliferating cells (figure 5.7a-b). Scoring the percentage of Ki-67 positive cells per acinus revealed that proliferation in *PBCre*$^{+}$*Catnb*$^{+/\Delta ex3}$ lesions (57%) was significantly different compared to *wild-type* and control cohorts (4%), throughout the course of tumour progression ($p = 0.0404$, Mann Whitney). Furthermore, Ki-67 staining remained constant during disease progression from PIN-like squamous metaplasia to adenocarcinoma (figure 5.7c).

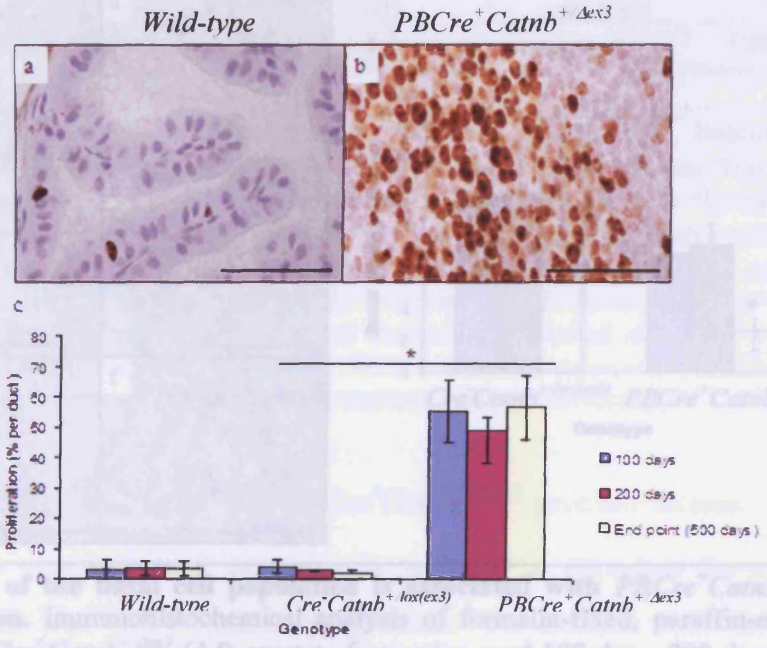


**Figure 5.7: *PBCre*$^{+}$*Catnb*$^{+/\Delta ex3}$ prostate lesions are highly proliferative.** Immunohistochemistry of formalin-fixed, paraffin-embedded end point anterior prostate sections to detect the proliferation marker Ki-67 in *wild-type* (a) and *PBCre*$^{+}$*Catnb*$^{+/\Delta ex3}$ adenocarcinoma revealed a dramatic increase in the rate of proliferation (b). Images were taken at 40x magnification and scale bars represent 50 μm. The chart in (c) shows the percentage of proliferating cells in prostate epithelium (20 acini were scored per mouse, n = 3 for each genotype). *PBCre*$^{+}$*Catnb*$^{+/\Delta ex3}$ prostate showed a significant increase in proliferation compared to *wild-type* and control tissue at all time points ($p = 0.0404$). Error bars represent standard deviation and statistical analysis was carried out using a non-parametric Mann Whitney test using "MiniTab" software (95% confidence interval). Counting was carried out by Jennifer Howard (Undergraduate student, Cardiff University).

Basal cells were detected by immunohistochemistry using an anti-p63 antibody (Shappell *et al.*, 2004). The basal cell population was reduced in prostate lesions expressing activated β-catenin compared to control tissue at each time point (figure 5.8a-f). Control prostate demonstrated the basal cell population comprised ~11% of the prostatic

epithelium at all time points (figure 5.8g), consistent with the literature (Collins *et al.*, 2001). Squamous metaplasia and adenocarcinoma at 100 days and 200 days respectively showed a significant reduction in p63 positive cells (8-9%, p = 0.0404, Mann Whitney). Interestingly, end point adenocarcinomas showed a further reduction in p63 (2.7%, p = 0.0404, Mann Whitney). In parallel with this data, depletion of the basal cell population has been demonstrated during the progression of human prostate cancer and p63 expression has been deemed necessary for the development of squamous metaplasia (Bruxvoort *et al.*, 2007). Similarly, bladder tumours show a progressive reduction in p63 with progression (Urist *et al.*, 2002).

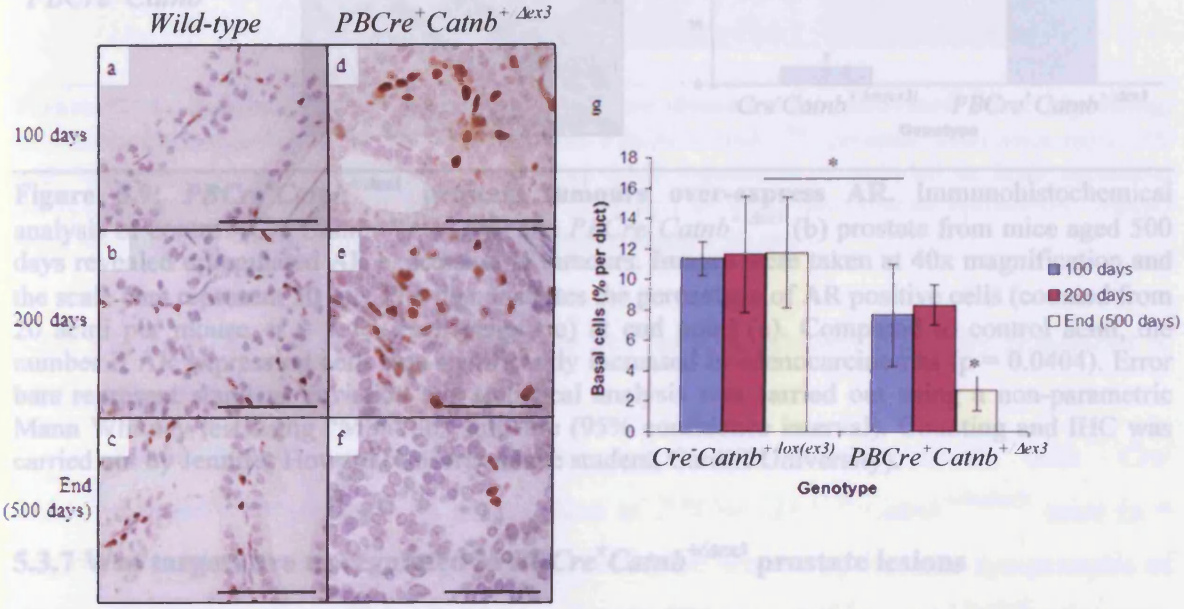


**Figure 5.8: Loss of the basal cell population is associated with *PBCre$^{+}$Catnb$^{+/\Delta ex3}$* prostate cancer progression.** Immunohistochemical analysis of formalin-fixed, paraffin-embedded *wild-type* (a-c) and *PBCre$^{+}$Catnb$^{+\ \Delta ex3}$* (d-f) prostate from mice aged 100 days, 200 days and end point (up to 500 days) revealed a reduction in the expression of the basal cell marker p63. Images were taken at 40x magnification and the scale bars represent 50 μm. The chart in (g) demonstrates the percentage of basal cells per acinus (20 acini were scored per mouse, n = 3 for each genotype). The basal cell population is significantly decreased in prostate tumours (p = 0.0404). Furthermore, p63 expression does not change with age in control prostate tissue (p = 0.6625). Error bars represent standard deviation and statistical analysis was carried out using a non-parametric Mann Whitney test using "MiniTab" software (95% confidence interval). Counting and immunohistochemistry was carried out by Jennifer Howard (Undergraduate student, Cardiff University).

Immunohistochemistry to detect AR revealed that dominant stabilisation of β-catenin results in an increase in the number of cells expressing nuclear AR compared to control prostate tissue (figure 5.9a-b). AR was present in 5.3% of the control prostate epithelium and was elevated 10-fold in adenocarcinomas (52.6%, p = 0.0404, Mann Whitney) (figure 5.9c). This suggests that β-catenin-mediated AR transcription and

signalling may further facilitate tumour progression in *PBCre*$^{+}$*Catnb*$^{+/lox(ex3)}$ mice (Terry *et al.*, 2006; Truica *et al.*, 2000; Yang *et al.*, 2006).

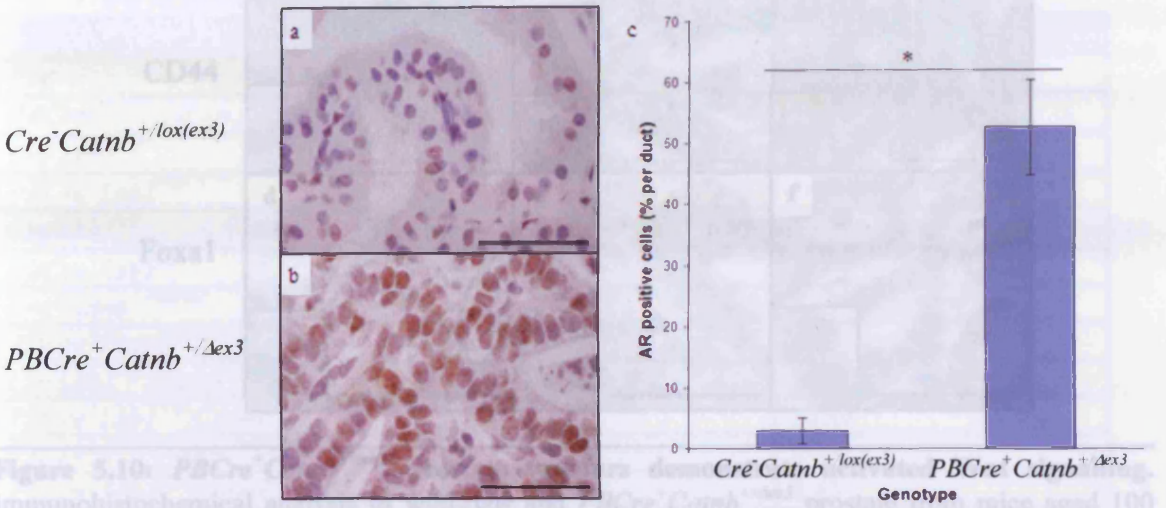


**Figure 5.9: *PBCre*$^{+}$*Catnb*$^{+/\Delta ex3}$ prostate tumours over-express AR.** Immunohistochemical analysis of control (*Cre*$^{-}$*Catnb*$^{+\ lox3(ex3)}$) (a) and *PBCre*$^{+}$*Catnb*$^{+\ \Delta ex3}$ (b) prostate from mice aged 500 days revealed upregulated AR expression in tumours. Images were taken at 40x magnification and the scale bars represent 50 μm. Plot demonstrates the percentage of AR positive cells (counted from 20 acini per mouse, n = 3 for each genotype) at end point (c). Compared to control acini, the number if AR expressing cells was significantly increased in adenocarcinomas ($p = 0.0404$). Error bars represent standard deviation and statistical analysis was carried out using a non-parametric Mann Whitney test using "MiniTab" software (95% confidence interval). Counting and IHC was carried out by Jennifer Howard (Undergraduate student, Cardiff University).

### 5.3.7 Wnt targets are upregulated in *PBCre*$^{+}$*Catnb*$^{+/\Delta ex3}$ prostate lesions

Dominant stabilisation of β-catenin is predicted to stimulate the transcription of Wnt target genes that drive tumour progression. To confirm that elevated nuclear accumulation of β-catenin in prostate lesions results in the expression of Wnt target genes, immunohistochemistry was employed to analyse the expression of the migration marker CD44 and the proto-oncogene Foxa1 (figure 5.10). CD44 was not detected in *wild-type* prostate (figure 5.10a) while mutant PIN-like squamous metaplasia lesions and adenocarcinomas both showed over-expression of CD44 (figure 5.10b-c). Foxa1 was also upregulated in *PBCre*$^{+}$*Catnb*$^{+/\Delta ex3}$ squamous metaplasia and adenocarcinoma compared to *wild-type* tissue (figure 5.10d-f). Together, this indicates that hyperactivation of β-catenin in prostate epithelium stimulates the transcription of Wnt target genes, which potentially act to drive tumour progression. This is consistent with other studies which have strongly implicated deregulated Wnt signalling in cancer (Polakis, 2000; Yardy and Brewster, 2005).

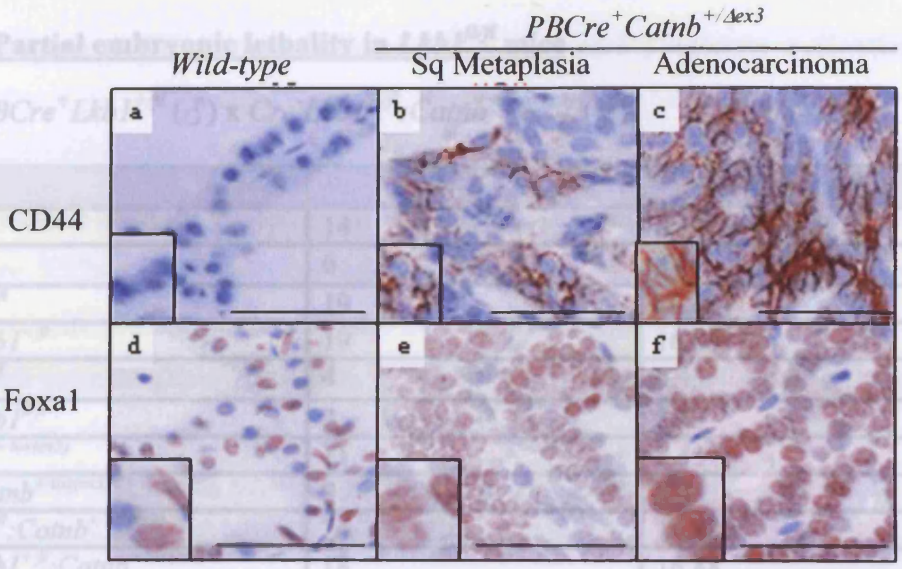


**Figure 5.10: *PBCre$^{+}$Catnb$^{+/\Delta ex3}$* prostate tumours demonstrate activated Wnt signalling.** Immunohistochemical analysis of *wild-type* and *PBCre$^{+}$Catnb$^{+/\Delta ex3}$* prostate from mice aged 100 and 500 days revealed CD44 (a-c) and Foxa1 (d-f) expression is induced in both squamous metaplasia and adenocarcinoma lesions (a-c) compared to *wild-type* prostate epithelium. Images were taken at 40x magnification and the scale bars represent 50 μm.

### 5.3.8 *PBCre$^{+}$Lkb1$^{+/fl}$:Catnb$^{+/lox(ex3)}$* mice do not show decreased longevity compared to *PBCre$^{+}$Catnb$^{+/lox(ex3)}$* mice

*PBCre$^{+}$Lkb1$^{+/fl}$* transgenic male mice were inter-crossed with *Cre$^{-}$ Lkb1$^{+/fl}$;Catnb$^{+/lox(ex3)}$* females. A male cohort of *PBCre$^{+}$Lkb1$^{+/fl}$;Catnb$^{+/lox(ex3)}$* mice (n = 10) was generated and aged to 500 days or harvested when they became symptomatic of disease. Unfortunately, sufficient numbers of male *PBCre$^{+}$Lkb1$^{fl/fl}$;Catnb$^{+/lox(ex3)}$* mice were not generated within the time course of the project (n = 2). Chi-squared analysis determined that the observed Mendelian frequencies did not fit the expected ratios ($\chi^2$ = 19.785, p = 0.0484, n = 135). This suggests that there is some lethality in a number of the genotypes. Expected ratios shown in Table 5.2 indicate that the number of *Lkb1$^{fl/fl}$* mice is lower than expected, however the cohort size of this genotype is relatively small. Consistent with this data, Sakamoto *et al* (2005) have reported that *Lkb1$^{fl/fl}$* mice are born at a frequency ~30% lower than the expected Mendelian ratio, suggesting partial embryonic lethality of this genotype. Mice carrying the dominant stable *β-catenin* transgene did not demonstrate partial lethality, although it is not clear from our data whether this construct may further enhance the partial embryonic lethality in *Lkb1$^{fl/fl}$* mice.

**Table 5.2 Partial embryonic lethality in *Lkb1*$^{fl/fl}$ mice**

**Cross:** *PBCre*$^{+}$*Lkb1*$^{+/fl}$ (♂) x *Cre*$^{-}$*Lkb1*$^{+/fl}$;*Catnb*$^{+/lox(ex3)}$ (♀)

| Genotype | Observed | Expected |
|---|---|---|
| *Cre*$^{-}$ | 14 | 8.43 |
| *PBCre*$^{+}$ | 6 | 8.43 |
| *Cre*$^{-}$*Lkb1*$^{+/fl}$ | 19 | 16.88 |
| *PBCre*$^{+}$*Lkb1*$^{+/fl}$ | 19 | 16.88 |
| *Cre*$^{-}$*Lkb1*$^{fl/fl}$ | 4 | 8.43 |
| *PBCre*$^{+}$*Lkb1*$^{fl/fl}$ | 2 | 8.43 |
| *Cre*$^{-}$*Catnb*$^{+lox(ex3)}$ | 11 | 8.43 |
| *PBCre*$^{+}$*Catnb*$^{+lox(ex3)}$ | 9 | 8.43 |
| *Cre*$^{-}$*Lkb1*$^{+/fl}$;*Catnb*$^{+lox(ex3)}$ | 24 | 16.88 |
| *PBCre*$^{+}$*Lkb1*$^{+/fl}$;*Catnb*$^{+lox(ex3)}$ | 18 | 16.88 |
| *Cre*$^{-}$*Lkb1*$^{fl/fl}$;*Catnb*$^{+lox(ex3)}$ | 4 | 8.43 |
| *PBCre*$^{+}$*Lkb1*$^{fl/fl}$;*Catnb*$^{+lox(ex3)}$ | 5 | 8.43 |
| Total | 135 | 135 |

A Kaplan-Meier survival plot (shown in figure 5.11) and Chi-squared analysis revealed double heterozygous transgenic mice (*PBCre*$^{+}$*Lkb1*$^{+/fl}$;*Catnb*$^{+/lox(ex3)}$) showed a significant reduction in lifespan (average survival 453 days, $\chi^2 = 26.07$, $p = 0.000$ compared to *wild-type* mice), but this did not differ from the *PBCre*$^{+}$*Catnb*$^{+/lox(ex3)}$ cohort (average survival 417 days, $\chi^2 = 2.825$, $p = 0.093$).

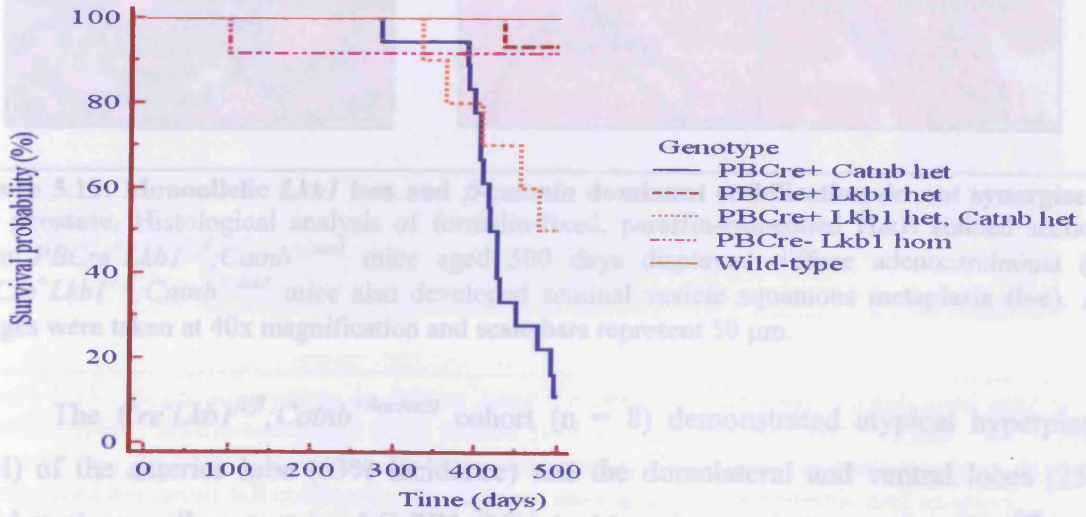


**Figure 5.11: *PBCre*$^{+}$*Lkb1*$^{+/fl}$*:Catnb*$^{+/lox(ex3)}$ male mice display reduced longevity.** A Kaplan-Meier plot of *wild-type* (n = 32), *PBCre*$^{+}$*Catnb*$^{+lox(ex3)}$ (n = 18), *PBCre*$^{+}$*Lkb1*$^{+fl}$ (n = 16), *Cre*$^{-}$*Lkb1*$^{fl/fl}$ (n = 12) and *PBCre*$^{+}$*Lkb1*$^{+fl}$;*Catnb*$^{+lox(ex3)}$ (n = 10) mice. *PBCre*$^{+}$*Lkb1*$^{+fl}$;*Catnb*$^{+lox(ex3)}$ mice displayed a small yet significant decrease in survival compared to *wild-type* mice (average survival 453 days, $\chi^2 = 26.07$, $p = 0.000$). This reduction was similar to *PBCre*$^{+}$*Catnb*$^{+/lox(ex3)}$ mice (average survival 417 days, $\chi^2 = 2.825$, $p = 0.093$). Statistical analysis was carried out using a Chi-squared test using "MiniTab" software and the Kaplan-Meier plot was generated using "MedCalc" software.

### 5.3.9 Investigating the cooperativity of Lkb1 loss and β-catenin activation in the prostate

Histological analysis of H&E sections from *PBCre*$^{+}$*Lkb1*$^{+/fl}$;*Catnb*$^{+/lox(ex3)}$ mice displayed prostate adenocarcinoma with 100% incidence, resembling *PBCre*$^{+}$*Catnb*$^{+/lox(ex3)}$ mice (figure 5.12a). This probably reflects the fact that *PBCre*$^{+}$*Lkb1*$^{+/fl}$ mice did not develop a prostate phenotype. Compound mutants were also predisposed to bulbourethral, preputial and urethral gland squamous metaplasia with 100%, 100% and 30% incidence respectively (as shown in figures 5.5 and 5.6). In addition, seminal vesicle squamous metaplasia (50% incidence) was observed in the double transgenic line which was not detected in single transgenics, suggesting heterozygous inactivation of the *Lkb1* gene may cause prostate cancer invasion into the adjacent male accessory organ (figure 5.12b-e).

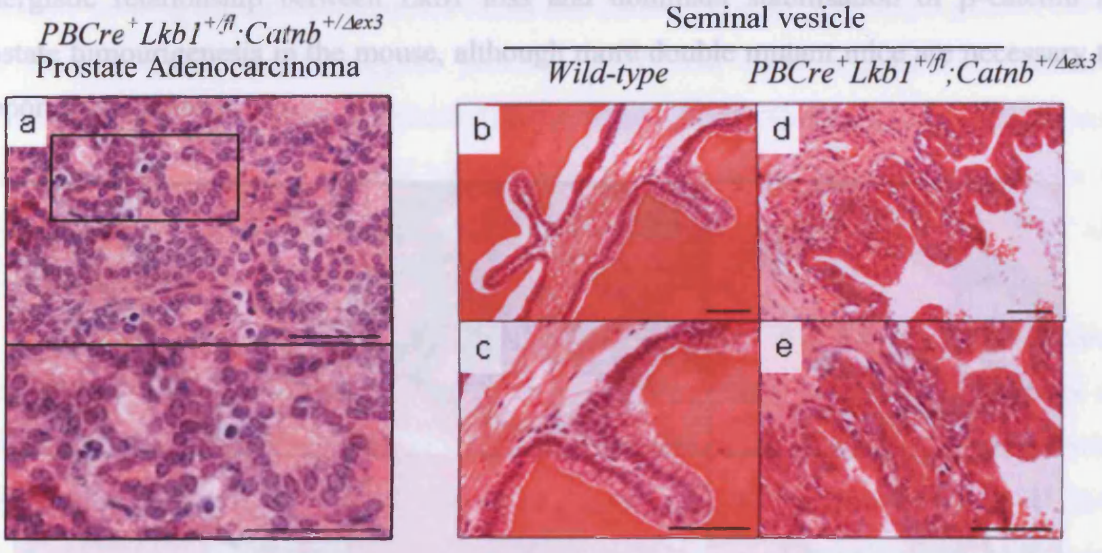


**Figure 5.12: Monoallelic *Lkb1* loss and *β-catenin* dominant stabilisation do not synergise in the prostate.** Histological analysis of formalin-fixed, paraffin-embedded H&E stained sections from *PBCre*$^{+}$*Lkb1*$^{+/fl}$;*Catnb*$^{+/\Delta ex3}$ mice aged 500 days displayed diffuse adenocarcinoma (a). *PBCre*$^{+}$*Lkb1*$^{+/fl}$;*Catnb*$^{+/\Delta ex3}$ mice also developed seminal vesicle squamous metaplasia (b-e). All images were taken at 40x magnification and scale bars represent 50 μm.

The *Cre*$^{-}$*Lkb1*$^{fl/fl}$;*Catnb*$^{+/lox(ex3)}$ cohort (n = 8) demonstrated atypical hyperplasia (AH) of the anterior lobe (63% incidence) and the dorsolateral and ventral lobes (25% incidence) as well as anterior LG-PIN (25% incidence), correlating to *Cre*$^{-}$*Lkb1*$^{fl/fl}$ mice (shown previously in Table 3.2) and reflecting the hypomorphic nature of the *Lkb1* floxed construct (figure 3.28d-f).

To date, only two male *PBCre$^{+}$Lkb1$^{fl/fl}$;Catnb$^{+/lox(ex3)}$* mice have been generated. Histological analysis of these mice at 100 days revealed that these mice were predisposed to PIN-like keratinised squamous metaplasia of all four prostate lobes, concomitant with epithelial cells that contained large cytoplasmic vacuoles with basal and compressed nuclei (figure 5.13), reminiscent of mucinous metaplasia observed in p63 null prostate (Kurita *et al.*, 2004) and *PB-H-ras$^{V12}$* mice (Scherl *et al.*, 2004). The *PBCre$^{+}$Lkb1$^{fl/fl}$;Catnb$^{+/lox(ex3)}$* phenotype resembles aspects of both *PBCre$^{+}$Catnb$^{+/lox(ex3)}$* mice at this time point (figure 5.3b) and *PBCre$^{+}$Lkb1$^{fl/fl}$* mice aged to 500 days (figure 3.28), suggesting an acceleration of the *Lkb1* deficient phenotype. In addition, both *PBCre$^{+}$Lkb1$^{fl/fl}$;Catnb$^{+/lox(ex3)}$* mice analysed were sterile (hypospermatogenesis) and developed preputial gland, bulbourethral gland and urethra keratinised squamous metaplasia. Together, this data implicates a synergistic relationship between Lkb1 loss and dominant stabilisation of β-catenin in prostate tumourigenesis in the mouse, although more double mutant mice are necessary to support this notion.

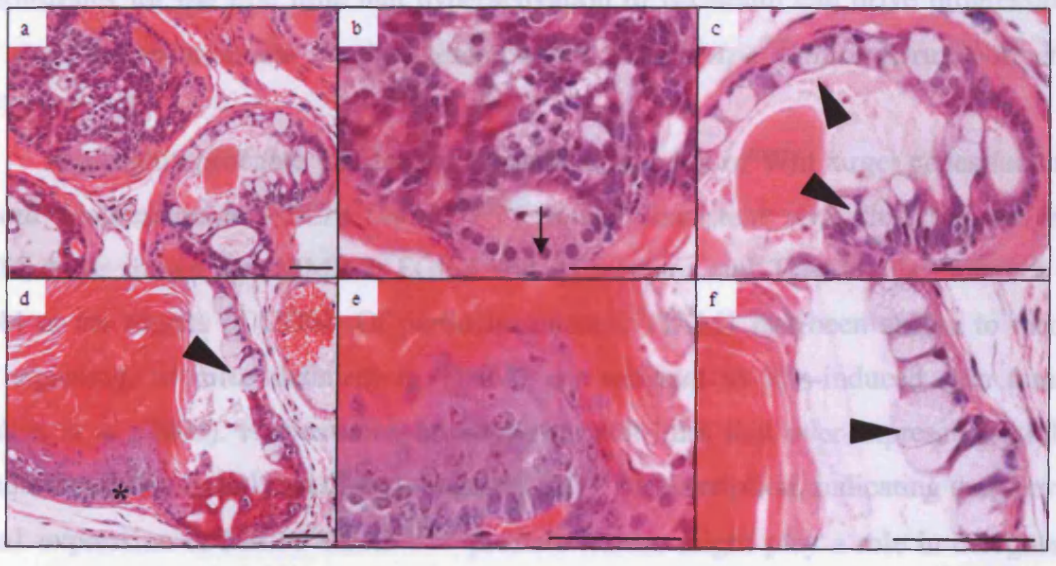


**Figure 5.13: Potential synergy in *PBCre$^{+}$Lkb1$^{fl/fl}$;Catnb$^{+/\Delta ex3}$* prostate.** Histological analysis of formalin-fixed, paraffin-embedded H&E stained sections from *PBCre$^{+}$Lkb1$^{fl/fl}$;Catnb$^{+/lox(ex3)}$* mice aged 100 days revealed all four prostate lobes were predisposed to several distinct lesions. PIN-like lesions (a-b) displayed tall columnar cells (arrow), nuclear atypia and mitotic and apoptotic figures shown in (b), mucinous-like epithelial cells that contained large vacuoles with compressed, basally located nuclei (arrow heads) shown in (c) and at high power in (d) and (f). Keratinised squamous metaplasia (*) was also observed (d), displaying flattened epithelial cells and nuclear atypia, shown at high power in (e). All images were taken at 40x magnification and scale bars represent 50 μm.

## 5.4 Discussion

### 5.4.1 Dominant stabilisation of β-catenin is sufficient to cause prostate adenocarcinoma

In this chapter, the role of Wnt/β-catenin signalling in prostate tumourigenesis was investigated using a conditional transgenic approach that led to dominant stabilisation of β-catenin in prostate epithelial cells and subsequent oncogenic transformation. Male *PBCre*$^{+}$*Catnb*$^{+/lox(ex3)}$ mice showed reduced longevity owing to tumour burden (>1 cm) and displayed an average survival of 417 days. Hyperactivation of β-catenin led to the development of squamous metaplasia at 100 days which progressed to adenocarcinoma by 200 days which became locally invasive at 500 days. This phenotype was characterised by β-catenin nuclear translocalisation and increased transcription of Wnt target genes (CD44 and Foxa1). These results support previous work that showed β-catenin dominant stabilisation causes prostate neoplasia (Bierie *et al.*, 2003; Gounari *et al.*, 2002) and demonstrates for the first time that hyperactivation of β-catenin can drive progression to late stage adenocarcinoma *in vivo*, resembling a *PBCre*$^{+}$*Apc*$^{fl/fl}$ mice (Bruxvoort *et al.*, 2007).

It is highly probable that the upregulated expression of Wnt target genes facilitates tumour progression in *PBCre*$^{+}$*Catnb*$^{+/lox(ex3)}$ mice. Consistent with this, Sansom *et al* (2004) have shown that MMP-7, FGF-4 and its receptor and TIAM1 may interact with CD44 or are targets of CD44. Of particular interest, TIAM1 has been shown to mediate Ras signaling, as mice deficient in TIAM1 are resistant to Ras-induced skin tumours (Malliri *et al.*, 2002). Furthermore, breast cancer cell lines that over-express Foxa1 have demonstrated that Foxa1 can directly regulate p27$^{Kip1}$ transcription, indicating that elevated Foxa1 expression in *PBCre*$^{+}$*Catnb*$^{+/\Delta ex3}$ prostate lesions might play a role in deregulating the cell cycle (Williamson *et al.*, 2006). Taken together, this evidence provides rational for prostate tumourigenesis in *PBCre*$^{+}$*Catnb*$^{+/lox(ex3)}$ mice via activation of the Wnt pathway, which leads to the upregulation of oncogenic Wnt target genes.

### 5.4.2 *PBCre*$^{+}$*Catnb*$^{+/\Delta ex3}$ prostate tumours show a progressive reduction in p63 expression with progression

Previous work has demonstrated that a reduction in p63 staining correlated directly with human prostate disease progression (Kwabi-Addo *et al.*, 2001; Parsons *et al.*, 2001;

Signoretti *et al.*, 2000) and more recently has been correlated with tumour stage in bladder cancer (Urist *et al.*, 2002). The human p63 gene is located on chromosome 3, within a region which is frequently amplified in squamous cell carcinomas (Moll *et al.*, 2001). Squamous metaplasia of the lung (Ji *et al.*, 2007), breast (Koker and Kleer, 2004) and prostate (Bruxvoort *et al.*, 2007) display a decrease in p63 expression upon progression to advanced stages of the disease, strongly resembling the *PBCre*$^{+}$*Catnb*$^{+/\Delta ex3}$ prostate phenotype. Clusters of p63 cells with altered morphology and localisation observed in the *PBCre*$^{+}$*Catnb*$^{+/\Delta ex3}$ metaplastic lesions may represent expansion of the transit-amplifying cells, suggesting that *PBCre*-mediated dominant stabilisation of *β-catenin* may result in the activation of prostate stem cells (Wang *et al.*, 2006b). The reduction in p63 expression in advanced lesions may reflect the fact that basal cells of normal epithelium, including the epidermis, strongly express p63 proteins (predominantly the ΔNp63α isotype) and lose them as soon as these cells withdraw from the stem cell compartment (Moll *et al.*, 2001). Alternatively, trans-differentiation of the p63$^{+}$ cells may also account for the reduction in p63 expression within the tumours. In addition, Notch signalling activation could be investigated, since keratinocytes have been shown to down-regulate p63 expression in response to Notch signalling (Nguyen *et al.*, 2006).

Human prostate cancer does not typically demonstrate squamous metaplasia (Melissari *et al.*, 2006) however, squamous metaplasia initiation has been linked to estrogen receptor (ER) signalling (Chang and Prins, 1999; Cunha *et al.*, 2004). Long-term exposure to exogenous or endogenous estrogen, in addition to studies using ERα knockout mice, have revealed squamous metaplasia initiation is mediated by ERα signalling and is usually reversible by removal of the estrogen stimulus (Chang and Prins, 1999; Cunha *et al.*, 2004). ER signalling has been directly linked to elevated Wnt signalling by rapidly upregulating the expression of Wnt4 and Wnt5a of the Wnt family and frizzled-2 of the Wnt receptor family in the mouse uterus to promote uterine growth (Hou *et al.*, 2004). Both ERα and ERβ have been detected in the adult rat reproductive tissues, and ERβ was prominent in the prostate (Chang and Prins, 1999) and together, this evidence suggests that squamous metaplasia in *PBCre*$^{+}$*Catnb*$^{+/lox(ex3)}$ mice may be a consequence of disrupted balance between AR and ER signalling in prostate epithelium (Risbridger *et al.*, 2007). To address this, immunohistochemistry to detect ER is necessary.

### 5.4.3 Dominant stabilisation of β-catenin drives androgen-independent tumourigenesis

Prostate cells require androgens for growth and survival and their effects are mediated by AR, which translocates into the nucleus in its ligand bound form to stimulate the upregulation of genes that promote proliferation and survival (detailed in section 1.1.8). β-catenin has been shown to bind AR to mediate androgen signalling and drive transcription of the *AR* gene and may provide a direct mechanism for prostate tumourigenesis (Yardy and Brewster, 2005). The interaction of β-catenin and the ligand-bound AR has also been shown to introduce a steroid-specific response, possibly linking aberrant Wnt signalling to hormone-refractory disease that maintains high levels of the AR protein (Truica *et al.*, 2000; Verras and Sun, 2005). Consistent with this, androgen ablation experiments in $PBCre^{+}Apc^{fl/fl}$ mice revealed that adenocarcinoma lesions were androgen-independent (Bruxvoort *et al.*, 2007). Given that AR is significantly over-expressed in $PBCre^{+}Catnb^{+/\Delta ex3}$ adenocarcinomas that were phenotypically similar to androgen-independent $PBCre^{+}Apc^{fl/fl}$ adenocarcinomas, it is hypothesised that $PBCre^{+}Catnb^{+/lox(ex3)}$ mice could also provide a model for hormone refractory prostate cancer.

### 5.4.4 Potential synergy between *Lkb1* loss and dominant stabilisation of β-catenin

A synergistic relationship between Lkb1 loss and constitutive activation of β-catenin was not demonstrated in $PBCre^{+}Lkb1^{+/fl};Catnb^{+/lox(ex3)}$ mice. Given that $PBCre^{+}Lkb1^{+/fl}$ mice were not predisposed to prostate tumourigenesis, only a very strong synergy between the mutations would be detectable in $PBCre^{+}Lkb1^{+/fl};Catnb^{+/lox(ex3)}$ mice. The phenotype of $PBCre^{+}Lkb1^{fl/fl};Catnb^{+/\Delta ex3}$ mice at 100 days suggests that Lkb1 loss and β-catenin activation may cooperate in the prostate to drive tumourigenesis, however cohort numbers are not sufficient to confirm this and aging (>100 days) may be required to demonstrate further acceleration of the disease. In support of this hypothesis, Miyaki *et al* (2000) reported that PJS hamartomatous polyps that display LKB1 loss of heterozygosity can progress to form adenomatous and carcinomatous lesions, which contain β-catenin mutations (and occasional p53 mutation). This evidence suggests that a synergistic relationship may exist between *β-catenin* hyperactivation and *Lkb1* inactivation to promote gastrointestinal tumour progression (Miyaki *et al.*, 2000).

## 5.5 Summary

Using a Cre-LoxP approach, the expression of a constitutively active dominant form of β-catenin confirmed a link between activation of the Wnt pathway and prostate tumourigenesis. This supports the molecular analysis of *AhCre*$^{+}$*Lkb1*$^{fl/fl}$ mice, which implicated a role for Wnt in the development of prostate neoplasia (chapter 4). No evidence for synergy was determined between Lkb1 loss and activation of the Wnt pathway, although investigations were limited to *PBCre*$^{+}$*Lkb1*$^{+/fl}$*:Catnb*$^{+/lox(ex3)}$ mice and preliminary analysis of *PBCre*$^{+}$*Lkb1*$^{fl/fl}$*:Catnb*$^{+/lox(ex3)}$ mice did not rule out this possibility.

# Chapter 6: Wnt and Ras signalling synergise to accelerate prostate tumourigenesis

## 6.1 Introduction

Activating mutations in *Ras* and *β-catenin* have been shown to synergise in colorectal (Janssen *et al.*, 2006; Li *et al.*, 2005), kidney (Sansom *et al.*, 2006), mammary (Jang *et al.*, 2006) and liver (Harada *et al.*, 2004) tumours, resulting in accelerated tumour progression. Furthermore, aberrant Ras and Wnt signalling are emerging as key events in the multi-step nature of prostate tumourigenesis and progression (Weber and Gioeli, 2004; Yardy and Brewster, 2005). To address whether synergy between Ras and Wnt occurs in the prostate, the *PBCre* transgenic line was used to drive expression of a dominant stabilised form of β-catenin (*Catnb*$^{+/lox(ex3)}$) and an activating mutant form of K-ras (K-*ras*$^{+/V12}$).

### 6.1.1 Alterations in Ras signalling promotes prostate tumourigenesis

Although *Ras* activating mutations are infrequent in human prostate cancer, aberrant Ras signalling is emerging as a common event in prostate tumour formation and progression (discussed in section 1.5). Raf, a mitogen-activated protein kinase kinase kinase (MAPKKK) and PI3K, a phosphatidyloinositol kinase, two principle Ras effectors, are also common to human prostate cancer (Carey *et al.*, 2007; Papatsoris *et al.*, 2007). Raf triggers the MEK/ERK MAPK cascade (Gioeli *et al.*, 1999) and PI3K regulates AKT signalling (Liao *et al.*, 2003), which stimulate proliferation and survival, thus driving tumourigenesis (Malumbres and Pellicer, 1998). Ras signalling can also stimulate AR, further facilitating prostate growth or tumourigenesis (Carey *et al.*, 2007; Papatsoris *et al.*, 2007).

To date, *in vivo* prostate cancer models expressing activating mutations in *Ras* have not generated consistent prostate phenotypes. This is considered to reflect differences in the transgenes and the genetic background employed (Scherl *et al.*, 2004). Ha-*RasT24* is an endogenous H-*ras* mutation from the T24 human bladder carcinoma cell line (Cohen and Levinson, 1988). This is an oncogenic form of the gene, which contains a point mutation at position 12 (replacing glycine with valine) and a second point mutation in intron 4 that causes a 10-fold increase in H-Ras protein expression (Cohen and Levinson, 1988). Transgenic mice expressing Ha-*RasT24* under control of the *PB* promoter (the initial 454 bp of the flanking sequence of the *probasin* gene) developed atypical hyperplasia (AH) in the dorsolateral and ventral lobes of the prostate between 6-12 months of age (Barrios *et al.*,

1996). This model also reported epithelial hyperplasia of the epididymis and focal destruction of the seminiferous tubules. Conversely, the same group reported that Ha-*RasT24* expression mediated by the PSA promoter predisposed to salivary gland and gastrointestinal tract neoplasms, but no prostate phenotype was observed. Consistent with this study, rats expressing both the SV40 T antigen and c-Ha-*ras* (H-*ras128*) under minimal probasin promoter control did not develop any additional prostate phenotype compared to the *PB-SV40 T-Ag* single transgenic line that develops prostate adenocarcinoma (Hokaiwado *et al.*, 2003). The human c-Ha-*ras128* also has an activating mutation at position 12 (128 refers to the transgenic rat strain) (Hokaiwado *et al.*, 2003).

More recently, Scherl et al (2004) showed that mice expressing Ha-*RasT24* (termed H-$Ras^{V12}$) expression under the control of the minimal *PB* promoter (-426/+28 bp of the *probasin* gene), displayed LG-PIN that exhibits a high incidence of intestinal metaplasia by 3 months. It is important to note that the H-$RAS^{V12}$ transgene was not detected in this model ≥12 months, resulting in a decrease in PIN incidence with age. This evidence suggests that PB expression decreases with reduced androgen levels in older mice and that aberrant Ras signalling might be required to maintain the phenotype (Scherl *et al.*, 2004).

v-H-*ras* activating mutations have also been shown to promote prostate tumour progression. Subcutaneous injections of the AT2.1 Dunning rat prostate adenocarcinoma cell line transfected with v-H-*ras* DNA developed metastasis with 80% incidence, compared to just 10% in AT2.1 inoculated mice (Treiger and Isaacs, 1988).

### 6.1.2 Derivation of mice expressing activated K-ras

The cancer prone K-$ras^{+/V12}$ mouse (detailed in figure 6.1) has been employed to investigate the role of aberrant Ras signalling within many tissues, including the intestine, kidney and pancreas (Guerra *et al.*, 2003). This transgene allows conditional activation of K-ras via *Cre* mediated deletion of a STOP codon upstream of Exon1 (Guerra *et al.*, 2003; Sansom *et al.*, 2006). *CMV-*$Cre^{+/T}$ mediated recombination throughout the body revealed that only a percentage of K-$ras^{V12}$-expressing lung bronchiolo-alveolar cells undergo malignant transformation, leading to the formation of multiple adenomas and adenocarcinomas by eight months (Guerra *et al.*, 2003). These results indicate that tumourigenesis induced by the K-$ras^{V12}$ oncogene depends upon cellular context.

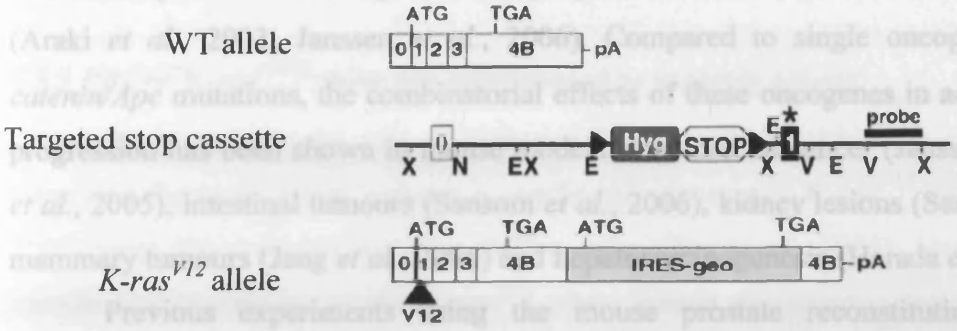


**Figure 6.1: Schematic representation of *wild-type* and activated K-*ras*$^{V12}$ alleles.** To generate the conditional K-*ras*$^{V12}$ transgene the *wild-type* (WT) K-*ras* allele (top) was manipulated by homologous recombination to replace the endogenous first exon with sequences carrying a mutant codon 12, encoding a valine residue, common to human tumours (*). In addition, a transcriptional STOP sequence was targeted to the first intron together with a PKG-Hygro cassette (Hyg) flanked by LoxP sites (arrow heads), middle panel. *Cre*-recombinase excises the STOP codon and the activated K-*ras*$^{V12}$ allele is expressed, bottom panel. The construct also harbours an internal ribosome entry site-*β-geo* cassette (IRES-geo) in the untranslated region allowing bicistronic translation of *β-geo* sequences driven by the endogenous K-*ras* promoter, which may be detected by X-gal staining. This figure is adapted from Guerra *et al* (2003).

Although the Ras isoforms show similar structural and functional properties, *Ras* gene mutations in cancer are dependent on both the tissue type and oncogenic Ras isoform (detailed in section 1.5). This is considered to relate to their differential expression within subcellular compartments and separate post-translational modification events (Schubbert *et al.*, 2007). In addition, sequence differences have demonstrated that K-*ras* (and not H-*ras* or N-*ras*) is susceptible to protein kinase C (PKC) phosphorylation (Malumbres and Pellicer, 1998) and only K-*ras* null mice are embryonic lethal, indicating this isoform plays a distinct role in embryonic development, possibly owing to stem/progenitor cell expression (Schubbert *et al.*, 2007). Consistent with this, activating K-*ras* mutations are predominant in somatic human diseases (30%) and H-*ras* activating mutations are less abundant (< 1%) (Schubbert *et al.*, 2007).

### 6.1.3 Activated Ras and Wnt signalling synergise to drive tumour progression

Cancer development is a multi-step process through which cells accumulate genetic mutations (Hanahan and Weinberg, 2000). Investigations that further our understanding of the cooperativity of these genetic transformations provide an insight into the aetiology of the disease and present targets for chemotherapeutic intervention. Synchronous activation of K-ras and activated Wnt signalling has been demonstrated in many transgenic models and the convergence of these pathways have been shown to upregulate the expression of genes that

function to promote tumourigenesis and progression, such as COX-2, c-Myc, AR and VEGF (Araki *et al.*, 2003; Janssen *et al.*, 2006). Compared to single oncogenic K-*ras* or *β-catenin/Apc* mutations, the combinatorial effects of these oncogenes in accelerating tumour progression has been shown in mouse models of colorectal cancer (Janssen *et al.*, 2006; Li *et al.*, 2005), intestinal tumours (Sansom *et al.*, 2006), kidney lesions (Sansom *et al.*, 2006), mammary tumours (Jang *et al.*, 2006) and hepatocarcinogenesis (Harada *et al.*, 2004).

Previous experiments using the mouse prostate reconstitution (MPR) model (described in section 1.2.2) have demonstrated synergy between vHa-*Ras* and *c-Myc* activating mutations. UGS transfected with activated *vHa-Ras* and *c-Myc* mutations and transplanted under the renal capsule of a male host revealed accelerated progression to a more advanced phenotype, highlighting the multi-step nature of prostate cancer and synergism between Wnt and Ras signalling (Thompson *et al.*, 1989).

## 6.2 Aim

Elevated Ras signalling has been linked to prostate tumourigenesis, but to date murine models that express oncogenic *H-Ras* have only developed hyperplastic foci or LG-PIN. Activating mutations of K-*RAS* in human prostate cancer are more common than any other isoform (Schubbert *et al.*, 2007). Therefore, activation of K-Ras in the mouse prostate is predicted to drive tumour progression. To test this hypothesis, the *PBCre* transgenic line was used to drive monoallelic K-$ras^{V12}$ expression in prostate epithelium. This model was examined for signs of neoplasia and characterised by means of immunohistochemistry and PCR.

To address whether synergy between Ras and Wnt signalling occurs in the prostate, the *PBCre* transgenic line was used to drive expression of a dominant stabilised form of β-catenin and an activating mutation in K-*ras* simultaneously in the mouse prostate. The phenotype of double mutants was characterised using immunohistochemistry and qRT-PCR.

## 6.3 Results

### 6.3.1 *PBCre*$^{+}$K-*ras*$^{+/V12}$ mice are predisposed to prostate cancer

To investigate the role of activated Ras signalling within the prostate, K-*ras*$^{+/V12}$ mice (see figure 6.1) that harbour a conditional oncogenic K-*ras*$^{V12}$ allele (Guerra *et al.*, 2003) were inter-crossed with the *PBCre* mice (Wu *et al.*, 2001). Cre-LoxP technology permits the expression of the K-*ras*$^{V12}$ allele within the prostate following endogenous *PBCre*-mediated excision of a floxed transcriptional inhibitory STOP sequence situated upstream from Exon 1 (Guerra *et al.*, 2003), shown in figure 6.1. Male cohorts of control (*PBCre*$^{+}$K-*ras*$^{+/+}$ and *Cre*$^{-}$K-*ras*$^{+/lox}$) and mutant (*PBCre*$^{+}$K-*ras*$^{+/V12}$) mice were generated and observed for signs of illness. To monitor disease progression we examined mice at 100 days (n = 6) and 200 days (n = 6), while the majority of histological analysis was carried out on cohorts aged to 500 days (n ≥ 15). All mice survived until the specified end point (average survival was 500 days). *PBCre*$^{+}$K-*ras*$^{+/V12}$ mice were predisposed to atypical hyperplasia (AH) that demonstrated progression to LG-PIN in all four lobes of the prostate (Table 6.1). No additional phenotypes were observed in non-prostate tissues.

**Table 6.1 Phenotype incidence in *PBCre*$^{+}$K-*ras*$^{+/V12}$ mice**

| Genotype / Phenotype | *Controls* (500 d) | *PBCre*$^{+}$ K-*ras*$^{+/V12}$ (100 d) | *PBCre*$^{+}$ K-*ras*$^{+/V12}$ (200 d) | *PBCre*$^{+}$ K-*ras*$^{+/V12}$ (500 d) |
|---|---|---|---|---|
| Prostate AH | 0% | 100% | 100% | 93% |
| Prostate LG-PIN | 0% | 0% | 67% | 60% |
| Prostate adenocarcinoma | 0% | 0% | 0% | 7% (1 mouse) |

At 100 days, *PBCre*$^{+}$K-*ras*$^{+/V12}$ mice displayed low severity focal atypical hyperplasia (AH), predominantly in the anterior prostate (100% incidence), when compared to control mice (*wild-type* or *Cre*$^{-}$K-*ras*$^{+/lox}$ mice) (figure 6.2a-b). AH comprised of focal tufting with nuclear abnormalities, including enlargement and the increased prominence of nucleoli. At 200 days, discrete AH foci were observed (100% incidence), which demonstrated progression to small LG-PIN foci (67% incidence), predominantly within the anterior prostate (data not shown as same phenotype as figure 6.2c). AH and LG-PIN lesions were both observed at 500 days with 93% and 60% incidence. LG-PIN foci comprised 2-3 cell layers within luminal epithelial cell compartments that demonstrated

nuclear atypia (figure 6.2c). In addition to LG-PIN, one *PBCre*$^{+}$K-*ras*$^{+/V12}$ mouse also displayed diffuse adenocarcinoma that showed elevated angiogenesis at 500 days (figure 6.2d).

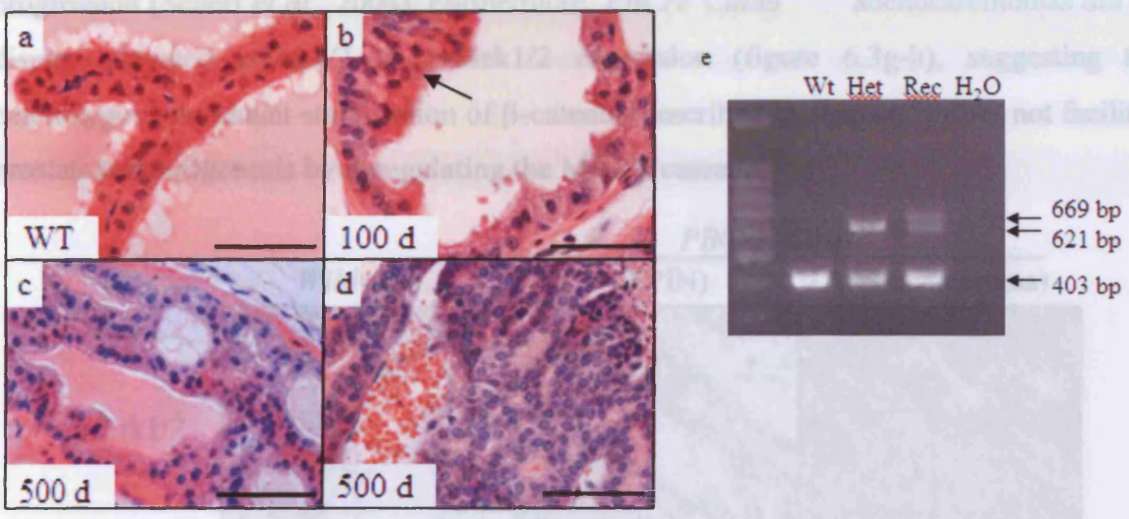


**Figure 6.2: *PBCre*$^{+}$K-*ras*$^{+/V12}$ mice are predisposed to prostate neoplasia.** Histological analysis of 10% formalin-fixed, paraffin-embedded GU sections determined that compared to *wild-type* or *Cre*$^{-}$ K-*ras*$^{+/lox}$ prostate shown in (a), *PBCre*$^{+}$K-*ras*$^{+/V12}$ mice were predisposed to focal AH at 100 days (b) which progressed to LG-PIN at 200-500 days (c) and in one case, adenocarcinoma (d). All images were taken at 40x magnification and scale bars represent 50 μm. (e) PCR analysis of tail biopsies determined *wild-type* (WT) mice were not recombined and only expressed the wild-type K-*ras* allele (403 bp). *PBCre*$^{+}$K-*ras*$^{+/V12}$ tail DNA expressed one *wild-type* and one K-*ras*$^{V12}$ allele (621 bp) and was not recombined. Recombined prostate lesions (Rec) expressed wild-type, K-*ras*$^{V12}$ floxed and the recombined (621 bp) K-*ras*$^{V12}$ alleles (e).

To confirm the *PBCre* transgene successfully targeted recombination and hyperactivation of K-*ras* in prostate epithelium, DNA was extracted from *PBCre*$^{+}$K-*ras*$^{+/V12}$ anterior prostate (at 500 days) and a PCR specific for the recombined, floxed and wild-type K-*ras* alleles was performed as described previously (Guerra *et al.*, 2003). PCR analysis determined excision of the transcriptional STOP cassette within the K-*ras*$^{+/V12}$ transgene is specific to prostate lesions. *Wild-type* and *PBCre*$^{+}$K-*ras*$^{+/V12}$ tail DNA served as negative controls (figure 6.2e).

### 6.3.2 Activated Ras signalling in *PBCre*$^{+}$K-*ras*$^{+/V12}$ prostate neoplasia

To validate the hyperactivation of K-*ras*, we monitored the expression of two proteins that participate in the MAPK cascade stimulated by Ras using immunohistochemistry. Nuclear and cytoplasmic levels of activated p-Erk1/2 (Thr202/Tyr204) and its upstream kinase p-Mek1/2 (Ser 221) were significantly elevated in

K-*ras*$^{+/V12}$ prostate lesions compared to *wild-type* controls (figure 6.3). Indeed, upregulation of the Ras signalling components corresponded to increased severity of the lesions, suggesting that sustained activation of the MAPK pathway might be required for tumour progression (Scherl *et al.*, 2004). Furthermore, *PBCre*$^{+}$*Catnb*$^{+/\Delta ex3}$ adenocarcinomas did not display elevated p-Erk1/2 or p-Mek1/2 expression (figure 6.3g-h), suggesting that heterozygous dominant stabilisation of β-catenin (described in chapter 5) does not facilitate prostate tumourigenesis by deregulating the MAPK cascade.

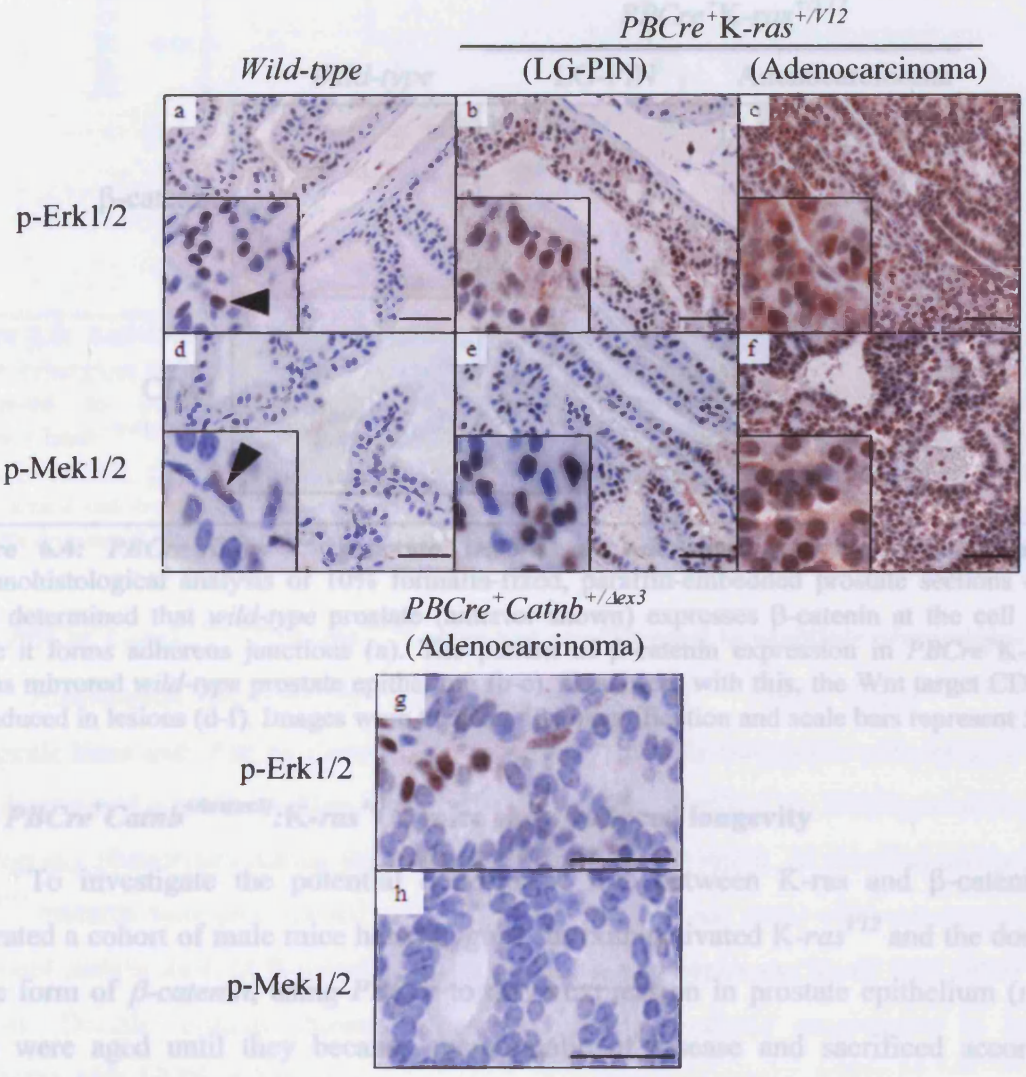


**Figure 6.3: The MAPK cascade is activated in *PBCre*$^{+}$K-*ras*$^{+/V12}$ mutant prostate lesions.** Histological analysis of 10% formalin-fixed, paraffin-embedded prostate sections (at 500 days) determined that *wild-type* prostate (anterior shown) expresses low levels of p-Erk1/2 (Thr202/Tyr204) (a), which was over-expressed in *PBCre*$^{+}$K-*ras*$^{+/V12}$ LG-PIN (b) and adenocarcinoma (c) lesions. A similar pattern of expression was observed for p-Mek1/2 (Ser221) (d-f). Over-expression of p-Erk1/2 and p-Mek1/2 was not demonstrated in *PBCre*$^{+}$*Catnb*$^{+/\Delta ex3}$ adenocarcinomas at 500 days. All images were taken at 40x magnification and scale bars represent 50 μm.

To determine whether aberrant Ras signalling deregulated the Wnt pathway we monitored the expression of β-catenin and the downstream Wnt signalling target CD44 using immunohistochemistry (figure 6.4). No difference in β-catenin expression was observed in K-*ras*$^{+/V12}$ LG-PIN lesions compared to control prostate epithelium (figure 6.4a-c). Accordingly we detected negligible levels of the migration marker CD44 in *wild-type* and K-*ras* mutants (figure 6.4d-f). These data demonstrate that active Ras signalling does not deregulate Wnt signalling in the prostate.

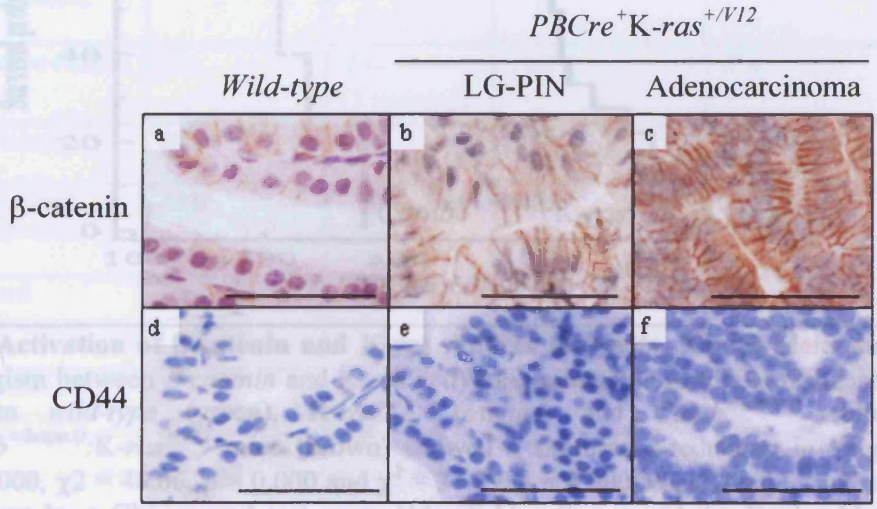


**Figure 6.4: *PBCre*$^{+}$K-*ras*$^{+/V12}$ prostate lesions do not show activated Wnt signalling.** Immunohistological analysis of 10% formalin-fixed, paraffin-embedded prostate sections (at 500 days) determined that *wild-type* prostate (anterior shown) expresses β-catenin at the cell surface where it forms adherens junctions (a). The pattern of β-catenin expression in *PBCre*$^{+}$K-*ras*$^{+/V12}$ lesions mirrored *wild-type* prostate epithelium (b-c). Consistent with this, the Wnt target CD44 was not induced in lesions (d-f). Images were taken at 40x magnification and scale bars represent 50 μm.

### 6.3.3 *PBCre*$^{+}$*Catnb*$^{+/lox(ex3)}$:K-*ras*$^{+/V12}$ mice show reduced longevity

To investigate the potential cooperative role between K-ras and β-catenin, we generated a cohort of male mice heterozygous for both activated K-*ras*$^{V12}$ and the dominant stable form of *β-catenin*, using *PBCre* to drive expression in prostate epithelium (n = 6). Mice were aged until they became symptomatic of disease and sacrificed accordingly (figure 6.5). Chi-squared tests determined *PBCre*$^{+}$*Catnb*$^{+/lox(ex3)}$:K-*ras*$^{+/V12}$ longevity was significantly reduced (average survival time 211 days) compared to *wild-type*, K-*ras*$^{+/V12}$ and *Catnb*$^{+/lox(ex3)}$ single transgenic mice ($\chi^2 = 48.66$, $p = 0.000$, $\chi^2 = 48.66$, $p = 0.000$ and $\chi^2 = 31.89$, $p = 0.000$ respectively). *Wild-type* and *PBCre*$^{+}$K-*ras*$^{+/V12}$ cohorts showed normal survival (at 500 days) while *PBCre*$^{+}$*Catnb*$^{+/lox(ex3)}$ mutants showed a significant reduction in

survival (average 417 days, $\chi^2 = 34.56$, p = 0.000). These data suggest that activation of K-ras and β-catenin cooperate to accelerate tumourigenesis in the prostate.

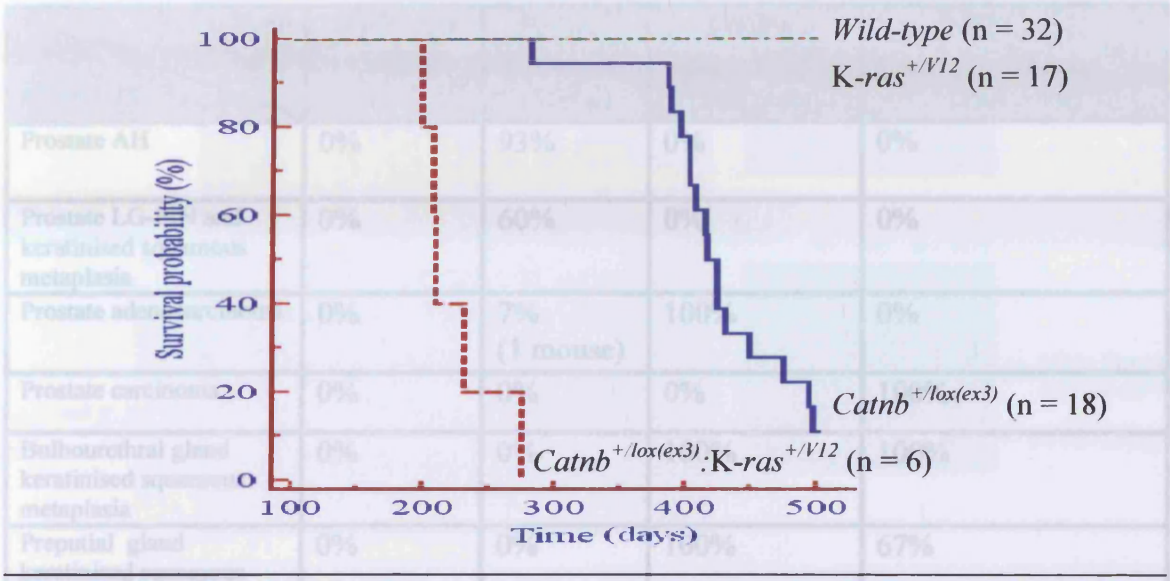


**Figure 6.5: Activation of β-catenin and K-ras reduces longevity.** Kaplan-Meier survival curve shows synergism between *β-catenin* and K-*ras* activating mutations results in decreased longevity. Compared to *wild-type* (green), K-*ras*$^{+V12}$ (orange) and *Catnb*$^{+lox(ex3)}$ (blue) cohorts, *PBCre*$^{+}$*Catnb*$^{+/lox(ex3)}$:K-*ras*$^{+/V12}$ mice (brown) showed a significant reduction in longevity ($\chi 2$ = 48.66, p = 0.000, $\chi 2$ = 48.66, p = 0.000 and $\chi^2$ = 31.89, p = 0.000 respectively). Statistical analysis was carried out by a Chi-squared test using 'MiniTab' software and the Kaplan-Meier plot was generated using 'MedCalc' software.

### 6.3.4 *PBCre*$^{+}$*Catnb*$^{+/lox(ex3)}$:K-*ras*$^{+/V12}$ mice are predisposed to multiple phenotypes

Histological analysis of *PBCre*$^{+}$K-*ras*$^{+/V12}$ and *PBCre*$^{+}$*Catnb*$^{+/lox(ex3)}$ single transgenic lines and *PBCre*$^{+}$*Catnb*$^{+/lox(ex3)}$:K-*ras*$^{+/V12}$ double transgenic cohorts aged to 500 days determined a predisposition to multiple phenotypes (Table 6.2). *Wild-type* mice did not develop any phenotypes during the time course of the experiment. At terminal end points K-*ras*$^{+/V12}$ mutants were predisposed to AH, LG-PIN and (in one case) adenocarcinoma, while dominant stabilisation of β-catenin led to diffuse adenocarcinoma in all four lobes of the prostate. Double mutants showed accelerated prostate cancer progression to invasive carcinoma with 100% incidence.

The *PBCre*$^{+}$*Catnb*$^{+/\Delta ex3}$ cohort also developed BUG, preputial gland and urethral keratinised squamous metaplasias (100%, 100% and 28% incidence respectively), which were also identified in the *PBCre*$^{+}$*Catnb*$^{+/lox(ex3)}$:K-*ras*$^{+/V12}$ cohort (100%, 67% and 17% incidence respectively). In addition, 83% of the *PBCre*$^{+}$*Catnb*$^{+/lox(ex3)}$:K-*ras*$^{+/V12}$ cohort were infertile.

**Table 6.2 Phenotype incidence in *PBCre$^{+}$Catnb$^{+/lox(ex3)}$*:K-*ras$^{+/V12}$* mice compared to single transgenic lines (at end point)**

| Genotype / Phenotype | *Wild-type* (500 d) | *PBCre$^{+}$* K-*ras$^{+/V12}$* (500 d) | *PBCre$^{+}$ Catnb$^{+/\Delta ex3}$* (End point) | *PBCre$^{+}$ Catnb$^{+/\Delta ex3}$*:K-*ras$^{+/V12}$* (End point) |
|---|---|---|---|---|
| Prostate AH | 0% | 93% | 0% | 0% |
| Prostate LG-PIN and keratinised squamous metaplasia | 0% | 60% | 0% | 0% |
| Prostate adenocarcinoma | 0% | 7% (1 mouse) | 100% | 0% |
| Prostate carcinoma | 0% | 0% | 0% | 100% |
| Bulbourethral gland keratinised squamous metaplasia | 0% | 0% | 100% | 100% |
| Preputial gland keratinised squamous metaplasia | 0% | 0% | 100% | 67% |
| Urethra keratinised squamous metaplasia | 0% | 0% | 28% (5 mice) | 17% |
| Infertile | 0% | 0% | 0% | 83% |

### 6.3.5 Activated K-ras and β-catenin synergise to accelerate prostate tumour progression

Histological analysis of the prostate from each cohort was carried out at terminal end points or 500 days. *PBCre$^{+}$Catnb$^{+/lox(ex3)}$*:K-*ras$^{+/V12}$* mice demonstrated accelerated tumour progression compared to single transgenic lines, predisposing to invasive carcinoma that developed from solid or sheet-like proliferations with frequent rosette structures, nuclear atypia, apoptotic bodies and mitosis (figure 6.6a-f). *PBCre$^{+}$Catnb$^{+/lox(ex3)}$*:K-*ras$^{+/V12}$* carcinomas also demonstrated elevated angiogenesis which facilitates tumour progression. PCR analysis of DNA isolated from *PBCre$^{+}$Catnb$^{+/lox(ex3)}$*:K-*ras$^{+/V12}$* carcinomas revealed that these tumours expressed one wild-type and one recombined allele of the dominant stabilised *β-catenin* (figure 6.6g) and K-*ras$^{V12}$* (figure 6.6h) transgenes.

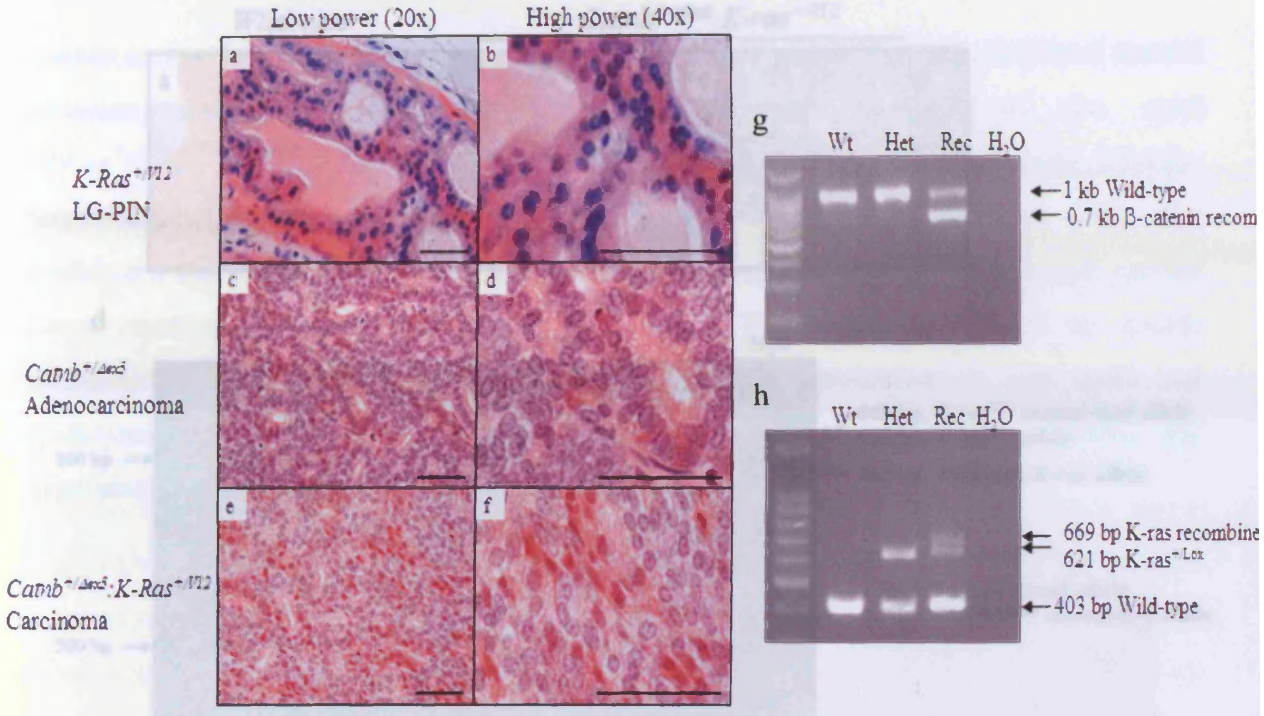


**Figure 6.6: *PBCre*$^{+}$*Catnb*$^{+/lox(ex3)}$:K-*ras*$^{+/V12}$ mice develop invasive prostate carcinoma.** Histological analysis of 10% formalin-fixed, paraffin-embedded GU sections from end point mice determined that compared to *PBCre*$^{+}$K-*ras*$^{+/V12}$ LG-PIN (a-b) and *PBCre*$^{+}$*Catnb*$^{+/\Delta ex3}$ adenocarcinoma (c-d), *PBCre*$^{+}$*Catnb*$^{+/\Delta ex3}$:K-*ras*$^{+/V12}$ mice are predisposed to invasive carcinoma (e-f). All images were taken at 40x magnification and scale bars represent 50 μm. PCR analysis of *wild-type* (Wt) and *PBCre*$^{+}$*Catnb*$^{+/lox(ex3)}$:K-*ras*$^{+/V12}$ (Het) tail biopsies and prostate lesions (Rec) determined that invasive carcinoma lesions express both the recombined *β-catenin* allele (g) and the recombined K-*ras* allele (h).

Invasive carcinoma frequently predisposes to metastasis (Shappell *et al.*, 2004). Histological analysis of the liver in *PBCre*$^{+}$*Catnb*$^{+/lox(ex3)}$:K-*ras*$^{+/V12}$ mice revealed that 83% of the cohort developed an infiltration of immune cells in the liver, concomitant with mitotic figures (figure 6.7a-b). To address the possibility that these deposits were in fact metastatic, immunohistochemistry to detect AR was carried out. Normal liver tissue does not express AR while a subset of the potential metastatic liver deposits stained positively for the AR in the cytoplasm, suggesting that these cells might be derived from the prostate tumours (figure 6.7c). However, PCR analysis of *PBCre*$^{+}$*Catnb*$^{+/lox(ex3)}$:K-*ras*$^{+/V12}$ liver DNA did not detect recombination of the K-*ras*$^{V12}$ or *Catnb*$^{+/lox(ex3)}$ alleles (figure 6.7d), indicating that the observed liver abnormality is more likely to be a consequence of an immune infiltration, reflecting the deterioration of health in these mice following the development of prostate carcinoma. Tail DNA from *wild-type* and *PBCre*$^{+}$*Catnb*$^{+/lox(ex3)}$:K-*ras*$^{+/V12}$ mice served as a negative control for recombination and *PBCre*$^{+}$*Catnb*$^{+/\Delta ex3}$:K-*ras*$^{+/V12}$ carcinoma served as a positive control.

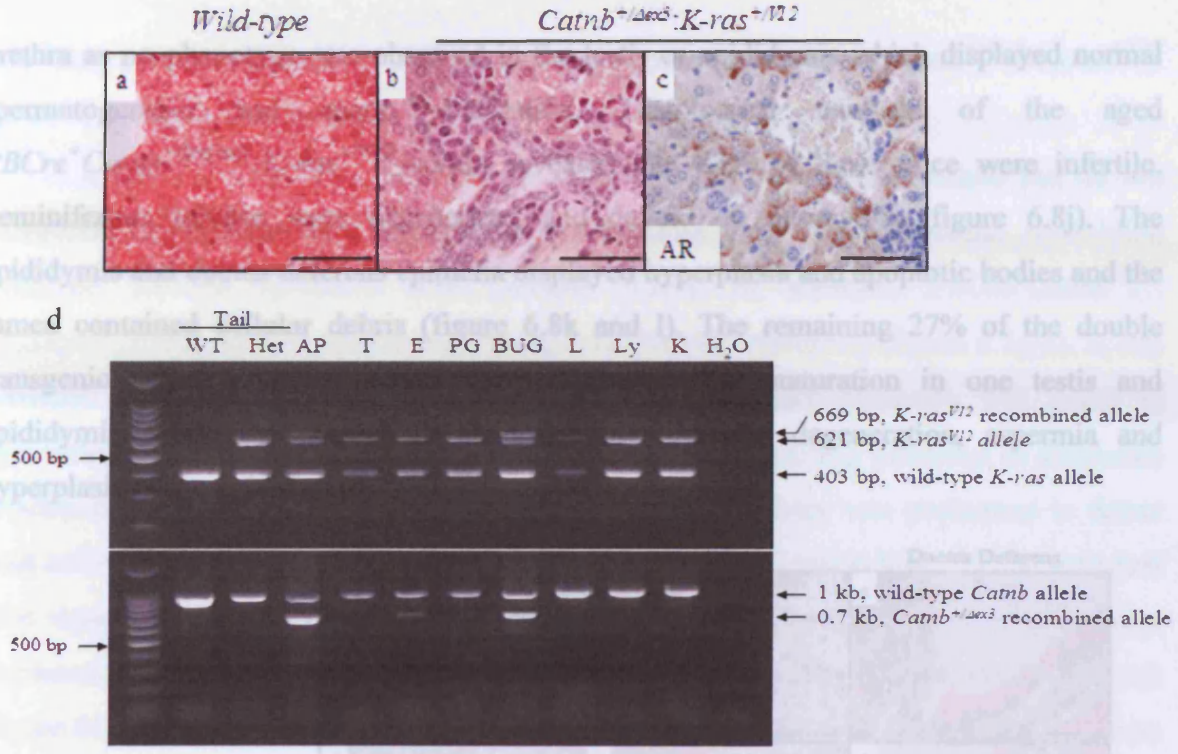


**Figure 6.7: Analysis of *PBCre*$^{+}$*Catnb*$^{+/lox(ex3)}$:K-*ras*$^{+/V12}$ mice to detect any metastasis.** Formalin-fixed, paraffin-embedded H&E stained sections from end point mice were analysed. *Wild-type* (a) and *Catnb*$^{+/lox(ex3)}$:K-*ras*$^{+/V12}$ (b) liver determined the presence of mitotic cells and inflammation in double mutants, which were not observed in single transgenic lines. Immunohistochemistry to detect AR revealed that some of the aberrant cells in the liver of compound mutants expressed AR (c). All images were taken at 40x magnification and scale bars represent 50 μm. To address the possibility of metastasis, K-*ras* and *β-catenin* recombined specific PCR analysis was carried out (d). The top gel indicates that anterior prostate carcinoma (AP), the epididymis (E) and the BUG all express a recombined K-*ras*$^{V12}$ allele while the testis (T), preputial gland (PG), liver (L), lymph node (Ly) and kidney (K) were heterozygous for the K-*ras*$^{V12}$ transgene, but not recombined. A similar pattern of recombination was determined for the *β-catenin* dominant stable allele (bottom gel) indicating the liver is not recombined.

Interestingly, DNA isolated from the epididymis and bulbourethral glands was recombined, correlating to the *PBCre*-mediated pattern of recombination determined by LacZ staining (figure 3.31). In addition, no recombination of the K-*ras*$^{V12}$ or *Catnb*$^{+/lox(ex3)}$ alleles was detected in the testis, preputial gland, lymph node or kidney (figure 6.7d).

### 6.3.6 *PBCre*$^{+}$*Catnb*$^{+/lox(ex3)}$:K-*ras*$^{+/V12}$ transgenic mice are infertile

*Wild-type* and K-*ras*$^{+/V12}$ cohorts were fertile and showed normal seminiferous tubule, epididymal and ductus deferens histology (figure 6.8a-f). Although *PBCre*$^{+}$*Catnb*$^{+/lox(ex3)}$ mice show normal spermatogenesis, sperm maturation and no abnormalities of the seminiferous tubule, epididymis and ductus deferens epithelia (figure 6.8g-i). It was noted that aging *PBCre*$^{+}$*Catnb*$^{+/lox(ex3)}$ males became sterile, concomitant with disease progression. Sterility is hypothesised to reflect prostate growth constricting the

urethra as no phenotype was observed in the testis or epididymis which displayed normal spermatogenesis and sperm maturation. Histological analysis of the aged *PBCre*$^{+}$*Catnb*$^{+/lox(ex3)}$:K-*ras*$^{+/V12}$ cohort revealed that 83% of these mice were infertile. Seminiferous tubules were degenerated and devoid of spermatids (figure 6.8j). The epididymis and ductus deferens epithelia displayed hyperplasia and apoptotic bodies and the lumen contained cellular debris (figure 6.8k and l). The remaining 27% of the double transgenic cohort showed normal spermatogenesis and maturation in one testis and epididymis, while the second set demonstrated testicular degeneration, aspermia and hyperplasia of the epididymis.

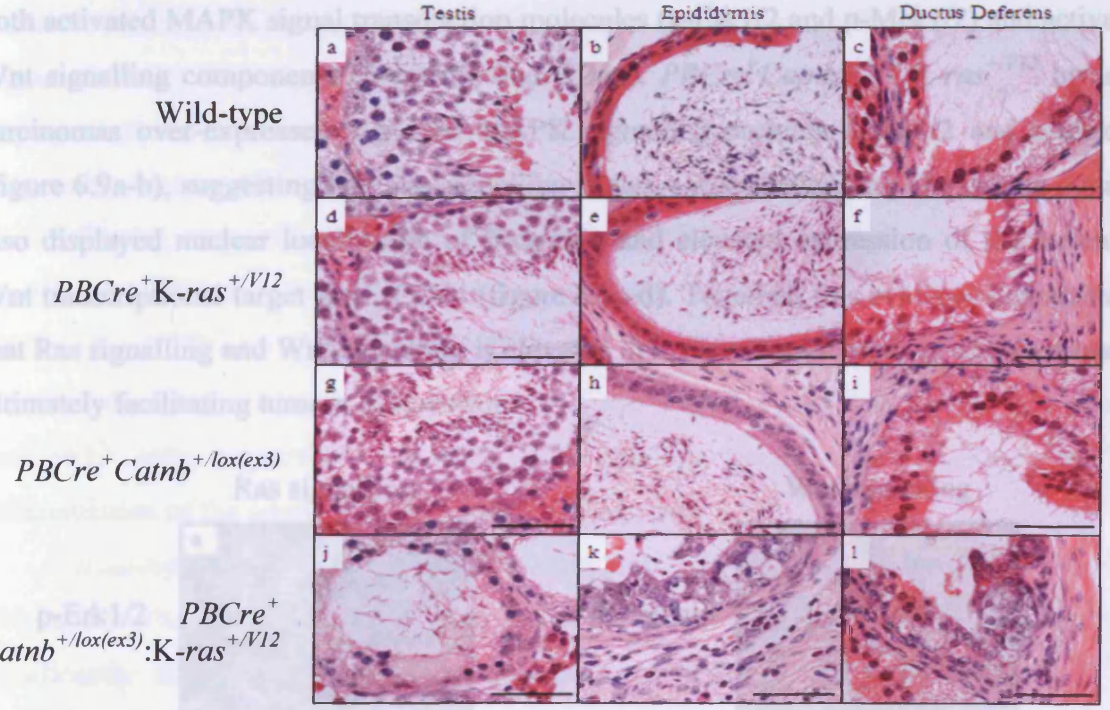


**Figure 6.8: *PBCre*$^{+}$*Catnb*$^{+/lox(ex3)}$:K-*ras*$^{+/V12}$ male mice are infertile.** Formalin-fixed, paraffin-embedded H&E stained sections from end point mice were analysed. *Wild-type* (a-c), K-*ras*$^{+/V12}$ (d-f) and *Catnb*$^{+/lox(ex3)}$ (g-i) cohorts display normal seminiferous tubule, epididymal and ductus deferens epithelium respectively and sperm was present in all organs. *PBCre*$^{+}$*Catnb*$^{+/lox(ex3)}$:K-*ras*$^{+/V12}$ males were infertile. Seminiferous tubules were degenerated (j) and the epididymal (k) and ductus deferens (l) epithelium showed hyperplastic foci and apoptosis and the lumen contained cellular debris. All images were taken at 40x magnification and scale bars represent 50 μm.

This evidence suggests a synergistic relationship between activating K-*ras*$^{V12}$ and dominant stable *β-catenin* mutations in the testis and epididymis, given that single transgenics were fertile. Although recombination was not detected in testis using PCR (figure 6.7), the pattern of recombination driven by the *PBCre* construct indicates that the Leydig cells are recombined (figure 3.9a).

### 6.3.7 Ras and Wnt signalling pathways are upregulated in *PBCre*$^{+}$*Catnb*$^{+/\Delta ex3}$:K-*ras*$^{+/V12}$ invasive prostate carcinoma

K-*ras*$^{+/V12}$ mice have been shown to upregulate the MAPK cascade but do not deregulate the Wnt pathway, as β-catenin was localised to the cell membrane, resembling *wild-type* prostate epithelial cells (section 6.2.3). In addition, *PBCre*$^{+}$Catnb$^{+/\Delta ex3}$ adenocarcinomas did not demonstrate upregulated MAPK signalling (figure 6.3g-h). It was predicted that oncogenic transformation of both K-*ras* and *β-catenin* will result in hyperactivation of both Ras-mediated and Wnt-mediated signalling pathways to accelerate prostate tumourigenesis. To address this, immunohistochemistry was performed to detect both activated MAPK signal transduction molecules (p-Erk1/2 and p-Mek1/2) and activated Wnt signalling components (β-catenin and CD44). *PBCre*$^{+}$*Catnb*$^{+/\Delta ex3}$:K-*ras*$^{+/V12}$ invasive carcinomas over-expressed activated MAPK signalling proteins p-Erk1/2 and p-Mek1/2 (figure 6.9a-b), suggesting that Ras signalling is active in these lesions. The double mutants also displayed nuclear localisation of β-catenin and elevated expression of the canonical Wnt transcriptional target gene, CD44 (figure 6.9c-d). Together, this evidence demonstrates that Ras signalling and Wnt signalling is elevated in invasive carcinomas of double mutants, ultimately facilitating tumour progression.

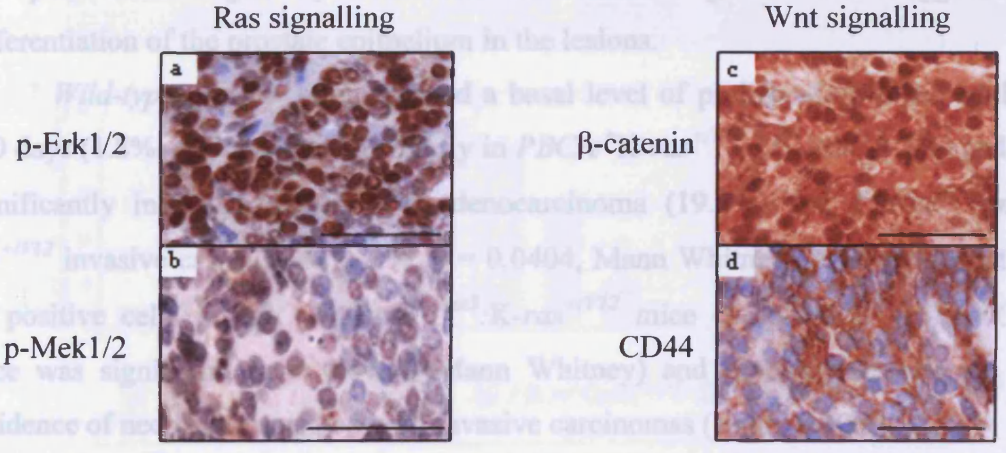


**Figure 6.9: *PBCre*$^{+}$*Catnb*$^{+/\Delta ex3}$:K-*ras*$^{+/V12}$ carcinomas demonstrate elevated MAPK and Wnt signalling cascades.** Histological analysis of 10% formalin-fixed, paraffin-embedded prostate sections at end point determined that *PBCre*$^{+}$*Catnb*$^{+/\Delta ex3}$:K-*ras*$^{+/V12}$ prostate carcinoma displays upregulated MAPK cascade molecules p-Erk1/2 (Thr202/Tyr204) (a) and p-Mek1/2 (Ser221) (b). Activation of the Wnt pathway was also detected in carcinomas as β-catenin was highly expressed in the nucleus (c) and the downstream Wnt target CD44 was over-expressed (d). All images were taken at 40x magnification and scale bars represent 50 μm.

### 6.3.8 Activated β-catenin and K-ras synergise to accelerate prostate cancer progression

To characterise the synergistic relationship between dominant stabilisation of *β-catenin* and K-*ras*$^{V12}$ oncogenic transformations, immunohistochemistry was performed on lesions from *PBCre*$^{+}$K-*ras*$^{+/V12}$, *PBCre*$^{+}$*Catnb*$^{+/\Delta ex3}$ and *PBCre*$^{+}$*Catnb*$^{+/\Delta ex3}$:K-*ras*$^{+/V12}$ mice to monitor the expression of the proliferation marker Ki-67, the basal cell marker p63 and AR. Ki-67, was rarely expressed in control prostate epithelium, however it was significantly elevated in epithelial cells throughout prostate tumours in PB*Cre*$^{+}$K-*ras*$^{+/V12}$ (LG-PIN), *PBCre*$^{+}$*Catnb*$^{+/\Delta ex3}$ (adenocarcinoma) and double heterozygous (invasive carcinoma) mice (figure 6.10a-d). Basal cells were detected using an antibody against p63, revealing a marked reduction in the presence of this lineage, concomitant with disease progression (figure 6.10e-h). Notably, all prostate lesions contained small clusters of p63$^{+}$ cells that displayed altered cytological morphology. Detection of AR showed that as the tumour stage progresses, nuclear AR accumulates in the neoplastic cells (figure 6.10i-l).

Scoring the percentage of cells expressing Ki-67, p63 and the AR determined a significant difference between *wild-type* prostate epithelium and PB*Cre*$^{+}$K-*ras*$^{+/V12}$, *PBCre*$^{+}$*Catnb*$^{+/\Delta ex3}$ and *PBCre*$^{+}$*Catnb*$^{+/\Delta ex3}$:K-*ras*$^{+/V12}$ mice (at end point), (figure 6.10m-o). Notably, the number of cells expressing Ki-67 and AR increased with disease progression and p63$^{+}$ cells negatively correlated with tumour grade. This suggests impaired differentiation of the prostate epithelium in the lesions.

*Wild-type* prostate demonstrated a basal level of proliferation of the adult gland at 500 days (1.8%) which elevated slightly in *PBCre*$^{+}$K-*ras*$^{+/V12}$ LG-PIN (3.7%) and increased significantly in *PBCre*$^{+}$*Catnb*$^{+/\Delta ex3}$ adenocarcinoma (19.5%) and *PBCre*$^{+}$*Catnb*$^{+/\Delta ex3}$:K-*ras*$^{+/V12}$ invasive carcinoma (18.3%, $p = 0.0404$, Mann Whitney). A slight reduction in Ki-67 positive cells in *PBCre*$^{+}$*Catnb*$^{+/\Delta ex3}$:K-*ras*$^{+/V12}$ mice compared to *PBCre*$^{+}$*Catnb*$^{+/\Delta ex3}$ mice was significant ($p = 0.0404$, Mann Whitney) and probably reflects the increased incidence of necrosis associated with invasive carcinomas (figure 6.10m).

The basal cell population was detected using the p63 marker and the number of positive prostate epithelial cells counted. In *wild-type* mice, 10.8% of the prostate epithelial cells were p63$^{+}$ (figure 6.10n), corresponding to previous work (Signoretti *et al.*, 2000). Analysis of K-*ras* and *β-catenin* mutant mice revealed that p63 expression decreases with advancing prostate tumour progression. LG-PIN lesions in *PBCre*$^{+}$K-*ras*$^{+/V12}$ mice at 500 days were reduced to 7.1% and *PBCre*$^{+}$*Catnb*$^{+/\Delta ex3}$ adenocarcinomas demonstrated a further reduction (2.9%). Interestingly, invasive carcinoma tumours in double transgenics rarely

expressed p63 positive cells (0.1%), mimicking human prostate cancer (Parsons *et al.*, 2001) and bladder tumours (Urist *et al.*, 2002). The observed loss of p63 expression may reflect the withdrawal of the basal cells or transit-amplifying cells from the stem cell compartment (Moll *et al.*, 2001), as discussed in section 5.4.2.

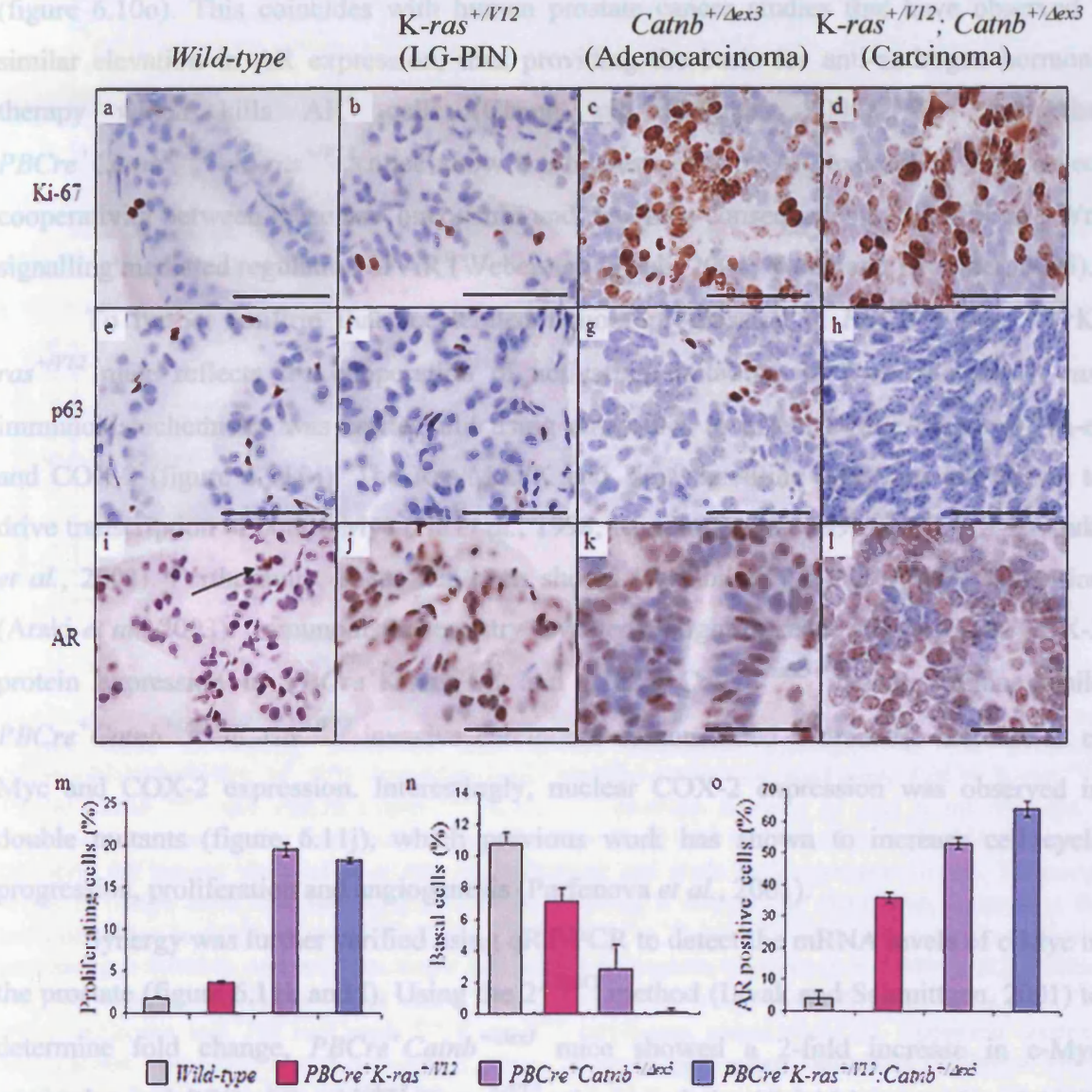


**Figure 6.10: Characterisation of activated β-catenin and K-ras synergy in the prostate.** Histological analysis of 10% formalin-fixed, paraffin-embedded (anterior) prostate sections determined an increase in the proliferation marker Ki-67 (a-d), a decrease in p63 (e-h) and elevated AR expression (i-l) in *PBCre*$^{+}$K-*ras*$^{+/V12}$, *PBCre*$^{+}$*Catnb*$^{+/\Delta ex3}$ and *PBCre*$^{+}$*Catnb*$^{+/\Delta ex3}$:K-*ras*$^{+/V12}$ prostate tumours (at end time points), which correlated with disease progression. All images were taken at 40x magnification and scale bars represent 50 μm. The percentage of Ki-67 (m), p63 (n) and AR (n) positive neoplastic cells at end point was counted (20 acini were scored per mouse, n = 3 for each genotype). K-ras and β-catenin single and double mutant prostates showed a significant difference in Ki-67, p63 and AR expression compared to wild-type mice ($p = 0.0404$) and to each other ($p = 0.0404$). Error bars represent standard deviation and statistical analysis was carried out using a non-parametric Mann Whitney test using "MiniTab" software (95% confidence interval).

Counting AR positive cells revealed that AR is not highly expressed in *wild-type* anterior prostate at 500 days (5.3%). Transgenic mice displayed a significant elevation in the level of AR expression with tumour aggression; K-*ras* mutant LG-PIN (35.8%), *β-catenin* mutant adenocarcinoma (52.6%) and double mutant invasive carcinoma (63.9%), (figure 6.10o). This coincides with human prostate cancer studies that have observed a similar elevation in AR expression, thus providing the basis for anti-androgen hormone therapy which kills $AR^+$ cells (Chang and Heinlein, 2004). The fact that *PBCre*$^+$*Catnb*$^{+/\Delta ex3}$:K-*ras*$^{+/V12}$ mice show the highest level of AR expression may reflect cooperativity between these two oncogenes and may be a consequence of MAPK and Wnt signalling mediated regulation of AR (Weber and Gioeli, 2004; Yardy and Brewster, 2005).

To further confirm that accelerated tumour progression in *PBCre*$^+$*Catnb*$^{+/\Delta ex3}$:K-*ras*$^{+/V12}$ mice reflects the cooperation of activating mutations in *β-catenin* and K-*ras*, immunohistochemistry was carried out using antibodies to detect c-Myc (figure 6.11a-e) and COX-2 (figure 6.11f-j). The Ras/MAPK and Wnt signalling pathways are known to drive transcription of both c-Myc (He *et al.*, 1998; Kerkhoff *et al.*, 1998) and COX-2 (Araki *et al.*, 2003). Furthermore, K-ras has been shown to stabilise COX-2 mRNA expression (Araki *et al.*, 2003). Immunohistochemistry revealed a slight increase in c-Myc and COX-2 protein expression in PB*Cre*$^+$K-*ras*$^{+/V12}$ and *PBCre*$^+$*Catnb*$^{+/\Delta ex3}$ prostate lesions while *PBCre*$^+$*Catnb*$^{+/\Delta ex3}$:K-*ras*$^{+/V12}$ invasive carcinoma demonstrated a dramatic increase in c-Myc and COX-2 expression. Interestingly, nuclear COX-2 expression was observed in double mutants (figure 6.11j), which previous work has shown to increase cell cycle progression, proliferation and angiogenesis (Parfenova *et al.*, 2001).

Synergy was further verified using qRT-PCR to detect the mRNA levels of c-Myc in the prostate (figure 6.11k and l). Using the $2^{\wedge-\Delta\Delta Ct}$ method (Livak and Schmittgen, 2001) to determine fold change, *PBCre*$^+$*Catnb*$^{+/\Delta ex3}$ mice showed a 2-fold increase in c-Myc expression and *PBCre*$^+$*Catnb*$^{+/\Delta ex3}$:K-*ras*$^{+/V12}$ mice revealed a 17-fold increase ($p = 0.0404$, Mann Whitney). This evidence suggests synergy between activation of the Ras and Wnt pathways in the prostate, ultimately accelerating tumour progression beyond that observed in the single transgenic lines.

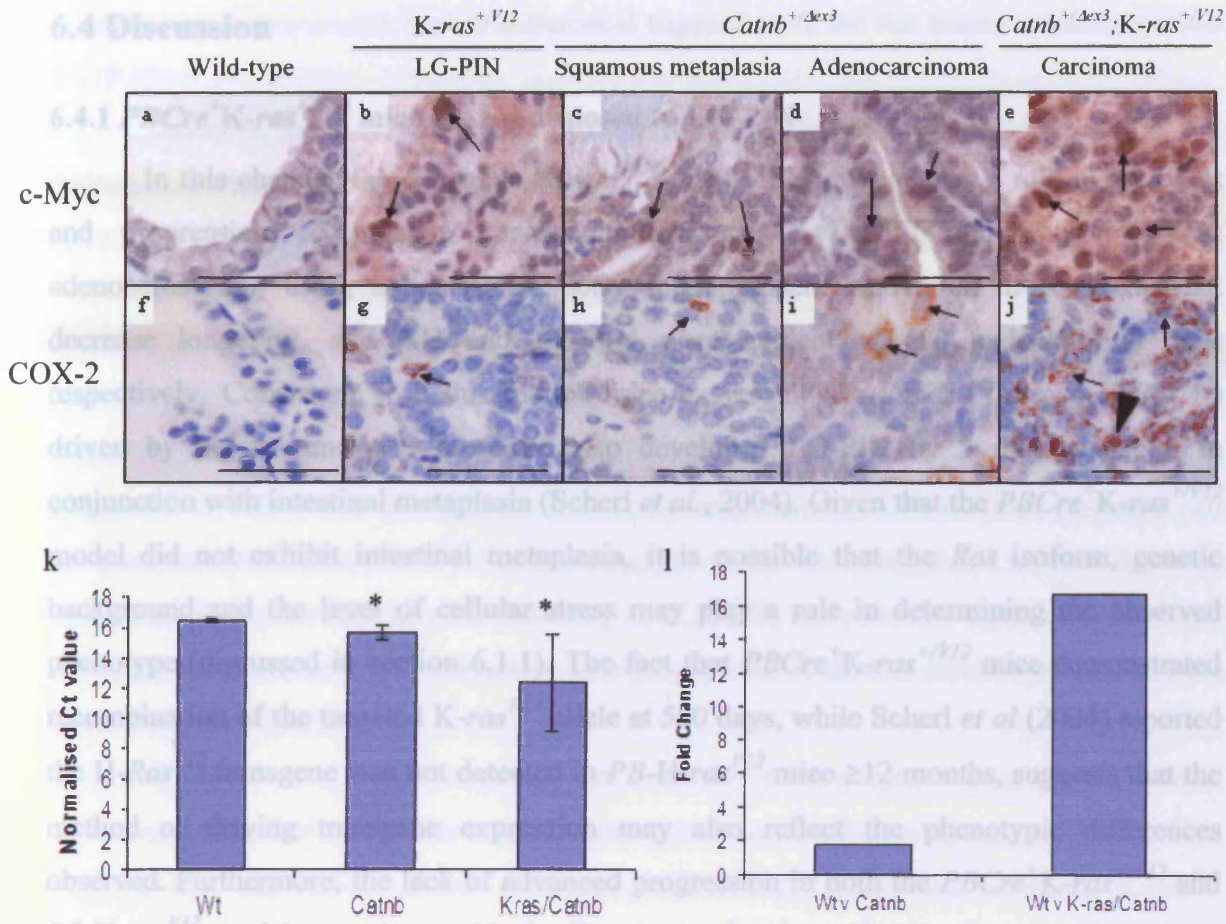


**Figure 6.11: Activating *β-catenin* and K-*ras* mutations synergise in the prostate.** Immunohistochemistry of 10% formalin-fixed, paraffin-embedded *wild-type*, *PBCre*$^{+}$K-*ras*$^{+/V12}$, *PBCre*$^{+}$*Catnb*$^{+/\Delta ex3}$ and *PBCre*$^{+}$*Catnb*$^{+/\Delta ex3}$;K-*ras*$^{+/V12}$ prostate sections at end point revealed a significant increase in the expression level of c-Myc (a-e) and COX-2 (f-j) in double transgenic tumours. All images were taken at 40x magnification and scale bars represent 50 μm. Transcript levels of c-Myc were detected using qRT-PCR revealing a statistically significant increase in the level of c-Myc in *PBCre*$^{+}$*Catnb*$^{+/\Delta ex3}$;K-*ras*$^{+/V12}$ and *PBCre*$^{+}$*Catnb*$^{+/\Delta ex3}$ mice compared to *wild-type* prostate ($p = 0.0404$), and between single and double transgenic tumours ($p = 0.0404$), (k). Plotting the fold change revealed a 2-fold and 17-fold increase in c-Myc mRNA in *PBCre*$^{+}$*Catnb*$^{+/\Delta ex3}$ adenocarcinoma and *PBCre*$^{+}$*Catnb*$^{+/\Delta ex3}$;K-*ras*$^{+/V12}$ carcinoma respectively (l). Statistical analysis was carried out using a non-parametric Mann Whitney test using "MiniTab" software (95% confidence interval) on the original $^{\Delta}$Ct values. qRT-PCR analysis was carried out by Dr. Toby Phesse (Cardiff University).

## 6.4 Discussion

### 6.4.1 *PBCre*$^{+}$K-*ras*$^{+/V12}$ mice are predisposed to LG-PIN

In this chapter, the oncogene K-*ras*$^{+/V12}$ has been shown to play a role in the onset and progression of prostate cancer predisposing to LG-PIN (and in one case adenocarcinoma) using a conditional activation approach. Activation of K-ras did not decrease longevity, and AH and LG-PIN were evident at 100 and 200-500 days respectively. Consistent with this model, mice expressing Ha-*RasT24* (termed H-*Ras*$^{V12}$) driven by the minimal *PB* promoter also developed LG-PIN by 3 months, albeit in conjunction with intestinal metaplasia (Scherl *et al.*, 2004). Given that the *PBCre*$^{+}$K-*ras*$^{+/V12}$ model did not exhibit intestinal metaplasia, it is possible that the *Ras* isoform, genetic background and the level of cellular stress may play a role in determining the observed phenotype (discussed in section 6.1.1). The fact that *PBCre*$^{+}$K-*ras*$^{+/V12}$ mice demonstrated recombination of the targeted K-*ras*$^{V12}$ allele at 500 days, while Scherl *et al* (2004) reported the H-*Ras*$^{V12}$ transgene was not detected in *PB*-H-*ras*$^{V12}$ mice ≥12 months, suggests that the method of driving transgene expression may also reflect the phenotypic differences observed. Furthermore, the lack of advanced progression in both the *PBCre*$^{+}$K-*ras*$^{+/V12}$ and *PB*-H-*ras*$^{V12}$ models correlates with the literature, whereby activating *Ras* mutations alone rarely progress to a metastatic/invasive tumourigenic state, which typically requires combinatorial genetic/epigenetic events (Janssen *et al.*, 2006). Together, these data implicate that K-*ras*$^{V12}$ mutation and concomitant upregulation of Ras effector pathways can promote tumour formation and early stage neoplasia *in vivo*.

The *PBCre*$^{+}$K-*ras*$^{+/V12}$ model also mimics aspects of human prostate cancer. Firstly, immunohistochemistry to detect p-Erk1/2 and p-Mek1/2 expression determined K-ras activation stimulates the Raf/Mek/Erk MAPK pathway in *PBCre*$^{+}$K-*ras*$^{+/V12}$ prostate lesions (figure 6.3). The majority of human studies have reported that p-ERK upregulation correlates with tumour grade (Bakin *et al.*, 2003; Gioeli *et al.*, 1999; Price *et al.*, 1999), although one study has demonstrated that ERK is down-regulated in advanced tumours (Malik SN, 2002). Consistent with this, the TRAMP transgenic prostate cancer model (described in section 1.2.3) has also demonstrated elevated MAPK signalling during tumour initiation and progression, while poorly differentiated, advanced adenocarcinomas and androgen-independent tumours showed reduced Erk1/2 and Mek1/2 expression (Uzgare *et al.*, 2003). It is possible that discrepancy in the literature regarding MAPK activation in

prostate cancer may correspond to differential expression of the Raf kinase inhibitor protein RKIP (Fu *et al.*, 2003).

Secondly, an increase in AR expression in *PBCre*$^{+}$K-*ras*$^{+/V12}$ AH and LG-PIN lesions also mimics human prostate cancer progression and may reflect previous reports that have shown Ras activation can play a causal role in driving prostate cancer cells towards decreased hormone dependence (Weber and Gioeli, 2004).

Thirdly, a reduction in p63 expression was observed, correlating to human prostate adenocarcinomas that usually express markers for secretory cells (Bruxvoort *et al.*, 2007; Signoretti *et al.*, 2000). Consistent with this, the reduction in p63 expression has been speculated to reflect the fact that the neoplastic cells have withdrawn from the stem cell compartment (Moll *et al.*, 2001). Furthermore, p63 is also down-regulated in head and neck squamous carcinoma cells *in vitro* (Matheny *et al.*, 2003) and previous work has shown that a progressive decrease in p63 correlates with progression in bladder carcinomas (Park *et al.*, 2000; Urist *et al.*, 2002).

Signoretti *et al* (2000) reported that secretory cells originate from the p63$^{+}$ basal cells, suggesting that p63$^{+}$ cells may also represent the transit-amplifying population. This suggests that expression of the dominant stabilised *β-catenin* and activated K-*ras*$^{V12}$ transgenes may result in the activation of prostate stem cells. Previous work has shown that activation of H-ras in the mouse results in mucinous metaplasia (Scherl *et al.*, 2004), resembling impaired basal cell differentiation (Kurita *et al.*, 2004). It is possible that activation of the MAPK cascade may regulate p63 expression through Src (Kurita *et al.*, 2004). Src is typically active in a proportion of the basal cells in the proliferation-quiescent state of the adult prostate, indicating its presence in normal adult prostate. Kurita *et al* (2004) grafted UGS from *p63* null mice into adult nude male mice revealing that prostate development can occur in the absence of basal cells. In this model, luminal cells show upregulated Ras signalling following expression of c-Src in the luminal cells in an androgen-dependent manner (Kurita *et al.*, 2004). Additionally, ΔNp63 has been shown to block β-catenin phosphorylation and nuclear accumulation in squamous cell carcinoma cell lines, suggesting that down-regulation of the ΔNp63 isoform may play a role in further enhancing Wnt signalling (Reis-Filho *et al.*, 2003).

Interestingly, p63 expression is suppressed by Notch1 activation in human and mouse keratinocytes (Nguyen et al., 2006). This suggests that aberrant Notch signalling may also play a role in prostate tumourigenesis in *PBCre*$^{+}$K-*ras*$^{+/V12}$, *PBCre*$^{+}$*Catnb*$^{+/\Delta ex3}$ and

*PBCre*$^{+}$*Catnb*$^{+/\Delta ex3}$;K-*ras*$^{+/V12}$ mice. To address whether Notch regulation of p63 is deregulated within these models, immunohistochemistry to detect Notch and Notch signalling components, such as γ-secretase, could be carried out to determine whether prostate lesions display reduced Notch signalling, providing a direct mechanism for the loss of p63 expression and stem cell activation (Nguyen *et al.*, 2006).

### 6.4.2 Dominant stabilised *β-catenin and* K-*ras*$^{V12}$ mutations synergise to accelerate prostate cancer progression

The life-span of *PBCre*$^{+}$*Catnb*$^{+/\Delta ex3}$:K-*ras*$^{+/V12}$ transgenic mice was significantly reduced compared to *wild-type* and single transgenic lines (figure 6.5). Histological analysis revealed the development of invasive carcinoma as the primary cause of reduced longevity, demonstrating that activating mutations of *β-catenin* and K-*ras* are synergistic in promoting prostate tumourigenesis and progression. Consistent with this, tumours displayed elevated proliferation concomitant with a decrease in p63 expression and elevated Wnt/β-catenin and MAPK signalling, ultimately facilitating tumour progression by stimulating AR, c-Myc and COX-2 expression beyond that observed in single transgenic neoplastic prostate epithelium. The findings of this investigation have been summarised in (figure 6.12).

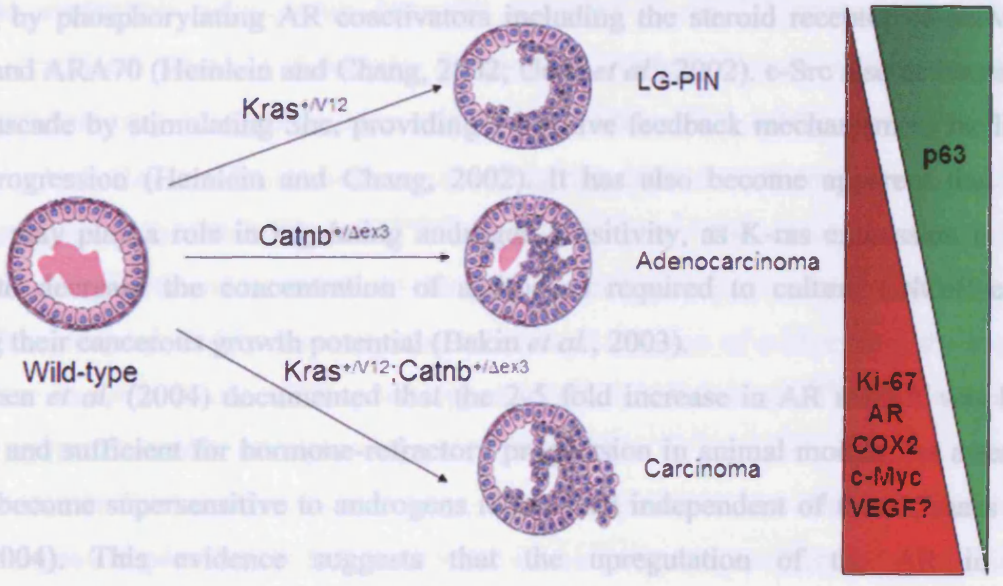


**Figure 6.12: Schematic diagram illustrating synergy between activated Ras and Wnt/β-catenin signalling in the prostate.** *PBCre*$^{+}$K-*ras*$^{+/V12}$ mice were predisposed to LG-PIN at 500 days while end-point *PBCre*$^{+}$*Catnb*$^{+/lox(ex3)}$ mice displayed adenocarcinoma. Synergy between Ras and Wnt signalling was demonstrated in *PBCre*$^{+}$*Catnb*$^{+/lox(ex3)}$;K-*ras*$^{+/V12}$ mice that showed accelerated tumour progression to invasive carcinoma concomitant with a reduction in p63 expression and upregulation of the proliferation marker Ki-67, AR, COX-2, c-Myc and angiogenesis (suggesting upregulated VEGF transcription).

*Wild-type* mice displayed the highest level of p63 expression, while LG-PIN in *PBCre*$^{+}$K-*ras*$^{+/V12}$ mice, *PBCre*$^{+}$*Catnb*$^{+/\Delta ex3}$ adenocarcinomas and invasive carcinomas in *PBCre*$^{+}$*Catnb*$^{+/lox(ex3)}$;K-*ras*$^{+/V12}$ mice demonstrated a marked reduction in p63 expression that correlated with tumour progression. This evidence suggests that both the Wnt and MAPK cascades may regulate p63 expression, and that the p63 positive cells observed in the *PBCre*$^{+}$*Catnb*$^{+/\Delta ex3}$:K-*ras*$^{+/V12}$ lesions are likely to be androgen-independent, as both these pathways regulate androgen signalling (Carey *et al.*, 2007; Weber and Gioeli, 2004; Yardy and Brewster, 2005). The ramifications of these cells are unclear but it is speculated that this evidence may reflect both the activation of prostate stem cells and the development of androgen-independent prostate growth.

Recent publications have demonstrated that AR regulation by Ras and Wnt signalling is a complex process (Weber and Gioeli, 2004; Yardy and Brewster, 2005). Upregulation of AR in *PBCre*$^{+}$*Catnb*$^{+/\Delta ex3}$:K-*ras*$^{+/V12}$ carcinomas provides a direct mechanism whereby synergism occurs following activation of both K-ras and β-catenin. The role Wnt/β-catenin signalling plays in elevating AR expression is detailed in section 5.1.1. The MAPK pathway has been shown to regulate an AR element-inducible reporter in human prostate cancer cell lines (Carey *et al.*, 2007) and p-ERK can mediate androgen signalling by phosphorylating AR coactivators including the steroid receptor co-activator (SRC-1) and ARA70 (Heinlein and Chang, 2002; Ueda *et al.*, 2002). c-Src also activates the MAPK cascade by stimulating Shc, providing a positive feedback mechanism to facilitate tumour progression (Heinlein and Chang, 2002). It has also become apparent that Ras signalling may play a role in regulating androgen sensitivity, as K-ras expression is also reported to decrease the concentration of androgens required to culture LNCaP cells, increasing their cancerous growth potential (Bakin *et al.*, 2003).

Chen *et al.* (2004) documented that the 2-5 fold increase in AR mRNA was both necessary and sufficient for hormone-refractory progression in animal models. As a result, cells can become supersensitive to androgens rather than independent of them (Isaacs and Isaacs, 2004). This evidence suggests that the upregulation of the AR in the *PBCre*$^{+}$*Catnb*$^{+/\Delta ex3}$ and *PBCre*$^{+}$*Catnb*$^{+/\Delta ex3}$;K-*ras*$^{+/V12}$ adenocarcinomas and invasive carcinomas respectively may be sufficient to promote androgen-independent prostate growth, correlating to human disease progression. Consistent with this, castration revealed that *PBCre*$^{+}$*Apc*$^{fl/fl}$ prostate tumours demonstrated androgen independence (Bruxvoort *et al.*, 2007). It would be interesting to investigate this possibility further by carrying out anti-

androgen therapy or castration experiments to determine whether tumour regression occurs in *PBCre*$^{+}$*Catnb*$^{+/lox(ex3)}$;K-*ras*$^{+/V12}$ mice. Additionally, analysis of co-regulators and co-repressors of the AR that are mediated by the MAPK and Wnt signalling pathways might further our understanding of the molecular events underlying the cooperativity of these pathways in accelerating tumour progression, which is hypothesised to be androgen-independent. To address this, hormone ablation therapy, castration or qRT-PCR analysis to detect androgen independence, such as Anxa7, is required.

Importantly, the Wnt pathway did not appear to be upregulated in *PBCre*$^{+}$K-*ras*$^{+/V12}$ lesions, as β-catenin expression was not nuclear and the Wnt target CD44 was undetected. This suggests that the augmented tumour multiplicity and malignant behaviour in compound transgenic mutants is not related to a K-ras-induced increase in Wnt/β-catenin signalling, as shown previously in intestinal studies (Janssen *et al.*, 2006). Expression of activated K-ras (pVillin-K-*ras*$^{V12G}$) was reported to upregulate β-catenin nuclear translocation in intestinal tumours, which was further increased in combination with an *Apc* deficiency (*Apc*$^{+/1638N}$) (Janssen *et al.*, 2006). The fact that activation of K-ras did not induce Wnt signalling in the *PBCre*$^{+}$K-*ras*$^{+/V12}$ prostate cancer model suggests that this may be a tissue specific event, or could reflect differences in genetic background and stress levels.

The synergistic relationship between activated K-*ras*$^{+/V12}$ expression and the dominant stabilised form of β-catenin in prostate epithelium was demonstrated by immunohistochemistry to detect c-Myc and COX-2. Given that c-Myc and COX-2 are regulated by both Ras and Wnt/β-catenin signalling, this provides rationale for accelerated tumour progression in *PBCre*$^{+}$*Catnb*$^{+/lox(ex3)}$;K-*ras*$^{+/V12}$ mice. The oncogene c-Myc is a regulator of cell growth and mutations in this gene are common in a wide variety of human cancers (Bernard *et al.*, 2003). Recently, the conditional deletion of c-Myc from the murine intestine was shown to rescue all the phenotypes of induced *AhCre*$^{+}$*Apc*$^{fl/fl}$ mice (Sansom *et al.*, 2007). These results strongly suggest that c-Myc is required for Wnt-induced tumourigenesis in the intestine. Furthermore, c-Myc expression has also been shown to confer androgen-independence in human prostate cancer cells *in vitro* (Bernard *et al.*, 2003). The Raf/Mek/Erk cascade has also been shown to stimulate transcription of c-Myc transcription *in vitro*, however c-Myc activation was dependent on TCF sites in its promoter region, demonstrating that activation was via the canonical Wnt pathway (Kerkhoff *et al.*, 1998).

These data are consistent with previous work *in vitro* studies and activated c-Myc and v-H-ras expression in rats has been shown to drive prostate cancer progression (Lehr *et al.*, 1998; Lu *et al.*, 1992). Compound mouse prostate reconstitution (MPR) models harbouring activating vHa-*Ras* and *Myc* mutations have also showed progression to carcinoma, illustrating the cooperativity of these oncogenes in prostate carcinogenesis (Thompson *et al.*, 1989). Together, these models demonstrate synergy between activation of Ras and c-Myc to drive prostate tumourigenesis and demonstrate the multi-step nature of tumourigenesis.

COX-2 is a regulatory factor in aracidonate metabolism that is undetectable in normal tissues and participates in proliferation, differentiation and tumourigenesis (Narayanan *et al.*, 2006). Previous studies have shown that COX-2 can be regulated by Wnt and Ras signalling (Araki *et al.*, 2003). COX-2 contains a TCF-4 binding element and its expression elevates following β-catenin nuclear localisation (Araki *et al.*, 2003). In addition, activated K-ras has been shown to increase COX-2 expression and stabilise COX-2 mRNA (Araki *et al.*, 2003). The *PBCre*$^{+}$*Catnb*$^{+/\Delta ex3}$:K-*ras*$^{+/V12}$ mice demonstrate cooperativity between these pathways and their convergence at the level of COX-2 *in vivo*. To address the role that COX-2 upregulation plays during prostate tumourigenesis, it would be interesting to determine how tumour formation and progression is effected upon treating *PBCre*$^{+}$*Catnb*$^{+/\Delta ex3}$:K-*ras*$^{+/V12}$ mice with a COX-2 inhibitor, such as Aspirin or Colecoxib (non-steroidal anti-inflammatory drugs). Narayanan *et al* (2006) reported that Celecoxib inhibits adenocarcinoma of the TRAMP model in a dose-dependent manner, and thus limits the growth of metastatic prostate cancer and men that take Aspirin regularly, over a long period of time, have been reported to reduce the risk of developing prostate cancer (Jacobs *et al.*, 2005).

*PBCre*$^{+}$*Catnb*$^{+/lox(ex3)}$:K-*ras*$^{+/V12}$ carcinomas demonstrated elevated angiogenesis. Consistent with this, *in vitro* studies in colon cancer cells have shown that both Wnt and Ras signalling pathways can regulate VEGF expression, a key regulator of angiogenesis, via a TCF-4 binding element in the VEGF promoter (Araki *et al.*, 2003). Angiogenesis is modulated through cross-talk between the tumour and stroma and COX-2 has been linked to this process, providing an additional route for enhanced angiogenesis that drives tumour progression (Banerjee *et al.*, 2003). Taken together, this evidence implies that activation of Ras and Wnt signalling may cooperate in *PBCre*$^{+}$*Catnb*$^{+/lox(ex3)}$:K-*ras*$^{+/V12}$ mice to further promote prostate cancer progression by stimulating angiogenesis via VEGF.

### 6.4.3 *PBCre*$^{+}$*Catnb*$^{+/lox(ex3)}$:K-*ras*$^{+/V12}$ mice are predisposed to multiple GU tract phenotypes

In addition to invasive carcinoma of the prostate, *PBCre*$^{+}$*Catnb*$^{+/lox(ex3)}$:K-*ras*$^{+/V12}$ mice developed squamous metaplasia of the preputial gland, bulbourethral gland and urethra, reminiscent of *PBCre*$^{+}$*Catnb*$^{+/lox(ex3)}$ mice. The fact that dominant stabilisation of β-catenin also predisposed to these lesions (discussed in chapter 5), indicates that oncogenic transformation of K-*ras* does not accelerate tumour growth in these lesions. This is consistent with the lack of these tumours in the *PBCre*$^{+}$K-*ras*$^{+/V12}$ transgenic line.

The *PBCre*$^{+}$*Catnb*$^{+/lox(ex3)}$:K-*ras*$^{+/V12}$ cohort was predisposed to testis degeneration (83% incidence), resulting in infertility. Mice harbouring single activating mutations were not prone to infertility, suggesting combinatorial effects of activated K-ras and β-catenin. This phenotype may be a consequence of several potential scenarios. Firstly, LacZ expression showed that *PBCre*-mediated recombination occurs in the Leydig cells of the testis, which function to produce testosterone in response to luteinising hormone (LH) and follicle stimulating hormone (FSH) (section 1.1.8). This suggests that recombination and subsequent activation of K-ras and β-catenin may occur in the Leydig cells, predisposing to the observed testis degeneration in *PBCre*$^{+}$*Catnb*$^{+/lox(ex3)}$:K-*ras*$^{+/V12}$ mice. Consistent with this, activation of Ras signalling by Src has been shown to cause loss of LH responsiveness in MA10 Leydig cells (Taylor, 2002). This suggests that elevated Ras signalling in *PBCre*$^{+}$K-*ras*$^{+/V12}$ mice may desensitise the Leydig cells to hormone regulation, leading to testis degeneration. The fact that *PBCre*$^{+}$K-*ras*$^{+/V12}$ male mice were fertile indicates that the combined activation of the Ras and Wnt pathways is required to cause male infertility in this model.

Ras and Wnt pathways have been shown to regulate AR expression, suggesting that disturbed paracrine communication between testicular cells may cause the observed testis degeneration/hypospermatogenesis, rather than an endocrine defect. This is consistent with *PBCre*-mediated recombination taking place in the interstitial cells of the testis (figure 3.29d). However, it is also possible that the *PBCre* construct drives recombination at an alternative site such as the hypothalamus or anterior pituitary, resulting in reduced levels of FSH, LH or testosterone. The fact that mature spermatids were observed in occasional hypospermatogenic seminiferous tubules in *PBCre*$^{+}$*Catnb*$^{+/lox(ex3)}$:K-*ras*$^{+/V12}$ mice suggests impairment of early germ cell proliferation or survival and not a specific block during sperm maturation (Behr *et al.*, 2007), as postulated for *Cre*$^{-}$*Lkb1*$^{fl/fl}$ mice (section 3.4.4).

It is clear that further analysis of this phenotype is required to establish the cause of male infertility in *PBCre*$^{+}$*Catnb*$^{+/lox(ex3)}$:K-*ras*$^{+/V12}$ mice. Detecting FSH, LH and testosterone serum levels and determining whether *PBCre* recombination occurs in the hypothalamus, anterior pituitary or adrenal cortex may provide insights into the mechanism leading to male sterility. In addition, laser capture microdissection of the Leydig cells would confirm whether they have undergone recombination in *PBCre*$^{+}$*Catnb*$^{+/lox(ex3)}$:K-*ras*$^{+/V12}$ mice.

## 6.5 Summary

Using a Cre-LoxP approach, the expression of activated K-ras demonstrated that elevated Ras signalling is sufficient to predispose to AH and LG-PIN in the mouse prostate. Expression of activated K-ras in combination with the dominant stabilised form of β-catenin was shown to accelerate tumourigenesis and cause invasive prostate carcinoma, demonstrating synergy between activation of the Ras and Wnt/β-catenin signalling pathways, which cooperate to stimulate AR, c-Myc and COX-2 to facilitate tumour formation. *PBCre*$^{+}$*Catnb*$^{+/\Delta ex3}$:K-*ras*$^{+/V12}$ carcinomas also mimicked aspects of human prostate cancer, demonstrating a reduction in p63 and an increase in AR expressing cells, suggestive of androgen-independent growth. To conclude, the *PBCre*$^{+}$*Catnb*$^{+/lox(ex3)}$:K-*ras*$^{+/V12}$ model further establishes the link between aberrant Ras and Wnt signalling in the multistep nature of prostate tumourigenesis and progression correlating to colorectal cancer (Janssen *et al.*, 2006; Li *et al.*, 2005), intestinal (Sansom *et al.*, 2006), kidney (Sansom *et al.*, 2006), mammary (Jang *et al.*, 2006) and liver (Harada *et al.*, 2004) cancers.

# Chapter 7: Summary

The development of novel models of prostate cancer is crucial to increasing our understanding of the molecular events underlying prostate tumourigenesis and progression, as well as providing novel therapeutic targets. To this end, this thesis has investigated the role of Lkb1, β-catenin and K-ras in prostate cancer with the aim of identifying potential therapeutic targets.

### 7.1 Loss of Lkb1 predisposes to prostate neoplasia

Germ-line mutation of *LKB1* is the key molecular event underlying Peutz-Jegher's syndrome (PJS), a dominantly inherited condition characterised by a predisposition to a range of malignancies, including those of the reproductive system (Boardman *et al.*, 1998). Recently, somatic deletion of *LKB1* has been linked to lung (Ji *et al.*, 2007), pancreatic and biliary tumourigenesis (Su *et al.*, 1999) and malignant melanomas (Guldberg *et al.*, 1999), further implicating LKB1 as a tumour suppressor. This evidence raises the possibility that LKB1 may function as a tumour suppressor in several organs.

This thesis has investigated the role of Lkb1 in the murine prostate using a conditional transgenic approach. Deletion of *Lkb1* in prostate epithelium predisposed to prostate intra-epithelial neoplasia *in vivo*, indicating that the tumour suppressive functions of Lkb1 extend to the murine prostate and raises the possibility of a similar association in man.

Lkb1 regulates numerous signalling pathways to exert its tumour suppressive function (Alessi *et al.*, 2006). It is clear from this thesis that Lkb1 loss deregulates both the Wnt pathway and PI3K/AKT signalling to promote tumourigenesis in the murine prostate. This is consistent with loss of Lkb1-mediated phosphorylation of Par1A, resulting in Wnt signalling and loss of cell polarity (Spicer *et al.*, 2003) and loss of Lkb1:Pten interactions, speculated to cause Pten inactivation, which ultimately leads to Akt activation, promoting cell growth and proliferation (Mehenni *et al.*, 2005; Song *et al.*, 2007). This evidence suggests that the Wnt and PI3K/Akt pathways are potential therapeutic targets in prostate tumours that display reduced Lkb1 expression or inactivating *Lkb1* mutations. However, before therapies against inhibition of Wnt/PI3K signalling in the prostate are considered, it is essential to establish the role of endogenous Wnt and PI3K signalling in both the murine and human prostate.

In the mouse, we have detected a low level of nuclear β-catenin expression in normal prostate epithelium, together with a high level of membrane immunoreactivity. This data is consistent with a human study, where nuclear and membrane β-catenin expression was detected in 0-5% and 100% of the prostate epithelial cells respectively (Horvath *et al.*, 2005). The fact that Wnt signalling is known to regulate stem cell self-renewal in many tissues (Reya and Clevers, 2005), suggests that nuclear β-catenin expression may be specific to the prostate stem/progenitor cells. A definitive answer to this question could be determined by over-expressing the Wnt inhibitor Dickkopf-1 (DKK1) in the murine prostate using the *PBCre* transgenic line to determine whether normal tissue homeostasis altered. This experiment has been performed previously in adult murine intestine and colon, where adenoviral expression of DKK1 inhibited proliferation and resulted in the failure of crypts, villi and glandular structures to develop within 7 days (Kuhnert *et al.*, 2004). Decreased DKK1 expression (>10 days) resulted in regeneration of the crypts and villi, highlighting the important role of Wnt signaling in intestinal homeostasis (Kuhnert *et al.*, 2004).

Given that Lkb1 is considered to suppress the Wnt pathway to prevent tumourigenesis (Spicer *et al.*, 2003), a synergistic relationship between Lkb1 loss and the activation of Wnt signalling oncogenic targets is predicted to promote tumourigenesis. Owing to partial embryonic lethality of mice expressing biallelic LoxP-flanked *Lkb1* alleles, it was not possible to generate a cohort of $PBCre^{+}Lkb1^{fl/fl}Catnb^{+/lox(ex3)}$ mice to address whether synergy occurred. Preliminary data from this thesis suggests that Lkb1 loss and activated Wnt signalling accelerates tumour progression, following histological analysis of two $PBCre^{+}Lkb1^{fl/fl}Catnb^{+/lox(ex3)}$ mice aged 100 days. The development of an aged cohort of $PBCre^{+}Lkb1^{fl/fl}Catnb^{+/lox(ex3)}$ mice is necessary to confirm the synergy between loss of Lkb1 and induction of the Wnt pathway.

Lkb1 has also been shown to negatively regulate AMPK/mTOR signalling under low energy conditions, to decrease cell growth and proliferation (Alessi *et al.*, 2006). Lkb1 loss in prostate epithelium is subsequently predicted to decrease p-AMPK expression and elevate mTOR signalling. However, data from this thesis suggested that mTOR signalling was not upregulated in Lkb1 deficient prostate epithelium. Indeed, the expression of active p-mTOR was markedly reduced, concomitant with increased p-AMPK expression (figure 4.1), suggesting that a feedback mechanism compensates for Lkb1 loss and prevents mTOR signalling by phosphorylating AMPK. Further investigation revealed that p-PDK1, postulated to be an AMPK kinase (Zou *et al.*, 2003), may fulfil this task as p-PDK1 expression was upregulated in Lkb1 deficient PIN lesions. Taken together, this evidence

indicates that treatment of prostate cancer with the mTOR inhibitor Rapamycin, may not be beneficial in Lkb1 deficient prostate lesions. To validate the observed down-regulation of mTOR signalling, staining for additional AMPK and mTOR downstream targets, such as p-ACC (phospo-Acetyl CoA Carboxylase), an AMPK target (Conde *et al.*, 2007), PKC (an mTORC2 target), and targets of mTORC1, such as CLIP-170, LIPIN, and STAT3 (Guertin and Sabatini, 2007) could be carried out. Unfortunately, attempts to obtain protein samples by laser capture were not successful, preventing western blot analysis of PIN lesions.

To date, the mechanisms employed by Rapamycin to inhibit tumour growth are not fully understood, which is in part owing to our lack of knowledge regarding the role of the mTORC1 (mTOR:Raptor) and mTORC2 (mTOR:Rictor) complexes and the intricate series of feedback mechanisms that regulate their activity (Guertin and Sabatini, 2007). Rapamycin typically inhibits the mTORC1 complex and has been shown to inhibit the Akt activating mTORC2 complex in a handful of cell types, including endothelial cells (Guertin and Sabatini, 2007). Since mTORC2 activates Akt, many studies have shown that PI3K inhibitors in combination with Rapamycin derivatives (e.g. RAD001) prevent cell growth, more so than Rapamycin alone (Sun *et al.*, 2005; Van-Der-Poel *et al.*, 2003).

An elevation in p-AMPK and subsequent reduction in p-mTOR$^{Ser2448}$ expression in *AhCre*$^{+}$*Lkb1*$^{fl/fl}$ PIN lesions does not correspond to previous work. Shaw *et al* (2004) reported elevated mTOR signalling in gastrointestinal hamartomas from heterozygous *Lkb1* knockout mice, suggesting that Lkb1 negatively regulates mTOR signalling in the intestine. Moreover, Rapamycin, which is proposed to inhibit mTOR, has been shown to inhibit the growth of PC-3 and LNCaP prostate cancer cells lines, which is further inhibited in combination with the PI3K inhibitor LY294002 (Van-Der-Poel *et al.*, 2003). Combined use of Rapamycin and PI3K inhibitors is thought to further inhibit cell growth by targeting both the mTORC1 complex and mTORC2-mediated activation of Akt respectively (Van-Der-Poel *et al.*, 2003), since Rapamycin does not target the mTORC2 complex in all tissues (Guertin and Sabatini, 2007). In addition, the MPAKT mouse prostate model in, which ventral prostate expresses human *AKT1,* has shown regression of neoplastic lesions upon Rapamycin treatment (Majumder *et al.*, 2003).

Together, these data suggest that mTOR signalling is elevated in prostate cancer, indicating Rapamycin treatment is beneficial in reducing prostate cancer growth. However, one caveat of these studies is that the method employed to detect elevated mTOR signalling was an increase in p-S6K and its substrate p-Rsp6, instead of directly observing activated p-mTOR$^{Ser2448}$ levels. S6K is also regulated by mTOR-independent pathways, such as

PI3K/PDK1 signalling (Pullen *et al.*, 1998) and the MAPK pathway (Martin and Blenis, 2002), indicating that these studies have not specifically demonstrated elevated mTOR signalling.

Convincing evidence for elevated mTOR signalling in human prostate cancer has been demonstrated recently by a morphoproteomic approach that assessed p-mTOR$^{Ser2448}$ expression in HG-PIN and prostate cancer biopsies (Brown *et al.*, 2008). Near to 100% of samples analysed displayed activated mTOR in prostate lesions compared to normal tissue (Brown *et al.*, 2008). This presents several scenarios; (a) the lack of p-mTOR$^{Ser2448}$ staining in *AhCre*$^{+}$*Lkb1*$^{fl/fl}$ mice is a false negative, (b) p-mTOR$^{Ser2448}$ staining in the human prostate samples analysed by Brown *et al* (2008) is a false positive, (c) Lkb1 is not lost in the human lesions analysed by Brown *et al* (2008) or (d) Lkb1-mediated regulation of AMPK/mTOR signalling in human and mouse prostate is distinct. To address this, p-mTOR$^{Ser2448}$ immunohistochemistry would need to be carried out on *LKB1* deficient human prostate cancer, in combination with downstream targets specific to mTOR signalling. The lack of LKB1 deficient human prostate tissue clearly presents a problem, although it has not yet been determined whether LKB1 loss is a common event in human prostate cancer. The development of human prostate glands in culture from ES cells (Risbridger *et al.*, 2007), may provide a useful tool for generating LKB1 deficient human prostate tissue in the future.

### 7.2 Does Lkb1 loss drive prostate cancer progression?

Progression to advanced prostate lesions was not observed in Lkb1 deficient mice, suggesting that Lkb1 loss may only be sufficient to initiate early stages of the disease. However, progression may have been hindered by *Cre*-mediated recombination taking place in non-prostate tissue compartments or in a subset of prostate epithelial cells that either prevent tumourigenesis or are not tumour initiating. However, the development of bulbourethral gland cysts in the *AhCre*$^{+}$*Lkb1*$^{fl/fl}$ model resulted in death at around 2-4 months, and therefore progression from PIN to later stages of disease could not be studied.

Interestingly, disrupted ZO-1 expression revealed Lkb1 deficient PIN lesions had lost cellular polarity (figure 4.3m), an event not typically associated with initiation of the disease (Wodarz and Näthke, 2007). In addition, loss of E-cadherin was observed at the surface membrane (figure 4.3d), which is commonly associated with a more invasive phenotype (Wodarz and Näthke, 2007). Taken together, this evidence suggests that Lkb1 loss is capable of initiating prostate cancer and shows elements of early disease progression, from atypical hyperplasia to HG-PIN. Subsequently, it is speculated that derivation of a

model that drives Lkb1 loss specifically in the prostate may permit disease progression. PSP94 (prostate specific secretory protein of 94 amino acids) has been shown to be specifically expressed in the murine prostate (Thorta *et al.*, 2003). It is hypothesised that the by employing the *PSP94* promoter to drive Cre recombinase expression, it may be possible to deleting *Lkb1* specifically within the murine prostate, allowing us to determine whether Lkb1 loss can facilitate tumour progression to the later stages of the disease, avoiding complicated phenotypes owing to Lkb1 loss in non-prostate tissues.

To confirm whether the *PBCre* and *AhCre* $Lkb1^{fl/fl}$ models demonstrate androgen-dependent prostate tumourigenesis, castration and androgen ablation studies could be carried out.

### 7.3 Lkb1 loss mediated by the *PBCre* transgene may alter differentiation of prostate lineages

The notion that the basal cell lineage (p63 positive) contains the prostate stem cells is widely accepted, although not definitively demonstrated. Consistent with this notion, Signoretti *et al* (2000) have shown that *p63* null mice develop defects in prostatic bud development, suggesting that the basal cells are required to restrict UGS endodermal cells to a prostate lineage and that p63 positive cells are required for luminal cell maintenance. Experiments grafting *p63* null UGS into adult nude male hosts revealed that p63 deficient grafts developed ducts where basal cells were absent, preventing maintenance of normal luminal cell differentiation (Kurita *et al.*, 2004). The $PBCre^{+}Lkb1^{fl/fl}$ prostate lesions displayed luminal cell mucinous-like metaplasia foci, resembling the phenotype observed in p63 null prostate. This suggests that loss of Lkb1 might also impair basal cell differentiation, providing rationale for occasional luminal cell metaplasia. To verify whether Lkb1 loss in prostate epithelial cells (targeted by the *PBCre* construct) results in impaired basal cell differentiation, immunohistochemistry to detect basal cell markers, such as p63, could be carried out. Furthermore, it would be interesting to determine the consequence of Lkb1 deletion specifically within the basal cell population (as oppose to the luminal cell population targeted by the *PBCre* construct) by applying the keratin-5 promoter to drive Cre-recombinase expression. The data from this thesis suggests that these mice are likely to display loss of basal cell differentiation markers, concomitant with metaplastic transformation of the luminal lineage to mucinous-like cells, similar to the p63 null prostate described by Kurita *et al.*, 2004.

Interestingly, mucinous metaplasia was also observed in *PB*-H-*ras* mice that express an activated form of H-*ras* in the prostate (Scherl *et al.*, 2004). To address whether Lkb1 loss results in mucinous metaplasia by deregulating Ras signalling, components of Ras effector pathways in Lkb1 deficient prostate lesions could be detected using immunohistochemistry. Also, $PBCre^{+}Lkb1^{fl/fl}$ mice could be inter-crossed to mice expressing activated Ras, where double mutants are expected to demonstrate synergy and promote the development of prostate mucinous metaplasia, should Lkb1 loss lead to elevated Ras signalling.

In contrast to the $PBCre^{+}Lkb1^{fl/fl}$ model that displayed hyperplasia and mucinous metaplasia, $AhCre^{+}Lkb1^{fl/fl}$ mice were predisposed to HG-PIN, concomitant with clusters of $p63^{+}$ cells that exhibited altered morphology. Clustering of $p63^{+}$ cell has been associated with expansion of the transit-amplifying cells and co-staining for p63 and transit-amplifying cell markers, such as PSCA or c-MET might provide an insight into the function of these cells (Tran *et al.*, 2002; Van-Leenders *et al.*, 2002). Furthermore, staining to detect prominin (CD133) may also determine whether the loss of Lkb1 results in activation of the proposed prostate stem cells (Tsujimura *et al.*, 2007).

### 7.4 Lkb1 plays a role in male fertility

It is clear from this thesis that Lkb1 also plays a role in fertility, as all male mice bearing biallelic Lox-P-flanked *Lkb1* alleles were sterile, consistent with previous work (Sakamoto *et al.*, 2005). Histological analysis revealed hypospermatogenesis and Sertoli-cell only syndrome in $AhCre^{+}$ and $PBCre^{+}$ $Lkb1^{fl/fl}$ mice respectively (figure 3.9 and 3.27). Previous work has shown that loss of Lkb1 disrupts cellular polarity, by switching the role of Par1A in HeLa cells *in vitro* (Spicer et al., 2003) and by disrupting expression of the tight junction protein ZO-1 in intestinal cells *in vitro* (Baas *et al.*, 2004b).

Maintenance of cellular polarity is critical during spermatogenesis. Closing and opening of Sertoli cell tight junctions that constitute the blood-testis barrier is necessary to allow preleptotene and leptotene spermatocytes in the basal compartment to translocate to the adluminal compartment of seminiferous epithelium (figure 3.32), so that fully developed spermatids (spermatozoa) may be released into the tubular lumen at spermiation (Fink *et al.*, 2006; Liu *et al.*, 2003). The regulation of this process is not yet fully understood, but has been linked to TGFβ, PKA and PKC (Liu *et al.*, 2003). This thesis reports that ZO-1 expression is disrupted in Lkb1 deficient testis, providing rationale for male infertility. To further investigate the potential role of LKB1 in male fertility, it would be interesting to

determine whether human testicular cancers frequently display reduced Lkb1 expression or *Lkb1* inactivating mutations and to establish if ZO-1 deficient seminiferous tubules display a similar phenotype to *Lkb1* deficient mice. In addition, ZO-1 is known to be phosphorylated and regulated at tyrosine residues by kinases such as c-Src (Toyofuku *et al.*, 2001). It is not thought that LKB1 directly regulates ZO-1 owing to the fact that it is a serine/threonine kinase. Of particular interest, TGFβ has been shown to regulate tight junctions, although the mechanism involved is not fully established (Liu *et al.*, 2003). Lkb1 has been shown to regulate TGFβ signalling by forming a heterotrimeric complex together with LIP1 and SMAD4 (Smith *et al.*, 2001). Taken together, this evidence suggests that Lkb1 loss may cause sterility in male mice by deregulating tight junctions through TGFβ. Consequently, immunohistochemistry to detect TGFβ deregulation in Lkb1 deficient testes may provide a further insight into the role of Lkb1 in male fertility.

In humans, male infertility is frequently associated with Karatagener's syndrome, where the dynein arms that are normally attached to the nine microtubule doublets of cilia and flagella are lacking, causing immotility and sterility (Guichard *et al.*, 2001). It is speculated that Lkb1's role as a microtubule sensor (Yoo *et al.*, 2002) may be important for sperm motility and further analysis of sperm in Lkb1 deficient mice by electron microscopy may determine whether Lkb1 loss disrupts microtubule arrangements in the flagella, causing male infertility.

### 7.5 Synchronous activation of Ras and Wnt signalling synergise to drive prostate cancer progression

Cancer development is a multi-step process through which cells accumulate genetic mutations (Hanahan and Weinberg, 2000). Investigations that further our understanding of the cooperativity of these genetic transformations provide an insight into the aetiology of the disease and present targets for chemotherapeutic intervention. Synchronous activation of K-ras and β-catenin has been demonstrated in many transgenic models illustrating their cooperation during intestinal, colorectal and liver tumourigenesis (Harada *et al.*, 2004; Janssen *et al.*, 2006; Sansom *et al.*, 2006). This evidence suggests a similar cooperativity in other tissues.

This thesis also investigated the synergistic relationship between the Wnt and Ras signalling pathways in prostate cancer, revealing that conditional activation of β-catenin and K-ras in the murine prostate also demonstrate cooperativity between activated Ras and Wnt signalling, raising the possibility of a similar association in humans. Convergence of the Ras

and Wnt pathways has been shown to upregulate the expression of genes that function to promote tumourigenesis and progression, such as COX-2, c-Myc, AR and VEGF (Araki *et al.*, 2003; He *et al.*, 1998; Kerkhoff *et al.*, 1998; Terry *et al.*, 2006; Weber and Gioeli, 2004). Immunohistochemical analysis of *PBCre*$^{+}$*K-ras*$^{+/V12}$;*Catnb*$^{+/\Delta ex3}$ prostate carcinomas determined Ras and Wnt signalling synergise to promote tumour progression by upregulating c-Myc and COX-2 via the canonical Wnt pathway, presenting a target for chemotherapeutic intervention. It is speculated that treating double mutant mice with a COX-2 inhibitor, such as Aspirin or Colecoxib, would drastically repress tumourigenesis (Narayanan *et al.*, 2006). Additionally, it is predicted that crossing the compound mutant mice to mice harbouring a conditional inactivating cMyc transgene would rescue the phenotype, as demonstrated previously in Apc deficient murine intestine (Sansom *et al.*, 2007).

Interestingly, Lkb1 is also known to play a role in regulating COX-2 expression by interacting with and phosphorylating PEA3 (Upadhyay *et al.*, 2006). Investigations into the phosphorylation status of PEA3 and COX-2 expression in *Lkb1*$^{fl/fl}$ prostate might provide an insight into whether COX-2 inhibitors would also be beneficial in preventing tumourigenesis in prostate lesions deficient in Lkb1.

Elevated Ras and Wnt signalling revealed an increase in the number of cells expressing AR. This indicates that these neoplastic cells are likely to be hypersensitive to androgen levels. It is predicted that these lesions are androgen-independent, as demonstrated in Apc deficient mice that displayed a similar phenotype (Bruxvoort *et al.*, 2007). To address whether activated K-ras and/or β-catenin results in androgen-independent tumourigenesis, androgen ablation experiments could be performed. It is predicted that androgen ablation in *PBCre*$^{+}$*Catnb*$^{+/lox(ex3)}$ and *PBCre*$^{+}$*K-ras*$^{+/V12}$;*Catnb*$^{+/lox(ex3)}$ mice will not cause tumour regression, confirming androgen-independent prostate cancer growth.

An elevation in AR expression is thought to represent aberrant differentiation of the basal and luminal cells and to address this, double staining for basal/luminal cell markers could be carried out to determine whether they are co-expressed. Cells expressing both luminal and basal cell markers are considered to be transit-amplifying cells, representing activation of the stem cells (Tran *et al.*, 2002).

### 7.5 Reduced p63 expression correlates with prostate cancer progression

A reduction in p63 expression has been observed to correlate to tumour progression in the human prostate (Parsons *et al.*, 2001), bladder (Urist *et al.*, 2002) and head and neck

cancer (Matheny *et al.*, 2003). Immunohistochemistry revealed a reduction in the basal cell marker p63 in association with tumour progression in *K-ras* and *β-catenin* mutants. Previous work has shown that p63 expression in keratinocytes is mediated by Notch signalling (Nguyen *et al.*, 2006). To establish whether this mechanism exists in prostate epithelium, immunohistochemistry to detect Notch signalling activity is required, in conjunction with p63 staining.

In addition, further investigation into the mechanism resulting in the loss of p63 expression may present a new route for chemotherapeutic intervention, as $PBCre^{+}K\text{-}ras^{+/V12};Catnb^{+/lox(ex3)}$ mice demonstrated loss of p63 in parallel with elevated AR (figure 6.10). Double staining for AR and p63 or Ki-67 might determine the role of AR expression and whether the few remaining p63 positive cells are proliferating. This staining would also provide an insight into whether the lesions are heterogeneous, resembling human prostate cancer.

### 7.5 Conclusions

Much of the challenge that remains lies in interpreting the molecular events underlying the predisposition to prostate cancer and androgen-independent prostate tumourigenesis. This thesis goes some way to addressing some of these questions by establishing the first correlation between Lkb1 loss and prostate neoplasia and by demonstrating the cooperativity between activated Ras and Wnt signalling. These models provide a valuable resource for genetic based studies that recapitulate the nature of human prostate cancer.

Mice have become the primary model organism for studying human diseases as they are easy to manipulate genetically, they are prone to several diseases and cancers and they display similar genetics and physiology to humans. However, there are still some crucial differences, preventing a direct comparison and one central limitation is the lack of common human and mouse prostate stem/progenitor cell and prostate specific markers. Consequently, it is important to be cautious when translating the outcomes of murine studies into the clinic. In the future, it is hoped that deriving human prostate in culture from embryonic stem cells may provide a powerful tool for studying the genetic and biochemical events that take place during prostate tumourigenesis. It is also hoped that gene therapy will hold the key to inhibiting prostate cancer.

# References


Abate-Shen C, Banach-Petrosky W, Sun X, Economides K, Desai N, Gregg J, Borowsky A, Cardiff R, Shen M. 2003. Nkx3.1; Pten mutant mice develop invasive prostate adenocarcinoma and lymph node metastasis. Cancer Res 63:3886-3890.

Abate-Shen C, Shen MM. 2002. Mouse models of prostate carcinogenesis. Trends Genet 18:S1-5.

Abdulkadir S, Magee J, Peters T, Kaleem Z, Naughton C, Humphrey P, Milbrandt J. 2002. Conditional loss of Nkx3.1 in adult mice induces prostatic intraepithelial neoplasia. Mol Cell Biol 22:1495-1503.

Abdulkadir SA, Garabodian ZQ, Song SA, Peters J. 2001. Impaired prostate tumourigenesis in Erg1-deficient mice. Nature 7:101-107.

Adhami VM, Siddiqui IA, Ahmad N, Gupta S, Mukhtar H. 2004. Oral consumption of green tea polyphenols inhibits insulin-like growth factor-I-induced signaling in an autochthonous mouse model of prostate cancer. Cancer Res 64:8715-8722.

Al-Khouri AM, Ma Y, Togo SH, Williams S, Mustelin T. 2005. Cooperative phosphorylation of the tumor suppressor phosphatase and tensin homologue (PTEN) by casein kinases and glycogen synthase kinase 3beta. J Biol Chem 280:35195-35202.

Alessi D, Sakamoto K, Bayascas J. 2006. LKB1-dependent signaling pathways. Annu Rev Biochem 75:137-163.

Alhopuro P, Katajisto P, Lehtonen R, Ylisaukko-Oja S, Näätsaari L, Karhu A, Westerman A, Wilson J, de-Rooij F, Vogel T, Moeslein G, Tomlinson I, Aaltonen L, Mäkelä T, Launonen V. 2005. Mutation analysis of three genes encoding novel LKB1-interacting proteins, BRG1, STRADalpha, and MO25alpha, in Peutz-Jeghers syndrome. Br J Cancer 92:1126-1129.

Amanatullah DF, Reutens AT, Zafonte BT, Fu M, Mani S, Pestell RG. 2000. Cell-cycle dysregulation and the molecular mechanisms of prostate cancer. Front Biosci 5:D372-390.

Araki Y, Okamura S, Hussain S, Nagashima M, He P, Shiseki M, Miura K, Harris C. 2003. Regulation of cyclooxygenase-2 expression by the Wnt and Ras pathways. Cancer Res 63:728-734.

Avizienyte E, Roth S, Loukola A, Hemminki A, Lothe R, Stenwig A, Fosså S, Salovaara R, Aaltonen L. 1998. Somatic mutations in LKB1 are rare in sporadic colorectal and testicular tumours. Cancer Res 58:2087-2090.

Baas AF, Kuipers J, van der Wel NN, Batlle E, Koerten HK, Peters PJ, Clevers HC. 2004a. Complete polarization of single intestinal epithelial cells upon activation of LKB1 by STRAD. Cell 116:457-466.

Baas AF, Smit L, Clevers H. 2004b. LKB1 tumor suppressor protein: PARtaker in cell polarity. Trends Cell Biol 14:312-319.

Bakin R, Gioeli D, Sikes R, Bissonette E, Weber M. 2003 Constitutive activation of the Ras/mitogen-activated protein kinase signaling pathway promotes androgen hypersensitivity in LNCaP prostate cancer cells. Cancer Res 63:1981-1989.

Banach-Petrosky W, Ouyang X, Gao H, Nader K, Ji Y, Suh N, DiPaola R, Abate-Shen C. 2006. Vitamin D inhibits the formation of prostatic intraepithelial neoplasia in Nkx3.1; Pten mutant mice. Clin Cancer Res 12:5895-5901.

Banerjee AG, Liu J, Yuan Y, Gopalakrishnan VK, Johansson SL, Dinda AK, Gupta NP, Trevino L, Vishwanatha JK. 2003. Expression of biomarkers modulating prostate cancer angiogenesis: differential expression of annexin II in prostate carcinomas from India and USA. Mol Cancer 2:34.

Barrios R, Lebovitz RM, Wiseman A.L, Weisoly DL, Matusik RJ, DeMayo F, Lieberman MW. 1996. RasT24 driven by a probasin promoter induces prostatic hyperplasia in transgenic mice. Transgenics 2:23-28.

Bayascas JR, Leslie NR, Parsons R, Fleming S, Alessi DR. 2005. Hypomorphic mutation of PDK1 suppresses tumorigenesis in PTEN(+/-) mice. Curr Biol 15:1839-1846.

Behr R, Sackett S, Bochkis I, Le P, Kaestner K. 2007. Impaired male fertility and atrophy of seminiferous tubules caused by haploinsufficiency for Foxa3. Dev Biol 306:636-645.

Belandia B, Powell S, García-Pedrero J, Walker M, Bevan C, Parker M. 2005. Hey1, a mediator of notch signaling, is an androgen receptor corepressor. Mol Cell Biol 25:1425-1436.

Benten W, Lieberherr M, Giese G, Wrehlke C, Stamm O, Sekeris C, Mossmann H, Wunderlich F. 1999. Functional testosterone receptors in plasma membranes of T cells. FASEB J 13:123-133.

Benten W, Lieberherr M, Sekeris C, Wunderlich F. 1997. Testosterone induces Ca2+ influx via non-genomic surface receptors in activated T cells. FEBS Lett 407:211-214.

Bernard D, Pourtier-Manzanedo A, Gil J, Beach D. 2003. Myc confers androgen-independent prostate cancer cell growth. J Clin Invest 112:1724-1731.

Besnard V, Wert SE, Hull WM, Whitsett JA. 2004. Immunohistochemical localization of Foxa1 and Foxa2 in mouse embryos and adult tissues. Gene Expr Patterns 5:193-208.

Bhatia-Gaur R, Donjacour AA, Sciavolino PJ, Kim M, Desai N, Young P, Norton CR, Gridley T, Cardiff RD, Cunha GR, Abate-Shen C, Shen MM. 1999. Roles for Nkx3.1 in prostate development and cancer. Genes Dev 13:966-977.

Bierie B, Nozawa M, Renou J, Shillingford JM, Morgan F, Oka T, Taketo MM, Cardiff RD, Miyoshi K, Wagner K, Robinson GW, Hennighausen. 2003. Activation of b-catenin in prostate epithelium induces hyperplasias and squamous transdifferentiation. Oncogene 22:3875-3887.

Boardman LA, Thibodeau SN, Schaid DJ, Lindor NM, McDonnell SK, Burgart LJ, Ahlquist DA, Podratz KC, Pittelkow M, Hartmann LC. 1998. Increased risk for cancer in patients with the Peutz-Jeghers syndrome. Ann Intern Med 128:896-899.

Bonkhoff H, Remberger K. 1996. Differentiation pathways and histogenetic aspects of normal and abnormal prostatic growth: a stem cell model. Prostate 28:98-106.

Bos J. 1989. Ras oncogenes in human cancer: a review. Cancer Res 49:4682-4689.

Bosman FT. 1999. The hamartoma-adenoma-carcinoma sequence. J Pathol 188:1-2.

Bostwick D, Pacelli A, Lopez-Beltran A. 1996. Molecular biology of prostatic intraepithelial neoplasia. Prostate 29:117-134.

Boudeau J, Baas AF, Deak M, Morrice NA, Kieloch A, Schutkowski M, Prescott AR, Clevers HC, Alessi DR. 2003. MO25alpha/beta interact with STRADalpha/beta enhancing their ability to bind, activate and localize LKB1 in the cytoplasm. Embo J 22:5102-5114.

Brawer MK. 2005. Prostatic Intraepithelial Neoplasia: An overview. Urology 7:S11-S18.

Brown R, Zotalis G, Zhang P, Zhao B. 2008. Morphoproteomic confirmation of a constitutively activated mTOR pathway in high grade prostate intra-epithelial neoplasia and prostate cancer. Int J Clin Exp Pathol 1:333-342.

Bruxvoort KJ, Charbonneau HM, Giambernardi TA, Goolsby JC, Qian CN, Zylstra CR, Robinson DR, Roy-Burman P, Shaw AK, Buckner-Berghuis BD, Sigler RE, Resau JH, Sullivan R, Bushman W, Williams BO. 2007. Inactivation of Apc in the mouse prostate causes prostate carcinoma. Cancer Res 67:2490-2496.

Bultman S, Herschkowitz J, Godfrey V, Gebuhr T, Yaniv M, Perou C, Magnuson T. 2007. Characterization of mammary tumors from Brg1 heterozygous mice. Oncogene 27:460-468.

Burger P, Xiong X, Coetzee S, Salm S, Moscatelli D, Goto K, Wilson E. 2005. Sca-1 expression identifies stem cells in the proximal region of prostatic ducts with

high capacity to reconstitute prostatic tissue. Proc Natl Acad Sci U S A 102:7180-7185.

Campbell SJ, Carlotti F, Hall PA, Clark AJ, Wolf CR. 1996. Regulation of the CYP1A1 promoter in transgenic mice: an exquisitely sensitive on-off system for cell specific gene regulation. J Cell Sci 109:2619-2625.

Carey A, Pramanik R, Nicholson L, Dew T, Martin F, Muir G, Morris J. 2007. Ras-MEK-ERK signaling cascade regulates androgen receptor element-inducible gene transcription and DNA synthesis in prostate cancer cells. Int J Cancer 121:520-527.

Chang C, Heinlein C. 2004. Androgen receptor in prostate cancer. Endocrine Reviews 25:276-308.

Chang W, Prins G. 1999. Estrogen receptor-beta: implications for the prostate gland Prostate 40:115-124.

Chen B, Liu J, Chang H, Chang C, Lo W, Kuo W, Yang C, Lin D. 2007. Hedgehog is involved in prostate basal cell hyperplasia formation and its progressing towards tumorigenesis. Biochem Biophys Res Commun 357:1084-1089.

Chen C, Welsbie D, Tran C, Baek S, Chen R, Vessella R, Rosenfeld M, Sawyers C. 2004. Molecular determinants of resistance to antiandrogen therapy. Nat Med 10:33-39.

Chesire D, Ewing C, Gage W, Isaacs W. 2002. In vitro evidence for complex modes of nuclear beta-catenin signaling during prostate growth and tumorigenesis. Oncogene 21:2679-2694.

Chesire DR, Dunn TA, Ewing CM, Luo J, Isaacs WB. 2004. Identification of aryl hydrocarbon receptor as a putative Wnt/beta-catenin pathway target gene in prostate cancer cells. Cancer Res. 64:2523-2533.

Chin JL, Reiter RE. 2004. Molecular markers and prostate cancer prognosis. Clin Prostate Cancer 3:157-164.

Cinar B, De-Benedetti A, Freeman M. 2005. Post-transcriptional regulation of the androgen receptor by mammalian target of rapamycin Cancer Res 65:2547-2553.

Clarke AR, editor. 2002. Transgenic Techniques: Principles and Protocols, 2 ed. New Jersey: Humana Press Inc.

Clements W, Kimelman D. 2003. Wnt signalling gets XEEKy. Nat Cell Biol 5:861-863.

Clevers H. 2006. Wnt/beta-catenin signaling in development and disease. Cell 127:469-480.

Cohen J, Levinson A. 1988. A point mutation in the last intron responsible for increased expression and transforming activity of the c-Ha-ras oncogene. Nature 334.

Collins A, Berry P, Hyde C, Stower M, Maitland N. 2005. Prospective identification of tumourigenic prostate cancer stem cells. Cancer Res 65:10946-10951.

Collins A, Habib F, Maitland N, Neal D. 2001. Identification and isolation of human prostate epithelial stem cells based on alpha(2)beta(1)-integrin expression. J Cell Sci 114:3865-3872.

Collins SP, Reoma JL, Gamm DM, Uhler MD. 2000. LKB1, a novel serine/threonine protein kinase and potential tumour suppressor, is phosphorylated by cAMP-dependent protein kinase (PKA) and prenylated in vivo. Biochem J 345 Pt 3:673-680.

Conde E, Suarez-Gauthier A, García-García E, Lopez-Rios F, Lopez-Encuentra A, García-Lujan R, Morente M, Sanchez-Verde L, Sanchez-Cespedes M. 2007. Specific pattern of LKB1 and phospho-acetyl-CoA carboxylase protein immunostaining in human normal tissues and lung carcinomas. Hum Pathol 38:1351-1360.

Corradetti MN, Inoki K, Bardeesy N, DePinho RA, Guan KL. 2004. Regulation of the TSC pathway by LKB1: evidence of a molecular link between tuberous sclerosis complex and Peutz-Jeghers syndrome. Genes Dev 18:1533-1538.

CRUK. 2004. UK prostate cancer incidence statistics. London, Cancer Research UK http://info.cancerresearchuk.org/cancerstats/types/prostate/incidence/.

Cunha G, Donjacour A, Cooke P, Mee S, Bigsby R, Higgins S, Sugimura Y. 1987. The endorcinology and developmental biology of the prostate. Endocr Rev 8:338-362.

Cunha G, Hayward S, Wang Y, Ricke W. 2003. The role of the stromal microenvironment in carcinogenesis of the prostate. Int J Cancer 107:1-10.

Cunha GR, Cooke PS, Kurita T. 2004. Role of stromal-epithelial interactions in hormonal responses. Arch Histol Cytol 67:417-434.

Curtis MW, Evans AJ, Srigley JR. 2005. Mucin-producing urothelial-type adenocarcinoma of prostate: report of two cases of a rare and diagnostically challenging entity. Mod Pathol 18:585-590.

Danielpour D. 1999. Transdifferentiation of NRP-152 rat prostatic basal epithelial cells toward a luminal phenotype: regulation by glucocorticoid, insulin-like growth factor-I and transforming growth factor-beta. J Cell Sci 112:169-179.

deKok J, Verhaegh G, Roelofs R, Hessels D, Kiemeney L, Aalders T, Swinkeis D, Schalken J. 2002. DD3(PCA3), a very sensitive and specific marker to detect prostate tumours. Cancer Res 62:2695-2698.

DeLaTaille A, Rubin M, Chen M, Vacherot F, de-Medina S, Burchardt M, Buttyan R, Chopin D. 2003. Beta-catenin-related anomalies in apoptosis-resistant and hormone-refractory prostate cancer cells. Clin Cancer Res 9:1801-1807.

DeMarzo A, Marchi V, Epstein J, Nelson W. 1999. Proliferative inflammatory atrophy of the prostate: implications for prostate carcinogenesis. Am J Pathol 155:1985-1992.

DeMarzo AM, Nelson WG, Isaacs WB, Epstein JI. 2003. Pathological and molecular aspects of prostate cancer. Lancet 361:955-964.

Deras I, Aubin S, Blase A, Day J, Koo S, Partin A, Ellis W, Marks L, Fradet Y, Rittenhouse H, Groskopf J. 2008. PCA3: A molecular urine assay for predicting prostate biopsy outcome. J Urol [epub ahead of print].

Di Cristofano A, De Acetis M, Koff A, Cordon-Cardo C, Pandolfi PP. 2001. Pten and p27KIP1 cooperate in prostate cancer tumor suppression in the mouse. Nat Genet 27:222-224.

Di Cristofano A, Pesce B, Cordon-Cardo C, Pandolfi PP. 1998. Pten is essential for embryonic development and tumour suppression. Nat Genet 19:348-355.

DiGiovanni J, Kiguchi K, Frijhoff A, Wilker W, Bol D, Beltran L, Moats S, Ramirez A, Jorcano J, Conti C. 2000. Deregulated expression of insulin-like growth factor-1 in prostate epithelial cells leads to neoplasia in transgenic mice. Proc Natl Acad Sci USA 97.

Ding V, Chen R, McCormick F. 2000. Differential regulation of glycogen synthase kinase-3beta by insulin and Wnt signalling. J Biol Chem 275:32475-32481.

Dmochowski L, Horning E. 1946. Induction of prostate tumours in mice. Brit. J. Cancer 1:59-63.

Duchesne G. 2001. Radiation for prostate cancer Lancet Oncology 2:73-81.

Dunker N, Aumuller G. 2002. Transforming growth factor-beta 2 heterozygous mutant mice exhibit Cowper's gland hyperplasia and cystic dilations of the gland ducts (Cowper's syringoceles). J Anat 201:173-183.

Eid M, Kumar M, Iczkowski K, Bostwick D, Tindall D. 1998. Expression of early growth response genes in human prostate cancer. Cancer Res 58:2461-2468.

English HF, Kyprianou N, Isaacs JT. 1989. Relationship between DNA fragmentation and apoptosis in the programmed cell death in the rat prostate following castration. Prostate 15:233-250.

Esteller M, Avizienyte E, Com P, Lothe R, Baylin S, Aaltanen L, Herman F. 2000. Epigenetic inactivation of LKB1 in primary tumours associated with the Peutz-Jeghers syndrome. Oncogene 19:164-168.

Fair WR, Cordonnier JJ. 1978. The pH of prostatic fluid: a reappraisal and therapeutic implications. J Urol 120:695-698.

Faith D, Han S, Lee D, Friedl A, Hicks J, DeMarzo A, Jarrard D. 2005. p16 is upregulated in proliferative inflammatory atrophy of the prostate. Prostate 65.

Feng L, Ravindranath N, Dym M. 2000. SCF/c-kit up-regulates cyclin D3 and promotes cell cycle progression through the PI3K/AKT/mTOR/p70S6K pathway in spermatogonia. J Biol Chem 275:25572-25576.

Fink C, Weigel R, Hembes T, Lauke-Wettwer H, Kliesch S, Bergmann M, Brehm R. 2006. Altered expression of ZO-1 and ZO-2 in Sertoli cells and loss of blood-testis barrier integrity in testicular carcinoma in situ. Neoplasia 8:1019-1027.

Forcet C, Etienne-Manneville S, Gaude H, Fournier L, Debilly S, Salmi M, Baas A, Olschwang S, Clevers H, Billaud M. 2005. Functional analysis of Peutz-Jeghers mutations reveals that the LKB1 C-terminal region exerts a crucial role in regulating both the AMPK pathway and the cell polarity. Hum Mol Genet 14:1283-1292.

Foster C, Dodson A, Karavana V, Smith P, Ke Y. 2002 Prostatic stem cells. J Pathol 197:551-565.

Friedman J, Kaestner K. 2006. The Foxa family of transcription factors in development and metabolism. Cellular and Molecular Life Sciences 63:2317-2328.

Fu Z, Smith PC, Zhang L, Rubin MA, Dunn RL, Yao Z, Keller ET. 2003. Effects of Raf Kinase Inhibitor Protein Expression on Suppression of Prostate Cancer Metastasis. J. Natl. Cancer Inst. 95:878-889.

Gakunga P, Frost G, Shuster S, Cunha G, Farmby B, Stern R. 1997. Hyluronan is a prerequisite for ductal branching morphogenesis. Development 124:3987-3997.

Gao N, Zhang J, Rao M, Case T, Mirosevich J, Wang Y, Jin R, Gupta A, Rennie P, Matusik R. 2003. The role of hepatocyte nuclear factor-3 alpha (Forkhead Box A1) and androgen receptor in transcriptional regulation of prostatic genes. Mol Endocrinol 17:1484-1507.

Garabedian EM, Humphrey PA, Gordon JI. 1998. A transgenic mouse model of metastatic prostate cancer originating from neuroendocrine cells. Proc Natl Acad Sci U S A 95:15382-15387.

Gerstein A, Almeida T, Zhao G, Chess E, Shih I, Buhler K, Pienta K, Rubin M, Vessella V, Papadopoulos N. 2002. APC/CTNNB1 (beta-catenin) pathway alterations in human prostate cancers. Genes Chromosomes Cancer 34:9-16.

Giardiello E, Welsh S, Hamilton S, Offerhaus G, Gittelsohn A, Booker S, Krush A, Yardley J, Luk G. 1987. Increased risk of cancer in the Peutz-Jeghers syndrome. N Engl J Med 316:1511-1514.

Gioeli D, Mandell J, GR GP, Frierson HJ, Weber M. 1999. Activation of mitogen-activated protein kinase associated with prostate cancer progression. Cancer Res 59:279-284.

Gipp J, Gu G, Crylen C, Kasper S, Bushman W. 2007. Hedgehog pathway activity in the LADY prostate tumor model. Mol Cancer Ther 6:19.

Glinka A, Wu W, Delius H, Monaghan A, Blumenstock C, Niehrs C. 1998. Dickkopf-1 is a member of a new family of secreted proteins and functions in head induction. Nature 391:357-362.

Gottardi CJ, Arpin M, Fanning AS, Louvard D. 1996. The junction-associated protein, zonula occludens-1, localizes to the nucleus before the maturation and during the remodeling of cell-cell contacts. Proc Natl Acad Sci U S A 93:10779-10784.

Gounari F, Signoretti S, Bronson R, Klein L, Sellers WR, Kum J, Siermann A, Taketo MM, von Boehmer H, Khazaie K. 2002. Stabilization of beta-catenin induces lesions reminiscent of prostatic intraepithelial neoplasia, but terminal squamous transdifferentiation of other secretory epithelia. Oncogene 21:4099-4107.

Green JB. 2004. Lkb1 and GSK3-beta: kinases at the center and poles of the action. Cell Cycle 3:12-14.

Greenberg NM, DeMayo F, Finegold MJ, Medina D, Tilley WD, Aspinall JO, Cunha GR, Donjacour AA, Matusik RJ, Rosen JM. 1995. Prostate cancer in a transgenic mouse. Proc Natl Acad Sci U S A 92:3439-3443.

Groszer M, Erickson R, Scripture-Adams D, Dougherty J, Lebelle J, Zack J, Geschwind D, Liu X, Kornblum H, Wu H. 2006. Pten negatively regulates neural stem cell self-renewal by modulating G0-G1 cell cycle entry. Proc Natl Acad Sci USA 103:111-116.

Gruber S, Entius M, Petersen G, Laken S, Longo P, Boyer R, Levin A, Mujumdar U, Trent J, Kinzler K, Vogelstein B, Hamilton S, Polymeropoulos M, Offerhaus G, Giardiello F. 1998. Pathogenesis of adenocarcinoma in Peutz-Jeghers syndrome. Cancer Res 58:5267-5270.

Guerra C, Mijimolle N, Dhawahir A, Dubus P, Barradas M, Serrano M, Campuzano V, Barbacid M. 2003. Tumor induction by an endogenous K-ras oncogene is highly dependent on cellular context. Cancer Cell 4:111-120.

Guertin D, Sabatini D. 2007. Defining the role of mTOR in cancer. Cancer Cell 12:9-22.

Guichard C, Horricane M, Laffitte J, Godard P, Zaegel M, Tuck V, Lalau G, Bouvagnet P. 2001. Axonemal dynein intermediate-chain gene (DNAI1) mutations result in situs inversus and primary ciliary dyskinesia (Kartaganer syndrome). Am J Hum Genet 68:1030-1035.

Guldberg P, thor-Straten P, Ahrenkiel V, Seremet T, Kirkin A, Zeuthen J. 1999. Somatic mutation of the Peutz-Jeghers syndrome gene, LKB1/STK11, in malignant melanoma. Oncogene 18:1777-1780.

Haegel H, Larue L, Ohsugi M, Fedorov L, Herrenknecht K, Kemler R. 1995. Lack of b-catenin affects mouse development at gastrulation. Development 232:3529-3537.

Hagen T, Vidal-Puig A. 2002. Characterisation of the phosphorylation of beta-catenin at the GSK-3 priming site Ser45. Biochem Biophys Res Commun 294:324-328.

Hanahan D, Weinberg R. 2000. The hallmarks of cancer. Cell 100:57-70.

Harada N, Oshima H, Katoh M, Tamai Y, Oshima M, Taketo M. 2004. Hepatocarcinogenesis in mice with beta-catenin and Ha-ras gene mutations. Cancer Res 64:48-54.

Harada N, Tamai Y, Ishikawa T, Sauer B, Takaku K, Oshima M, Taketo MM. 1999. Intestinal polyposis in mice with a dominant stable mutation of the beta-catenin gene. Embo J 18:5931-5942. .

Hardie D. 2005. New roles for the LKB1-->AMPK pathway. Curr Opin Cell Biol 17:167-173.

Hawley SA, Boudeau J, Reid JL, Mustard KJ, Udd L, Makela TP, Alessi DR, Hardie DG. 2003. Complexes between the LKB1 tumor suppressor, STRAD alpha/beta and MO25 alpha/beta are upstream kinases in the AMP-activated protein kinase cascade. J Biol 2:28.

Hayward S, Haughney P, Rosen M, Greulich K, Weier H, Dahiya R, Cunha G. 1998. Interactions between adult human prostatic epithelium and rat urogenital sinus mesenchyme in a tissue reconstitution model. Differentiation 63:131-140.

Hayward SW, Cunha GR. 2000. The prostate: development and physiology. Radiol Clin North Am 38:1-14.

He T, Sparks A, Rago C, Hermeking H, Zawel L, da-Costa L, Morin P, Vogelstein B, Kinzler K. 1998. Identification of c-MYC as a target of the APC pathway. Science 281:1509-1512.

Heinlein C, Chang C. 2002. The roles of androgen receptors and androgen-binding proteins in nongenomic androgen actions. Mol Endocrinol 16:2181-2187.

Hernan I, Roig I, Martin B, Gamundi M, Martinez-Gimeno M, Carballo M. 2004. De novo germline mutation in the serine-threonine kinase STK11/LKB1 gene associated with Peutz–Jeghers syndrome. Clin. Genet 66:58-62.

Hill R. 2005. Development and characterisation of a mouse model of human prostate cancer. In: ProQuest company, UMI. Chapel Hill: University of North Carolina. p 1-148.

Hoess RH, Abremski K. 1984. Interaction of the bacteriophage P1 recombinase Cre with the recombining site loxP. Proc Natl Acad Sci U S A 81:1026-1029.

Hokaiwado N, Asamoto M, Cho YM, Tsuda H, Shirai T. 2003. Lack of effect of human c-Ha-ras proto-oncogene overexpression on prostate carcinogenesis in probasin/SV40 T antigen transgenic rats. Cancer Sci 94:1042-1045.

Holyrood. 1997. Prostate Gland Development, Accessed Jan 2007. In: http://www.ana.ed.ac.uk/database/prosbase/prosdev.html

Horvath L, Henshall S, Soon-Lee C, Kench J, Golovsky D, Brenner P, O'Neill G, Kooner R, Stricker P, Grygiel J, Sutherland R. 2005. Lower levels of nuclear beta-catenin predict for a poorer prognosis in localised prostate cancer. Int J Cancer 113:415-422.

Hou X, Tan Y, Li M, Dey S, Das S. 2004. Canonical Wnt signaling is critical to estrogen-mediated uterine growth. Mol Endocrinol 18:3035-3049.

Huang J, Powell W, Khodavirdi A, Wu J, Makita T, Cardiff R, Cohen M, Sucov H, Roy-Burman P. 2002. Prostatic intraepithelial neoplasia in mice with conditional disruption of the retinoid X receptor alpha allele in the prostate epithelium. Cancer Res 62:4812-4819.

Hurov J, Stappenbeck T, Zmasek C, White L, Ranganath S, Russell J, Chan A, Murphy K, Piwnica-Worms H. 2001. Immune system dysfunction and autoimmune disease in mice lacking Emk (Par-1) protein kinase. Mol Cell Biol 21:3206–3219.

Hurt E, Kowasaki B, Klarmann G, Thomas S, Farrar W. 2008. CD44(+) CD24(-) prostate cells are early cancer progenitors/stem cells that provide a model for patients with poor prognosis. Br J Cancer 98:756-765.

Huss W, Maddison L, Greenberg N. 2001. Autochthonous mouse models for prostate cancer: past, present and future. Cancer Biol 11:245-259.

Ikediobi O, Davies H, Bignell G, Edkins S, Stevens C, O'Meara S, Santarius T, Avis T, Barthorpe S, Brakenbury L, Buck G, Butler A, Clements J, Cole J, Dicks E, Forbes S, Gray K, Halliday H, Harrison R, Hills K, Hinton J, Hunter C, Jenkinson A, Jones D, Kosmidou V, Lugg R, Menzies A, Miranenko T, Parker A, Perry J, Raine K, Richardson D, Shepherd S, Small A, Smith R, Solomon H, Stephens P, Teague J, Tofts C, Varian J, Webb T, West S, Widaa S, Yates A, Reinhold W, Weinstein J, Stratton M, Futreau P, Wooster R. 2006.

Mutation analysis of 24 known cancer genes in the NCI-60 cell line set. Mol Cancer Ther 5:2606-2612.

Ireland H, Kemp R, Houghton C, Howard L, Clarke AR, Sansom OJ, Winton DJ. 2004. Inducible Cre-mediated control of gene expression in the murine gastrointestinal tract: effect of loss of beta-catenin. Gastroenterology 126:1236-1246. .

Isaacs J, Isaacs W. 2004. Androgen receptor outwits prostate cancer drugs. Nat Med 10:26-27.

Jackson E, Willis N, Mercer K, Bronson R, Crowley D, Montoya R, Jacks T, Tuveson D. 2001. Analysis of lung tumor initiation and progression using conditional expression of oncogenic K-ras. Genes Dev 15:3243-3248.

Jacobs E, Rodriguez C, Mondul A, Connell C, Henley S, Calle E, Thun M. 2005. A large cohort study of aspirin and other nonsteroidal anti-inflammatory drugs and prostate cancer incidence. J Natl Cancer Inst 97:975-980.

Jang J, Boxer R, Chodosh L. 2006. Isoform-specific ras activation and oncogene dependence during MYC- and Wnt-induced mammary tumorigenesis. Mol Cell Biol 26:8106-8121.

Janssen K, Alberici P, Fsihi H, Gaspar C, Breukel C, Franken P, Rosty C, Abal M, El-Marjou F, Smits R, Louvard D, Fodde R, Robine S. 2006. APC and oncogenic KRAS are synergistic in enhancing Wnt signaling in intestinal tumor formation and progression. Gastroenterology 131:1096-1109.

Jenne DE, Reimann H, Nezu J, Friedel W, Loff S, Jeschke R, Muller O, Back W, Zimmer M. 1998. Peutz-Jeghers syndrome is caused by mutations in a novel serine threonine kinase. Nat Genet 18:38-43.

Ji H, Ramsey MR, Hayes DN, Fan C, McNamara K, Kozlowski P, Torrice C, Wu MC, Shimamura T, Perera SA, Liang MC, Cai D, Naumov GN, Bao L, Contreras CM, Li D, Chen L, Krishnamurthy J, Koivunen J, Chirieac LR, Padera RF, Bronson RT, Lindeman NI, Christiani DC, Lin X, Shapiro GI, Janne PA, Johnson BE, Meyerson M, Kwiatkowski DJ, Castrillon DH, Bardeesy N, Sharpless NE, Wong KK. 2007. LKB1 modulates lung cancer differentiation and metastasis. Nature 448:807-810.

Jimenez A, Fernandez P, Dominguez O, Dopazo A, Sanchez-Cespedes M. 2003. Growth and molecular profile of lung cancer cells expressing ectopic LKB1: down-regulation of the phosphatidylinositol 3'-phosphate kinase/PTEN pathway. Cancer Res 63:1382-1388.

Johnson M, Hernandez I, Wei Y, Greenberg N. 2000. Isolation and characterization of mouse probasin: An androgen-regulated protein specifically expressed in the differentiated prostate. Prostate 43:255-262.

Karhadkar SS, Bova GS, Abdallah N, Dhara S, Gardner D, Maitra A, Isaacs JT, Berman DM, Beachy PA. 2004. Hedgehog signalling in prostate regeneration, neoplasia and metastasis. Nature 431:707-712.

Karuman P, Gozani O, Odze R, Zhu X, Shaw R, Brien T, Bozzuto C, Odi D, Cantley L, Yuan J. 2001. The Peutz-Jegher gene product is a mediator of p53-dependent cell death. Mol Cell 7:1307-1319.

Kasper S. 2005. Survey of genetically engineered mouse models for prostate cancer: analyzing the molecular basis of prostate cancer development, progression, and metastasis. J Cell Biochem 94:279-297.

Kasper S, Matusik RJ. 2000. Rat probasin: structure and function of an outlier lipocalin. Biochim Biophys Acta 1482:249-258.

Katajisto P, Vallenius T, Vaahtomeri K, Ekman N, Udd L, Tiainen M, Mäkelä T. 2007. The LKB1 tumor suppressor kinase in human disease. Biochim Biophys Acta 1775:63-75.

Ke N, Zhou D, E. Chatterton J, Liu G, Chionis J, Zhang J, Tsugawa L, Lynn R, Yu D, Meyhack B, Wong-Staal F, Li Q-X. 2006. A new inducible RNAi xenograft model for assessing the staged tumor response to mTOR silencing. Experimental Cell Research 312:2726-2734.

Keith W, Thomson C, Howcroft J, Maitland N, Shay J. 2007. Seeding drug discovery: integrating telomerase cancer biology and cellular senescence to uncover new therapeutic opportunities in targeting cancer stem cells. Drug Discov Today 12:611-621.

Kerkhoff E, Houben R, Löffler S, Troppmair J, Lee J, Rapp U. 1998. Regulation of c-myc expression by Ras/Raf signalling. Oncogene 16:211-216.

Kikyo N, Williamson CM, John RM, Barton SC, Beechey CV, Ball ST, Cattanach BM, Surani MA, Peters J. 1997. Genetic and functional analysis of neuronatin in mice with maternal or paternal duplication of distal Chr 2. Dev Biol 190:66-77.

Kim C, Lee H. 1987. Sertoli Cell Only Syndrome. Korean J Urol 28:97-104.

Kim JH, Kim B, Cai L, Choi HJ, Ohgl KA, Tran C, Chen C, Chung CH, Huber O, Rose DW, Sawyers CL, Rosenfold MG, Baek SH. 2005. Transcriptional regulation of a metastasis supressor gene by Tip60 and b-catenin complexes. Nature 434:921-926.

Kim M, Bhatia-Gaur R, Banach-Petrosky W, Desai N, Wang Y, Hayward S, Cunha G, Cardiff R, Shen M, Abate-Shen C. 2002a. Nkx3.1 mutant mice recapitulate early stages of prostate carcinogenesis. Cancer Res 62:2999-3004.

Kim M, Cardiff R, Desai N, Banach-Petrosky W, Parsons R, Shen M, Abate-Shen C. 2002b. Cooperativity of Nkx3.1 and Pten loss of function in a mouse model of prostate carcinogenesis. Proc Natl Acad Sci USA 99:2884–2889.

Kinbara H, Cunha G, Boutin E, Hayashi N, Kawamura J. 1996. Evidence of stem cells in the adult prostatic epithelium based upon responsiveness to mesenchymal inductors. Prostate 29:107-116.

Koker M, Kleer C. 2004. p63 expression in breast cancer: a highly sensitive and specific marker of metaplastic carcinoma. Am J Surg Pathol 28:1506-1512.

Kolligs F, Bommer G, Göke B. 2002. Wnt/beta-catenin/Tcf signaling: a critical pathway in gastrointestinal tumorigenesis. Digestion 66:131-144.

Korinek V, Barker N, Morin P, Van-Wichen D, de-Weger R, Kinzler K, Vogelstein B, Clevers H. 1997. Constitutive transcriptional activation by a beta-catenin-Tcf complex in APC -/- colon carcinoma. Science 275:1784-1787.

Korkaya H, Wicha M. 2007. Selective targeting of cancer stem cells: a new concept in cancer therapeutics. BioDrugs 21:299-310.

Kranenburg O. 2005. The KRAS oncogene: past, present, and future. Biochim. Biophys. Acta 1756:81-82.

Kuefer R, Hofer MD, Zorn CS, Engel O, Volkmer BG, Juarez-Brito MA, Eggel M, Gschwend JE, Rubin MA, Day ML. 2005. Assessment of a fragment of e-cadherin as a serum biomarker with predictive value for prostate cancer. Br J Cancer 92:2018-2023.

Kuhnert F, Davies C, Wang H, Chu P, Lee M, Yuan J, Nusse R, Cuo C. 2004. Essential requirement for Wnt signalling in adult small intestine and colon revealed by adenoviral expression of Dickkopf-1. Proc Natl Acad Sci USA 101:266-271.

Kurita T, Medina R, Mills A, Cunha G. 2004. Role of p63 and basal cells in the prostate. Development 131:4955-4964.

Kwabi-Addo B, Giri D, Schmidt K, Podsypanina K, Parsons R, Greenberg N, Ittmann M. 2001. Haploinsufficiency of the Pten tumor suppressor gene promotes prostate cancer progression. Proc Natl Acad Sci USA 98:11563–11568.

Lakso M, Sauer B, Masinger B, Lee E, Manning R, Yu S, Mulder K, Westphal H. 1992. Targeted oncogene activation by site-specific recombination in transgenic mice. Proc. Natl. Acad. Sci. 89:6232-6236.

Lam J. 2006. Stem cells in prostate and prostate cancer development. Urol Oncol 24:131-140.

Lamb D, Zhang L. 2005. Challenges in prostate cancer research: animal models for nutritional studies of chemoprevention and disease progression. J Nutr 135:3009S-3015S.

Laramas M, Pasquier D, Filhol O, Ringeisen F, Descotes J, Cochet C. 2007. Nuclear localization of protein kinase CK2 catalytic subunit (CK2alpha) is associated with poor prognostic factors in human prostate cancer. Eur J Cancer 43:928-934.

Lattouf J, Srinivasan R, Pinto P, Linehan W, Neckers L. 2006. Mechanisms of disease: the role of heat-shock protein 90 in genitourinary malignancy. Nat Clin Pract Urol 3:590-601.

Lawson D, Witte O. 2007. Stem cells in prostate cancer initiation and progression. J Clin Invest 117:2044-2050.

Lawson D, Xin L, Lukacs R, Cheng D, Witte O. 2007. Isolation and functional characterization of murine prostate stem cells. Proc Natl Acad Sci U S A 104:282-286.

Le-Page C, Koumakpayi I, Alam-Fahmy M, Mes-Masson A, Saad F. 2006. Expression and localisation of Akt-1, Akt-2 and Akt-3 correlate with clinical outcome of prostate cancer patients. Br J Cancer 94:1906-1912.

Lee D, Chang C. 2003. Molecular communication between androgen receptor and general transcription machinery. J Steroid Biochem Mol Biol 84:41-49.

Lee M, Hwang JT, Yun H, Kim EJ, Kim MJ, Kim SS, Ha J. 2006. Critical roles of AMP-activated protein kinase in the carcinogenic metal-induced expression of VEGF and HIF-1 proteins in DU145 prostate carcinoma. Biochem Pharmacol 72:91-103.

Lefevre H, Bouvattier C, Lahlou N, Adamsbaum C, Bougneres P, Carel J. 2006. Prepubertal gynecomastia in Peutz-Jeghers syndrome: incomplete penetrance in a familial case and management with an aromatase inhibitor. Eur J Endocrinol 154:221-227.

Lehr J, Pienta K, Yamazaki K, Pilat M. 1998. A model to study c-myc and v-H-ras induced prostate cancer progression in the Copenhagen rat. Cell Mol Biol (Noisy-le-grand) 44:949-959.

Li H, Zhou J, Miki J, Furusato B, Gu Y, Srivastava S, McLeod D, Vogel J, Rhim J. 2007a. Telomerase-immortalized non-malignant human prostate epithelial cells retain the properties of multipotent stem cells. Exp Cell Res doi:10.1016/j.yexcr.2007.08.011.

Li J, Mizukami Y, Zhang X, Jo W, Chung D. 2005. Oncogenic K-ras stimulates Wnt signaling in colon cancer through inhibition of GSK-3beta. Gastroenterology 128:1907-1918.

Li X, Deng W, Lobo-Ruppert S, Ruppert J. 2007b. Gli1 acts through Snail and E-cadherin to promote nuclear signaling by beta-catenin. Oncogene 26:4489-4498.

Li Y, Welm B, Podsypanina K, Huang S, Chamorro M, Zhang X, Rowlands T, Egeblad M, Cowin P, Werb Z, Tan L, Rosen J, Varmus H. 2003. Evidence that transgenes encoding components of the Wnt signaling pathway preferentially induce mammary cancers from progenitor cells. Proc Natl Acad Sci USA 100:15853-15858.

Liao Y, Grobholz R, Abel U, Trojan L, Michel M, Angel P, Mayer D. 2003. Increase of AKT/PKB expression correlates with gleason pattern in human prostate cancer. Int J Cancer 107:676-680.

Lin-Marq N, Borel C, Antonarakis S. 2005. Peutz-Jeghers LKB1 mutants fail to activate GSK-3beta, preventing it from inhibiting Wnt signalling. Mol Gen Genomics 273:184-196.

Lin D, Hu Y, Lee D, Chang C. 2004a. Negative regulation of the androgen receptor transcriptional activity by Daxx. Mol Cell Biol 24:10529-10541.

Lin H, Hu Y, Lee D, Chang C. 2004b. Regulation of androgen receptor signaling by PTEN (phosphatase and tensin homolog deleted on chromosome 10) tumor suppressor through distinct mechanisms in prostate cancer cells. Mol Endocrinol 18:2409-2423.

Litvinov I, DeMarzo A, Isaacs J. 2003. Is the Achilles' Heel for Prostate Cancer Therapy a Gain of Function in Androgen Receptor Signaling? J Clin Endocrinol Metab 88:2972-2982.

Liu A, True L, LaTray L, Nelson P, Ellis W, Vessella R, Lange P, Hood L, Engh Gvd. 1997. Cell-cell interaction in prostate gene regulation and cytodifferentiation. Proc Natl Acad Sci U S A 94:10705-10710.

Liu W, Mruk D, Lee W, Cheng C. 2003. Sertoli cell tight junction dynamics: their regulation during spermatogenesis. Biol Reprod 68:1087-1097.

Livak KJ, Schmittgen TD. 2001. Analysis of relative gene expression data using real-time quantitative PCR and the 2(-Delta Delta C(T)) Method. Methods 25:402-408.

Lizcano JM, Goransson O, Toth R, Deak M, Morrice NA, Boudeau J, Hawley SA, Udd L, Makela TP, Hardie DG, Alessi DR. 2004. LKB1 is a master kinase that activates 13 kinases of the AMPK subfamily, including MARK/PAR-1. Embo J 23:833-843.

Lu X, Park S, Thompson T, Lane D. 1992. Ras-induced hyperplasia occurs with mutation of p53, but activated ras and myc together can induce carcinoma without p53 mutation. Cell 70:153-161.

Lui W, Mruk D, Lee W, Cheng C. 2003. Sertoli cell tight junction dynamics: their regulation during spermatogenesis. Biol Reprod 68:1087-1097.

Luukko K, Ylikorkala A, Tiainen M, Mäkelä T. 1999. Expression of LKB1 and PTEN tumor suppressor genes during mouse embryonic development. Mech Dev 83:187-190.

Lyons SK. 2005. Advances in imaging mouse tumour models in vivo. J Pathol 205:194-205.

Ma X, Ziel-van-der-Made A, Autar B, van-der-Korput H, Vermeij M, van-Duijn P, Cleutjens K, de-Krijger R, Krimpenfort P, Berns A, van-der-Kwast T, Trapman J. 2005. Targeted biallelic inactivation of Pten in the mouse prostate leads to prostate cancer accompanied by increased epithelial cell proliferation but not by reduced apoptosis. Cancer Res 65:5730-5739.

Maddison K, Clarke A. 2005 New approaches for modelling cancer mechanisms in the mouse. J Pathol 205:181-193.

Maddison L, Nahm H, DeMayo F, Greenberg N. 2000. Prostate specific expression of Cre recombinase in transgenic mice. Genesis 26:154-156.

Maitland N, Collins A. 2005. A tumour stem cell hypothesis for the origins of prostate cancer. BJU International 96:1219-1223.

Majumder PK, Yeh JJ, George DJ, Febbo PG, Kum J, Xue Q, Bikoff R, Ma H, Kantoff PW, Golub TR, Loda M, Sellers WR. 2003. Prostate intraepithelial neoplasia induced by prostate restricted Akt activation: the MPAKT model. Proc Natl Acad Sci U S A 100:7841-7846.

Malik S, Brattain M, Ghosh P, Troyer D, Prihoda T, Bedolla R, Kreisberg J. 2002. Immunohistochemical demonstration of phospho-Akt in high Gleason grade prostate cancer. Clin Cancer Res 8:1168-1171.

Malik SN BM, Ghosh PM, Troyer DA, Prihoda T, Bedolla R, Kreisberg JI. 2002. Immunohistochemical demonstration of phospho-Akt in high Gleason grade prostate cancer. Clin Cancer Res 8:1168-1171.

Malliri A, van-der-Kammen R, Clark K, van-der-Valk M, Michiels F, Collard J. 2002. Mice deficient in the Rac activator Tiam1 are resistant to Ras-induced skin tumours. Nature 417:867-871.

Malumbres M, Pellicer A. 1998. RAS pathways to cell cycle control and cell transformation. Front Biosci 3:d887-912.

Marignani P, Kanai F, Carpenter C. 2001. LKB1 associates with Brg1 and is necessary for Brg1-induced growth arrest. J Biol Chem 276:32415-32418.

Marignani P, Kanai F, Carpenter C. 2005. LKB1, the multitasking tumour suppressor kinase. J Clin Pathol 58:15-19.

Maroni P, Koul S, Meacham R, Koul H. 2004. Mitogen Activated Protein kinase signal transduction pathways in the prostate. Cell Commun Signal 2:5.

Martin K, Blenis J. 2002. Coordinate regulation of translation by the PI 3-kinase and mTOR pathways. Adv Cancer Res 86:1-39.

Matheny K, Barbieri C, Sniezek J, Arteaga C, Pietenpol J. 2003. Inhibition of epidermal growth factor receptor signaling decreases p63 expression in head and neck squamous carcinoma cells. Laryngoscope 113:936-939.

Maunsbach A, Bjorn A. 1999. Biomedical Electron Microscopy: Practical Methods. Academic Press, London:p515-523.

Mehenni H, Lin-Marq N, Buchet-Poyau K, Reymond A, Collart MA, Picard D, Antonarakis SE. 2005. LKB1 interacts with and phosphorylates PTEN: a functional link between two proteins involved in cancer predisposing syndromes. Hum Mol Genet. 14:2209-2219.

Melissari M, Lopez-Beltran A, Mazzucchelli R, Froio E, Bostwick D, Montironi R. 2006. High grade prostatic intraepithelial neoplasia with squamous differentiation. J Clin Pathol 59:437-439.

Menke A, IJpenberg A, Fleming S, Ross A, Medine C, Patek C, Spraggon L, Hughes J, Clarke A, Hastie N. 2003. The wt1-heterozygous mouse; a model to study the development of glomerular sclerosis. J Pathol 200:667-674.

Mirosevich J, Gao N, Matusik RJ. 2005. Expression of Foxa transcription factors in the developing and adult murine prostate. Prostate 62:339-352.

Mitsumori K, Elwell MR. 1994. Tumours of the male accessory sex glands. IARC Sci Publ:431-449.

Miyaki M, Iijima T, Hosono K, Ishii R, Yasuno M, Mori T, Toi M, Hishima T, Shitara N, Tamura K, Utsunomiya J, Kobayashi N, Kuroki T, Iwama T. 2000. Somatic mutations of LKB1 and beta-catenin genes in gastrointestinal polyps from patients with Peutz-Jeghers syndrome. Cancer Res 60:6311-6313.

Miyoshi H, Nakau M, Ishikawa TO, Seldin MF, Oshima M, Taketo MM. 2002. Gastrointestinal hamartomatous polyposis in Lkb1 heterozygous knockout mice. Cancer Res 62:2261-2266.

Miyoshi Y, Iwao K, Nagasawa Y, Aihara T, Sasaki Y, Imaoka S, Murata M, Shimano T, Nakamura Y. 1998. Activation of the beta-catenin gene in primary hepatocellular carcinomas by somatic alterations involving exon 3. Cancer Res 58:2524-2527.

Moll U, Erster S, Zaika A. 2001. p53, p63 and p73 – solos, alliances and feuds among family members. Biochimica et Biophysica Acta (BBA) - Reviews on Cancer 1552:47-59.

Müller J, Ory S, Copeland T, Piwnica-Worms H, Morrison D. 2001 C-TAK1 regulates Ras signaling by phosphorylating the MAPK scaffold, KSR1. Mol Cell Biol 8:983-993.

Nakau M. 2002. Hepatacellular carcinoma caused by loss of heretrozygosity in Lkb1 gene knockout mice. Cancer Res 62:4549-4553.

Narayanan B, Narayanan N, Pittman B, Reddy B. 2006. Adenocarcinoma of the mouse prostate growth inhibition by celecoxib: downregulation of transcription factors involved in COX-2 inhibition. Prostate 66:257-265.

Navone NM, Logothetis CJ, von Eschenbach AC, Troncoso P. 1998. Model systems of prostate cancer: uses and limitations. Cancer Metastasis Rev 17:361-371.

Neville P, Conti D, Krumroy L, Catalona W, Suarez B, Witte J, Casey G. 2003. Prostate cancer aggressiveness locus on chromosome segment 19q12-q13.1 identified by linkage and allelic imbalance studies. Genes Chromosomes Cancer 36:332-339.

Nguyen B, Lefort K, Mandinova A, Antonini D, Devgon V. 2006. Cross-regulation between Notch and p63 in keratinocyte commitment to differentiation. Genes Dev 20:1028-1042.

Niessen C. 2007. Tight junctions/adherens junctions: basic structure and function. J Invest Dermatol 127:2525-2532.

Nollet F, Berx G, Molemans F, Roy Fv. 1996. Genomic organization of the human beta-catenin gene (CTNNB1). Genomics 32:413-424.

Odom DG, Donatucci CF, Deshon GE. 1986. Mucinous adenocarcinoma of the prostate. Hum Pathol 17:863-865.

Okahara F, Ikawa H, Kanaho Y, Maehama T. 2004. Regulation of PTEN phosphorylation and stability by a tumor suppressor candidate protein. J Biol Chem 279:45300-45303.

Oshima R, Baribault H, Caulín C. 1996. Oncogenic regulation and function of keratins 8 and 18. Cancer Metastasis Rev 15:445-471.

Ossipova O, Bardeesy N, DePinho RA, Green JB. 2003. LKB1 (XEEK1) regulates Wnt signalling in vertebrate development. Nat Cell Biol 5:889-894.

Pandha H, Eaton J, Greenhalgh R, Soars D, Dalgleish A. 2005. Immunotherapy of murine prostate cancer using whole tumor cells killed ex vivo by herpes simplex viral thymidine kinase/ganciclovir suicide gene therapy. Cancer Gene Ther 12:572-578.

Papatsoris A, Karamouzis M, Papavassiliou A. 2007. The power and promise of "rewiring" the mitogen-activated protein kinase network in prostate cancer therapeutics. Mol Cancer Ther 6:811-819.

Parfenova H, Parfenov V, Shlopov B, Levine V, Falkos S, Pourcyrous M, Leffler C. 2001. Dynamics of nuclear localisation sites for COX-2 in vasculature endothelial cells. Am J Physiol Cell Physiol 281:C116-C178.

Park B, Lee S, Kim J, Lee S, Lee C, Chang S, Park J, Chi S. 2000. Frequent alteration of p63 expression in human primary bladder carcinomas. Cancer Res 60:3370-3374.

Parsons J, Gage W, Nelson W, De-Marzo A. 2001. p63 protein expression is rare in prostate adenocarcinoma: implications for cancer diagnosis and carcinogenesis Urology 58.

Pflug BR, Pecher SM, Brink AW, Nelson JB, Foster BA. 2003. Increased fatty acid synthase expression and activity during progression of prostate cancer in the TRAMP model. Prostate 57:245-254.

Pineau C, Sharpe R, Saunders P, Gerard N, Jegou B. 1990. Regulation of Sertoli cell inhibin production and of inhibin [alpha]-subunit mRNA levels by specific germ cell types. Mol Cell Endocrinol 72.

Pinheiro PF, Almeida CC, Segatelli TM, Martinez M, Padovani CR, Martinez FE. 2003. Structure of the pelvic and penile urethra--relationship with the ducts of the sex accessory glands of the Mongolian gerbil (Meriones unguiculatus). J Anat 202:431-444.

Podsypanina K, Ellenson L, Nemes A, Gu J, Tamura M, Yamada K, Cordon-Cardo C, Catoretti G, Fisher P, Parsons R. 1999. Mutation of Pten/Mmac1 in mice causes neoplasia in multiple organ systems. Proc Natl Acad Sci USA 96:1563-1568.

Pointisa G, Fiorinia C, Defamiea N, Segretainb D. 2005. Gap junctional communication in the male reproductive system. Biochimica et Biophysica Acta (BBA) - Biomembranes 1719:102-116.

Polakis P. 2000. Wnt signaling and cancer. Genes Dev. 14:1837-1851.

Polnaszek N, Kwabi-Addo B, Peterson L, Ozen M, Greenberg N, Ortega S, Basilico C, Ittmann M. 2003. Fibroblast growth factor 2 promotes tumour progression in an autochthonous mouse model of prostate cancer. Cancer Res 63:5754-5760.

Pommery N, Henichart J. 2005. Involvement of PI3K/Akt Pathway in Prostate Cancer - Potential Strategies for Developing Targeted Therapies. Mini Reviews in Medicinal Chemistry 5:1125-1132.

Price D. 1963. Comparative Aspects of Development and Structure in the Prostate. Natl Cancer Inst Monogr 12:1-27.

Price D, Rocca GD, Guo C, Ballo M, Schwinn D, Luttrell L. 1999. Activation of extracellular signal-regulated kinase in human prostate cancer. J Urol 162:1537-1542.

Prins GS, Birch L, Greene GL. 1991. Androgen receptor localization in different cell types of the adult rat prostate. Endocrinology 129:3187-3199.

Pullen N, Dennis PB, Andjelkovic M, Dufner A, Kozma SC, Hemmings BA, Thomas G. 1998. Phosphorylation and activation of p70s6k by PDK1. Science 279:707-710.

Qanungo S, Haldar S, Basu A. 2003. Restoration of silenced Peutz-Jeghers syndrome gene, LKB1, induces apoptosis in pancreatic carcinoma cells. Neoplasia 5:367-374.

Quade G. 2005. Treatment statement for health professionals: Prostate cancer. In: National Institute of Cancer, Med News.

Raghow S, Hooshdaran M, Katiyar S, Steiner M. 2002. Toremifene prevents prostate cancer in the transgenic adenocarcinoma of mouse prostate model. Cancer Res 62:1370-1376.

Rankin T, Tsuruta K, Holland M, Griswold M, Orgebin-Crist M. 1992. Isolation, immunolocalization, and sperm-association of three proteins of 18, 25, and 29 kilodaltons secreted by the mouse epididymis. Biol Reprod 46:747-766.

Reis-Filho J, Simpson P, Fulford L, Martins A, Schmitt F. 2003. P63-driven nuclear accumulation of beta-catenin is not a frequent event in human neoplasms. Pathol Res Pract 199:785-793.

Resta N, Stella A, Susca FC, Di Giacomo M, Forleo G, Miccolis I, Rossini FP, Genuardi M, Piepoli A, Grammatico P, Guanti G. 2002. Two novel mutations and a new STK11/LKB1 gene isoform in Peutz-Jeghers patients. Hum Mutat 20:78-79.

Reya T, Clevers H. 2005. Wnt signalling in stem cells and cancer. Nature 434:843-850. .

Richardson G, Robson C, Lang S, Neal D, Maitland N, Collins A. 2004. CD133, a novel marker for human prostatic epithelial stem cells. J Cell Sci 117.

Rider M. 2006. The ubiquitin-associated domain of AMPK-related protein kinases allows LKB1-induced phosphorylation and activation. Biochem J 394:e7-e9.

Risbridger G, Ellem S, McPherson S. 2007. Estrogen action on the prostate gland: a critical mix of endocrine and paracrine signaling. J Mol Endocrinol 39:183-188.

Robinson E, Neal D, Collins A. 1998. Basal cells are progenitors of luminal cells in primary cultures of differentiating human prostatic epithelium. Prostate 37:149-160.

Rossi D, Ylikorkala A, Korsisaari N, Salovaara R, Luukko K, Launonen V, Henkemeyer M, Ristimaki A, Aaltonen L, Makela T. 2002. Induction of cyclooxygenase-2 in a mouse model of Peutz-Jeghers polyposis. Proc Natl Acad Sci U S A 99:12327-12332.

Rowan A, Churchman M, Jefferey R, Hanby A, Poulsom R, Tomlinson I. 2000. In situ analysis of LKB1/STK11 mRNA expression in human normal tissues and tumours. J Pathol 192:203-206.

Roy-Burman P, Wu H, Powell WC, Hagenkord J, Cohen MB. 2004. Genetically defined mouse models that mimic natural aspects of human prostate cancer development. Endocr Relat Cancer 11:225-254.

Saito S, Egawa S, Endoh M, Ueno S, Ito A, Numahata K, Satoh M, Kuwao S, Baba S, Hakomori S, Arai Y. 2005. RM2 antigen (beta1,4-GalNAc-disialyl-Lc4) as a new marker for prostate cancer. Int J Cancer 115:105-113.

Sakamoto K, McCarthy A, Smith D, Green KA, Grahame Hardie D, Ashworth A, Alessi DR. 2005. Deficiency of LKB1 in skeletal muscle prevents AMPK activation and glucose uptake during contraction. Embo J 24:1810-1820.

Sanchez-Cespedes M, Parrella P, Esteller M, Nomoto S, Trink B, Engles JM, Westra WH, Herman JG, Sidransky D. 2002. Inactivation of LKB1/STK11 is a common event in adenocarcinomas of the lung. Cancer Res 62:3659-3662.

Sanchez P, Hernandez A, Stecca B, Kahler A, DeGueme A, Barrett A. 2004. Inhibition of prostate cancer proliferation by interference with Sonic hedgehog-Gli-1 signalling Proc Natl Acad Sci USA 101:12561.

Sancho E, Batlle E, Clevers H. 2004. Signaling pathways in intestinal development and cancer. Annu Rev Cell Dev Biol 20:695-723.

Sansom O, Griffiths D, KR KR, Winton D, Clarke A. 2005. Apc deficiency predisposes to renal carcinoma in the mouse. Oncogene 24:8205-8210.

Sansom O, Menial V, Wilkins J, Cole A, Oien K, Marsh V, Jamieson T, Guerra C, Ashton G, Barbacid M, Clarke A. 2006. Loss of APC allows phenotypic manifestation of the transforming properties of an endogenous K-ras oncogene in vivo. PNAS 103:14122-14127.

Sansom OJ, Meniel VS, Muncan V, Phesse TJ, Wilkins JA, Reed KR, Vass JK, Athineos D, Clevers H, Clarke AR. 2007. Myc deletion rescues Apc deficiency in the small intestine. Nature 446:676-679.

Sansom OJ, Reed KR, Hayes AJ, Ireland H, Brinkmann H, Newton IP, Batlle E, Simon-Assmann P, Clevers H, Nathke IS, Clarke AR, Winton DJ. 2004. Loss

of Apc in vivo immediately perturbs Wnt signaling, differentiation, and migration. Genes Dev 18:1385-1390.

Santagata S, Demichelis F, Riva A, Varambally S, Hofer MD, Kutok JL, Kim R, Tang J, Montie JE, Chinnaiyan AM, Rubin MA, Aster JC. 2004. JAGGED1 expression is associated with prostate cancer metastasis and recurrence. Cancer Res 64:6854-6857.

Sawicki J, Rothman C. 2002. Evidence for stem cells in cultures of mouse prostate epithelial cells. Prostate 50:46-53.

Schalken J, Hessels D, Verhaegh G. 2003. New targets for therapy in prostate cancer: differential display code 3 (DD3/PCA3), a highly prostate cancer specific gene. Urology 62:34-43.

Scher H, Buchanan G, Gerald W, Butler L, Tilley W. 2004. Targeting the androgen receptor: improving outcomes for castration-resistant prostate cancer Endocrine-Related Cancer 11:459-476.

Scherl A, Li JF, Cardiff RD, Schreiber-Agus N. 2004. Prostatic intraepithelial neoplasia and intestinal metaplasia in prostates of probasin-RAS transgenic mice. Prostate 59:448-459.

Schmelz M, Moll R, Hess U, Prasad A, Gandolfi J, Hasan S, Bartholdi M, Cress A. 2005. Identification of a stem cell candidate in the normal human prostate gland. Eur J Cell Biol 84:341-354.

Schmitz M, Grignard G, Margue C, Dippel W, Capesius C, Mossong J, Nathan M, Giacchi S, Scheiden R, Kieffer N. 2007. Complete loss of PTEN expression as a possible early prognostic marker for prostate cancer metastasis. Int J Cancer 120:1284-1292.

Schubbert S, Shannon K, Bollag G. 2007. Hyperactive Ras in developmental disorders and cancer. Nat Rev Cancer 7:295-308.

Shappell SB, Thomas GV, Roberts RL, Herbert R, Ittmann MM, Rubin MA, Humphrey PA, Sundberg JP, Rozengurt N, Barrios R, Ward JM, Cardiff RD. 2004. Prostate pathology of genetically engineered mice: definitions and classification. The consensus report from the Bar Harbor meeting of the Mouse Models of Human Cancer Consortium Prostate Pathology Committee. Cancer Res 64:2270-2305.

Sharma M, Chuang W, Sun Z. 2002. Phosphatidylinositol 3-kinase/Akt stimulates androgen pathway through GSK3beta inhibition and nuclear beta-catenin accumulation. J Biol Chem 277:30935-30941.

Shaw A, Bushman W. 2007. Hedgehog signalling in the prostate. J Urol 177:832-838.

Shaw RJ, Bardeesy N, Manning BD, Lopez L, Kosmatka M, DePinho RA, Cantley LC. 2004. The LKB1 tumor suppressor negatively regulates mTOR signaling. Cancer Cell 6:91-99.

Sheng T, Li C, Zhang X, Chi S, He N, Chen K, McCormick F, Gatalica Z, Xie J. 2004. Activation of the hedgehog pathway in advanced prostate cancer. Mol Cancer 3:13.

Shorning BY, Zabkiewicz J, McCarthy A, Sansom OJ, Pearson HB, Winton DJ, Ashworth A, Clarke AR. 2007. Lkb1 maintains the normal differentiation programme in the small intestine Submitted to Gastroenterology.

Shukla S, Maclennon G, Marengo S, Resnick M, Gupta S. 2005. Constitutive activation of PI3K-Akt and NF-kB during prostate cancer progression in autochthonous transgenic mouse model. The Prostate 64:224-239.

Signoretti S, Loda M. 2006 Defining cell lineages in the prostate epithelium. Cell Cycle 5:138-141.

Signoretti S, Waltregny D, Dilks J, Isaac B, Lin D, Garraway L, Yang A, Montironi R, McKeon F, Loda M. 2000. p63 is a prostate basal cell marker and is required for prostate development. Am J Pathol 157:1769-1775.

Singh S, Clarke I, Terasaki M, Bonn V, Hawkins C, Squire J, Dirks P. 2003. Identification of a Cancer Stem Cell in Human Brain Tumors. Cancer Res 63.

Singh S, Hawkins C, Clarke I, Squire J, Bayani J, Hide T, Henkelmen R, Cusimano M, Dirks P. 2004. Identification of human brain tumour initiating cells. Nature 432:396-401.

Sinner D, Rankin S, Lee M, Zorn AM. 2004. Sox17 and beta-catenin cooperate to regulate the transcription of endodermal genes. Development 131:3069-3080.

Smit V, Boot A, Smits A, Fleuren G, Cornelisse C, Bos J. 1988. KRAS codon 12 mutations occur very frequently in pancreatic adenocarcniomas. Nucleic Acids Res 16:7773-7782.

Smith D, Rayter S, Neiderlander C, Spicer J, Jones C, Ashworth A. 2001. LIP1, a cytoplasmic protein functionally linked to the Peutz-Jeghers syndrome kinase LKB1. Hum Mol Genet 10:2869-2877.

Song P, Wu Y, Xu J, Xie Z, Dong Y, Zhang M, Zou M. 2007. Reactive nitrogen species induced by hyperglycemia suppresses Akt signaling and triggers apoptosis by upregulating phosphatase PTEN (phosphatase and tensin homologue deleted on chromosome 10) in an LKB1-dependent manner. Circulation 116:1585-1595.

Soriano P. 1999. Generalized lacZ expression with the ROSA26 Cre reporter strain. Nat Genet 21:70-71.

Spicer J, Ashworth A. 2004. LKB1 kinase: master and commander of metabolism and polarity. Curr Biol 14:R383-385.

Spicer J, Rayter S, Young N, Elliott R, Ashworth A, Smith D. 2003. Regulation of the Wnt signalling component PAR1A by the Peutz-Jeghers syndrome kinase LKB1. Oncogene 22:4752-4756.

Staack A, Donjacour AA, Brody J, Cunha GR, Carroll P. 2003. Mouse urogenital development: a practical approach. Differentiation 71:402-413.

Steiner H, Godoy-Tundidor S, Rogatsch H, Berger A, Fuchs D, Comuzzi B, Bartsch G, Hobisch A, Culig Z. 2003. Accelerated in Vivo Growth of Prostate Tumors that Up-Regulate Interleukin-6 Is Associated with Reduced Retinoblastoma Protein Expression and Activation of the Mitogen-Activated Protein Kinase Pathway. Am J Pathol 162:655–663.

Stingl J, Eirew P, Ricketson I, Shackleton M, Vaillant F, Choi D, Li H, Eaves C. 2006. Purification and unique properties of mammary epithelial stem cells. Nature 439:993-997.

Su G, Hruban R, Bansal R, Bova G, Tang D, Shekher M, Westerman A, Entius M, Goggins M, Yeo C, Kern S. 1999. Germline and somatic mutations of the STK11/LKB1 Peutz-Jeghers gene in pancreatic and biliary cancers. Am J Pathol 154:1835-1840.

Sugimura Y, Cunha GR, Donjacour AA. 1986. Morphogenesis of ductal networks in the mouse prostate. Biol Reprod 34:961-971.

Sun A, Tawfik O, Gayed B, Thrasher J, Hoestje S, Li C, Li B. 2007. Aberrant expression of SWI/SNF catalytic subunits BRG1/BRM is associated with tumor development and increased invasiveness in prostate cancers. Prostate 67:203-213.

Sun M, Wang G, Paciga J, Feldman R, Yuan Z, Ma X, Shelley S, Jove R, Tsichlis P, Nicosia S, Cheng J. 2001a. AKT1/PKBalpha kinase is frequently elevated in human cancers and its constitutive activation is required for oncogenic transformation in NIH3T3 cells. Am J Pathol 159:431–437.

Sun S, Rosenberg L, Wang X, Zhou Z, Yue P, Fu H, Khuri F. 2005. Activation of Akt and eIF4E survival pathways by rapamycin-mediated mammalian target of rapamycin inhibition. Cancer Res 65:7052-7058.

Sun TQ, Lu B, Feng JJ, Reinhard C, Jan YN, Fantl WJ, Williams LT. 2001b. PAR-1 is a Dishevelled-associated kinase and a positive regulator of Wnt signalling. Nat Cell Biol 3:628-636.

Suttie AW, Dinse GE, Nyska A, Moser GJ, Goldsworthy TL, Maronpot RR. 2005. An investigation of the effects of late-onset dietary restriction on prostate cancer development in the TRAMP mouse. Toxicol Pathol 33:386-397.

Suzuki A, Yamaguchi M, Ohteki Y, Sasaki T, Kaisho T, Kimura Y, Yoshida R, Wakeham A, Higuchi T, Fukumoto M, Subata T, Ohashi P, Koyasu S, Penninger J, Nakano T, Mak T. 2001. T-Cell specific loss of Pten leads to defects in central and peripheral tolerance. Immunity 14:523-534.

Taboga S, de-Souza R, dos-Santos D, Oliani S. 1999. Spontaneous germ cell death by apoptosis in epididymis of the adult bat Artibeus lituratus. Cytobios 99:39-45.

Tang D, Patrawala L, Calhoun T, Bhatia B, Choy G, Schneider-Broussard R, Jeter C. 2007 Prostate cancer stem/progenitor cells: identification, characterization, and implications. Mol Carcinog 46:1-14.

Taylor C. 2002. Src tyrosine kinase-induced loss of luteinizing hormone responsiveness is via a Ras-dependent, phosphatidylinositol-3-kinase independent pathway. Biol Reprod 67:789-794.

Terry S, Yang X, Chen M, Vacherot F, Buttyan R. 2006. Multifaceted interaction between the androgen and Wnt signaling pathways and the implication for prostate cancer. J Cell Biochem 99:402-410.

Thompson T, Southgate J, Kitchener G, Land H. 1989. Multistage carcinogenesis induced by ras and myc oncogenes in a reconstituted organ. Cell Commun Signal 56:917-930.

Thomson DM, Porter BB, Tall JH, Kim HJ, Barrow JR, Winder WW. 2007. Skeletal muscle and heart LKB1 deficiency causes decreased voluntary running and reduced muscle mitochondrial marker enzyme expression in mice. Am J Physiol Endocrinol Metab 292:E196-202.

Thorson P, Swanson P, Vollmer R, Humphrey P. 2003. Basal cell hyperplasia in the peripheral zone of the prostate. Mod Pathol 16:598-606.

Thorta A, Karajgikar M, Duan W, Gabril M, Chan F, Wong Y, Sakai H, Chin J, Moussa M, Xuan J. 2003. Mouse PSP94 expression is prostate tissue-specific as demonstrated by a comparison of multiple antibodies against recombinant proteins. J Cellular Biochem 88:999-1011.

Tianen M, Vaahtomeri K, Ylikorkala A, Makela T. 2002. Growth arrest by the LKB1 tumour suppressor: induction of p21(WAF1/CIP1). Hum Mol Genet 11:1497-1504.

Tokar E, Ancrile B, Cunha G, Webber M. 2005. Stem/progenitor and intermediate cell types and the origin of human prostate cancer. Differentiation 73:463-473.

Toyofuku T, Akamatsu Y, Zhang H, Kuzuya T, Tada M, Hori M. 2001. C-Src regulates the interaction between connexin-43 and ZO-1 in cardiac myocytes. J Biol Chem 270:1780-1788.

Tran C, Lin C, Yamashiro J, Reiter R. 2002. Prostate stem cell antigen is a marker of late intermediate prostate epithelial cells. Molecular Cancer Research 1:113-121.

Treiger B, Isaacs J. 1988. Expression of a transfected v-Harvey-ras oncogene in a Dunning rat prostate adenocarcinoma and the development of high metastatic ability. J Urol 140:1580-1586.

Trotman LC, Niki M, Dotan ZA, Koutcher JA, Cristofano AD, Xiao A, Khoo AS, Roy-Burman P, Greenberg NM, Dyke TV, Cordon-Cardo C, Pandolfi P. 2003. Pten dose dictates cancer progression in the prostate. PLoS Biol 1:E59.

Trotman LC, Pandolfi PP. 2003. PTEN and p53: who will get the upper hand? Cancer Cell 3:97-99.

Truica C, Byers S, Gelmann E. 2000. Beta-catenin affects androgen receptor transcriptional activity and ligand specificity. Cancer Res 60:4709-4713.

Tsujimura A, Fujita K, Komori K, Takao T, Miyagawa Y, Takada S, Matsumiya K, Nonomur N, Okuyama A. 2007. Prostatic stem cell marker identified by cDNA microarray in mouse. J Urol 178:686-691.

Tsujimura A, Kolikawa Y, Salm S, Takao T, Coetzee S, Moscatelli D, Shapiro E, Lepar H, Sun T, Wilson E. 2002. Proximal location of mouse prostate epitehlial stem cells: A model of prostatic homeostasis. J Cell Biol 157:1257-1265.

Tysnes B, Bjerkvig R. 2007. Cancer initiation and progression: involvement of stem cells and the microenvironment. Biochim Biophys Acta 1775:283-297.

Ueda T, Mawji N, Bruchovsky N, Sadar M. 2002. Ligand-independent activation of the androgen receptor by interleukin-6 and the role of steroid receptor coactivator-1 in prostate cancer cells. J Biol Chem 277:38087-38094.

Upadhyay S, Liu C, Chatterjee A, Hoque M, Kim M, Engles J, Westra W, Trink B, Ratovitski E, Sidransky D. 2006. LKB1/STK11 suppresses cyclooxygenase-2 induction and Cellular invasion through PEA3 in lung cancer Cancer Res 66:7870-7879.

Urist MJ, Di Como CJ, Lu M-L, Charytonowicz E, Verbel D, Crum CP, Ince TA, McKeon FD, Cordon-Cardo C. 2002. Loss of p63 Expression Is Associated with Tumor Progression in Bladder Cancer. Am J Pathol 161:1199-1206.

Uzgare A, Kaplan P, Greenberg N. 2003. Differential expression and/or activation of P38MAPK, erk1/2, and jnk during the initiation and progression of prostate cancer. Prostate 55:128-139.

Uzgare A, Xu Y, Isaacs J. 2004. In vitro culturing and characteristics of transit amplifying epithelial cells from human prostate tissue. J Cell Biochem 91:196-205.

Van-Der-Poel H, Hanrahan C, Zhang H, Simons J. 2003. Rapamycin induces smad activity in prostate cancer cell lines. Urol Res 30:380-386.

Van-Leenders G, Van-Balken B, Aalders T, Hulsberguen-van-de-kaa C, Ruiter D, Schalken J. 2002. Intermediate cells in normal and malignant prostate epithelium express c-MET: implications for prostate invasion. Prostate 51:98-107.

Veldscholte J, Berrevoets C, Brinkmann A, Grootegoed J, Mulder E. 1992. Anti-androgens and the mutated androgen receptor of LNCaP cells: differential effects on binding affinity, heat-shock protein interaction, and transcription activation. Biochemistry 31:2393-2399.

Verhagen A, Ramaekers F, Aalders T, Schaafsma H, Debruyne F, Schalken J. 1992. Colocalization of basal and luminal cell-type cytokeratins in human prostate cancer. Cancer Res 52:6182-6187.

Verras M, Sun Z. 2005. Beta-catenin is involved in insulin-like growth factor 1-mediated transactivation of the androgen receptor. Mol Endocrinol 19:391-398.

Verras M, Sun Z. 2006. Roles and regulation of Wnt signaling and beta-catenin in prostate cancer. Cancer Lett 237:22-32.

Voeller H, Truica C, Gelmann E. 1998. Beta-catenin mutations in human prostate cancer. Cancer Res 58:2520-2523.

Wang G, Ahmad K, Unger G, Slaton J, Ahmed K. 2006a. CK2 signaling in androgen-dependent and -independent prostate cancer. J Cellular Biochem 99:282-291.

Wang L, Lin H, Hu Y, Xie S, Yang L, Chang C. 2004a. Suppression of androgen receptor-mediated transactivation and cell growth by the glycogen synthase kinase 3 beta in prostate cells. J Biol Chem 279:32444-32452.

Wang S, Gao J, Lei Q, Rozengurt N, Pritchard C, Jiao J, Thomas GV, Li G, Roy-Burman P, Nelson PS, Liu X, Wu H. 2003. Prostate-specific deletion of the murine Pten tumor suppressor gene leads to metastatic prostate cancer. Cancer Cell 4:209-221.

Wang S, Garcia A, Wu M, Lawson D, Witte O, Wu H. 2006b. Pten deletion leads to the expansion of a prostatic stem/progenitor cell subpopulation and tumor initiation. Proc Natl Acad Sci U S A 103:1480-1485.

Wang X, Leow C, Zah J, Tang Z, Modrusan Z, Aguet M, deSauvage F, Gao W. 2006c. Notch signalling is required for normal prostatic epithelial cell proliferation and differentiation. Dev Biol 290:66-80.

Wang XD, Shou J, Wong P, French DM, Gao WQ. 2004b. Notch1-expressing cells are indispensable for prostatic branching morphogenesis during development

and re-growth following castration and androgen replacement. J Biol Chem 279:24733-24744.

Wang Y, Hayward S, Cao M, Thayer K, Cunha G. 2001. Cell differentiation lineage in the prostate. Differentiation 68:270-279.

Watabe T, Lin M, Ide H, Donjacour AA, Cunha GR, Witte ON, Reiter RE. 2002. Growth, regeneration, and tumorigenesis of the prostate activates the PSCA promoter. Proc Natl Acad Sci U S A 99:401-406.

Weber MJ, Gioeli D. 2004. Ras signaling in prostate cancer progression. J Cell Biochem 91:13-25.

Wechter W, Leipold D, Murray E, Quiggle D, McCracken J, Barrios R, Greenberg N. 2000. E-7869 (R-Flurbiprofen) inhibits progression of prostate cancer in the TRAMP model. Cancer Res 60:2203-2208.

Wei C, Amos CI, Rashid A, Sabripour M, Nations L, McGarrity TJ, Frazier ML. 2003. Correlation of staining for LKB1 and COX-2 in hamartomatous polyps and carcinomas from patients with Peutz-Jeghers syndrome. J Histochem Cytochem 51:1665-1672.

Wells A, Souto J, Solava J, Kassis J, Bailey K, Turner T. 2002. Luteinizing hormone releasing hormone agonist limits DU-145 prostate cancer growth by attenuating epidermal growth factor receptor signalling. Clin Cancer Res 8:1251-1257.

Westerman A, Wilson J. 1999. Peutz-Jeghers syndrome: risks of a hereditary condition. Scand J Gastroenterol Suppl 230:64-70.

Wielenga VJM, Smits R, Korinek V, Smit L, Kielman M, Fodde R, Clevers H, Pals ST. 1999. Expression of CD44 in APC and Tcf mutant mice implies regulation by the WNT pathway. Am. J. Pathol 154:515-523.

Willert K, Nusse R. 1998. Beta-catenin: a key mediator of Wnt signaling. Curr Opin Genet Dev 8:95-102.

Williamson E, Wolf I, O'Kelly J, Bose S, Tanosaki S, Koeffler H. 2006. BRCA1 and FOXA1 proteins coregulate the expression of the cell cycle-dependent kinase inhibitor p27(Kip1) Oncogene 25:1391-1399.

Wissmann C, Wild PJ, Kaiser S, Roepcke S, Stoehr R, Woenckhaus M, Kristiansen G, Hsieh JC, Hofstaedter F, Hartmann A, Knuechel R, Rosenthal A, Pilarsky C. 2003. WIF1, a component of the Wnt pathway, is down-regulated in prostate, breast, lung, and bladder cancer. J Pathol 201:204-212.

Wodarz A, Näthke I. 2007. Cell polarity in development and cancer. Nature Cell Biology 9:1016-1024.

Woods A, Dickerson K, Heath R, Hong S, Momcilovic M, Johnstone S, Carlson M, Carling D. 2005. Ca2+/calmodulin-dependent protein kinase kinase-beta acts upstream of AMP-activated protein kinase in mammalian cells. Cell Metab 2:21-33.

Woods A, Johnstone SR, Dickerson K, Leiper FC, Fryer LG, Neumann D, Schlattner U, Wallimann T, Carlson M, Carling D. 2003. LKB1 is the upstream kinase in the AMP-activated protein kinase cascade. Curr Biol 13:2004-2008.

Wright K, Wilson P, Morland S, Campbell I, Walsh M, Hurst T, Ward B, Cummings M, Chenevix-Trench G. 1999. Beta-catenin mutation and expression analysis in ovarian cancer, exon 3 mutations and nuclear translocation in 16% of endometrioid tumours. Int J Cancer 82:625-629.

Wu X, Wu J, Huang J, Powell WC, Zhang J, Matusik RJ, Sangiorgi FO, Maxson RE, Sucov HM, Roy-Burman P. 2001. Generation of a prostate epithelial cell-specific Cre transgenic mouse model for tissue-specific gene ablation. Mech Dev 101:61-69. .

Xie X, Luo Z, Slawin KM, Spencer DM. 2004. The EZC-prostate model: noninvasive prostate imaging in living mice. Mol Endocrinol 18:722-732.

Xin L, Lawson D, Witte O. 2005. The Sca-1 cell surface marker enriches for a prostate-regenerating cell sub-population that can initiate prostate tumourigenesis. PNAS 102:6942-6947.

Xu J, Meyers D, Freije D, Isaacs S, Wiley K, Nusskern D, Ewing C, Wilkens E, Bujnovszky P, Bova GS, Walsh P, Isaacs W, Schleutker J, Matikainen M, Tammela T, Visakorpi T, Kallioniemi OP, Berry R, Schaid D, French A, McDonnell S, Schroeder J, Blute M, Thibodeau S, Trent J, et al. 1998. Evidence for a prostate cancer susceptibility locus on the X chromosome. Nat Genet 20:175-179.

Xue L, Yang K, Newmark H, Lipkin M. 1997a. Induced hyperproliferation in epithelial cells of mouse prostate by a Western-style diet. Carcinogenesis 18:995-999.

Xue Y, Smedts F, Umbas R, Aalders TW, Debruyne FM, de la Rosette JJ, Schalken JA. 1997b. Changes in keratin expression during the development of benign prostatic hyperplasia. Eur Urol 32:332-338.

Xue Y, Verhofstad A, Lange W, Smedts F, Debruyne F, de la Rosette J, Schalken J. 1997c. Prostatic neuroendocrine cells have a unique keratin expression pattern and do not express Bcl-2: cell kinetic features of neuroendocrine cells in the human prostate. Am J Pathol 151:1759-1765.

Yang G, Timme T, Frolov A, Wheeler T, Thompson T. 2005. Combined c-Myc and caveolin-1 expression in human prostate cancer predicts prostate carcinoma progression. Cancer 103:1186-1194.

Yang X, Chen M, Terry S, Vacherot F, Bemis D, Capodice J, Kitajewski J, delaTaille A, Benson M, Guo Y, Buttyan R. 2006. Complex regulation of human androgen receptor expression by Wnt signaling in prostate cancer cells. Oncogene 25:3436-3444.

Yardy GW, Brewster SF. 2005. Wnt signalling and prostate cancer. Prostate Cancer Prostatic Dis 8:119-126.

Yin A, Miraglia S, Zanjani E, Almeida-Porada G, Ogawa M, Leary A, Olweus J, Kearney J, Buck D. 1997. AC133, a novel marker for human haematopoietic stem and progenitor cells. Blood 90:5002-5012.

Ylikorkala A, Rossi DJ, Korsisaari N, Luukko K, Alitalo K, Henkemeyer M, Makela TP. 2001. Vascular abnormalities and deregulation of VEGF in Lkb1-deficient mice. Science 293:1323-1326.

Yoo LI, Chung DC, Yuan J. 2002. LKB1--a master tumour suppressor of the small intestine and beyond. Nat Rev Cancer 2:529-535.

Yoshimoto M, Cunha I, Coudry R, Fonseca F, Torres C, Soares F, Squire J. 2007. FISH analysis of 107 prostate cancers shows that PTEN genomic deletion is associated with poor clinical outcome. Br J Cancer 97:678-685.

Yu X, Gupta A, Wang Y, Suzuki K, Mirosevich J, Orgebin-Crist M, Matusik R. 2005. Foxa1 and Foxa2 interact with the androgen receptor to regulate prostate and epididymal genes differentially. Ann N Y Acad Sci 1061:77-93.

Yuan H, Mao J, Li L. 1999. Suppresion of glycogen synthase kinase activity is not sufficient for leukemia enhancer factor-1 activation. J Biol Chem 274:30419-30423.

Zaichick V, Sviridova TV, Zaichick SV. 1997. Zinc in the human prostate gland: normal, hyperplastic and cancerous. Int Urol Nephrol 29:565-574.

Zeng P, Berger S. 2006. LKB1 is recruited to the p21/WAF1 promoter by p53 to mediate transcriptional activation. Cancer Res 66:10701-10708.

Zhang J, Lipinski R, Shaw A, Gipp J, Bushman W. 2007. Lack of demonstratable autocrine Hh Signalling in prostate cancer cell lines. J Urol 177:1179-1185.

Zhang L, Li J, Young L, Caplan M. 2006. AMP-activated protein kinase regulates the assembly of epithelial tight junctions. PNAS 103:17272-17277.

Zhang X, Lee C, Ng P, Rubin M, Shabsigh A, Buttyan R. 2000. Prostatic neoplasia in transgenic mice with prostate-directed overexpression of the c-myc oncoprotein. Prostate 43:278-285.

Zhang X, Podsypanina K, Huang S, Mohsin S, Chamness G, Hatsell S, Cowin P, Schiff R, Li Y. 2005. Estrogen receptor positivity in mammary tumors of Wnt-

1 transgenic mice is influenced by collaborating oncogenic mutations. Oncogene 24:4220-4231.

Zhou Z, Flesken-Nikitin A, Nikitin A. 2007. Prostate cancer associated with p53 and Rb deficiency arises from the stem/progenitor cell-enriched proximal region of prostatic ducts. Cancer Res 67:5683-5690.

Zhuang Z, Di G, Shen Z, Ding J, Shao Z. 2006. Enhanced expression of LKB1 in breast cancer cells attenuates angiogenesis, invasion, and metastatic potential. Mol Cancer Res 4:843-849.

Zitzmann M, Gromoll J, von Eckardstein A, Nieschlag E. 2003. The CAG repeat polymorphism in the androgen receptor gene modulates body fat mass and serum concentrations of leptin and insulin in men. Diabetologia 46:31-39.

Zou M, Hou X, Shi C, Kirkpatrick S, Liu F, Goldman M, Cohen R. 2003. Activation of 5'-AMP-activated kinase is mediated through c-Src and phoshoinositide 3-kinase activity during hypoxia-reoxygeneation of bovine aortic endothelial cells. Role of peroxynitrite. J Biol Chem 278:34003-34010.

# Appendix 1: Laboratory reagents, enzymes and suppliers

| Product | Supplier |
|---|---|
| Proteinase K (14-22 mg/ml) | #03115844001, Roche |
| Cell lysis solution | Gentra |
| Protein precipitation buffer | Gentra |
| Nuclease-free water | Sigma |
| PicTaq | Cancer Research UK |
| 25mM $MgCl_2$ | Sigma |
| 10x Platinum Taq buffer | Invitrogen |
| Platinum Taq | #10966-034, Invitrogen |
| 5x GoTaq Flexi Buffer | #M890A, Promega |
| GoTaq | #M830B, Promega |
| 25 mM dNTPs | Sigma |
| 10% formalin | Sigma |
| 10x citrate buffer (pH 6.0) | #AP-9003-500, Labvision |
| Standard Vectastain Kit | #PK6100, Vectastain |
| Rabbit Envision Kit | #K4010, DAKO |
| Mouse Envision Kit | #K4006, DAKO |
| Diaminobenzidine (DAB) kit | #K3467, DAKO |
| Invitrogen Superscript II Kit | #18064071, Invitrogen |
| RNA Later solution | #R0901, Sigma |
| TRIzol reagent | #15596-026, Invitrogen |
| DNase TURBO kit | #1907, Ambion |
| DyNAmo HS SYBR Green qPCR kit | #F-410L, GRI |
| Polyethylene naphthol membrane-coated slides | #415101-4401-000, PALM |
| QIAamp DNA Micro Kit | #56304, Qiagen |
| Adhesive capped tubes (0.2 ml) | #415101-4400-245, PALM |
| Genomiphi DNA amplification kit | #25-6600-00, Amersham |
| DIG Labelling kit | #BM 1175025, Roche |
| RNA polymerase T3, 20 units/µl | #1031163, Roche |
| RNA polymerase T7, 20 units/µl | #881767, Roche |
| DIG RNA Labelling mix 10x solution | #1277073, Roche |
| RNase inhibitor, 10-50 units/µl | #799017, Roche |
| Anti-digoxigenin Fab fragments | #11327723, Roche |
| DNase1, RNase free 20-50 units/µl | #776785, Roche |
| Paraformaldehyde | #P6148, Sigma |
| BM purple substrate | #11442074001, Roche |
| 20x SSC (pH 5) | #S6639, Sigma |
| Formamide | #47671, Sigma |
| Heparin | #H4784, Sigma |
| Calf liver tRNA | #R4752-100N, Sigma |
| Triethanolamine hydrochloride | #T1377, Sigma |

# Appendix 2: Publications

Research Article

# *Lkb1* Deficiency Causes Prostate Neoplasia in the Mouse

Helen B. Pearson,[1] Afshan McCarthy,[2] Christopher M.P. Collins,[3] Alan Ashworth,[2] and Alan R. Clarke[1]

[1]Cardiff University, School of Biosciences, Cardiff, Wales, United Kingdom; [2]Breakthrough Breast Cancer Research Center, The Institute of Cancer Research, London, United Kingdom; and [3]Bristol Royal Infirmary, Department of Pathology, Bristol, United Kingdom

## Abstract

**Mutation of *LKB1* is the key molecular event underlying Peutz-Jeghers syndrome, a dominantly inherited condition characterized by a predisposition to a range of malignancies, including those of the reproductive system. We report here the use of a *Cre-LoxP* strategy to directly address the role of Lkb1 in prostate neoplasia. Recombination of a *LoxP*-flanked *Lkb1* allele within all four murine prostate lobes was mediated by spontaneous activation of a *p450 CYP1A1*-driven *Cre recombinase* transgene (termed *AhCre*). Homozygous mutation of *Lkb1* in males expressing *AhCre* reduced longevity, with 100% manifesting atypical hyperplasia and 83% developing prostate intraepithelial neoplasia (PIN) of the anterior prostate within 2 to 4 months. We also observed focal hyperplasia of the dorsolateral and ventral lobes (61% and 56% incidence, respectively), bulbourethral gland cysts associated with atypical hyperplasia (100% incidence), hyperplasia of the urethra (39% incidence), and seminal vesicle squamous metaplasia (11% incidence). PIN foci overexpressed nuclear β-catenin, p-Gsk3β, and downstream Wnt targets. Immunohistochemical analysis of foci also showed a reduction in Pten activation and up-regulation of both p-PDK1 (an AMPK kinase) and phosphorylated Akt. Our data are therefore consistent with deregulation of Wnt and phosphoinositide 3-kinase/Akt signaling cascades after loss of Lkb1 function. For the first time, this model establishes a link between the tumor suppressor Lkb1 and prostate neoplasia, highlighting a tumor suppressive role within the mouse and raising the possibility of a similar association in the human.** [Cancer Res 2008;68(7):1–10]

## Introduction

Prostate cancer is the second most common malignancy next to lung cancer in men (1). A central limitation to studying prostate cancer has been the lack of suitable animal models that recapitulate all the stages of human disease progression. This has at least in part been alleviated by the generation of a range of mouse strains with prostate phenotypes, including those mutant for RB, PTEN, AR, AKT, and, more recently, β-catenin (2). However, it remains of paramount importance to develop novel models of prostate cancer to further our understanding of the molecular mechanisms and genetic events underlying prostate cancer.

LKB1 encodes a serine-threonine kinase that was first identified as a gene whose multiple germ line mutations abrogate enzymatic function and are associated with familial Peutz-Jeghers syndrome (PJS; ref. 3). The disorder is characterized by melanin deposits on the buccal mucosa, lips, and digits and the risk of intestinal hamartomas and extraintestinal cancers, such as stomach, pancreas, thyroid, and those of the reproductive organs is at least 10-fold higher than the general population (4). The molecular mechanisms underlying this enhanced tumor predisposition remain to be fully elucidated, but LKB1 has been implicated in the regulation of multiple pathways associated with tumor prevention (3–7). These include chromatin remodeling, angiogenesis, p53-dependent apoptosis, cell cycle arrest, energy metabolism, fatty acid biosynthesis, Wnt signaling, proliferation, polarity, and differentiation (4, 8–11). Recently, somatic deletion of *Lkb1* has been linked to lung tumorigenesis and mutation screening of human lung cancer patients revealed *LKB1* inactivation is a common event in lung adenocarcinomas (34%) and squamous cell carcinomas (19%), further implicating Lkb1 as a tumor suppressor (12). In addition, somatic mutation of *Lkb1* has been reported in pancreatic and biliary cancers (13), as well as malignant melanomas (14).

LKB1 is a member of the Snf1 family of kinases and has been shown to phosphorylate at least 13 members of the AMPK subfamily, many of which play a fundamental role in metabolic regulation (7). In particular, Lkb1 can activate AMPK by phosphorylating $Thr^{172}$ within the T-loop (11, 15). This leads to mTOR inhibition via TSC2 (tuberin) to suppress cell growth and proliferation (16), as well as down-regulating fatty acid and cholesterol biosynthesis and enhancing glucose uptake and glycolysis (17, 18). However, to date, there is little published data to support a direct role for AMPK deregulation in prostate tumorigenesis (19).

With respect to the Wnt pathway, it has been reported that loss of function of LKB1 elevates Wnt signaling via its regulation of MARK3 (Par1A, cTAK). In the absence of Lkb1, Par1A is unphosphorylated and available to participate in the Wnt cascade, instigating translocation of β-catenin into the nucleus where it instructs transcription of target genes to stimulate proliferation (8). This gives a direct mechanism, whereby mutation of LKB1 may lead to activated Wnt signaling. The potential relevance of such deregulation to prostate cancer has been indicated through studies of human prostate cancer that have identified both mutations in *β-catenin* and aberrant β-catenin expression (20). Further evidence in support of such a link is derived from Cre-Lox–based models, which develop high-grade PIN and squamous metaplasia after Cre-mediated activation of a constitutive β-catenin mutation (20, 21). Most recently, the rat probasin promoter (*PB-Cre4*) has been used to drive *Cre*-mediated deletion of *Apc* in the prostate, and this has been shown to predispose to adenocarcinoma of the prostate (22).

LKB1 has also been shown to interact with the tumor suppressor PTEN and thereby the phosphoinositide 3-kinase (PI3K)/Akt and mTOR pathways. The most direct evidence for this interaction was

**Requests for reprints:** Alan Clarke, University of Cardiff, Museum Avenue, Cardiff, South Glamorgan, CF10 3US, United Kingdom. Phone: 44-0-2920-879115; Fax: 44-02920 874116; E-mail: Clarkear@cardifff.ac.uk.



doi:10.1158/0008-5472.CAN-07-5169

derived from *in vitro* studies that have shown LKB1 to bind and phosphorylate PTEN (3, 23). This interaction has been speculated to result in PTEN stabilization and activation (23). Further indirect evidence for an interaction comes from the observation that ~70% of PJS patients also harbor mutation or display loss of at least one allele of *PTEN* (24). Any potential interaction between PTEN and LKB1 is of particular relevance to prostate neoplasia, as PTEN is well established as a tumor suppressor within this tissue. In humans, *PTEN* has been reported to be frequently deleted in prostate adenocarcinomas (24). In mice, homozygous inactivation of *Pten* leads to embryonic lethality (25), whereas heterozygosity predisposes to prostate carcinoma within 9 to 16 months (50%). This phenotype can be accelerated by additional homozygous deletion of *Cdkn1b*, with carcinomas occurring within 3 months on this background (26). Prostate-specific deletion of *Pten* has also been achieved using the *PB-Cre4* construct to drive recombination of a LoxP-flanked *Pten* allele. This model recapitulates the full spectrum of human prostate cancer progression from hyperplasia, low-grade PIN, high-grade PIN, carcinoma, and metastasis (27). Finally, it has also been argued that progressive depletion of *Pten* levels correlates with a more aggressive prostate phenotype and elevated Akt signaling (24), frequently associated with human prostate cancer (28).

There is currently little in the literature to directly link *LKB1* mutation with human or murine prostate neoplasia. However, the fact that somatic LKB1 mutations have been observed in human lung cancer and the observation of Lkb1-driven lung tumorigenesis in the mouse suggests that Lkb1 may have a broad tumor suppressive role in epithelial tissues (12).

In the prostate, LKB1 protein has been detected in the cytoplasm of luminal cells using immunohistochemistry (29) and low levels of *Lkb1* mRNA are detectable (30). Sequencing studies have reported that *LKB1* is mutated in one of five sequenced human prostate carcinoma cell lines, with a frame-shift deletion (p.K178fs*86) within the kinase domain of DU145 cells (31). Further support for a tumor suppressive role for Lkb1 comes from a whole-genome scan study that identified an association between chromosome segments 19q12-q13.11 and prostate cancer aggressiveness (32). The chromosome segment 19p13.3 harbors the LKB1 tumor suppressor gene and also contains members of the kalikrein family (such as KLK3, PSA) and the *MUC16* gene that encodes the ovarian cancer antigen CA125 (32). Deletions, amplifications, and structural rearrangements of chromosome 19 have also been reported in a variety of tumors, including pancreatic adenocarcinomas, both benign and anaplastic thyroid tumors and stomach cancers (reviewed in ref. 32). Interestingly, prostate cancer has also been anecdotally reported in a PJS patient (66 years old) after the development of colon cancer (6). The presence of prostate cancer in PJS patients is not a frequent occurrence, possibly as a consequence of the normal age of onset of disease. Prostate cancer is typically diagnosed in the seventh decade of life, whereas PJS patients have an average life span of 57 years (4).

Together with the biochemical evidence of pathway interaction, these observations suggest a potential role for deregulated LKB1 signaling in prostate cancer. To directly assess this possibility *in vivo*, we have characterized the phenotype of mice deficient for *Lkb1* within the prostate. Mice engineered to carry floxed (fl) *Lkb1* alleles ($Lkb1^{fl/fl}$; ref. 33), where the kinase domain has been replaced by a cDNA cassette encoding exons 5 to 7, enabled *Lkb1* deletion within the prostate by using the *AhCre* promoter to drive expression of *Cre* recombinase (34). By applying this strategy, we show that loss of *Lkb1* predisposes to atypical hyperplasia (AH) that progressed to PIN in the anterior lobe and focal hyperplasia associated with nuclear atypia of the dorsolateral and ventral lobes within 2 to 4 months. Within PIN lesions, we observe elevation of both the PI3K/Akt and Wnt signaling pathways, supporting the concept that loss of *Lkb1* promotes neoplasia through deregulation of these pathways.

## Materials and Methods

**Generation of *AhCre*$^+$*Lkb1*$^{fl/fl}$ mice.** All animal studies and breeding were carried out under a UK Home Office project license. $Lkb1^{fl/fl}$ mice and the *AhCre* transgenic mice have been described previously (33, 34). The *Lkb1* and *AhCre* alleles were backcrossed six times onto a C57BL/6 background. Mice containing one wild-type *Lkb1* allele and one floxed allele ($Lkb1^{+/fl}$) were mated with *AhCre*-positive mice carrying the *Rosa26* reporter allele (35). The *Lkb1* heterozygous progeny from this cross was intercrossed to generate *AhCre*$^+$$Lkb1^{fl/fl}$ mice (as $Lkb1^{fl/fl}$ males are sterile; ref. 33). Cohorts were aged, and the male genitourinary (GU) tract was harvested when mice developed symptoms. Mice were genotyped by PCR using DNA isolated from tail biopsies. The wild-type and LoxP-flanked *Lkb1* alleles were detected using the primers *Lkb1fwd*, 5′-GATTTCCGCCAGCTGATTGA-3′ and *Lkb1rev*, 3′-AGTGTGACCCCAGCTGACCA-5′ producing 320-bp (wild-type) and 280-bp (floxed) PCR fragments. Recombined *Lkb1* was detected using *Lkb1rec1* 5′-CAGAATCACATCCCCTGGTT-3′ and *Lkb1rec2*, 3′-TTCCCCTCCTCCTGCTAGAT-5′, producing a PCR product of 500 bp. *Cre recombinase* activity was induced in control mice by four i.p. injections of 80 mg/kg β-naphthoflavone within 24 h. Recombined liver tissue was harvested 7 d later.

**β-Galactosidase analysis.** To determine the pattern of recombination at the *Rosa26R* reporter locus, sectioned material was analyzed as previously described, except X-gal staining was reduced to 1 h at 37°C (34).

**Tissue isolation.** Tissue was harvested as described previously (36) and fixed for no longer than 24 h in 10% neutral buffered formaldehyde at 4°C before being embedded in paraffin and sectioned at 5 μm. Frozen sections were prepared by snap-freezing in liquid nitrogen, embedded in OCT on dry ice, and sectioned at 10 μm.

**Histology, immunohistochemistry, and immunofluorescence.** For histology, sections were stained with H&E. For immunohistochemistry, antigen retrieval was performed by incubating the slides in 1× citrate buffer (pH 6.0) in the microwave on full power for 15 min, and endogenous peroxidase activity was inactivated in a solution containing 1.5% $H_2O_2$ in deionized water. Detection and visualization was carried out using the 3,3′-diaminobenzidine chromagen (DAKO Cytomation) according to the manufacturer's protocol. Images were taken at 40× magnification using "AnalySIS" software (Olympus Soft Imaging System GMBH)", and scale bars were added to represent 50 μm. Control slides known to be positive for each antibody were incorporated. Primary antibodies were obtained from the following sources: anti-androgen receptor 1:100 dilution (Lab Vision Corporation), anti-β-catenin 1:50 dilution (Transduction Laboratories), CD44 1:50 dilution (PharMingen), anti-Foxa1 1:800 dilution (Clone 2F83, Seven Hills Bioreagents), anti-pGsk3β ($Ser^9$) 1:50 dilution (Cell Signaling Technology), anti-Keratin-5 1:1000 dilution (Covance), anti-Ki-67 1:200 dilution (Vector Laboratories), anti-p63 1:50 dilution (Lab Vision Corporation), anti-p-PTEN ($Ser^{380}$/$Thr^{382/383}$) 1:25 dilution (Cell Signaling Technology), anti-PTEN 1:100 dilution (Cell Signaling Technology), anti-p-AKT ($Ser^{473}$) 1:50 dilution (Cell Signaling Technology), anti-PDK1 ($Ser^{241}$) 1:50 dilution (Abcam), anti-Keratin-18 1:20 dilution (Progen), anti-p-AMPK ($Thr^{172}$) 1:50 dilution (Cell Signaling Technology), anti-p-mTOR ($Ser^{2448}$) 1:100 dilution (Cell Signaling Technology), anti-p-p70-S6K ($Thr^{421}$/$Ser^{424}$) 1:100 dilution (Cell signaling Technology), and anti-p-S6 ribosomal protein (p-Rps6; $Ser^{240/244}$) 1:100 dilution (Cell Signaling Technology).

For immunofluorescence, the frozen sections were treated with pepsin solution (Zymed) and incubated with the primary rabbit polyclonal anti-zona occludens 1 (ZO-1) antibody 1:20 dilution (Zymed). The primary was detected using the AlexaFluor-488 Nanogold Fab fragment of goat anti-rabbit

IgG (Molecular Probes) 1:200 dilution. Slides were mounted with Vectashield HardSet + 4′,6-diamidino-2-phenylindole mounting medium (Vector Laboratories), and fluorescence was detected using the *Leica TCS SP2 AOBS* confocal microscope.

***In situ* hybridization.** The Qiagen midi-prep kit was used to produce large-scale preparation of the *Lkb1* insert, an *Lkb1* full-length cDNA clone inserted in the *pYX-Asc* vector (IRAVp968E05123D, RZPD). Templates were prepared by linearization with *Eco*R1 or *Not*1 (Promega); DNA phenol chloroform was extracted, and ethanol was precipitated. The plasmid sequence was checked by automated sequencing, confirming 100% identity of the *Lkb1* clone with the National Center for Biotechnology Information Sequence (accession number BC052379). Anti-sense and sense RNA probes were then obtained by *in vitro* transcription using T3 and T7 RNA polymerases (Roche) and labeled using the DIG RNA labeling kit (BM 1175025, Roche). *In situ* hybridization was carried out as described previously on 10% formalin-fixed paraffin-embedded sections (37). Briefly, sections were fixed in 4% paraformaldehyde at 4°C for 15 min, treated with proteinase K (20 mg/mL), and hybridized with the probes overnight at 65°C. The sections were washed at 65°C and adsorbed with alkaline phosphatase-conjugated anti-DIG antibody (Roche) overnight at 4°C. Alkaline phosphatase activity was detected by using BM purple AP solution (Roche).

**Laser capture microdissection and DNA isolation and amplification.** Frozen tissue was sectioned (at 15–20 μm) onto polyethylene naphthol membrane-coated glass slides (PALM Microlaser Technologies) and lightly stained with 1% cresyl violet acetate. Laser capture microdissection (LCMD) was performed immediately and did not exceed 30 min. DNA was isolated with the QIAamp DNA microkit (Qiagen) and amplified using the Genomiphi DNA amplification kit (Amersham). PCR reactions were performed in the log phase of amplification using 100 ng of LCMD–amplified DNA in a 50-μL reaction.

## Results

**AhCre$^+$Lkb1$^{fl/fl}$mice have a reduced life span.** *AhCre$^+$* mice were intercrossed with mice carrying a LoxP-flanked *Lkb1* allele and the *Rosa26* reporter allele. Cohorts of *wild-type* (*AhCre$^+$Lkb1$^{+/+}$*), *AhCre$^+$Lkb1$^{+/fl}$* *AhCre$^-$Lkb1$^{fl/fl}$*, and *AhCre$^+$Lkb1$^{fl/fl}$* mice were generated and aged. Each cohort contained a minimum of 20 males. Animals were then monitored for signs of illness and killed when they became symptomatic of disease (Fig. 1*A*). *Wild-type*, *AhCre$^+$Lkb1$^{+/fl}$*, and *AhCre$^-$Lkb1$^{fl/fl}$* cohorts showed average survival times exceeding 450 days and did not significantly differ from each other ($\chi^2$ test). However, all *AhCre$^+$Lkb1$^{fl/fl}$* mice became ill by 200 d, with a significantly reduced average survival of 83 d compared with *wild-type* ($P < 0.0001$, $\chi^2 = 39.85$).

***AhCre$^+$Lkb1$^{fl/fl}$* mice develop multiple GU phenotypes, including *PIN*.** Histologic analysis of the GU tract was performed in accordance with the consensus report from the Bar Harbor meeting of the mouse models of human cancer consortium prostate pathology committee (36). No gross phenotype was observed in *wild-type* ($n = 21$), *AhCre$^+$Lkb1$^{+/fl}$* ($n = 18$), and *AhCre$^-$Lkb1$^{fl/fl}$* ($n = 19$) mice, whereas the *AhCre$^+$Lkb1$^{fl/fl}$* cohort ($n = 20$) was predisposed to a number of GU phenotypes.

The anterior prostate from *AhCre$^+$Lkb1$^{fl/fl}$* mice between 2 to 4 months of age revealed atypical hyperplastic foci (100% incidence) and progression to prostate neoplasia predominantly in the proximal region of the duct (Fig. 2*A*). PIN was observed as early as 8 weeks when mice became sick (83% incidence). Within these lesions, solid and cribriform intraluminal proliferation of markedly atypical epithelial cells was accompanied by cytologic (nuclear) atypia, such as nuclear enlargement, pleomorphism, chromatin abnormalities, and an increased prominence of nucleoli, along with apparent focal rosetting that contained mitotic bodies (38). This process was also coupled to thickened stroma surrounding the acini and scattered interstitial infiltrate of lymphocytes and plasma cells. Sparse lymphocytes were also observed within some AH and PIN lesions and in severe cases obstructing prostate acini, resulting in gross tubular dilation. Dorsolateral and ventral lobes displayed a less severe phenotype, where cells exhibited nuclear atypia associated with focal epithelial hyperplasia with 61% and 56% incidence, respectively (Fig. 2*B*).

In addition to PIN, *AhCre$^+$Lkb1$^{fl/fl}$* mice displayed other GU phenotypes. The cohort could be identified visually from 6 to 8 weeks of age because 100% of the mice developed swellings at the base of the tail. Histologic analysis from this region revealed bulbourethral gland (BUG) cysts associated with atypical hyperplasia (Fig. 2*C*). The acinar mucosal epithelium of these cysts was characterized by a loss of cell polarity and was composed primarily of ductal cells, consistent with reduced secretory function indicative of the depleted foamy cytoplasm, similar to an Nkx3.1 deficiency (39, 40). The presence of interstitial, AH, and PIN inflammatory cells is probably linked to disruption of the cystic BUGs. It is unlikely that the inflammation predisposes to the prostate phenotype, because lesions were not regenerative. We also identified urethral gland hyperplasia in 39% of *AhCre$^+$Lkb1$^{fl/fl}$* mice (Fig. 2*Di,ii*). Nodular hyperplasia of the membranous urethra transitional epithelium (UGH) within the lamina propria and a predisposition to cytologic atypia was apparent. There were also two cases (11%) of seminal vesicle squamous metaplasia (SV SqM; Fig. 2*Diii-iv*). Interestingly, somatic mutation of *Lkb1* in the lung has been shown to predispose to squamous metaplasia (12). Finally, all *Lkb1$^{fl/fl}$* mice were sterile, correlating with previous reports (33). PIN is not a likely cause of our observed reduced longevity. Health of the *AhCre$^+$Lkb1$^{fl/fl}$* male cohort deteriorated, owing to a combination of phenotypes. These include the development of both cystic BUGs (susceptible to rupture) and subsequent infection

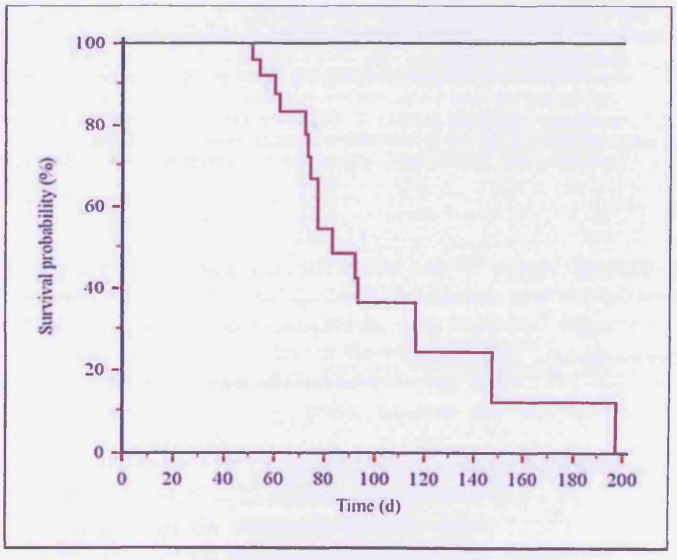


**Figure 1.** *AhCre$^+$Lkb1$^{fl/fl}$* male mice display reduced longevity. Kaplan-Meier plot of the *AhCre$^+$Lkb1$^{+/+}$* ($n = 26$), *AhCre$^+$Lkb1$^{fl/+}$* ($n = 41$), *AhCre$^-$Lkb1$^{fl/fl}$* ($n = 20$) cohorts were all represented in green, and *AhCre$^+$Lkb1$^{fl/fl}$* mice ($n = 26$) were illustrated in purple. *AhCre$^+$Lkb1$^{fl/fl}$* mice show decreased longevity, where 100% of the cohort did not survive past 200 d. $\chi^2$ tests confirmed *AhCre$^+$Lkb1$^{fl/fl}$* mice exhibit a significantly reduced average survival of 83 d compared with *wild-type* ($P < 0.0001$, $\chi^2 = 39.85$), *AhCre$^+$Lkb1$^{+/fl}$* ($P < 0.0001$, $\chi^2 = 59.01$), and *AhCre$^-$Lkb1$^{fl/fl}$* ($P < 0.0001$, $\chi^2 = 31.97$) cohorts.

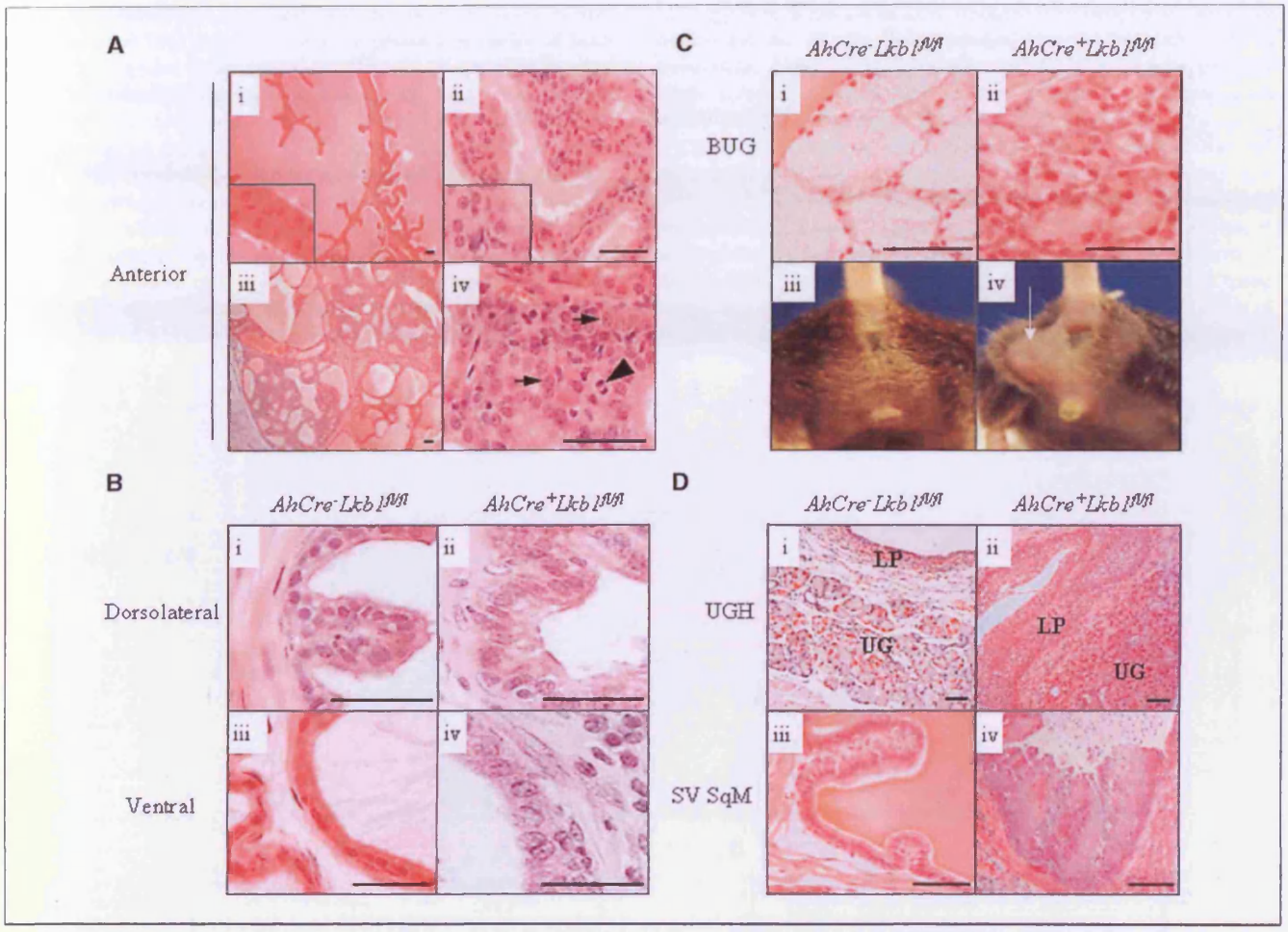


Figure 2. *AhCre*-mediated deletion of *Lkb1* predisposes to multiple GU phenotypes, including PIN. Histologic analysis of H&E sections from $AhCre^{-}Lkb1^{fl/fl}$ and $AhCre^{+}Lkb1^{fl/fl}$ cohorts aged 2 to 7 mo. *A*, $AhCre^{-}Lkb1^{fl/fl}$ anterior prostate developed normally (*i*). $AhCre^{+}Lkb1^{fl/fl}$ anterior prostate developed atypical hyperplasia (*ii*), which progressed to PIN and showed solid and cribriform patterned lesions (*iii*). High power magnification reveals mitotic cells present (*arrow heads*) and nuclear atypia (*arrows*), characteristic of PIN (*iv*). *B*, $AhCre^{+}Lkb1^{fl/fl}$ dorsolateral and ventral prostate lobes exhibited low-grade hyperplasia in association with nuclear atypia. *C*, the BUG displayed aberrant ductal architecture and chronic infection, suggesting cystic hyperplasia in $AhCre^{+}Lkb1^{fl/fl}$ mice compared with control cohorts (*i–ii*), which were identified by swellings near the base of the tail that developed between 6 and 8 wk (*iii–iv*). *D*, urethral gland and transitional epithelial hyperplasia developed in *Lkb1* mutants, where the lamina propria (*LP*) and urethral glands (*UG*) seem to have proliferated (*i* and *ii*). SV SqM was also observed in $AhCre^{+}Lkb1^{fl/fl}$ mice (*iii* and *iv*). Images were photographed at 20× magnification (low power) or 40× magnification (high power), and scale bars represent 50 μm.

of the GU tract. We assume these other phenotypes prevent progression of PIN to more advanced stages of prostate cancer, such as adenocarcinoma and metastasis. The fact that the $AhCre^{+}Lkb1^{fl/fl}$ lesions are not regenerative and also that not all PIN lesions were associated with inflammation strongly suggests that infection does not drive the development of PIN in this model.

**The AhCre transgene mediates recombination in the GU.** The observation of a GU phenotype in the $AhCre^{+}Lkb1^{fl/fl}$ mice implied recombination was occurring within these tissues, with subsequent loss of Lkb1 function. To characterize this pattern, we used mice bearing both the *AhCre* transgene and the Rosa26R reporter locus (35). Using this approach, *AhCre*-mediated excision, as reported by LacZ expression, was observed in all four lobes of the prostate and in a mosaic pattern in the urethral glands (Fig. 3*A*). Further LacZ analysis revealed that uninduced *AhCre*-mediated recombination also occurred in the kidney (41), as well as in the BUG, seminal vesicle, testis, epididymis, and vas deferens (not shown). Histologic analysis of the kidney from the $AhCre^{+}Lkb1^{fl/fl}$ cohort determined no abnormalities, whereas the testis, epididymis, and vas deferens showed male hypospermatogenesis and aspermia, respectively. Interestingly, *Lkb1* expression in the testis of $Lkb1^{fl/fl}$ hypomorphic male mice is dramatically reduced in the testis. The common 50-kDa isoform is 10-fold lower, whereas the 48-kDa form is completely absent (33).

**Recombination of the Lkb1 occurs within the GU and is associated with PIN.** To confirm that the Lkb1 kinase domain had been deleted in the neoplastic prostate tissue, LCMD and PCR amplification of extracted DNA samples was carried out. This approach was taken as insufficient tissue was available for Western blots and immunohistochemistry using anti-Lkb1 antibodies did not detect a product in control tissue and was therefore inappropriate to show loss of function. For PCR amplification, positive controls were derived from $AhCre^{+}Lkb1^{fl/fl}$ mice which had been exposed to β-naphthoflavone. This protocol delivers near

100% recombination of the target allele in the liver. Laser capture microdissected DNA from the anterior prostate epithelia of both normal (N) regions from *AhCre⁺Lkb1$^{fl/fl}$* and *AhCre⁻Lkb1$^{fl/fl}$* mice served as a negative control for a PCR specific for the recombined *Lkb1* allele (Fig. 3*B*). Semiquantitative densitometry of PIN in the anterior prostate from *AhCre⁺Lkb1$^{fl/fl}$* mice showed 64% recombination (when compared with fully recombined liver controls). This correlated with a reduction in the level of the unrecombined LoxP-flanked *Lkb1* allele. The fact that recombination was below 100% presumably reflects the observed stromal content in the PIN lesions. These observations establish that recombination of the LoxP-flanked *Lkb1* allele is associated with PIN, but cannot discriminate between loss of function and haploinsufficiency of *Lkb1*.

To confirm depletion of *Lkb1* transcripts in neoplastic tissue, we performed an *in situ* hybridisation specific for *Lkb1* mRNA transcripts. *Lkb1* mRNA was detected in all *wild-type* prostate lobes (ventral prostate not shown) but was not present in *AhCre⁺Lkb1$^{fl/fl}$* mice (Fig. 3*C*).

**Characterization of Lkb1-deficient PIN.** To characterize the prostate lesions at a molecular level, immunohistochemistry was performed. The proliferation marker Ki-67 was rarely expressed in control (*AhCre⁻Lkb1$^{fl/fl}$*) anterior prostate epithelium; however, it was significantly elevated in epithelial cells throughout the acini of *AhCre⁺Lkb1$^{fl/fl}$* mice (Fig. 4*A*). Basal cells were detected using F4
antibodies against p63 and Keratin-5 in the epithelial lining of anterior acini, indicating a marked accumulation and clustering of

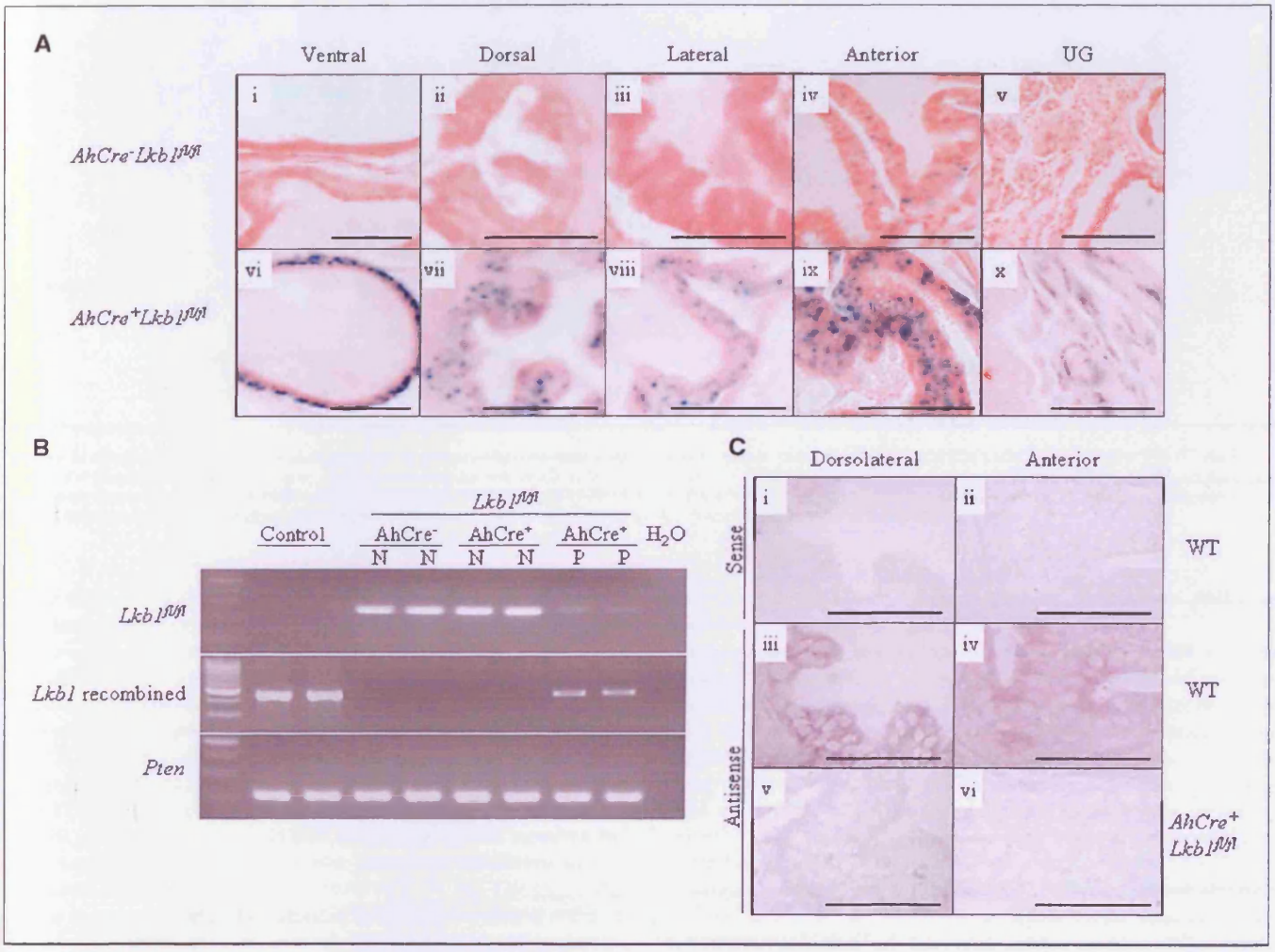


**Figure 3.** Recombination of *Lkb1* occurs within the GU and is associated with PIN. *A*, tissues from adult transgenic mice (ages, 6 mo) were harvested for the detection of Cre recombinase activity using X-gal staining (*blue stain*). Cross-sections of the four individual lobes of the murine prostate (ventral, dorsal, lateral, and anterior) and the urethral glands for *AhCre⁻Lkb1$^{fl/fl}$* control (*i–v*) and *AhCre⁺Lkb1$^{fl/fl}$* (*vi–x*) mice. Recombination events were apparent in *AhCre⁺* tissue after 1 h incubation with the X-gal solution, whereas controls were negative. Some punctate staining was observed in the *AhCre⁻Lkb1$^{fl/fl}$* anterior prostate, which is attributable to endogenous β-lactamase activity (*iv*). *B*, using LCMD, DNA was isolated from anterior prostate lobes of *AhCre⁻Lkb1$^{fl/fl}$* ($n = 3$) and *AhCre⁺Lkb1$^{fl/fl}$* mice ($n = 3$) and underwent PCR analysis. DNA isolated from induced liver tissue from *AhCre⁺Lkb1$^{fl/fl}$* mice was used as a positive control (near 100% recombination). The top gel represents the unrecombined LoxP-flanked *Lkb1* allele (280 bp), revealing none in the positive control, 100% presence in *AhCre⁻Lkb1$^{fl/fl}$* and *AhCre⁺Lkb1$^{fl/fl}$* normal (*N*) samples, and a reduced level of expression in *AhCre⁺Lkb1$^{fl/fl}$* PIN lesions (*P*). The middle gel refers to *Lkb1* recombined alleles (500 bp), confirming the positive control as ~100% recombined and the *AhCre⁺Lkb1$^{fl/fl}$* PIN samples partly recombined. Densitometry determined ~64% of *AhCre⁺Lkb1$^{fl/fl}$* PIN is recombined. *AhCre⁻Lkb1$^{fl/fl}$* anterior prostate served as a negative control, and the bottom gel depicts *Pten*, used as a loading control (230 bp). *C, in situ* hybridization to detect *Lkb1* mRNA in *wild-type* dorsolateral and anterior prostate lobes determined no unspecific binding using the sense probe (*i* and *ii*), whereas the antisense probe revealed *Lkb1* is expressed in *wild-type* prostate epithelia (*iii* and *iv*). *AhCre⁺Lkb1$^{fl/fl}$* dorsolateral and anterior prostate lesions show reduced *Lkb1* mRNA transcript levels (*v* and *vi*). Images were taken at 40× magnification, and scale bars represent 50 μm.

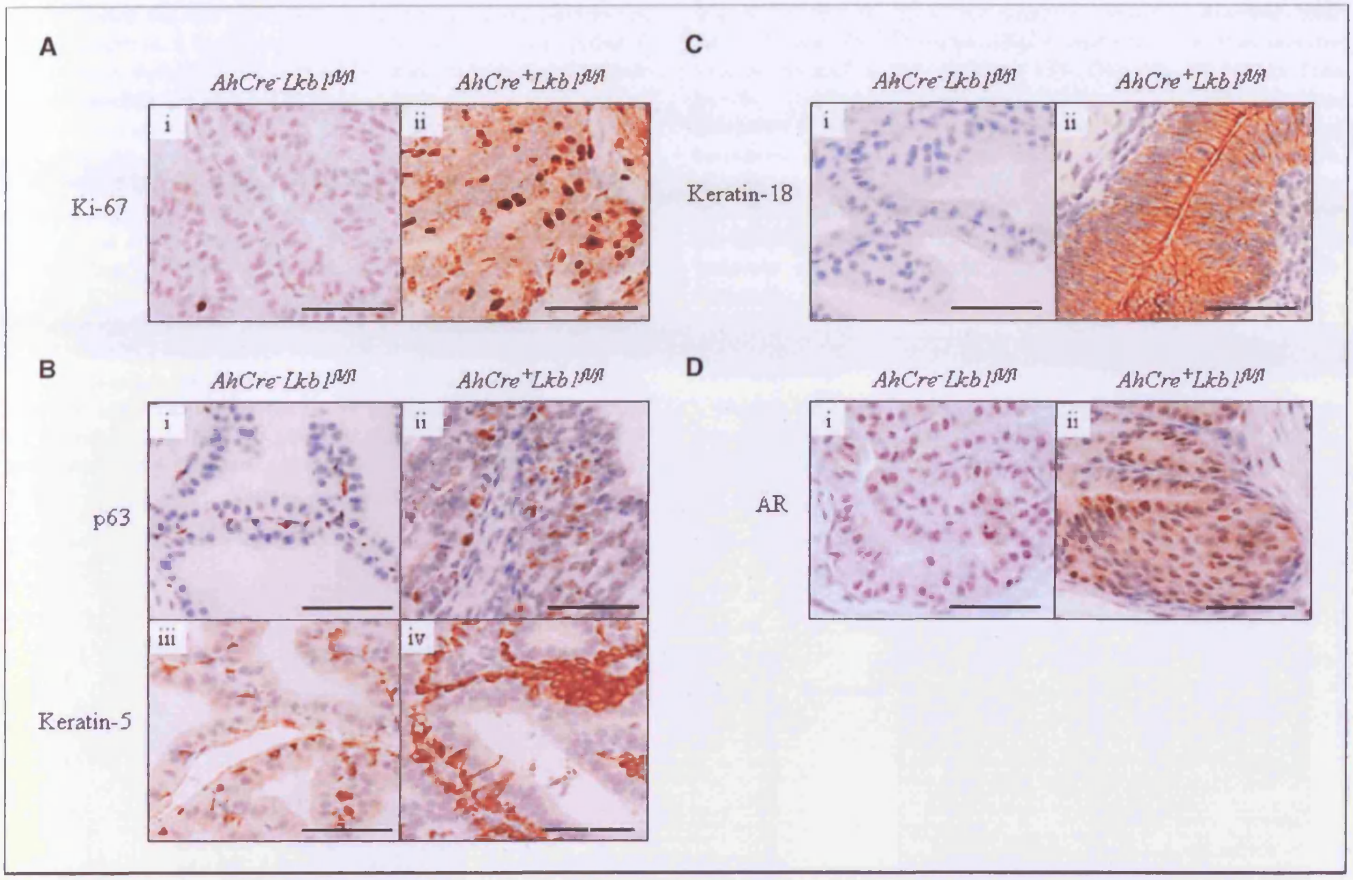


**Figure 4.** Characterisation of *Lkb1*-deficient PIN. *A*, immunohistochemical analysis of the anterior prostate of control (*AhCre⁻Lkb1$^{fl/fl}$*) and *AhCre⁺Lkb1$^{fl/fl}$* mice (ages, 2-7 mo) revealed an increase in proliferation using an anti–Ki-67 antibody. *B*, basal cell clustering was determined by monitoring p63 (*i* and *ii*) and Keratin-5 (*iii* and *iv*) expression. *C*, the luminal cell marker Keratin-18 is elevated in PIN foci. *D*, the androgen receptor (*AR*) is overexpressed in PIN lesions, suggesting deregulation of androgen signaling within neoplastic lesions. Images were taken at 40× magnification, and the scale bars represent 50 μm.

these cells within the lesions (Fig. 4*B*). This pattern of expression was also recently observed in lung tumors from mice bearing *Lkb1* inactivation (12). Keratin-18 is a luminal cell marker. Here, we show an elevation in Keratin-18 expression in PIN foci, mimicking human prostate cancer (Fig. 4*C*). We also show increased expression of the androgen receptor within the lesions, suggesting that PIN development in the context of mutant *Lkb1* is probably androgen sensitive (Fig. 4*D*).

**mTOR signaling is decreased in AhCre⁺Lkb1$^{fl/fl}$ PIN after p-AMPK activation.** Lkb1 is known to mediate mTOR signaling by the phosphorylation of AMPK under low-energy conditions within the small intestine and skeletal muscle (4, 7, 11, 15). Consequently, in the absence of *Lkb1*, the extent of this phosphorylation event is expected to decrease concomitantly with mTOR signaling activation. To establish on a molecular level whether the loss of *Lkb1* deregulates mTOR signaling in PIN foci, we used immunohistochemistry to stain for active p-AMPKα, p-mTOR, p-S6K (ribosomal protein S6 kinase, 70kDa), an mTOR downstream target, and its substrate p-Rps6 (Fig. 5*A*). We observed an increase in cytoplasmic p-AMPKα expression in association with loss of nuclear p-mTOR in *Lkb1*-deficient PIN lesions, contradicting S6K activation and phosphorylation of its substrate p-Rps6. This suggests that an alternative AMPK kinase (AMPKK) compensates for the absence of *Lkb1*, inhibiting mTOR production and stimulating S6K via an alternative mechanism or that Lkb1 does not regulate AMPK in prostatic epithelia.

**Wnt signaling is deregulated in AhCre⁺Lkb1$^{fl/fl}$ PIN.** Considering mTOR signaling is not stimulated in *Lkb1*-deficient prostate epithelium, we investigated alternative pathways mediated by Lkb1. To this end, we monitored the expression of a number of Wnt signaling components and downstream transcriptional targets using immunohistochemistry. The β-catenin (CTNNB1) oncogene plays a dual role in cells by participating in both Wnt signaling, essential for normal mammalian development, polarity, and migration, as well as forming adheren junctions at the cell surface membrane together with E-cadherin (42). We observed elevated nuclear β-catenin in PIN foci compared with control tissue, indicating activation of the Wnt signal cascade (Fig. 5*Bi,ii*). Aberrant Wnt signaling was further shown through overexpression of a number of β-catenin transcriptional targets. We detected elevated levels of the migration marker CD44 in PIN foci, a known immediate transcriptional target of Wnt signaling (ref. 43; Fig. 5*Biii,iv*). Foxa1, a Forkhead box factor involved in prostate development and an indirect Wnt target via Sox17 (44), was also up-regulated in PIN lesions (Fig. 5*Bv,vi*). Interestingly, we also observed high-cytoplasmic expression of inactivated p-Gsk3β ($Ser^9$), a negative regulator of β-catenin (Fig. 5*Bvii,viii*), which further implies perturbation of the Wnt cascade.

Considering the role Lkb1 plays in organizing cellular polarity via Par1A regulation, it is rational for *Lkb1*-deficient prostate epithelial cells to have undergone not only an elevation in Wnt signaling, but also to have lost cell polarity (11, 45). To this end, we analyzed the expression pattern of the tight junction protein ZO-1 using immunofluorescence. This revealed highly organized tight junctions located on the surface of the luminal cells in control tissues. In contrast, *AhCre*$^{+}$*Lkb1*$^{fl/fl}$ mice showed aberrant expression of ZO-1, being either principally lost completely or perturbed in a small subset of cells. In addition, reduced ZO-1 expression correlated with nuclear accumulation of ZO-1 (Fig. 5*Bix,x*), a phenomenon previously hypothesized to reflect altered regulation of cell polarity events (46).

**Deregulation of Pten and Akt in AhCre$^{+}$Lkb1$^{fl/fl}$ PIN.** Recently, Lkb1 has been linked to the Pten/PI3K/Akt pathway (3). To determine whether the PI3K/Akt pathway is deregulated upon loss of *Lkb1*, we used an antibody directed against total Pten (Fig. 6*Ai,ii*) and one that only recognizes inactive/phosphorylated (Ser$^{380,385}$ and Thr$^{382}$) p-Pten (Fig. 6*Aiii,iv*) to show that inactive Pten is elevated in *Lkb1*-deficient PIN. This suggests loss of Pten function/stability is a direct consequence of losing *Lkb1* function, ultimately facilitating a predisposition to PIN. Lkb1 activation and coincident stabilization of Pten has been shown by *in vitro* studies, supporting our data (3, 23). Consistent with this, the *Lkb1* mutant mice also exhibited increased activation of phosphorylated Akt and the AMPKK p-PDK1 (47) within PIN foci (Fig. 6*Av–viii*). This indicates that the PI3K/Akt pathway is deregulated after *Lkb1* mutation. F6

## Discussion

Murine prostate cancer models are becoming increasingly powerful in elucidating the mechanisms underlying prostate intraepithelial neoplasia, the most established precursor to

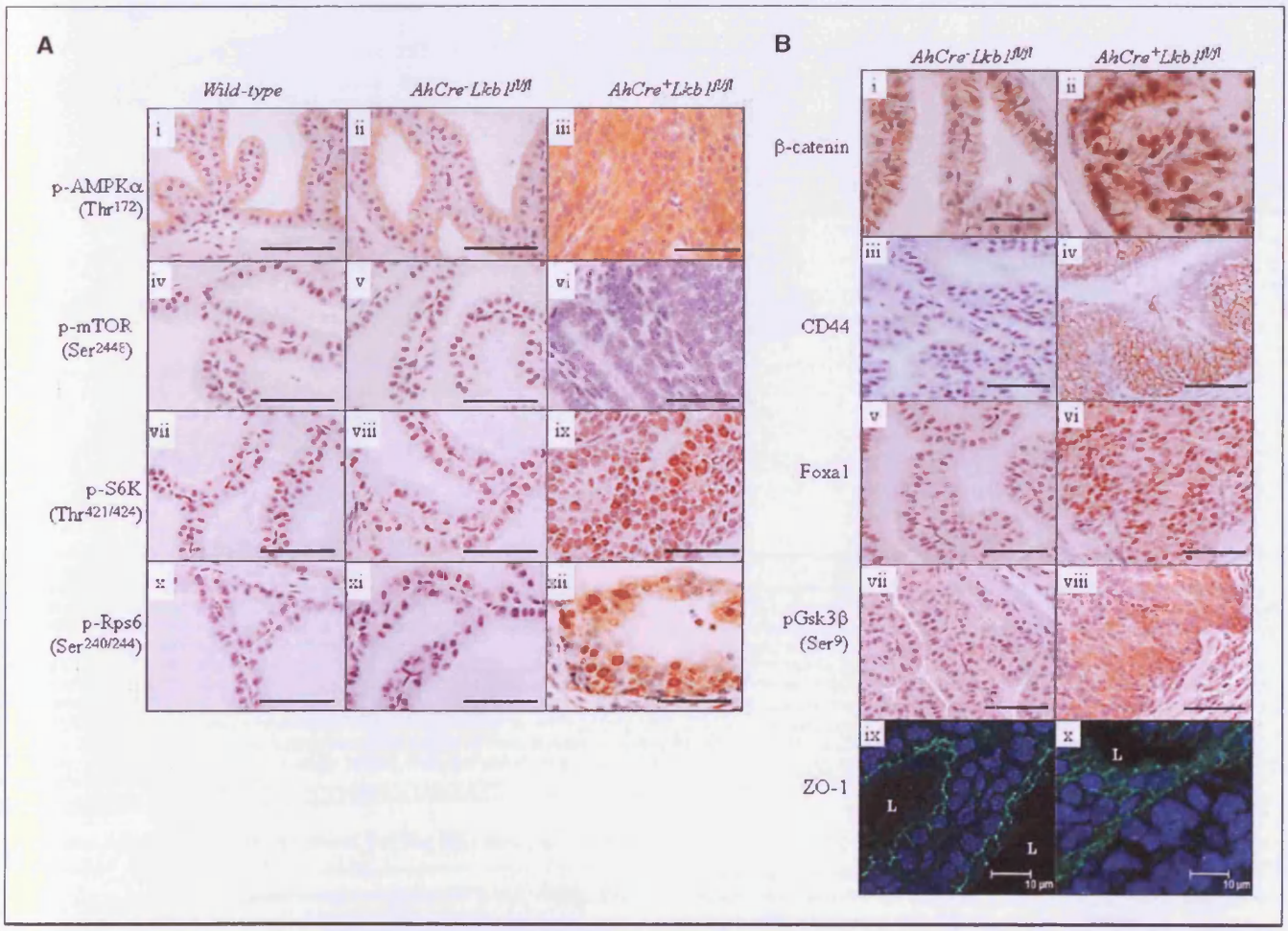


**Figure 5.** Wnt signaling is activated in *Lkb1*-deficient PIN. *A*, formalin-fixed, paraffin-embedded anterior prostate tissue sections from *AhCre*$^{-}$*Lkb1*$^{fl/fl}$ and *AhCre*$^{+}$*Lkb1*$^{fl/fl}$ mice were stained for p-AMPKα (*i–iii*), p-mTOR (*iv–vi*), p-S6K (*vii–ix*), and p-Rps6 (*x–xii*). Within PIN lesions, p-AMPKα expression was elevated throughout the cytoplasm, whereas p-mTOR expression is lost, along with a decrease in mTOR downstream signaling components p-S6K and p-Rps6. Lambda phosphatase treatment was used to determine the extent of any nonspecific staining after anti–p-AMPKα immunohistochemistry, which was observed weakly at the apical surface of the epithelium (as in *i* and *ii*). Similar controls for other antibodies used did not identify any nonspecific staining. *B*, investigations into Wnt signaling components determined β-catenin (*i* and *ii*), CD44 (*iii* and *iv*), Foxa1 (*v* and *vi*), and p-Gsk3β (*vii* and *viii*) were all elevated in *AhCre*$^{+}$*Lkb1*$^{fl/fl}$ PIN, indicating Wnt signaling is deregulated. Immunofluorescence for ZO-1 revealed ordered cellular polarity in control mice, whereas cell polarity is disrupted in *AhCre*$^{+}$*Lkb1*$^{fl/fl}$ PIN foci (*ix* and *x*). ZO-1 exhibited aberrant surface expression and punctate nuclear accumulation. Immunohistochemistry images were taken at 40× magnification, and scale bars represent 50 μm; confocal images were taken at 63× magnification, and scale bars represent 10 μm.

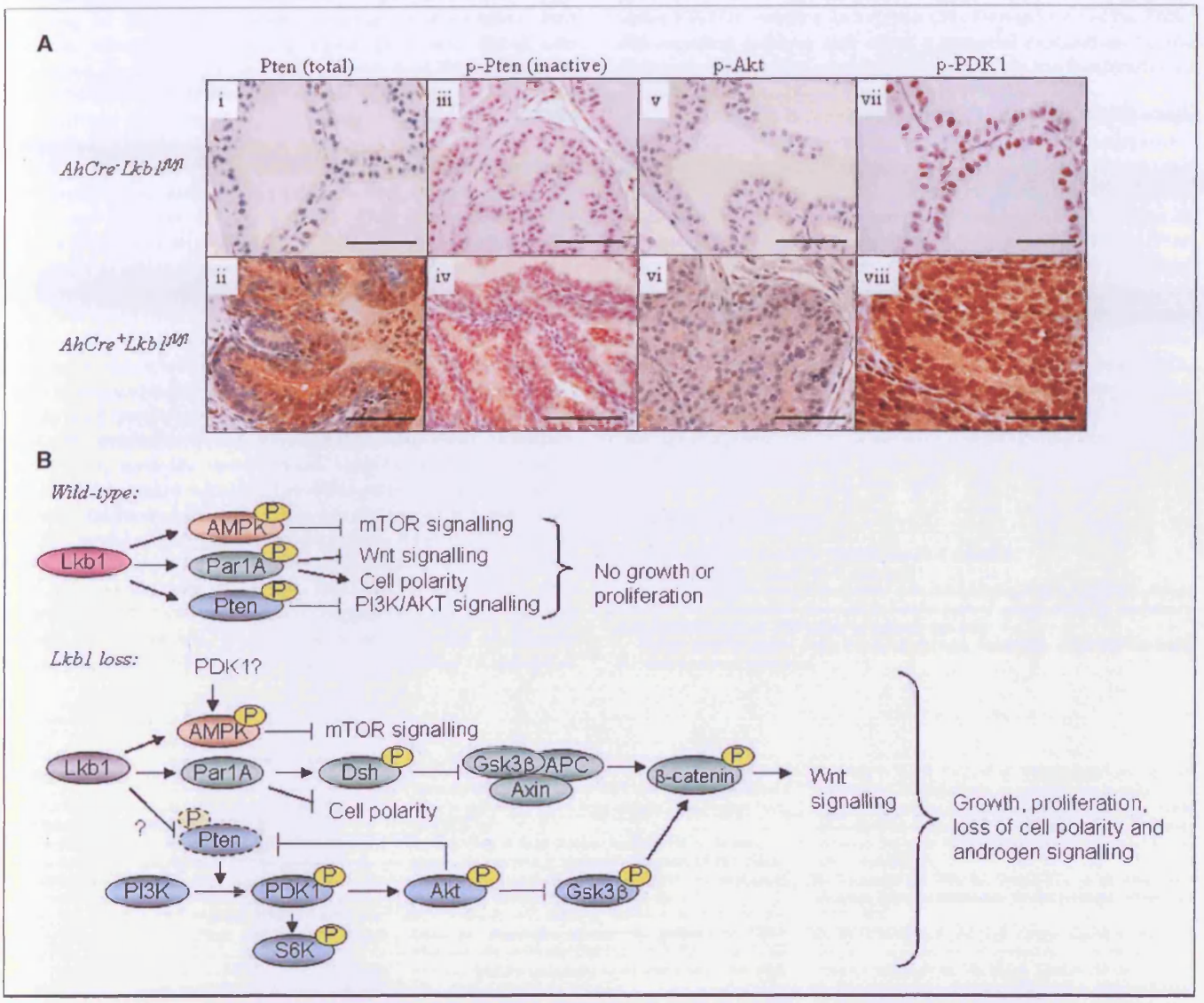


**Figure 6.** Loss of *Lkb1* stimulates the PI3K/Akt signaling cascade. *A*, immunohistochemistry of control and *AhCre*$^{+}$*Lkb1*$^{fl/fl}$ anterior prostate revealed total Pten (*i* and *ii*), inactive p-Pten (Ser$^{380}$/Thr$^{382/383}$; *iii* and *iv*), active phosphorylated Akt kinase (Ser$^{473}$; *v* and *vi*), and p-PDK1 (Ser$^{241}$; *vii* and *viii*) are all overexpressed in PIN lesions. Images were taken at 40× magnification, and scale bars represent 50 μm. *B*, a speculative schematic for signaling events mediated by Lkb1 (*top*) and those under *Lkb1* deficient conditions (*bottom*) within prostatic epithelia. Firstly, Lkb1 typically acts to phosphorylate AMPK to suppress mTOR signaling. Once Lkb1 is lost, mTOR signaling may proceed. Our investigations indicate an alternative AMPK kinase acts on behalf of Lkb1 (e.g., p-PDK1, which stimulates S6K) to sustain mTOR signaling inhibition. Secondly, Lkb1 phosphorylates Par1A to maintain cellular polarity. Upon loss of Lkb1 function, Par1A is redirected to stimulate Disheveled (*Dsh*) to inhibit the APC/Axin/Gsk3β complex, allowing β-catenin to translocate into the nucleus. Here, it stimulates transcription of downstream Wnt target genes and induces growth and proliferation, as well as androgen signaling (51). Finally, although the role of Lkb1 interaction and phosphorylation of Pten is still undefined, our data suggest that Lkb1 maintains Pten stability, inhibiting Akt activation. In the absence of Lkb1, we observed inactivation of Pten function, a common precursor to prostate cancer. Pten loss results in activated Akt and ultimately results in p-Gsk3β expression, which can act to maintain Wnt signaling and drive tumorigenesis.

prostatic carcinoma. Here, we show, for the first time, a role for the tumor suppressor Lkb1 in prostate cancer using Cre-LoxP technology to derive a conditional knockout of *Lkb1* within the prostate epithelial cells. Loss of *Lkb1* reduced male longevity and predisposed to hyperplasia, which progressed to high-grade PIN in the anterior lobe and mild hyperplasia, was also observed in the dorsolateral and ventral glands (within 2–4 months). This positively correlated with β-catenin nuclear translocation and up-regulation of the Wnt and PI3K/Akt signaling cascades within the prostate epithelium. Our immunohistochemical analysis suggests that mTOR signaling seems to decrease after an unexpected surge of p-AMPK in PIN lesions. It is feasible that either Lkb1 does not regulate AMPK within prostate tissue or that an alternative AMPKK compensates for the loss of Lkb1, resulting in suppression of the mTOR pathway. Our data indicate PDK1 is up-regulated in *Lkb1* deficient PIN and may therefore play a role in the observed AMPK phosphorylation and activation of pS6K (47). A speculative schematic of events occurring in the presence and absence of Lkb1 in prostate epithelium is depicted in Fig. 6*B*. One caveat of our studies is that we were limited to immunohistochemical analysis of these proteins, owing to the size of the lesions identified.

Our results from the *AhCre*$^{+}$*Lkb1*$^{fl/fl}$ mice parallel those of previous studies which have monitored the effects of aberrant Wnt signaling in the prostate, demonstrating an association with prostate tumorigenesis (20–22). Upon *Lkb1* loss, Par1A can propagate the translocation of β-catenin into the nucleus to initiate transcription of Wnt target genes, instigating tumorigenesis accompanied with loss of cellular polarity (8). This gives a direct mechanism whereby mutation of *Lkb1* may lead to activated Wnt signaling. The phenotype we observe is somewhat less severe than that reported for either constitutive activation of β-catenin or conditional deletion of *Apc* (20–22). This difference probably reflects differences in gene function (between *Lkb1* and either *Apc* or *β-catenin*) within the prostate, but may also reflect differences in the experimental approaches used, such as the pattern of *Cre*-mediated recombination.

The *Lkb1*-deficient prostate phenotype also parallels the phenotypic characteristics of *Pten*-deficient mice (25–27), although again being somewhat less severe. Loss of *Pten* results in HG-PIN which may progress into carcinoma, where tumorigenesis is positively correlated with the overexpression of p-PDK1, phosphorylated Akt, and its downstream targets, such as pGsk3β (24, 27). *Lkb1* mutant mice paralleled this pattern, and the elevation of both total Pten and inactive Pten was previously observed in the TRAMP model of prostate neoplasia where elevated Pten protein levels, as well as phosphorylation of stabilization sites, associated with inactivation ($Ser^{380}$, $Ser^{385}$, and $Thr^{382}$) correlated with progression (48). Our data therefore suggest loss of *Lkb1* function impairs Pten function, possibly as a consequence of directly interacting and regulating Pten stability (3), leading to enhanced PDK1 and Akt activity, and ultimately predisposing to PIN. This is consistent with an *in vitro* study that speculates LKB1 phosphorylates PTEN to stabilize its function (23). Deregulation of the PI3K/Akt signaling pathway also offers a potential explanation for the observed deregulation of the Wnt pathway via the inactivation of Gsk3β, which maintains Wnt signaling (49, 50).

In summary, we describe here a transgenic mouse model which provides the first link between mutation of the tumor suppressor gene *Lkb1* and prostate neoplasia. Conditional biallelic loss of *Lkb1* leads to the development of a PIN phenotype and to other lesions within the GU. The mechanism underlying this predisposition to PIN involves deregulation of both the Wnt and PI3K/Akt/Pten pathways. Indeed, the phenotype of *Lkb1* deficiency mirrors aspects of both *Pten* loss and Wnt deregulation. Surprisingly, we observed a decrease in mTOR signaling, which we hypothesize may occur as a consequence of a negative feedback mechanism whereby AMPK is activated by an alternate AMPKK to Lkb1, possibly PDK1, to suppress the mTOR pathway. Mechanisms for such deregulation and pathway crosstalk have already been described (Fig. 6*B*), both through the phosphorylation of Par1a and by altering Pten activity/stabilization.

## Acknowledgments

Received 8/23/2007; revised 1/15/2008; accepted 1/20/2008.

**Grant support:** Tenovus (H.B. Pearson).

The costs of publication of this article were defrayed in part by the payment of page charges. This article must therefore be hereby marked *advertisement* in accordance with 18 U.S.C. Section 1734 solely to indicate this fact.

We thank Mark Bishop, Lucie Pietzka, and Derek Scarbrough at Cardiff University for their technical assistance.

## References

1. Jemal A, Siegel R, Ward E, et al. Cancer statistics, 2006. CA Cancer J Clin 2006;56:106–30.
2. Chin JL, Reiter RE. Molecular markers and prostate cancer prognosis. Clin Prostate Cancer 2004;3:157–64.
3. Mehenni H, Lin-Marq N, Buchet-Poyau K, et al. LKB1 interacts with and phosphorylates PTEN: a functional link between two proteins involved in cancer predisposing syndromes. Hum Mol Genet 2005;14:2209–19.
4. Yoo LI, Chung DC, Yuan J. LKB1-a master tumour suppressor of the small intestine and beyond. Nat Rev Cancer 2002;2:529–35.
5. Giardiello FM, Welsh SB, Hamilton SR, et al. Increased risk of cancer in the Peutz-Jeghers syndrome. N Engl J Med 1987;316:1511–4.
6. Boardman LA, Thibodeau SN, Schaid DJ, et al. Increased risk for cancer in patients with the Peutz-Jeghers syndrome. Ann Intern Med 1998;128:896–9.
7. Lizcano JM, Goransson O, Toth R, et al. LKB1 is a master kinase that activates 13 kinases of the AMPK subfamily, including MARK/PAR-1. EMBO J 2004;23:833–43.
8. Spicer J, Rayter S, Young N, Elliott R, Ashworth A, Smith D. Regulation of the Wnt signaling component PAR1A by the Peutz-Jeghers syndrome kinase LKB1. Oncogene 2003;22:4752–6.
9. Marignani PA. LKB1, the multitasking tumour suppressor kinase. J Clin Pathol 2005;58:15–9.
10. Alessi DR, Sakamoto K, Bayascas JR. LKB1-dependent signaling pathways. Annu Rev Biochem 2006;75:137–63.
11. Spicer J, Ashworth A. LKB1 kinase: master and commander of metabolism and polarity. Curr Biol 2004;14:R383–5.
12. Ji H, Ramsey MR, Hayes DN, et al. LKB1 modulates lung cancer differentiation and metastasis. Nature 2007;448:807–10.
13. Su G, Hruban R, Bansal R, et al. Germline and somatic mutations of the STK11/LKB1 Peutz-Jeghers gene in pancreatic and biliary cancers. Am J Pathol 1999;154:1835–40.
14. Guldberg P, thor Straten P, Ahrenkiel V, Seremet T, Kirkin A, Zeuthen J. Somatic mutation of the Peutz-Jeghers syndrome gene, LKB1/STK11, in malignant melanoma. Oncogene 1999;18:1777–80.
15. Corradetti MN, Inoki K, Bardeesy N, DePinho RA, Guan KL. Regulation of the TSC pathway by LKB1: evidence of a molecular link between tuberous sclerosis complex and Peutz-Jeghers syndrome. Genes Dev 2004;18:1533–8.
16. Baas AF, Smit L, Clevers H. LKB1 tumor suppressor protein: PARtaker in cell polarity. Trends Cell Biol 2004;14:312–9.
17. Shaw RJ, Bardeesy N, Manning BD, et al. The LKB1 tumor suppressor negatively regulates mTOR signaling. Cancer Cell 2004;6:91–9.
18. Kyriakis JM. At the crossroads: AMP-activated kinase and the LKB1 tumor suppressor link cell proliferation to metabolic regulation. J Biol 2003;2:26.
19. Lee M, Hwang JT, Yun H, et al. Critical roles of AMP-activated protein kinase in the carcinogenic metal-induced expression of VEGF and HIF-1 proteins in DU145 prostate carcinoma. Biochem Pharmacol 2006;72:91–103.
20. Gounari F, Signoretti S, Bronson R, et al. Stabilization of β-catenin induces lesions reminiscent of prostatic intraepithelial neoplasia, but terminal squamous transdifferentiation of other secretory epithelia. Oncogene 2002;21:4099–107.
21. Bierie B, Nozawa M, Renou J, et al. Activation of b-catenin in prostate epithelium induces hyperplasias and squamous transdifferentiation. Oncogene 2003;22:3875–87.
22. Bruxvoort KJ, Charbonneau HM, Giambernardi TA, et al. Inactivation of Apc in the mouse prostate causes prostate carcinoma. Cancer Res 2007;67:2490–6.
23. Song P, Wu Y, Xu J, et al. Reactive nitrogen species induced by hyperglycemia suppresses Akt signaling and triggers apoptosis by upregulating phosphatase PTEN (phosphatase and tensin homologue deleted on chromosome 10) in an LKB1-dependent manner. Circulation 2007;116:1585–95.
24. Trotman LC, Niki M, Dotan ZA, et al. Pten dose dictates cancer progression in the prostate. PLoS Biol 2003;1:E59.
25. Di Cristofano A, Pesce B, Cordon-Cardo C, Pandolfi PP. Pten is essential for embryonic development and tumour suppression. Nat Genet 1998;19:348–55.
26. Di Cristofano A, De Acetis M, Koff A, Cordon-Cardo C, Pandolfi PP. Pten and p27KIP1 cooperate in prostate cancer tumor suppression in the mouse. Nat Genet 2001;27:222–4.
27. Wang S, Gao J, Lei Q, et al. Prostate-specific deletion of the murine Pten tumor suppressor gene leads to metastatic prostate cancer. Cancer Cell 2003;4:209–21.
28. Le Page C, Koumakpayi I, Alam Fahmy M, Mes Masson A, Saad F. Expression and localisation of Akt-1, Akt-2 and Akt-3 correlate with clinical outcome of prostate cancer patients. Br J Cancer 2006;94:1906–12.
29. Conde E, Suarez-Gauthier A, García-García E, et al. Specific pattern of LKB1 and phospho-acetyl-CoA carboxylase protein immunostaining in human normal tissues and lung carcinomas. Hum Pathol 2007;38:1351–60.
30. Collins SP, Reoma JL, Gamm DM, Uhler MD. LKB1, a novel serine/threonine protein kinase and potential tumour suppressor, is phosphorylated by cAMP-dependent protein kinase (PKA) and prenylated *in vivo*. Biochem J 2000;345:673–80.
31. Ikediobi ON, Davies H, Bignell G, et al. Mutation analysis of 24 known cancer genes in the NCI-60 cell line set. Mol Cancer Ther 2006;5:2606–12.
32. Neville P, Conti D, Krumroy L, et al. Prostate cancer aggressiveness locus on chromosome segment 19q12–13.1 identified by linkage and allelic imbalance studies. Genes Chromosomes Cancer 2003;36:332–9.

33. Sakamoto K, McCarthy A, Smith D, et al. Deficiency of LKB1 in skeletal muscle prevents AMPK activation and glucose uptake during contraction. EMBO J 2005;24:1810–20.
34. Ireland H, Kemp R, Houghton C, et al. Inducible Cre-mediated control of gene expression in the murine gastrointestinal tract: effect of loss of β-catenin. Gastroenterology 2004;126:1236–46.
35. Soriano P. Generalized lacZ expression with the ROSA26 Cre reporter strain. Nat Genet 1999;21:70–1.
36. Shappell SB, Thomas GV, Roberts RL, et al. Prostate pathology of genetically engineered mice: definitions and classification. The consensus report from the Bar Harbor meeting of the Mouse Models of Human Cancer Consortium Prostate Pathology Committee. Cancer Res 2004;64:2270–305.
37. Kikyo N, Williamson CM, John RM, et al. Genetic and functional analysis of neuronatin in mice with maternal or paternal duplication of distal Chr 2. Dev Biol 1997;190:66–77.
38. Brawer MK. Prostatic Intraepithelial Neoplasia: an overview. Urology 2005;7:S11–8.
39. Bhatia-Gaur R, Donjacour AA, Sciavolino PJ, et al. Roles for Nkx3.1 in prostate development and cancer. Genes Dev 1999;13:966–77.
40. Schneider A, Brand T, Zweigerdt R, Arnold H. Targeted disruption of the Nkx3.1 gene in mice results in morphogenetic defects of minor salivary glands: parallels to glandular duct morphogenesis in prostate. Mech Dev 2000;95:163–74.
41. Sansom O, Griffiths D, Reed KR, Winton D, Clarke A. Apc deficiency predisposes to renal carcinoma in the mouse. Oncogene 2005;24:8205–10.
42. Willert K, Nusse R. β-catenin: a key mediator of Wnt signaling. Curr Opin Genet Dev 1998;8:95–102.
43. Wielenga VJM, Smits R, Korinek V, et al. Expression of CD44 in APC and Tcf mutant mice implies regulation by the WNT pathway. Am J Pathol 1999;154:515–23.
44. Sinner D, Rankin S, Lee M, Zorn AM. Sox17 and β-catenin cooperate to regulate the transcription of endodermal genes. Development 2004;131:3069–80.
45. Forcet C, Etienne-Manneville S, Gaude H, et al. Functional analysis of Peutz-Jeghers mutations reveals that the LKB1 C-terminal region exerts a crucial role in regulating both the AMPK pathway and the cell polarity. Hum Mol Genet 2005;14:1283–92.
46. Gottardi CJ, Arpin M, Fanning AS, Louvard D. The junction-associated protein, zonula occludens-1, localizes to the nucleus before the maturation and during the remodelling of cell-cell contacts. Proc Natl Acad Sci U S A 1996;93:10779–84.
47. Bayascas JR, Leslie NR, Parsons R, Fleming S, Alessi DR. Hypomorphic mutation of PDK1 suppresses tumorigenesis in PTEN (+/-) mice. Curr Biol 15:1839–46. Q4
48. Shukla S, Maclennan GT, Marengo SR, Resnick MI, Gupta S. Constitutive activation of PI3K-Akt and NF-kB during prostate cancer progression in autochthonous transgenic mouse model. Prostate 2005;64:224–39.
49. Green JB. Lkb1 and GSK3-β: kinases at the center and poles of the action. Cell Cycle 2004;3:12–4.
50. Al-Khouri AM, Ma Y, Togo SH, Williams S, Mustelin T. Cooperative phosphorylation of the tumor suppressor phosphatase and tensin homologue (PTEN) by casein kinases and glycogen synthase kinase 3β. J Biol Chem 2005;280:35195–202.
51. Yardy GW, Brewster SF. Wnt signaling and prostate cancer. Prostate Cancer Prostatic Dis 2005;8:119–26.